

Technical University of Liberec

**Faculty of Mechatronics, Informatics and Interdisciplinary
Studies**



**Valorization of Tree Gum Polysaccharides in the Synthesis
of Nanostructures and Packaging Films**

PhD Thesis

Liberec 2022

Abhilash Venkateshaiah



Thesis topic: Valorization of tree gum polysaccharides in the synthesis of nanostructures and packaging films

Study program: P3942 Nanotechnology

Field of Study: 3942V001 Nanotechnology

Author: Abhilash Venkateshaiah

Supervisor: Dr. Vinod V.T. Padil, M.Sc.,B.Ed., Ph.D

Workplace: Institute for Nanomaterials, Advanced Technology and Innovation, Technical University of Liberec.



Declaration

I hereby certify that I have been informed that Act 121/2000, the Copyright Act of the Czech Republic, namely Section 60, School-work, applies to my Ph.D. thesis in full scope.

I acknowledge that the Technical University of Liberec (TUL) does not infringe my copyrights by using my Ph.D. thesis for TUL's internal purposes.

I am aware of my obligation to inform TUL on having used or licensed to use my Ph.D. thesis, in which event TUL may require compensation of costs incurred in creating the work at up to their actual amount.

I have written my Ph.D. thesis myself using literature listed therein after consulting with my supervisor.

I hereby also declare that the hard copy of my Ph.D. thesis is identical to its electronic form as saved at the IS STAG portal.

Date:

Signature:

Acknowledgements

I want to take this opportunity to thank a lot of eminent personalities, without whose help and support this work would be incomplete.

It gives me immense pleasure to express my profound and sincere gratitude to my supervisor Dr Vinod V.T. Padil, for his suggestions, support and guidance throughout my PhD. I learnt a lot from you. My deepest gratitude to Dr Stanisław Waclawek for his constant support and encouragement. I can't thank you enough for all your help and suggestions; you made my life so much easier here and it was an absolute pleasure to work with you. I offer my sincere thanks to Dr Miroslav Černík for being the coolest boss and providing an excellent platform to carry out my thesis. I also like to thank Dr Pavel Hrabák for being ever so helpful and considerate.

I also want to thank Mgr. Vít Novotný for his help and assistance over the years. I can't count the number of times I have troubled you. I also want to thank my friends and colleagues, Daniele Silvestri, Rohith Ramakrishnan, Kamil Krawczyk and Barbara Socha, for their help during my PhD. I also thank all colleagues and personnel of the Institute for Nanomaterials, Advanced Technology and Innovation who were directly or indirectly involved in the success of this work. My special thanks to Dr Malladi Nagalakshmaiah for his support and suggestions throughout the years.

I want to thank my dad for his everlasting support, encouragement, and love, which made this possible. Finally, I would like to thank my fiancée Amulya Raj for all the love, patience and motivation to always be a better version of myself.

Abstract

Tree gums exemplify sustainable and renewable biomacromolecules abundantly available from nature and possess excellent biodegradability, non-toxicity, low cost, physicochemical properties, structural attributes and diverse functional groups. Often known as tree gum polysaccharides or gum hydrocolloids, these biopolymers are obtained as the natural exudates of different tree species and represent a largely unexplored source of valuable natural products. Exudate gums have a wide range of applications in food and pharmaceutical industries as stabilizers, thickening agents, emulsifying agents, and binding agents. Recently there is a growing interest in the use of these exudate gums for non-food applications, including biomedical, food and pharmaceutical packaging, energy, and environmental applications. The discovery of novel uses for these gums has piqued people's attention in recent years.

This current thesis investigates the potential non-food applications of three important tree gums: arabic (*Acacia Senegal*, *Acacia Seyal*), karaya (*Sterculia Urens*), and kondagogu (*Cochlospermum Gossypium*), focusing their uses in food packaging. Abundant availability and biodegradability coupled with non-toxicity and low cost can make these materials ideal for the fabrication of packaging films to replace conventional plastics. However, these exudate gums have intrinsic limitations, including high hydrophilicity, poor film-forming ability, and low mechanical properties. To overcome these drawbacks, different strategies were employed, including chemical modifications, blending with different nanomaterials (graphene oxide, nanocellulose), 2D nanoclay coating, and blending with other natural polymers. The obtained packaging films demonstrated significant improvement in the physicochemical, mechanical, thermal and barrier properties while retaining the biodegradability of the gums.

Additionally, certain strategies have been developed to valorize tree gum wastes in the fabrication of nanostructures for advanced applications. The carbon-rich structure of the gum wastes has been

utilized in the development of carbon nanostructures with exceptionally high surface area. These carbon nanostructures have been further used in the development of energy harvesters. The abundant functional groups of the gums have been put to use in the development of graphene-supported nanoparticles for environmental remediation application.

To summarize, this work emphasizes the valorization of tree gums in food packaging, energy, and environmental applications. The results demonstrate the tremendous unexplored potential of the exudate gums for the fabrication of bioplastic packaging materials. Additionally, gum wastes with no commercial value can potentially be a great resource for the development of nanostructures for advanced applications.

Keywords: tree gums, karaya, kondagogu, arabic, bioplastics, food packaging, nanostructures, energy harvesters

Abstrakt

Rostlinné gummy představují udržitelné a obnovitelné biomakromolekuly dostupné z přírodních zdrojů, vyznačující se výtečnou biodegradabilitou, netoxicitou, nízkou cenou, zajímavými chemickými a fyzikálními vlastnostmi, strukturou a přítomností rozličných funkčních skupin. Jsou často označovány jako polysacharidy nebo hydrokoloidy z rostlinných gum. Tyto biopolymery jsou získávány jako přírodní exudáty z různých druhů dřevin a představují málo prozkoumaný zdroj cenných přírodních produktů. Exudátové gummy mají široké spektrum uplatnění v potravinářském a farmaceutickém průmyslu jako stabilizátory, zahušřovadla, emulgátory a pojiva. V poslední době je zvýšený zájem o jejich využití v nepotravinářských odvětvích, zvláště biomedicínských aplikacích, materiálech pro obaly, energetických a environmentálních aplikacích. Výzkumu nových využití těchto gum je tedy v současné době věnována pozornost mnoha subjektů.

Tato představovaná práce se zabývá nepotravinářskými aplikacemi tří důležitých materiálů – arabské gummy (získávané z *Acacia Senegal*, *Acacia Seyal*) gummy karaya (*Sterculia Urens*), a gummy kondagogu (*Cochlospermum Gossypium*) a soustředí se na jejich využití při výrobě obalových materiálů pro potravinářství. Dostupnost v dostatečném množství, biodegradabilita, netoxicity a cenová dostupnost činí tyto materiály ideálními pro výrobu obalových folií s nadějí, že nahradí konvenční plasty. Bohužel tyto exudáty mají v nezpracovaném stavu nedostatky, jako je vysoká hydrofilicita, špatná schopnost tvoření filmů, a nízká mechanická odolnost. Pro překonání těchto nevýhod bylo uplatněno několik strategií, včetně chemické modifikace, mísení

s různými nanomateriály (oxid grafenu, nanocelulóza), 2D nanojílové povlakování a mísení s jinými přírodními polymery. Výsledné obalové folie vykazovaly značné zlepšení fyzikálně-chemických, mechanických a tepelně izolačních vlastností i neprodyšnosti za zachování biodegradability rostlinných gum.

Také se nám podařilo vyvinout způsoby zušlechtění odpadů z výroby rostlinných gum umožňující jejich použití pro výrobu nanostruktur pro technologicky pokročilé aplikace. Struktura gum bohatá na uhlík byla využita k výrobě nanostruktur s obzvláště vysokým měrným povrchem. Tyto uhlíkaté nanostruktury byly využity k vývoji zařízení pro získávání energie. Početné funkční skupiny zkoumaných gum byly využity při vývoji nanočástic ukotvených na grafenu a pro jejich environmentálně sanační aplikace.

Tato práce tedy zahrnuje využití rostlinných gum pro potravinářské obaly, energetické a environmentální aplikace. Její výsledky odhalují obrovský dosud nevyužitý potenciál pro výrobu bioplastických obalových materiálů. Odpady z výroby těchto gum, které zatím nemají komerční hodnotu, se mohou stát ceněnou surovinou pro výrobu nanostruktur pro pokročilé technické aplikace.

Klíčová slova: rostlinné gummy, karaya guma, kondagogu, arabská guma, bioplasty, potravinářské obaly, nanostruktury, získávání energie

Contents

1. Abbreviations.....	11
2. Introduction.....	12
2.1. Biopolymers	13
2.2. Gums	15
2.3. Extraction of tree gum exudates.....	16
2.4. Physico-chemical properties of gums	18
2.4.1. Colour	18
2.4.2. Size and shape.....	19
2.4.3. Solubility.....	19
2.4.4. Taste and smell	19
2.4.5. Viscosity	19
2.4.6. Hardness and density	20
2.5. Tree gums of interest.....	20
2.5.1. Gum arabic.....	21
2.5.1.1. Chemistry of gum arabic	21
2.5.1.2. Properties of gum arabic.....	23
2.5.2. Gum karaya.....	23
2.5.2.1. Chemistry of gum karaya	24
2.5.2.2. Properties of gum karaya.....	25
2.5.3. Gum kondagogu.....	26
2.5.3.1. Chemistry of gum kondagogu	27
2.5.3.2. Properties of gum kondagogu.....	27
2.6. Common applications of tree gums.....	28
2.6.1. Food additives.....	28
2.6.2. Green synthesis of nanoparticles	29

2.6.3.	Miscellaneous applications	31
2.7.	Food packaging	32
2.7.1.	Biobased food packaging	33
2.8.	Packaging properties	34
2.8.1.	Barrier properties	34
2.8.2.	Mechanical properties	36
2.8.3.	Other properties	37
2.8.4.	Biodegradability.....	37
2.9.	Tree gums in food packaging	38
2.10.	Valorization of tree gum wastes in nanostructures synthesis	40
2.11.	Objectives	40
3.	Results and discussion	42
3.1.	Tree Gum–Graphene Oxide Nanocomposite Films as Gas Barriers	42
3.2.	Alkenyl succinic anhydride modified tree-gum kondagogu: A bio-based material with potential for food packaging	51
3.3.	High barrier, biodegradable nanocomposite films based on clay coated and chemically modified Gum Kondagogu	61
3.4.	Dialdehyde Modified Tree Gum Karaya: A Sustainable Green Crosslinker for Gelatin-Based Edible Films.	70
3.5.	Recycling non-food-grade tree gum wastes into nanoporous carbon for sustainable energy harvesting	80
3.6.	Gum Kondagogu/Reduced Graphene Oxide Framed Platinum Nanoparticles and Their Catalytic Role.....	92
4.	Conclusions.....	104
5.	Future prospects	106
6.	Publications.....	107
7.	References.....	109

1. Abbreviations

PET – Polyethylene terephthalate

PE – Polyethylene

PP – Polypropylene

PS – Polystyrene

PVC – Polyvinyl chloride

DDT – Dichlorodiphenyltrichloroethane

PCB – Polychlorinated biphenyls

PAH – Polycyclic aromatic hydrocarbons

GA – Gum arabic

GK – Gum karaya

KG – Gum kondagogu

FAO – Food and agriculture organization

GRAS – Generally recognized as safe

ASTM - American society for testing and materials

PVA – Polyvinyl alcohol

GO – Graphene oxide

RGO – Reduced graphene oxide

DDSA – Dodeceny succinic anhydride

2. Introduction

Polymers derived from petrochemical compounds are ubiquitous in our daily lives. These materials, which are derived from nonrenewable energy sources such as crude oil, may be modified to have a wide range of characteristics tailored to specific applications. Their exceptional versatility along with technical properties and lower manufacturing costs are the driving forces behind their widespread use and, consequently, a global reliance. The amount of plastics produced worldwide has increased exponentially from 2 million tons in 1950 to 367 million tons in 2020¹. The fact that more than half of all plastics ever produced were introduced to the market after 2000 reflects their prevalence in our everyday lives¹. Polyethylene terephthalate (PET), polyethylene (PE), polypropylene (PP), polystyrene (PS), and polyvinyl chloride (PVC) are some of the most commonly used plastics in the market. These conventional plastics are resistant to microbial degradation and persist in the environment for a long period of time, taking years to centuries to degrade in natural conditions, resulting in an untenable environment. When released into the environment, plastic waste can migrate from land to river and finally reach the ocean. Plastic pollution has spread across the environment, littering all of the main ocean basins, rivers, and bodies of water². Plastics can have a negative influence on the natural environment, animals, and even human health throughout their migration³. When ingested, microplastics, a kind of plastic waste, obstruct the digestive tracts of animals and marine life, posing a hazard to them. They are then translocated to the circulatory system and other tissues, allowing them to pass from prey to predator along the food chain⁴.

Furthermore, compounds such as monomers, oligomers, and additives have been shown to be released into the environment by plastics, suggesting that plastics can also be considered sources of some hazardous substances⁵. Moreover, plastics can also serve as “vehicles” for many other contaminants in the environment; heavy metals, dichlorodiphenyltrichloroethane (DDT),

polychlorinated biphenyls (PCB), polycyclic aromatic hydrocarbons (PAH), and nanoparticles have been detected on the plastic debris surface, creating a plastic-contaminant mixtures³. The creation of such mixtures not only accelerated the spread of these contaminants but also opened up a new environmental fate for them. Taking into consideration the innumerable pollutants released into the environment, it is still unclear if plastics may function as vectors for them, especially emerging contaminants. Further, plastics can aid in the dispersion and diffusion of microbes and pathogens in the ecosystem by serving as carriers, adding to their list of potential threats⁶.

Over the years, different techniques have been explored for dealing with plastic waste, including incineration, burying in landfills, and recycling. Nevertheless, most of these techniques have environmental consequences, and recycling has not been a viable option for many of these materials⁷. As a response to resolve these escalating environmental concerns and unknown future threats, the green chemistry approach and sustainable engineering are being viewed as a key alternative for the development of new generation materials, products, and processes. With the depletion of fossil fuel reserves and the introduction of new environmental regulations, a synergistic drive has emerged to develop new materials and products that are both ecologically friendly and are not reliant on petroleum. In recent years, many major steps have been taken to create a more cost-effective and environmentally friendly world. The development of biobased materials is an example of such an endeavour that fits nicely within this paradigm. Biobased materials are those whose primary components are derived from biological origins. Biopolymers are once such components that are derived from natural renewable biomass.

2.1. Biopolymers

Biopolymers are a diverse group of materials obtained from biological sources, including trees/plants, animals, and microbes and also involve materials chemically synthesized from

biological sources like sugars, oils, proteins, fats, exudates, and resins⁸. Biopolymers have several unique characteristics, including renewability, natural abundance, low cost, unique structures, non-toxicity, biodegradability, non-carcinogenic, non-thrombogenic, biocompatibility, and are carbon neutral⁹. Nature-derived biopolymers, in contrast to conventional polymers with a simpler structure, have a broad range of structural complexity, frequently dependent on several factors such as the species, source, technique of extraction, and the age of the plant. However, the commercialization of these natural polymers is hindered by economic and engineering constraints. Nevertheless, due to their versatility, abundance, and low cost, biopolymers hold a tremendous potential to replace petroleum-based conventional polymers in various applications, including packaging, biomedical, textile, structural materials, cosmetics, drug delivery, and food technology.

Biopolymers are classified using various criteria in the literature; however, they may be roughly classified into natural and synthetic biopolymers. Natural biopolymers are acquired directly from nature, while synthetic biopolymers involve human intervention and chemical synthesis techniques to obtain the polymers. Natural biopolymers extracted from biomass can be further subclassified as polysaccharides, proteins, and lipids. Among these, polysaccharides are the most abundant and diverse group of biopolymers available on the planet. They are an essential component that performs a variety of biological functions including, communication between the cells, molecular recognition, and cell adhesion¹⁰. These are complex carbohydrate polymers composed of monosaccharide units connected through glycosidic linkages forming linear or branched-chain molecules of various lengths. They are either glycosidically connected sugar residues or covalently bound to other structures such as amino acids, peptides, and lipids. The physical and chemical characteristics of the polysaccharides are influenced by the monosaccharide unit type, chain configuration, molecular weight, branching, type of linkages, and anomeric configuration¹⁰. The most common polysaccharides obtained from biomass are cellulose, starch,

chitin/chitosan, and gums. Since gums are the focus of the thesis, they will be addressed in-depth in the next section.

2.2. Gums

Gums are high molecular weight compounds, either hydrophilic or hydrophobic, forming gels or highly viscous solutions with their respective solvents. Gums are often referred to as hydrocolloids due to their hydrophilic nature and ability to dissolve in water. This is due to the vast number of hydroxyl groups that are generally arranged in a somewhat regular pattern throughout the molecule's backbone. Most gums are heterogeneous polysaccharides, meaning they are made up of different monosaccharide units and possess complex structures. There are different types of gums derived from various sources, such as tree exudates, plants, seaweeds, mucilage gums, and microbes (Figure 1).

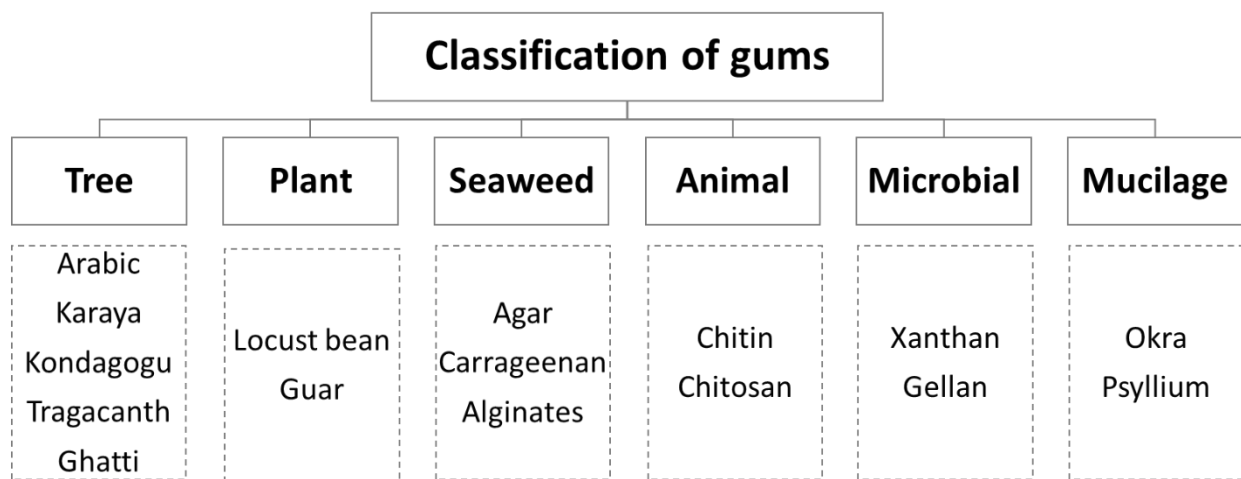


Figure 1. Classification of gums obtained from different sources.

Exudate gums have been utilized for various applications since ancient times and are even mentioned in the Bible as a source of food¹¹. Natural exudate gums are polysaccharides that trees exude as a defensive mechanism in response to mechanical damage, chemical injuries, microbial attacks, insect attacks, and water stress (Figure 2). Under these conditions, trees produce gums in the form of tears, masses, smeared buds, or lumps that are amorphous in nature; this process is

called gummosis. Usually, gums are not part of the typical tree metabolism, rather a product of abnormal and unfavourable circumstances. When the exuded gummy liquid dries in sunlight and air, it hardens into a hard-glassy mass of varied colour. This protects the injured part of the plant from subsequent infections and water losses by preventing the microbes from entering the internal tissues acting as a barrier. The trees exude gums quickly and abundantly during the summer, whereas it is relatively sluggish or non-existent during the winter¹².

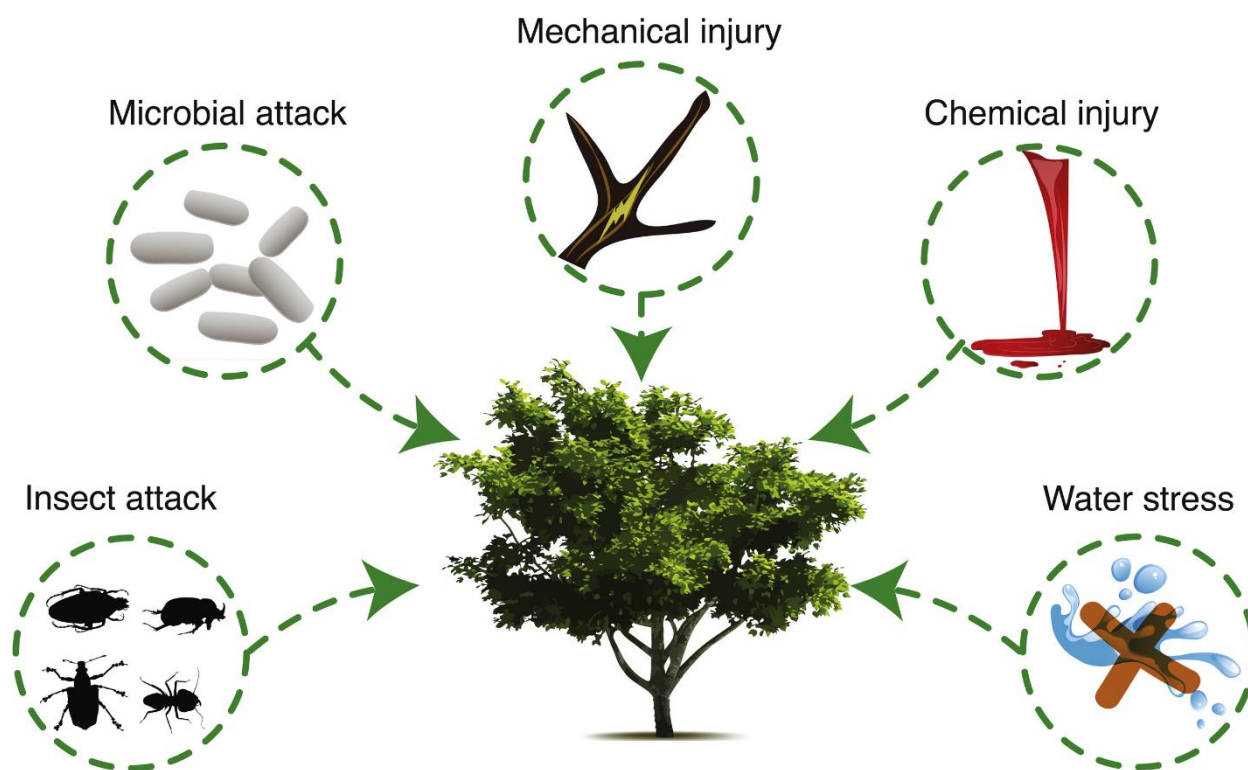


Figure 2. The most prevalent causes of gummosis in trees¹².

2.3. Extraction of tree gum exudates

Although harvesting and gathering naturally exuded gums from forest regions is still one of the most common approaches, tapping or blazing of trees is used to obtain large quantities of exudates. Making cuts and incisions in the bark of trees to increase gum exudation is a process known as tapping or blazing. The tapping procedure involves the removal of some sections of the bark with a sharp instrument and inflicting a sharp incision to trigger the exudation process¹¹. This

method requires a sharp instrument to slice off a chunk of bark and blaze the area underneath. Gums in the form of sticky liquid begin to pour from the wounds created on stems and branches. These viscous liquid tears start to harden and granulate upon exposure to sun and wind. It's critical to keep the tears on the trees for long enough for them to dry and to prevent clustering together. The tapping of gum trees is typically done in dry seasons until the beginning of the rainy season. Tapping incisions are usually made on the sun-facing sides of the trees to allow the gums to get substantial sunlight exposure and dry quickly. Successive tapping cycles can be used to further improve the yield of the gums. The earlier incisions are reopened during these tapping cycles by removing the bark from the top of the wounds and slicing the bottom edge even further. Until the end of the dry season, this repetitive tapping is carried out at an interval of 2-3 weeks. However, care should be taken to avoid unscientific and excessive tapping, which might result in tree's death. The timing of consecutive tapping is crucial. If the interval between tapplings is longer, the wounds inflicted will heal, and the trees will take a longer time to produce adequate and high-quality gums. Excessive tapping, on the other hand, may result in small/dusty tears of inferior quality or even the death of the tree.

Gum yields can also be improved by treating the trees with ethylene, a stress hormone in trees, or ethylene-releasing compounds like 2-chloroethylphosphonic acid (ethephon)¹³. Ethylene is biosynthesized by trees in response to environmental stress, especially drought. The concept behind using ethylene to boost gum yield is to speed up the tree's developmental response to stress by artificially supplying stress hormone, resulting in increased gum production¹⁴. Ethephon may replicate the effects of water stress by releasing the stress hormone ethylene in tree tissues, and it has been observed that gum synthesis increases as ethephon concentration increases¹⁴.

Gum is gathered manually as partly dried mass and is cleaned and graded before being sent to processors to be milled, sieved, and purified. Gums are graded based on colour and impurities;

lighter coloured gums with fewer impurities are of better quality, whereas darker coloured gums fall into lower grade¹⁵. Higher-grade gums are well-known for their numerous applications in the food industry. In baking and confectioneries, they are used as binding and stabilizing agents and as coatings for fruits¹⁶⁻¹⁸. They are also used as glazing agents for chewing gums and candies and flavour encapsulating agents, clouding or clarifying agents, and stabilizing agents in alcoholic and non-alcoholic beverages^{19,20}. Furthermore, their bioavailability, abundance, and non-toxicity have spurred their usage in the biomedical and pharmaceutical industry, cosmetics, and textiles²¹⁻²⁵. Lower-grade gums are usually discarded as they have high impurities and are unsuitable for use in the applications mentioned above.

2.4. Physico-chemical properties of gums

Natural gums' physical characteristics and appearance are some of the most crucial criteria in defining their commercial viability and intended usage. These characteristics of the natural gums are influenced by many factors, including the species of the tree, geographical source, harvesting season, and age of the tree²⁶. Furthermore, the exudate age, as well as the processing of the gum after harvestings, such as drying, washing, and storage temperature, also influence the physical characteristics²⁷.

2.4.1. Colour

Gums are generally valued commercially based on their colour, with light-coloured gums being considered higher quality. The dried gum exudates are sorted manually and graded based on their colour. It is often believed that darker colours result from the presence of contaminants. As a result, the commercial value of gums reduces as their colour becomes darker. When solid, gum colours range from virtually translucent white through different shades of yellow, amber, orange, brown, dark brown, and black, with hints of pink, red, and green in some gums.

2.4.2. Size and shape

Gums are available in a multitude of shapes and sizes when collected in their natural state. The exudate fragments are usually in the form of teardrops, globular, smeared buds, and lumps. Large pieces of exudates are frequently graded higher than siftings. The exudates can be further processed into kibbles and powders. Kibbled form is usually obtained by breaking down the large chunks of the exudates into smaller granules with uniform size distribution. While the powdered form is obtained by crushing or milling the granules into a fine powder then sieving it to the desired particle size. The powdered form can also be obtained via the spray drying technique²⁸. These processes facilitate the easy dissolution of gum in water.

2.4.3. Solubility

Most gums are partly soluble in water and leave behind some insoluble residues. The quantity of insoluble matter in low-quality dark-coloured gums is higher than in high-quality light-coloured gums. Moreover, certain gums are only partially soluble and only swell when exposed to water. As previously stated, processing can also improve the solubility of the gums since smaller particles dissolve more easily than bigger ones.

2.4.4. Taste and smell

Natural gums are nearly odourless compared to the resins that have a characteristic odour. They may have no discernible flavour and, in fact, lack any distinctive taste. However, some gums are mildly sweet or bitter, depending on the botanical origin. Some gums have a pronounced bitter taste, which is a significant drawback to be used in food applications.

2.4.5. Viscosity

The viscosity of gums is primarily responsible for their thickening characteristics in food systems. Owing to the intermolecular entanglements, gums can impart viscosity into solution mixtures. The viscosity of gums can be measured using various methods, some of which are

relatively simple, like the Bostwick flow method. This method estimates the flow speed of a liquid down a given slope over a certain period of time. However, the apparent viscosity of the gums is determined using advanced techniques using viscometers. These techniques allow for the variation of stress and shear rates, and the rheological properties can be determined as a relationship between the shear rate and apparent viscosity. The apparent viscosity of the gum solutions is influenced by various factors such as temperature, solvent concentration, impurities, pH, molecular structure, and salts present. The viscosity of all gum solutions increases with the increase in gum concentrations.

2.4.6. Hardness and density

The hardness and density of the gums vary widely depending on numerous factors and might not be a reliable factor in characterizing gums. Gum hardness is influenced by various factors, including moisture content, which typically ranges between 10 to 16%. However, when sufficiently dried, most gums break with a distinct glassy fracture and may be readily crushed. Furthermore, the density of the gums may also be an inaccurate element to consider because the density of gum from the same tree might vary based on the quantity of air that was incorporated when the exudate was being formed.

2.5. Tree gums of interest

The interest in different tree gums has increased over the years due to their distinctive characteristics. As a result, numerous gums of varied origins from diverse trees have been discovered worldwide. The most well-known tree gums include arabic, ghatti, karaya, kondagogu, and tragacanth. However, this work focuses mainly on arabic, karaya, and kondagogu gums. The following section provides an overview of these gums and their characteristics.

2.5.1. Gum arabic

Gum arabic (GA), also known as acacia gum, gum Sudani, Senegal gum, and Indian gum, is one of the oldest well-known gums with a history of nearly 5000 years²⁹. It is obtained from the exudates of *Acacia Senegal*, *Acacia Seyal* trees, and other species of *Acacia*, which belong to the *Leguminosae* family³⁰. Although genus *Acacia* has over 1000 species, only *Acacia Senegal* and *Acacia Seyal* are commercially important³¹. Due to a low amount of tannins, gums obtained from *Acacia Senegal* are regarded the highest in quality and account for the majority of worldwide trade, while gums from *Acacia seyal* are regarded as comparatively lower grade^{32,33}. These trees are usually found in sub-Saharan Africa, the Indian peninsula, and Australia. The majority of GA is obtained from Sudan, Nigeria, Senegal, Chad, Ethiopia, and Indian arid regions. The largest exporter of GA is Sudan, accounting for up to 80% of the total GA produced worldwide. The most significant GA markets are Europe and the United States of America, Japan being the leading Asian importer. *Acacia* trees have vast roots and can be cultivated in dry climates, making them beneficial to prevent soil erosion.



Figure 3. Native gum arabic tree and its exudate³⁴.

2.5.1.1. Chemistry of gum arabic

GA is a complex heteropolysaccharide with a branched structure that's neutral or slightly acidic. It consists of a main chain comprising 1,3-linked β -D-galactopyranosyl units and side

chains with 2-5 of the same units connected by 1, 6-linkages to the main chain³⁵. GA structure consists of α -L-arabinofuranosyl, α -L-rhamnopyranosyl, and 4-O-methyl- β -D-glucuronopyranosyl units (Figure 4)²⁶.

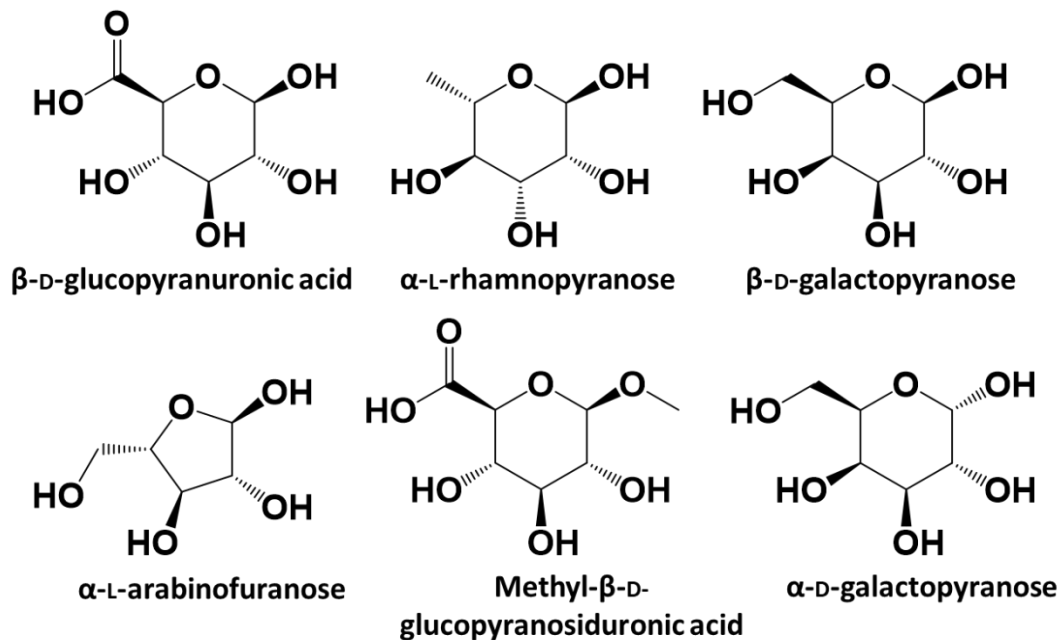


Figure 4. Sugar constituents of gum arabic.

This high molecular weight polysaccharide further contains calcium, potassium, and magnesium salts. Upon hydrolysis, GA yields polysaccharide and protein fractions, including arabinogalactan, arabinogalactan protein, and glycoprotein. The arabinogalactan component with low molecular weight (Mw ~300 KDa) accounts for 88% of the total gum weight and contains less than 1% protein concentration. The arabinogalactan protein component, primarily responsible for GA's emulsifying capabilities, accounts for 10% of the total gum weight. It has a high molecular weight (Mw ~1500 KDa) with a protein content of ~10%. The glycoprotein component accounting for less than 2% of the total gum weight has the lowest molecular weight of all the components (Mw ~250 KDa) and the highest protein content of up to 20-50%^{36,37}. GA obtained from different *Acacia* species include similar components, however in varying proportions. GA's chemical

composition has also been found to vary based on the source, harvest time, tree age, processing techniques and conditions³⁸⁻⁴¹.

2.5.1.2. Properties of gum arabic

Properties such as solubility, viscosity, and emulsifying ability of the gums have been the key variables in determining their industrial application. When compared to other industrial gums, GA has a high-water solubility. GA can form aqueous solutions with concentrations as high as 50% w/v and result in a solution that is tasteless, colourless, and acidic in nature. In addition, when compared to other industrial gums under identical conditions and concentrations, GA exhibits the lowest viscosity. Gums are typically difficult to work with at higher concentrations due to their high viscosity, while GA solutions are easier to prepare and handle owing to their low viscosity. Adding acids or bases, however, can alter the viscosity by changing the electrostatic charge on the polysaccharide. The pH of the solutions is generally about 4.5-5.5, however, at pH 6.0, maximum viscosity was observed. Because of its high amount of arabinogalactan protein, GA has exceptional emulsifying characteristics³⁶. The hydrophobic polypeptide backbone significantly adsorbs at the oil-water interface, while the carbohydrate units linked to it stabilize the emulsion through steric and electrostatic repulsion. Although emulsifying qualities typically increase with increasing molecular weight and protein concentration, studies indicate that mixtures of different fractions produce the best outcomes⁴².

2.5.2. Gum karaya

Gum karaya (GK), also known as kadaya, kullo is a native gum from India, which is the world's largest producer and exporter⁴³. GK is obtained from the exudates of the *Sterculia urens* tree belonging to the Sterculiaceae family. This large bushy tree is usually found in the arid rocky regions of the central, northern and west coast of India, as well as Myanmar's and Sri Lanka's dry forest regions⁴⁴. GK is also obtained from other trees of *Sterculia* species, such as *Sterculia*

serigera, which grows in Senegal and Mali, and *Sterculia villosa*, which grows in Pakistan and India. India produces and exports more than half of all GK in the world, with the remainder coming from North Africa. The USA, France, and the United Kingdom are the three biggest importers of GK. GK is also known as ‘Indian tragacanth’, as it has similar properties to gum tragacanth and was initially introduced to replace the same. However, owing to the low cost and superior properties of GK, it has now become the second most used gum after GA¹¹.



Figure 5. Native gum karaya tree and its exudate⁴⁵.

2.5.2.1. Chemistry of gum karaya

GK is a complex branched polysaccharide that is hydrophilic, and anionic in nature. It is a substituted form of acetylated rhamnogalacturonoglycan that exists as calcium and magnesium salts. GK has a very high molecular weight ranging between 9×10^6 to 16×10^6 Da. GK is composed of 13-26% of galactose, 15-30% of rhamnose, 40% of glucuronic and galacturonic acids and ~1% of protein content. When compared to other exudate gums, GK has a greater rhamnose content. The backbone of GK is comprised of α -L-rhamnose and α -D-galacturonic acid moieties. The side chains are attached to galacturonic acid of the main chain via 1,3-linkage of β -D-glucuronic acid or 1,2-linkage of β -D-galactose²¹. GK also has high acetyl content of ~8%, which is the main reason behind its insolubility in water and its swelling behaviour.

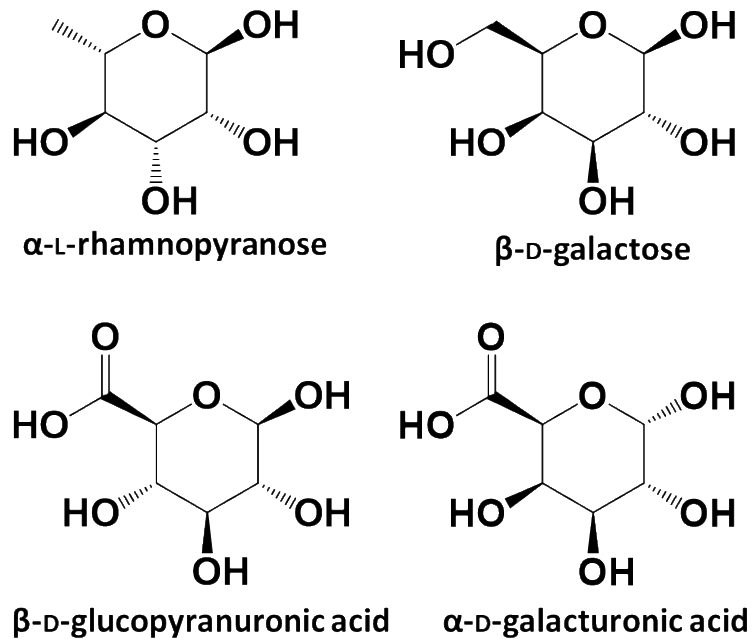


Figure 6. Sugar Constituents of gum karaya

2.5.2.2. Properties of gum karaya

GK has a slight acetic flavour, a fine dust appearance and colour ranging between white and brown depending on the impurity levels. GK exhibits one of the lowest solubilities among exudate gums. In cold water, native gum is only 10% soluble; however, in hot water, it is 30% soluble²⁶. In the presence of water, GK powder absorbs and swells up to 60-100 times its initial volume and forms a highly viscous dispersion. Previous studies have shown that alkali treatment using sodium hydroxide (NaOH), ammonium hydroxide (NH₄OH), potassium hydroxide (KOH), and lithium hydroxide (LiOH) increased the solubility of GK, indicating that GK deacetylation results in a soluble state, similar to other acetylated polysaccharides⁴⁶. Subsequently, the solubility of GK increased to up to 90% after deacetylation. As a result of its greater acid content, GK of Indian origin has a lower pH of 4.4-4.7 in water than its African counterpart with a pH of 4.7-5.2. Deacetylation occurs above pH 8, which causes viscosity to rise. GK possesses several distinctive characteristics, including high swelling, water retention, high acidic stability, and good viscosity.

The high acidic stability arises from the higher concentration of uronic acid moieties. Furthermore, GK is non-toxic and does not show any allergic, teratogenic or mutagenic effects.

2.5.3. Gum kondagogu

Gum kondagogu (KG) is another non-wood forest product obtained majorly from Indian forests. It is obtained from the exudates of *Cochlospermum gossypium* trees belonging to the Bixaceae family. These tree gum exudates are collected by the tribal people from the forests and are then marketed commercially. However, the Food and Agriculture Organization (FAO) classifies KG exudates as karaya gum since this gum does not have a distinct identity in the market and is commonly blended with karaya gum and marketed. Nevertheless, KG has many distinctive properties that separate it from karaya and are less expensive. Janaki and Sashidhar pioneered research into the physicochemical characteristics of KG and its potential as a novel food additive⁴⁷. In comparison to other well-known tree gums like gum arabic, gum tragacanth, and gum karaya, their research revealed that this gum has a unique identity. Furthermore, Vinod et al. conducted extensive qualitative and quantitative analysis to investigate the structural, physicochemical, morphological, rheological and compositional characteristics of this novel gum, which further validated its distinctive attributes⁴⁸⁻⁵².



Figure 7. Native gum kondagogu tree and its exudate⁵³.

2.5.3.1. Chemistry of gum kondagogu

KG is a complex anionic polysaccharide that belongs to a class of substituted rhamnogalactouronans type of gums based on its monosaccharide composition, due to the presence of a large number of rhamnose, uronic acids and galactose. The acidic sugar constituents of KG include D-glucuronic acids and α -D-galacturonic, β -D-galacturonic acids. The neutral sugar constituents include glucose, rhamnose, galactose and arabinose⁵⁴. This acidic gum has a high uronic acid content of 50-63% and remaining neutral sugar content⁴⁷. KG has an acetyl content of 12% and has a protein content of 5-6.3%, which was significantly higher than GK. Further, the tannin content and fibre content of KG is distinguishably different from GK validating its independent identity⁴⁷.

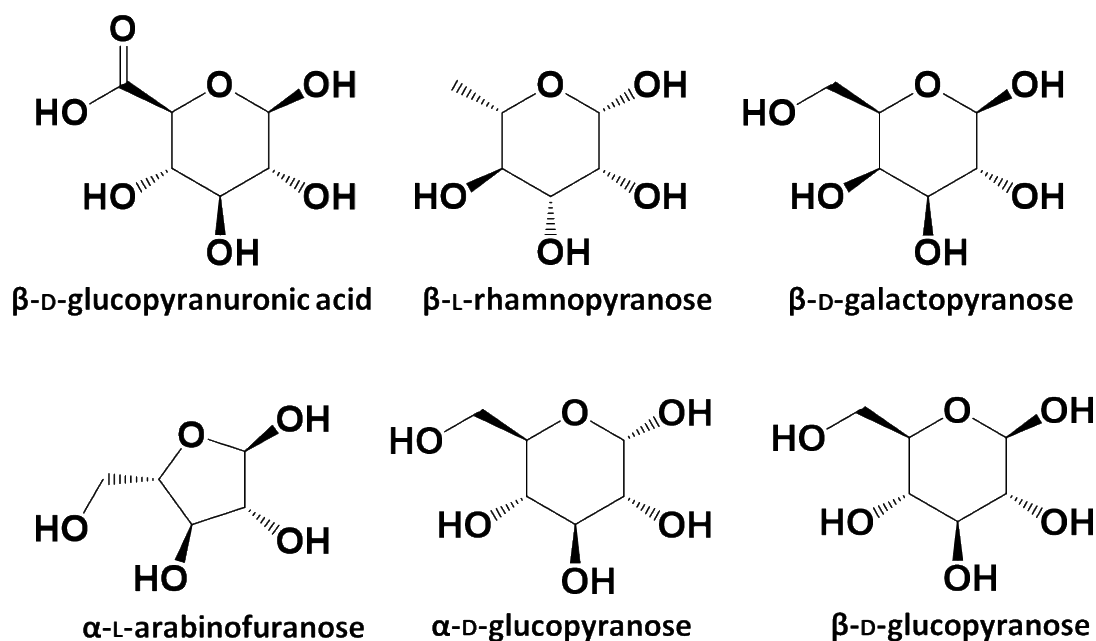


Figure 8. Sugar constituents of gum kondagogu

2.5.3.2. Properties of gum kondagogu

Despite being classified as the same material, there are considerable differences in the properties of both KG and GK. The physicochemical analysis revealed that gum kondagogu differs from gum karaya with respect to intrinsic viscosity, water-binding capacity, and pH⁴⁷. Similar to

GK, the solubility of KG is limited due to its high acetyl content and deacetylation results in an increase in the solubility. The presence of large acetyl groups, however, gives the gum good emulsifying capabilities. The molecule takes on an amphiphilic character wherein the acetyl groups are adsorbed on the oil surface, leaving the hydrophilic segments in the aqueous phase. Further, KG exhibits higher intrinsic viscosity than GK and other tree gums.

2.6. Common applications of tree gums

Exudate gums have been extensively used in food applications commercially. They have been utilized as food additives for decades owing to their distinctive properties. Additionally, they have also piqued interest in the production and stability of metal and metal oxide nanoparticles. Furthermore, gums have also been explored for several potential applications. Herein we briefly discuss the various applications of exudate gums.

2.6.1. Food additives

The unique characteristics of tree gums prompt their use in a wide array of applications. Gums have found extensive use in the food industry as an ingredient or an additive. The complex structure of these polysaccharides imparts specific characteristics which in turn gives rise to certain features like stabilization, emulsification, thickening, gelling, and moisture retention abilities. These characteristics determine their use in a variety of applications, including food, pharmaceuticals, and cosmetics. Gums like GA and GK have been provided with ‘Generally Recognized as Safe’ (GRAS) status and have been used as a food additive for decades⁵⁵⁻⁵⁸. Additionally, Physico-chemical and toxicological studies of KG have determined it to be a potential food additive^{47,59}.

GA is most commonly used in the production of encapsulated commodities including bioactive substances, oils and flavours, thereby improving their shelf life and rendering them suitable for dry mixes⁶⁰⁻⁶³. GA owing to its high-water solubility and low viscosity is used in baked

goods as an emulsifier, gloss enhancer and to allow flavour release⁶⁴. GA is used in confectionery items because of its ability to prevent sucrose crystallization and to emulsify fat components⁶⁵. It is also utilized in the production of sugar-free candies, which are soft and contain half as much sugar as hard candies^{66,67}. Because of its bulking ability without raising the product's calories, it is also employed in the manufacture of low-calorie dietary items^{11,68,69}. The emulsifying action of GA is put into use as a clouding agent and also in the stabilization of foams in beers and soft beverages^{70,71}.

GK has found its application in frozen dairy products as stabilizers. At 0.2-0.4% concentration GK improves the textural properties by regulating the ice crystal formation. This has been found to positively impact the mouth feel^{72,73}. It has been found to have a good stabilizing effect in low-acid beverages owing to its high acidic stability⁷³. GK is also used as a binding agent in bakery products and pasta and as an emulsifier in salad dressings⁷⁴. Due to GK's excellent water retention and binding abilities, it is also used in minced and ground meat products⁷³.

Extensive work has been done on KG to determine its physico-chemical, morphological, compositional, rheological and toxicological properties to evaluate KG as a food additive. These studies have concluded that KG could be a potential food additive with unique characteristics^{47-52,54}.

2.6.2. Green synthesis of nanoparticles

Recently, developing novel ecologically friendly methods to obtain nanomaterials has gained significant attention⁷⁵⁻⁷⁹. These processes conform to green chemistry principles and replace the harmful, hazardous chemicals with materials derived from natural origins^{80,81}. Tree gums owing to their renewability, non-toxicity and cost-effectiveness have been explored for the synthesis of nanoparticles⁸². A typical nanoparticle synthesis procedure involves the mixing of respective gum solutions with the metal salt solutions and heating them to a certain temperature.

Gums, in addition to serving as reducing agents, have also been shown to function as stabilizing agents, preventing nanoparticle aggregation⁸³. The presence of abundant functional groups (–OH, –C=O, –COO, and CH₃CO–) can assist in the reduction of metal salts into their respective nanoparticles. Further, these functional groups aid in the formation of complexes with the produced nanoparticles, preventing agglomeration and ensuring the long-term stability of the colloidal solutions. It has also been reported that the size and morphology of the nanoparticles may be controlled by controlling the synthesis parameters^{84,85}.

Table 1. Synthesis of various nanoparticles using exudate tree gums.

Gum	Nanoparticle	Size	Function	Ref
GA	Ag	~ 5 nm	Reducing and stabilizing agent	86
GA	Au	15-20 nm	Stabilizing agent	87
GA	Au	26.8±5.3 nm	Reducing and stabilizing agent	88
GA	Se	~34.9 nm	Stabilizing agent	89
GA	Pd	9.1±0.3 nm	Reducing and stabilizing agent	90
GA	Cu	19.6-35.1nm	Stabilizing agent	91
GA	MoO ₃	7-42 nm	Reducing agent	92
GK	Ag	2-4 nm	Reducing and stabilizing agent	93
GK	Au	8-22 nm	Reducing and stabilizing agent	94
GK	CuO	4.8±1.6 nm	Reducing agent	95
GK	Pt	~12 nm	Reducing and stabilizing agent	96
GK	Pd	~1.5 nm	Reducing and stabilizing agent	96
GK	nZVI	~20-100 nm	Stabilizing agent	97
KG	Ag	~3 nm	Reducing and stabilizing agent	98
KG	Au	12±2 nm	Reducing and stabilizing agent	99
KG	Pt	2.4±0.7 nm	Reducing and stabilizing agent	100

KG	TiO ₂	~ 11 nm	Reducing agent	101
KG	Fe	2-6 nm	Reducing and stabilizing agent	102
KG	Pd	6.5±2.3 nm	Reducing and stabilizing agent	103

2.6.3. Miscellaneous applications

Tree gums have been used in the fabrication of electrospun fibres. Electrospun fibres made from biopolymers offer a wide range of applications in biomedicine, including drug delivery, scaffolds, wound dressing, and tissue engineering. Tree gums have been explored in the production of electrospun fibres due to their non-toxicity, biocompatibility, biodegradability and low cost. Furthermore, the electrospinning process utilizes aqueous solvents making the process more sustainable. Despite these benefits, tree exudate gums are not electrospinnable on their own and are frequently blended with other biopolymers such as gelatin and chitosan, as well as synthetic biocompatible polymers such as poly(vinyl alcohol) (PVA)^{104–110}. These fibres are further used for various applications including environmental remediation, food packaging, tissue engineering and wound dressings.

In recent years, to broaden the horizons of applications of tree gums various strategies have been reported. These chemical modifications include grafting, interpenetrating polymer networks carboxymethylation, esterification, thiolation and crosslinking to improve the properties of the gums^{111,112}. Among these, the formation of 3D network structure via grafting, crosslinking and interpenetrating networks has shown great potential in biomedical and pharmaceutical fields. These gum polysaccharide-based 3D network hydrogels can store large amounts of water or biological fluids without deteriorating structurally^{111–115}.

Further, the gums have been used in the biosorption of environmental contaminants. Heavy metals such as Pb²⁺, Cd²⁺, Hg²⁺, Ni²⁺, U⁴⁺, Cr⁶⁺, and Cr³⁺ have been effectively removed from

wastewater using GK, KG and GA¹¹⁶⁻¹²⁰. The abundant functional groups found in gums such as hydroxyl (OH⁻), carboxyl (R-COO⁻), carbonyl (C=O), ether (C-O-C), acetyl (CH₃CO⁻), and aliphatic (CH⁻), interact with the metal ions and ensue effective biosorption. It was further observed that the gums interact with heavy metal ions via, physisorption, chemisorption, surface adsorption, ion exchange, and functional group exchanges to effectively bind the contaminants thereby enabling easy remediation¹¹⁶⁻¹²⁰.

2.7. Food packaging

Packaging is an integral part of the present modern world, which enables safe and easy transport of materials. Glass, metals, paper, and plastics have traditionally been the most utilized packaging materials. Among these, plastics remain a popular packaging material due to their low weight, transparency, and good performance-to-cost ratio. Since most consumer items purchased come with packaging, the use of plastic materials in packaging has grown exponentially in everyday life over the last three decades. The packaging industry represents one of the biggest sectors for the use of synthetic plastics worldwide. Food packaging is one of the fastest expanding segments in the packaging industry, as well as one of the largest consumers of synthetic plastics.

Food packaging has progressed in lockstep with an ever-changing lifestyle. In the older days, people used to eat food that was readily accessible in their immediate surroundings, and communities were self-sufficient in terms of their food demands. However, as time has passed and people's habits have changed, food transportation has become an essential aspect of the contemporary food system, which would not be conceivable without packaging. Following the industrial revolution, new production methods and materials were available. This enabled the development of various packaging techniques that deteriorated food degradation and extended their shelf life. Glass bottles fitted with corks and metal cans for food storage and transport were introduced. Plastic, on the other hand, was not widely used until the latter half of the twentieth

century, probably around World War II. Packaging began as a basic container for storing food, but it has since grown into a critical element for food quality preservation, acting as a barrier to oxygen, and moisture, while retaining flavour. Packaging's role has evolved throughout time to include not just ensuring food safety, but also being cost-effective for businesses and customers while having no detrimental effect on the environment. Recently, the negative environmental impact of food packaging materials has drawn considerable attention. These food packaging materials are referred to as single-use plastics since they are normally discarded once the product has been consumed. These single-use plastics contribute to the growing landfills, pollution and resulting greenhouse effects. Owing to these serious implications of conventional plastic packaging materials as well as their reliance on fossil fuel reserves, a great deal of research is focused on developing new packaging materials using biological alternatives.

2.7.1. Biobased food packaging

Customers' preferences have changed as a consequence of elevated environmental concerns and regulatory measures, prompting many industries and businesses to transition from synthetic conventional plastic packaging to sustainable alternatives that are ecologically friendly. Biobased packaging materials that are both biodegradable and naturally renewable are being investigated as a viable alternative to traditional plastics in single-use packaging applications. The considerable amount of research and development effort that is ongoing in the development of biobased and biodegradable packaging materials demonstrates that the packaging sector is heading in the direction of long-term sustainability. These naturally derived bioplastics are renewable and capable of degrading in bioactive environments like landfills either under the action of microorganisms via enzymatic catalytic processes or via non-enzymatic mechanisms such as chemical hydrolysis which results in the breakdown of polymer chains. Nowadays a lot of biodegradable plastics are available commercially, however, their biodegradability is under

scrutiny as they require specific conditions to breakdown that does not match the real conditions. As a result, compostable polymers, particularly those generated from renewable resources, are being encouraged and recognized as ecologically friendly packaging materials. The aim of these new bio-based packaging materials made from renewable resources is to increase shelf life and improve food quality while minimizing packaging waste. Despite the benefits, replacing traditional food packaging materials with biobased materials is still a daunting task. One of the primary issues is the durability of food packaging, which must be matched to the shelf life of the product. This implies that the packing material must be robust in terms of mechanical and barrier qualities, as well as perform well throughout storage and use. Further, the biodegradability of the bioplastics which might be beneficial in the composting of spoiled food can limit the use of packaging materials for short term applications. Thus, while developing biopackaging materials, biomaterial composition, microbial and water activity, storage temperature, and other factors that influence biodegradation and rate of biodegradation must be considered.

2.8. Packaging properties

To be an efficient packaging material, each packaging material must possess specific characteristics. Some of the most major characteristics to consider when developing biobased packaging materials include barrier properties, mechanical properties transparency, etc. These material characteristics aid in the protection of the encasing product, as well as influencing the product's shelf life.

2.8.1. Barrier properties

Barrier properties of the packaging material is an essential consideration when choosing food packaging systems. This corresponds to the ability of the material to prevent gases, water vapour, and aroma permeation through the packaging system. These are critical factors in the preservation of packaged food quality. Permeation of these gas phases through a packaging film

usually occurs via adsorption on the surface, diffusion through the material and desorption. Barrier properties are usually quantified in terms of transmission rates and permeability. Transmission rates correspond to the volume/weight of the permeant diffusing through the packaging film per unit surface area and time. While permeability considers the thickness of the film and is more reliable when comparing barrier properties of different materials. In addition to the nature of the material, the barrier properties are also influenced by temperature, pressure and relative humidity. Hence, barrier characteristics are often tested in a controlled setting under equilibrium moisture conditions^{121,122} and hygroscopic materials like biopolymers normally take a day or two to attain equilibrium. The oxygen and moisture barrier properties of the materials can be measured by numerous methods, however, the most standard one is using American Society for Testing and Materials (ASTM) standards with an analyzer from the MOCON company¹²¹⁻¹²³. In the literature, several SI units for barrier properties have been used, however, $\text{cm}^3 \cdot \mu\text{m} \cdot \text{m}^{-2} \cdot \text{day}^{-1} \cdot \text{bar}^{-1}$ for oxygen permeability and $\text{g} \cdot \mu\text{m} \cdot \text{m}^{-2} \cdot \text{day}^{-1} \cdot \text{bar}^{-1}$ for water vapour permeability are the most commonly used units as they are easily comprehensible. Depending on the type of food that has to be preserved, different moisture and oxygen transmission rates are required (Figure 9).

Many polysaccharides exhibit exceptional oxygen barrier properties owing to the hydrogen-bonded network structure between the polysaccharide chains resulting in very low free volume for the gas diffusion. As a matter of fact, biopolymers can replicate the oxygen permeability of a wide spectrum of conventional packaging materials based on synthetic plastics. However, humidity is a very critical parameter that influences the gas barrier properties of the biopolymers. Gas permeability through the film is known to increase with increasing humidity for both biopolymers and conventional plastics. Even plastics with high barrier characteristics, such as ethylvinyl alcohol and nylons, have reduced barrier properties when exposed to high levels of humidity¹²⁴⁻¹²⁶. The capacity to withstand humid environments is a fundamental hurdle in the

development of biobased packaging systems. Several strategies have been employed in this regard including, multilayer packaging, impermeable fillers, coatings etc¹²⁷⁻¹³⁰. When these biobased polymer systems are compared to petroleum-based polymer systems, it is clear that biobarriers can compete with conventional plastics in terms of water vapour transmission.

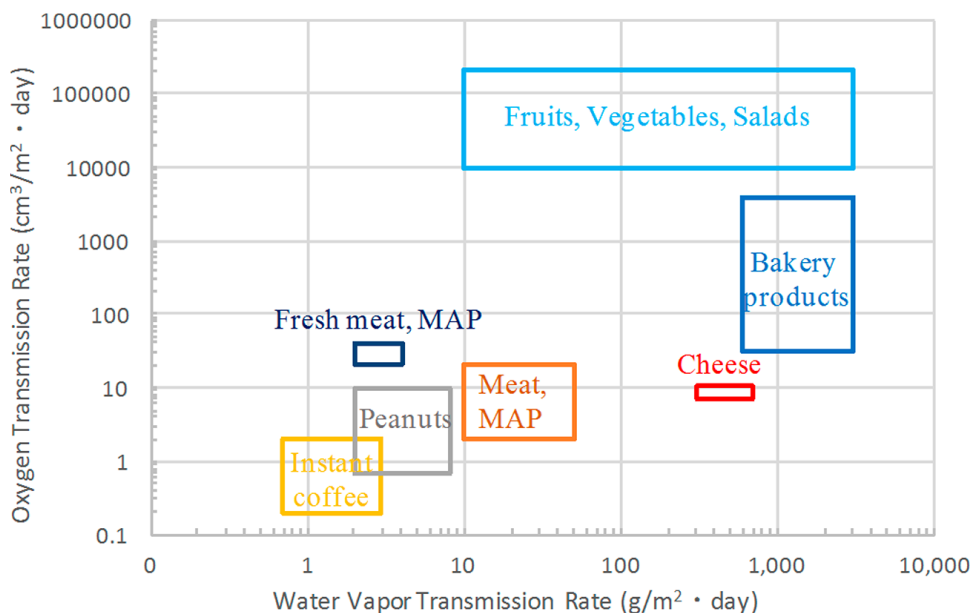


Figure 9. Barrier film packaging requirements for certain food products¹³¹.

2.8.2. Mechanical properties

As an effective packaging material, it must have acceptable mechanical properties to endure wear and tear throughout the packing, storage, and transportation of the goods. The mechanical characteristics of biopolymer films are studied primarily in terms of tensile strength, elongation at break, and Young's modulus. The flexibility and elasticity of films are determined by these characteristics, which is essential for the preservation of packaged foods. The mechanical properties requirements of the packing material vary depending on the sort of product it is encasing. Biopolymer packaging materials can be produced to have mechanical properties that are equivalent to those of petroleum sourced plastics. In terms of modulus and stiffness, biobased and petroleum-derived polymers have similar mechanical characteristics. Plasticizing, mixing with

other polymers or fillers, crosslinking, may all be used to further modify the modulus of biopolymer systems^{128,132–135}.

2.8.3. Other properties

Many packaging applications also require additional properties including transparency, antimicrobial activity and printability. Transparent packaging allows the customer to be able to see the product while also assuring them of its quality. Most polysaccharides are known to produce transparent films^{136–138}. However, the addition of components, coatings can significantly alter the transparency of the material. Antimicrobial packaging can effectively extend the shelf life of the product by protecting it against spoilage from microbial activity. The antimicrobial activity of packaging materials is influenced by barrier properties as well as oxygen and moisture scavengers, as the presence of oxygen and moisture inside the package can promote microbial activity and lead to quality loss^{139–143}. Incorporation of volatile antimicrobial substances, antimicrobial fillers/coatings, or the use of naturally antimicrobial polymers like chitosan are some of the other ways used to impart antimicrobial characteristics to biopackaging systems^{139–143}. Printability is also another parameter for consideration in packaging applications. This will enable the easy printing of information and be able to provide consumers with mandatory and optional information about the product¹⁴⁴.

2.8.4. Biodegradability

Another crucial characteristic that has recently been added to the list of packaging material requirements is biodegradability or compostability¹⁴⁵. A biodegradable plastic, according to the ASTM standards, is one that degrades due to naturally occurring microorganisms such as bacteria, algae, and fungi¹⁴⁶. The mechanism involved in biodegradation is the enzymatic activity of the microbes¹⁴⁷. A compostable plastic, on the other hand, degrades through biological processes to produce carbon dioxide, water, inorganic compounds, and biomass at a rate comparable to other

known compostable materials without leaving any hazardous byproducts¹⁴⁸. Thus, all compostable plastics are biodegradable, but not the other way around.

2.9. Tree gums in food packaging

Despite possessing a variety of unique characteristics such as biorenewability, biodegradability, nontoxicity, and low cost, tree gums have yet to be completely investigated in the food packaging industry. The reason for its limited usage in packaging applications can be due to its high hydrophilicity and low film-forming properties (Figure 10). Generally, tree gum films are fragile and brittle owing to the high intermolecular interactions like hydrogen bonding. To improve the mechanical characteristics of the material, a plasticizer should be added to minimize intermolecular interactions. Plasticizers like glycerol, sorbitol, polyethylene glycol are used as plasticizers with biopolymers to improve the flexibility and film-forming properties¹³⁵. However, the addition of these plasticizers can have a detrimental effect on the barrier properties of the films.

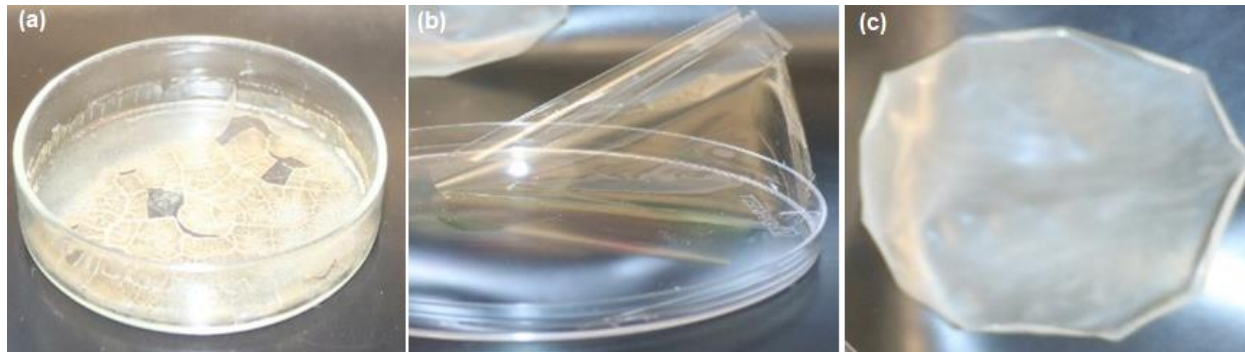


Figure 10. Brittle and fragile films of (a) gum arabic, (b) gum karaya and (c) gum kondagogu

Furthermore, the properties of the gum films can be enhanced via modifications and functionalization. These modifications and functionalization are often necessary to achieve molecular structures of interest depending on the final purpose of their use. Combining two or more biopolymers or combining with another component are some of the alternatives for polysaccharide modification to acquire more desirable features for usage in food packaging. It is

generally recognized that in order to provide the optimal packaging solution for specific food goods, a mix of more than two packaging materials is usually required.

Only a few studies have been published on the use of tree gums such as arabic, karaya, and kondagogu in food packaging. The reported articles are relatively recent and the majority are from our research group. Padil et al. prepared electrospun fibres based on arabic, karaya and kondagogu in combination with a water-soluble polymer like polyvinyl alcohol¹⁰⁶. These electrospun membranes, modified by methane plasma treatment demonstrated good stability and enhanced physicochemical properties with potential in food packaging applications¹⁰⁶. Further, the same group was involved in the development of electrospun membranes composed of karaya, polyvinyl alcohol, and incorporating silver nanoparticles¹⁴⁹. These membranes showed enhanced antibacterial properties toward a wide range of potentially pathogenic bacteria due to the presence of silver nanoparticles and demonstrated good potential for antibacterial packaging¹⁴⁹. Furthermore, they developed bioplastic fibres from gum arabic and PVA and treated them with ⁶⁰Co γ irradiation and methane plasma treatment¹⁰⁵. The treated membranes exhibited significant mechanical, thermal, and antibacterial properties, as well as good oxygen barrier properties, potent antioxidant activity, and promising biodegradability indicating that they could be used as an environmentally sustainable breathing food-packaging material for biodegradable bags¹⁰⁵. Cao et al., developed gum karaya films loaded with cloisite and cinnamaldehyde¹⁵⁰. The obtained films demonstrated good mechanical, barrier and antibacterial properties essentially rendering them suitable for biodegradable food packaging. Ramakrishnan et al. developed biomacromolecule assembly based on kondagogu and sodium alginate composites¹⁵¹. The obtained bicomponent films had improved mechanical attributes and hydrophobic nature with good barrier properties and biodegradability.

Building on these ideas, herein, we focus on the development of packaging films based on arabic, karaya and kondagogu gums by overcoming their limitations via various strategies. We develop numerous films with potential for food packaging applications by combining them with different 2D and 3D nanomaterials, chemical modifications, coating and blending with other biopolymers while retaining their inherent biodegradability. To ensure that these films were ideally suited for food packaging, their morphological, mechanical, thermal, barrier properties and biodegradability were analyzed.

2.10. Valorization of tree gum wastes in nanostructures synthesis

As mentioned earlier the lower grade gums cannot be used for food or pharmaceutical applications due to their highly acidic nature and presence of a large number of impurities. These lower grade gums possess no commercial value and are usually discarded. However, there are considerable benefits in using these lower grade gums as they still possess a carbon-rich structure with abundant functional groups and metal impurities that can be used to develop co-doped carbon nanostructures and the synthesis of other metal nanoparticles. These gum wastes possess multi-branched structures with enhanced physicochemical and mechanical properties, which can be adopted for various potential applications. Therefore, it is an enticing strategy to develop a facile and general synthetic process to utilize these gum wastes for functional use, rather than perpetually throwing the wastes in already overburdened disposal sites. To the best of my knowledge, there have been no reports of gum wastes being used to develop value-added products with advanced applications.

2.11. Objectives

Several objectives were defined based on the literature review, and the present thesis explores these in detail:

- 1) Development of mechanically stable, free-standing films by utilizing tree gum exudates with potential in food packaging.
- 2) Reduction in the hygroscopic nature of the tree gum polysaccharides via hydrophobic modifications.
- 3) Improving the barrier properties of the tree gum films to match their conventional counterparts via different strategies.
- 4) Development of completely biodegradable edible films utilizing tree gums.
- 5) Identifying viable strategies and techniques to utilize gum wastes for the development of value-added structures for advanced applications.

3. Results and discussion

3.1. Tree Gum–Graphene Oxide Nanocomposite Films as Gas Barriers

Abstract: To reduce the dependency on petro-based conventional plastics, research focusing on bioplastics derived from biological origin has gained precedence. Herein, we report an ecofriendly and a facile synthetic route to develop a freestanding nanocomposite film prepared from the combination of nonedible biodegradable tree gum waste and graphene oxide (GO). Three variants of bionanocomposite films such as GO–gum arabic (GA–GO), GO–gum karaya (GK–GO), and GO–kondagogu gum (KG–GO) were fabricated via solution casting of respective gums with GO (0.5% and 1.0%) in an aqueous environment. GO was thoroughly blended within different types of gum matrices via the hydrogen bond interaction and electrostatic attraction, thus forming interconnected homogeneous GO–gum layered structure. The addition of GO further transformed the brittle gum film into a freestanding film with substantial mechanical strength. Furthermore, the layered nanocomposite films demonstrated enhanced oxygen gas barrier property as well as reduced water vapor transmittance. The barrier properties are comparable to the plastics traditionally used in packaging, emphasizing the potential of tree gums nanocomposite films in packaging applications. Such frugally viable gums can be a cost-effective alternative in the development of nanocomposite films that could be readily used for applications in food packaging, pharmaceutical, and various biomedical industries.

Citation: **Abhilash Venkateshaiah**, Jun Young Cheong, Christoph Habel, Stanislaw Waclawek, Tomáš Lederer, Miroslav Černík, Il-Doo Kim, Vinod V. T. Padil, and Seema Agarwal, “**Tree Gum–Graphene Oxide Nanocomposite Films as Gas Barriers.**” *ACS Applied Nano Materials* 3 (1): 633–40 [2020]

Tree Gum–Graphene Oxide Nanocomposite Films as Gas Barriers

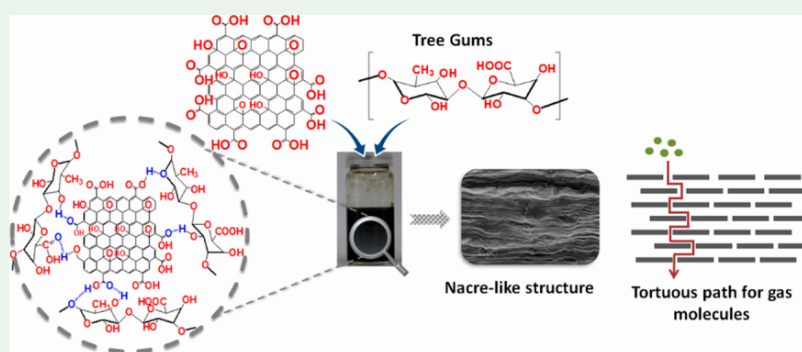
Abhilash Venkateshaiah,[†] Jun Young Cheong,[‡] Christoph Habel,[‡] Stanislaw Wacławek,[†] Tomáš Lederer,[†] Miroslav Černík,[†] Il-Doo Kim,[‡] Vinod V. T. Padil,^{*,†} and Seema Agarwal^{*,§}

[†]Department of Nanomaterials in Natural Sciences, Institute for Nanomaterials, Advanced Technologies and Innovation (CXI), Technical University of Liberec (TUL), Studentská 1402/2, Liberec 1, Czech Republic 461 17

[‡]Department of Materials Science and Engineering, Korea Advanced Institute of Science and Technology (KAIST), 291 Daehak-ro, Yuseong-gu, Daejeon 34141, Republic of Korea

[‡]Department of Chemistry and [§]Macromolecular Chemistry II, Bavarian Polymer Institute, University of Bayreuth, Universitätsstraße 30, 95447 Bayreuth, Germany

Supporting Information



ABSTRACT: To reduce the dependency on petro-based conventional plastics, research focusing on bioplastics derived from biological origin has gained precedence. Herein, we report an ecofriendly and a facile synthetic route to develop a freestanding nanocomposite film prepared from the combination of nonedible biodegradable tree gum waste and graphene oxide (GO). Three variants of bionanocomposite films such as GO–gum arabic (GA–GO), GO–gum karaya (GK–GO), and GO–kondagogu gum (KG–GO) were fabricated via solution casting of respective gums with GO (0.5% and 1.0%) in an aqueous environment. GO was thoroughly blended within different types of gum matrices via the hydrogen bond interaction and electrostatic attraction, thus forming interconnected homogeneous GO–gum layered structure. Morphological analysis revealed a natural nacre-like structure comprised of gum-intercalated graphene sheets, which was further confirmed by X-ray diffraction studies. The addition of GO further transformed the brittle gum film into a freestanding film with substantial mechanical strength. Furthermore, the layered nanocomposite films demonstrated enhanced oxygen gas barrier property as well as reduced water vapor transmittance. The barrier properties are comparable to the plastics traditionally used in packaging, emphasizing the potential of tree gums nanocomposite films in packaging applications. Such frugally viable gums can be a cost-effective alternative in the development of nanocomposite films that could be readily used for applications in food packaging, pharmaceutical, and various biomedical industries.

KEYWORDS: gums, graphene oxide, biodegradable, freestanding, food and biomedical packaging

INTRODUCTION

Development of bioplastic and biodegradable films, which will replace plastic derived from petroleum products, is key research focusing on greener stratagems.^{1–3} The major essential functionalities for biodegradable packing materials rely on their light weight, structural attributes, and high thermal, mechanical, and gas barrier properties besides degradability in compost or landfills.^{4–8} Current plastic packages are predominantly polyolefins (polypropylene (PP) and polyethylene (PE)) and aromatic polyesters (poly(ethylene terephthalate) (PET)) which are not biodegradable. Raising environmental safety concerns has brought these

conventional polymers under scrutiny due to their presence as microplastics in the environment and nonparticipation in the closed circular economy while causing greenhouse effects and depleting natural fossil fuels.^{1,9,10}

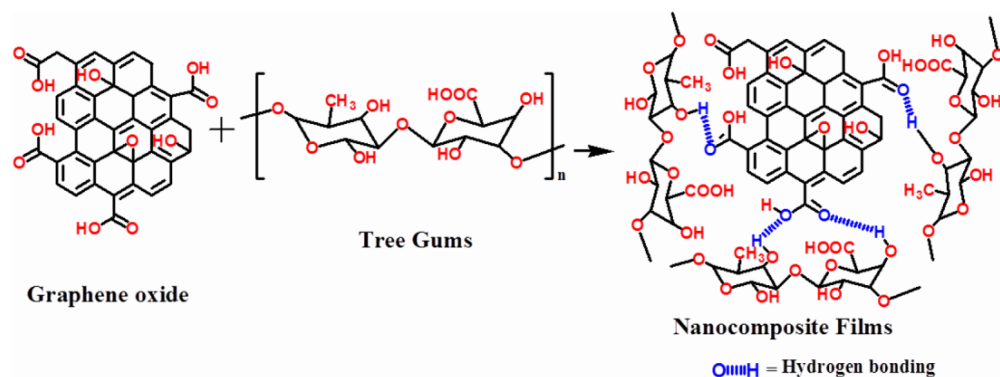
Biobased and biodegradable polymers could be an important addition to the packaging sector that generates a major portion of the total plastic waste. The probable candidates are aliphatic polyesters (poly(lactic acid) (PLA)^{11,12} and polyhydroxy-

Received: November 4, 2019

Accepted: December 18, 2019

Published: December 18, 2019

Scheme 1. Schematic Illustration for the Preparation of Tree Gum–Graphene Oxide Nanocomposites



alkanoates (PHA)^{13,14} extracted/prepared from various biomass sources. However, because of the high cost and processing difficulties, they are not able to fulfill the global huge demand for bioplastic in food packaging and other applications. Moreover, their degradability under environmental conditions in a reasonable time frame is under dispute. Therefore, more and more attention is being given to the bioplastics from natural biopolymers (cellulose, chitosan, and starch)^{15–19}

Gums are natural hydrocolloids with applications in food, pharmaceutical, environmental, tissue engineering, drug carrier, and biomedical fields.^{20–23} The nontoxicity, biodegradability, availability, and physicochemical properties make gums suitable biobased materials for food packaging applications. However, the use of pristine gums alone in food-packaging applications is restricted due to their hydrophilicity, lack of film-forming ability, brittleness/low flexibility, and low tensile properties. A facile way to fabricate flexible, biodegradable gum-based film with high barrier properties would be a great solution to the existing predicament.

Here, we present a successful fabrication of freestanding natural gum–graphene oxide nacre-like hybrid films via solution casting of biodegradable gums with graphene oxide (GO) nanosheets in an aqueous medium (Scheme 1). GO with its abundant surface functional groups coupled with nontoxic, biocompatibility, and exceptional mechanical and chemical stability is an ideal filler.^{24,25} Different driving forces (hydrogen bonding, electrostatic interaction, stacking, van der Waals interaction, and coordination) propel the homogeneous mixing between tree gums and GO.^{26–29} Three different gums [gum Arabic (GA), gum Karaya (GK), and Kondagogu gum (KG)] were combined with GO to form homogeneous dispersion, resulting in uniform, freestanding gum–GO hybrid film. Such gum–GO hybrid film exhibits excellent oxygen barrier as well as reduced water vapor permeability. This is an initial report on utilizing GO together with tree gums to fabricate an efficient film, which can also be extended to other kinds of gums and natural resources. This work builds up a milestone in combining GO together with tree gum to fabricate a malleable and environmentally friendly biodegradable film out of tree exudate-based polysaccharides.

EXPERIMENTAL SECTION

Materials. Nonedible grades of GA, GK, and KG were procured from the Grijian Cooperative Society, Hyderabad, India. The preparation and molecular characterization of GA, GK, and KG were reported earlier.³⁰ Graphite powder ($\leq 20 \mu\text{m}$, 99.99%), KMnO_4 ,

NaNO_3 , H_2SO_4 , HCl , glycerol, and other analytical-grade chemicals were procured from Sigma-Aldrich.

Fabrication of GO–GA, GO–GK, and GO–KG Composite Films. GO was prepared by using the modified Hummer's method.³¹ Briefly, the prepared GO with its characterization such as Raman spectroscopy, FTIR, HR-TEM, and XRD are presented in Figure S1 (Supporting Information). To prepare GA–GO, GK–GO, and KG–GO hybrid films by the solution casting method, GO was dispersed in deionized water and sonicated for 30 min. 1.0% w/v each of the GA, GK, and KG and 1% of glycerol were dispersed into various GO (0.5% and 1.0% w/v) loading (details are in Table S1). The individual mixtures of GA–GO, GK–GO, and KG–GO were stirred continuously and later sonicated (10 min) to obtain a homogeneous mixture. Then, the as-prepared nanocomposite solutions were immediately cast onto substrates and then kept at room temperature for drying. The dried GA–GO, GK–GO, and KG–GO composites films were obtained and used for further characterization and analysis.

RESULTS AND DISCUSSION

Fabrication of Gum–GO Films. Gum–GO hybrid films were fabricated by mixing GO (0.5% and 1.0% w/v each) with different kinds of tree gums (each gum 1.0% w/v). Prior to mixing, the GO was sonicated to completely exfoliate the GO nanosheets. The interaction between the functional groups of GO and gum ensures uniform dispersion of GO (Figure 1a). The resultant gum–GO hybrid film (Figure 1b–d) demonstrates flexibility and freestanding characteristics. The initial characterization of GO is presented in Figure S1. Gums are natural water-soluble hydrocolloids of proteins and poly-

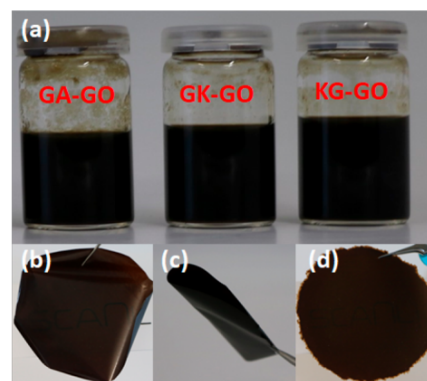


Figure 1. (a) Digital camera images of homogeneous GA–GO, GK–GO, and KG–GO mixture used for making composite films. Flexible freestanding hybrid films based on gum–GO: (b) GA–GO, (c) GK–GO, and (d) KG–GO.

saccharides. Usually, pristine gums do not have good film-forming properties (Figure S2), but the addition of GO could enhance the formation of mechanically stable and flexible films (Figure 1b–d).

SEM and TEM Characterization of Films. SEM images of GO and pristine gums are presented in Figures S1f and S3, respectively. The SEM images of all gums indicate highly lopsided structures, and SEM images of GO reveal a wrinkled surface of the graphene sheet. Based on the cross-sectional SEM images, it was observed that the introduction of GO ensued highly ordered structures (Figure 2a–c). This is a

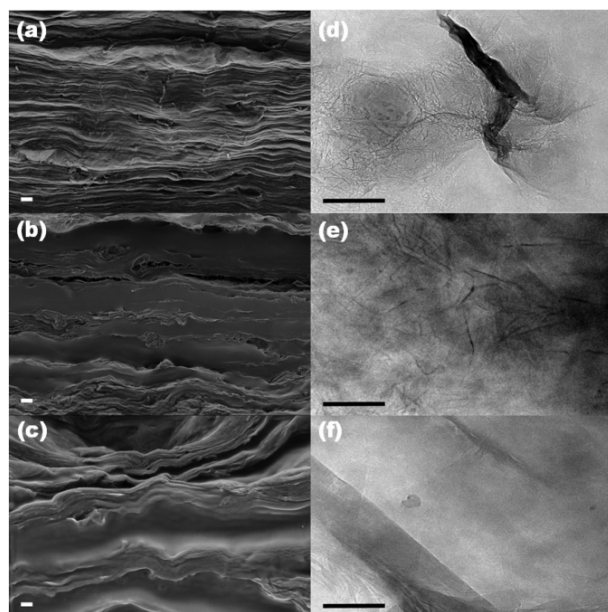


Figure 2. Cross-sectional SEM images of (a) GA-GO, (b) GK-GO, and (c) KG-GO hybrid film. TEM images of (d) GA-GO, (e) GK-GO, and (f) KG-GO hybrid film. The scale bar of SEM images in (a), (b), and (c) is 1.0 μm . The scale bar of TEM images in (d), (e), and (f) is 200 nm.

result of the two-dimensional orientation of the GO and gums upon drying. The cross-sectional SEM images of gum-GO indicate a highly rough morphology with dense parallel stacking, which is attributed to polysaccharide chains intercalation into GO nanosheets. The nacre-like gum-GO hybrid films showed well-arranged structure, comparable to the brick and mortar structure of natural nacre and nacre-like composites.^{32–34} Furthermore, TEM analysis of GA-GO, GK-GO, and KG-GO hybrid films (Figure 2d–f) suggests the clear presence of GO, which is partially exfoliated into individual layer structures within gum matrices. Both TEM and SEM analysis of gum-GO hybrid films indicate that the channels and surface roughness are present which might be generated by the interaction between GO (Figure S4; TEM images of GO) and gums. These observations are similar to the other natural polymers such as chitosan,³⁵ sodium alginate,³⁶ and lignin/starch³⁷ interaction with GO.

XRD Analysis. XRD analysis was further used to understand how the incorporation of GO into various kinds of gums resulted in changes in crystal structures. X-ray diffraction patterns of gums (GA, GK, and KG), GO, and gum-GO hybrid films with GO (1.0% w/v) are presented in Figure 3.

The XRD spectra of the gums suggest that the gums are amorphous in nature with no obvious diffraction peaks.^{38,39} The peak at $2\theta = 10.06^\circ$ corresponds to the (002) crystal plane in the GO spectrum. The interlayer spacing calculated by using Bragg's equation was found to be 0.88 nm.⁴⁰ In the case of gums-GO nanocomposite films, the characteristic GO peak shifted to $2\theta = 6.3^\circ$, 6.5° , and 5.17° for GA-GO, GK-GO, and KG-GO, respectively. The interlayer spacing of these nanocomposite films was calculated to be 1.40, 1.35, and 1.70 nm for GA/GO, KG/GO, and GK/GO, respectively. The increased interlayer spacing is due to the intercalation of polymeric chains into the GO galleries.⁴⁰ This is in correlation with the observations made by SEM images. These results suggest that the GO was completely exfoliated with a uniform distribution within the biopolymer matrix.

FTIR Interpretation. To probe into the chemical structure of GO, gums, and GO-gum hybrid film, the characteristic FTIR peaks present in native gums (GA, GK, and KG), GO and gum-GO films are analyzed and presented in Figure 4a. FTIR spectra of GO reveal peaks for -OH, C=O, and C-O stretching as mentioned in previous literature.⁴¹ The spectra of gums (GA, GK, and KG) reveal peaks at 3345 cm^{-1} , which are assigned to -OH stretching of carbohydrates; the peak at 2938 cm^{-1} is assigned to the C-H stretching mode of CH_2 groups. The peaks at 1720 and 1600 cm^{-1} can be assigned to the C=O stretching vibrations from the free carboxylic acids and glucuronic acid esters of the gums.³⁰ The peaks at 1241 cm^{-1} are indicative of $-\text{CH}_3\text{CO}$ groups, and peaks at 1371 cm^{-1} can be assigned to the $-\text{COO}-$ groups.⁴² The peak at 1033 cm^{-1} corresponds to the stretching vibration of C-O-C groups. The FT-IR spectra of the nanocomposite films retain all the above-mentioned peaks; however, the intensity of the peak in the range $3000\text{--}3600\text{ cm}^{-1}$ increased, which could be due to the increase in the oxygenated functional groups. In addition, broadness in this range suggests the probable hydrogen bonding between the components in the film.

Raman Spectra of GO and Gum-GO Films. The Raman spectra of GO and gum-GO (GA-GO, GK-GO, and KG-GO) nanocomposite films are depicted in Figure 4b. The intensity ratio I_D/I_G of D and G bands at 1341 and 1582 cm^{-1} for GO was found to be 0.96.⁴³ The D and G bands of GO were consistent in the Raman spectra of all the gum-GO nanocomposite films. The presence of these bands in the film spectra suggests the existence of GO in the gum matrix. Furthermore, negligible changes were observed in the GK-GO and KG-GO film spectra when compared with GO spectra. However, an additional significant peak at 2908 cm^{-1} was present in the case of GA-GO films. This can be due to the C-H vibrations from polysaccharides of gum.^{44,45} The sugar ring in gums ((C-O-C)) produced two peaks centered at around 850 and 940 cm^{-1} . The fluorescence from GO might have masked the other peaks and could not be observed in gum-GO hybrid films. Additionally, the I_D/I_G ratio of the GA-GO films was found to have increased to 1.11 from 0.96; this can be due to certain reduction of GO sheets into RGO sheets in the GA-GO films and can be attributed to a certain degree of restoration of sp^2 -hybridized carbon.⁴⁶

Thermal and Mechanical Properties of Films. Furthermore, the thermal and mechanical properties of the bioplastic nanocomposite films were studied. Thermal properties of the hybrid film play a pivotal role in deciding the end-use applications. To access the thermal stability of gum-GO nanocomposite films, GO, and native gums (GA, GK, and

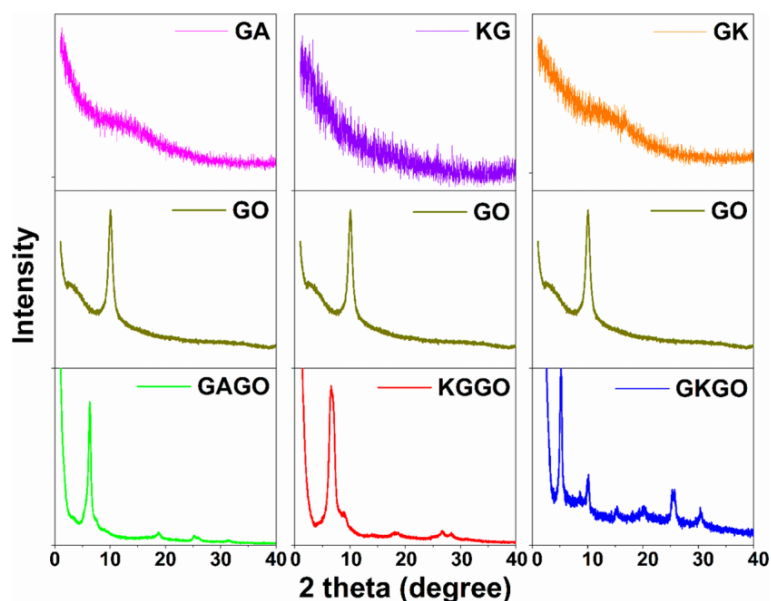


Figure 3. Comparison of XRD patterns of gum, GO, and gum–GO hybrid films.

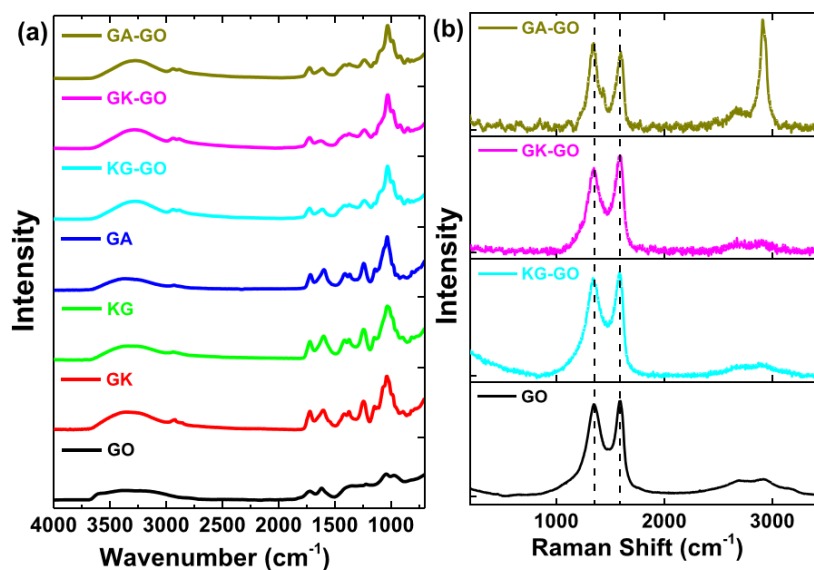


Figure 4. (a) FTIR spectra of gum–GO hybrid films and respective components. (b) Raman spectra of GO and gum–GO films.

KG), thermogravimetric analysis (TGA) was carried out. The resulting TGA and DTG curves are depicted in Figure 5a–d. GO undergoes multistep degradation, where it loses 12% of its initial weight up to 150 °C due to the loss of adsorbed water molecules. However, GO undergoes a drastic weight loss of up to 55% at around 200–250 °C due to the loss of oxygen functionalities. The TGA curves of the gums (GA, GK, and KG) are similar to that of GO and undergoes multistep degradation. The initial weight loss (<120 °C) was ascribed to the evaporation of moisture in the gums, and second weight loss (>250 °C) was due to the degradation of gums. The gum–GO nanocomposite films, however, show a weight loss at temperatures of 200 °C due to the removal of plasticizer (i.e., glycerol) and show higher thermal stability than GO without any rapid weight loss. This can be attributed to the hydrogen bonding between the GO and the gums (GA, GK, and KG),

which led to a decrease in the free –OH groups and stabilized the matrix. This suggests that there is a uniform mixing of the components in the film. The GA–GO hybrid film shows a synergistic effect and displays slightly increased thermal stability than the gum and GO alone, but the thermal stability of other gums lies in between that of GO and the pure gums. The thermal stability of the gum–GO hybrid films was tested again after a storage period of 3 months to determine any changes in the thermal properties upon storage. The results were very similar to the ones taken initially, suggesting that negligible changes to thermal stability over the storage period (more than 3 months) of these films.

Mechanical properties such as Young's modulus (E , MPa), tensile strength (σ , MPa), and elongation at break (ϵ , %) were assessed for gum–GO composite films. The mechanical properties of GO incorporated (0.5% and 1.0% w/v) into

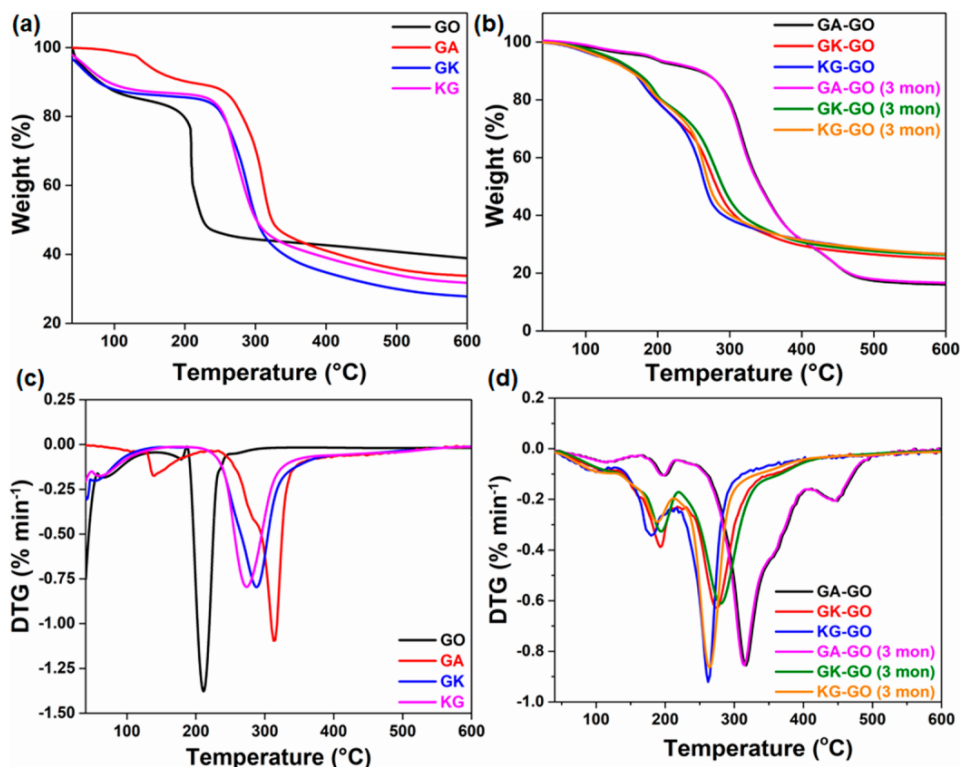


Figure 5. TGA curves of (a) GO, GA, GK, and KG. (b) Gum–GO nanocomposite films as-synthesized and after 3 months storage period. DTG curves (c) GO, GA, GK, and KG. (d) Gum–GO nanocomposite films as-synthesized and after 3 months storage period.

GA, GK, and KG polymers and their corresponding films (GA–GO, GK–GO, and KG–GO hybrid film) are presented in Table S2 and Figure 6, respectively. Pristine gums form

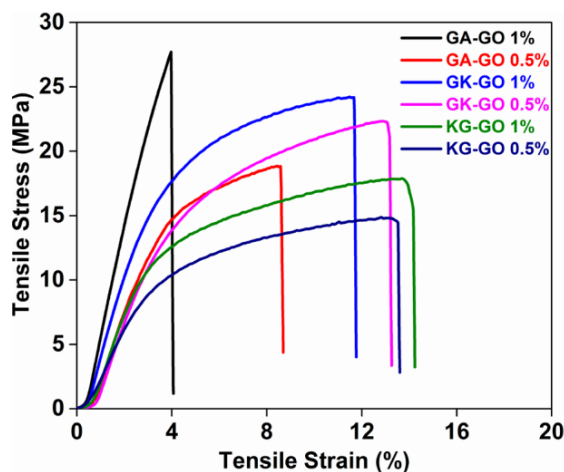


Figure 6. Stress–strain curve of the gum–GO hybrid film with different concentrations of GO incorporated (0.5 and 1.0 wt %).

highly brittle films, and hence their mechanical properties could not be evaluated. From Figure 6, we can observe that there is a linear increase in stress with strain at the beginning, and a nonlinear behavior is seen before attaining the maximum stress. It is clear from the data obtained that Young’s modulus and tensile strength increase with the increase in GO content. The highest increase was observed for GA–GO nano-

composite films with a 68% and 47% increase in E and σ , respectively. This could be due to the strong interaction of GO and GA matrix and the resulting highly ordered nacre-like structure observed in GA–GO films as shown in SEM analysis (Figure 2). This enhancement of mechanical properties (Young’s modulus and tensile strength) were due to the high dispersion, highly ordered structure, and interfacial interactions between the gums matrices and exfoliated GO nanolayers. The improved mechanical properties via the addition of GO have been observed in other natural polymers such as starch,⁴⁷ alginate,³⁶ poly(lactic acid),⁴¹ carboxymethyl cellulose,⁴⁸ and lignin/starch biocomposite.³⁷ However, the elongation at break (ϵ) does not follow the same trend as E and σ . From the results obtained, it was observed that the increase in GO content resulted in a decrease in ϵ values. GA–GO films showed the least elongation with only 8.5% and 3.9% elongation for 0.5% and 1% GO loading, respectively.

OTR, WVTR, Water Stability, and Biodegradability of Films. Efficient packaging material should possess superior barrier properties, as these dictate the shelf life of the products. Biopolymers, in general, are highly hydrophilic in nature and thus exhibit poor barrier performance because of the swelling of biopolymers at high humidity conditions. However, upon blending with layered nanomaterials like clay and GO, the barrier performance of the biopolymers expected to improve.⁴⁹ To determine the barrier performance of gum–GO nanocomposite films, oxygen transmission rate (OTR) studies were performed at a relative humidity (RH) of 65% and a temperature of 23 °C. The obtained results for all the gums are depicted in Figure 7a. We have chosen 65% RH as a standard for food packaging, as per the ISO 14663-2 method. GO is known to enhance the barrier properties in the films.

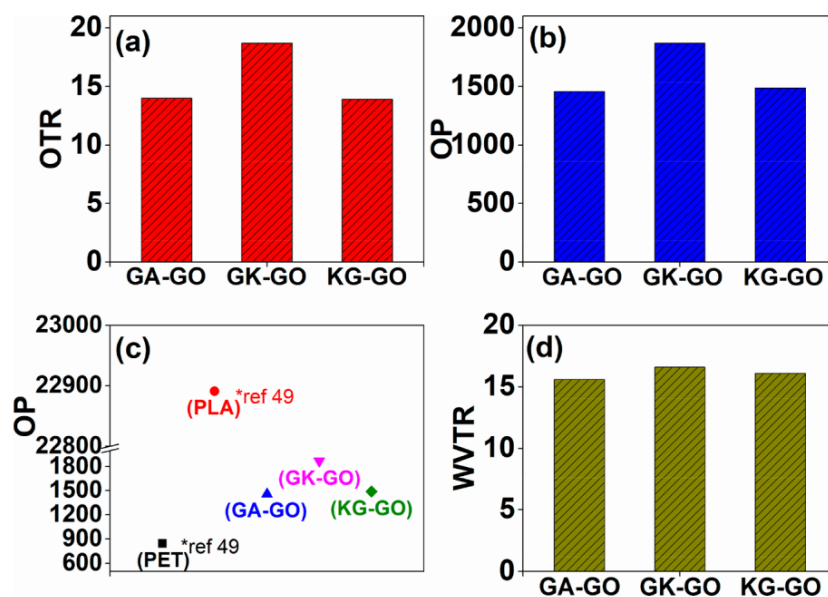


Figure 7. Graphs showing the barrier properties of different films: (a) OTR ($\text{cm}^3 \text{m}^{-2} \text{day}^{-1} \text{atm}^{-1}$), (b) OP ($\text{cm}^3 \mu\text{m m}^{-2} \text{day}^{-1} \text{atm}^{-1}$), (c) OP comparison with PLA and PET, and (d) WVTR ($\text{g m}^{-2} \text{day}^{-1}$).

The layered structure of the GO, when embedded in the polymer matrix, creates a tortuous path for the gases to diffuse through the film, thereby reducing the permeability. The OTR values of GA-GO, GK-GO, and KG-GO films were found to be 14.0, 18.7, and 13.9 $\text{cm}^3 \text{m}^{-2} \text{day}^{-1} \text{atm}^{-1}$. For a better comparison of these results, the transmission rates are converted into permeability values. The obtained oxygen permeability (OP) values were found to be 1456, 1870, and 1487 $\text{cm}^3 \mu\text{m m}^{-2} \text{day}^{-1} \text{atm}^{-1}$, respectively (Figure 7b). Our results are comparable with OP values of poly(ethylene terephthalate) (PET) films and less than poly(lactic acid) (PLA) films (Figure 7c), which indicates the suitability of GA-GO, GK-GO, and KG-GO films for food packaging application.^{49,50} The presence of GO ensures low oxygen permeation even in high humidity conditions (Figure 7b); this can be attributed to the decreased affinity for moisture as observed by the moisture absorption values. Biobased materials such as pectin, starch, chitosan, xylan, and lignin with layered nanofillers such as GO and clay have shown higher OP values compared to pristine samples.^{51,52} In addition, the water vapor transmission rate (WVTR) of the gum-GO composite films (GA-GO, GK-GO, and KG-GO) were analyzed. All the films showed approximately similar WVTR values with 15.6, 16.6, and 16.1 $\text{g m}^{-2} \text{day}^{-1}$ for GA-GO, GK-GO, and KG-GO respectively (Figure 7d). The presence of GO in small amounts (~ 1 wt %) in nanocomposites with gums increased the film stability in water. The nanocomposite films maintained their form in water for ~ 24 h at room temperature, if not stirred. Also, they showed ~ 16 – 21 wt % (Table S3) water absorption at 100 °C in 24 h in comparison to the pristine gums.

The preliminary results regarding the degree of aerobic biodegradability of gum-GO nanocomposite films in aqueous environment are obtained by measuring the oxygen demand in a closed respirometer. The nanocomposite films are exposed in an aqueous medium under laboratory conditions to an inoculum from activated sludge and oxygen demand was measured. The ongoing studies showed gum-GO nano-

composites to be biodegradable although with a slow degradation rate. The nanocomposite gum films with 1 wt % GO demonstrated a biodegradability of $\sim 29\%$ (Table S4) over a period of 672 h, and the process appears to continue further (Figure S5). A detailed biodegradation and biocompatibility study with focus on effect of the type of the gum and the amount of GO in different environments is under progress. Also, for improving their mechanical stability in water under stirring and rough handling conditions, further research is required using different cross-linkers.

CONCLUSION

Gum-GO-based hybrid films for enhanced thermal, mechanical, and barrier characteristics were fabricated. The high dispersibility of GO with gums assisted in the development of hybrid films with ordered structure and morphology that was similar to natural nacre and nacre-like composites as evidenced by SEM and TEM analyses. Intercalation of GO by gums was observed in SEM, which was further confirmed by XRD. The interaction of functional groups and hydrogen bonding between GO and gums was evidenced by ATR-FTIR. The thermal stability of the gum-GO films was found to be stable even after a storage period of 3 months. The enhancement of mechanical properties was ascribed to the dispersion and interfacial interactions between the gums and exfoliated GO nanolayers. The barrier properties are comparable with values of poly(ethylene terephthalate) (PET) films and much better than poly(lactic acid) (PLA) films, which indicates the suitability of GA-GO, GK-GO, and KG-GO films for food packaging applications.

ASSOCIATED CONTENT

Supporting Information

The Supporting Information is available free of charge at <https://pubs.acs.org/doi/10.1021/acsanm.9b02166>.

Figure S1: UV-vis spectra of GO showing a typical peak at 230 nm; (b) Raman spectra of GO with peaks corresponding to D band (1341 cm^{-1}) and G band

(1582 cm^{-1}); (c) FTIR spectra of GO with peaks at 3380 cm^{-1} ($-\text{OH}$ stretching), 1724 and 1619 cm^{-1} ($\text{C}=\text{O}$ stretching of carboxylic and/or carbonyl moiety functional groups), 1222 and 1041 cm^{-1} ($\text{C}-\text{O}$ stretching of epoxy and alkoxy groups); (d) TGA profile of GO; (e) XRD spectra of GO; (f) SEM image of GO with wrinkled surface of a graphene sheet and wormlike structure randomly aggregated; Figure S2: brittle gum films of (a) gum arabic, (b) gum karaya, and (c) gum kondagogu; Figure S3: SEM images of (a) GA, (b) GK, and (c) KG; Figure S4: TEM images of GO at different magnifications; Figure S5: representative biological oxygen demand of the nanocomposite films; Table S1: summary of mechanical properties of different films; Table S2: summary of the composition of different films; Table S3: moisture content of different films; Table S4: biodegradation analysis of nanocomposite films (PDF)

AUTHOR INFORMATION

Corresponding Authors

*E-mail: vinod.padil@tul.cz (V.V.T.P.).

*E-mail: agarwal@uni-bayreuth.de (S.A.).

ORCID

Stanislaw Waclawek: 0000-0002-8430-8269

Il-Doo Kim: 0000-0002-9970-2218

Vinod V. T. Padil: 0000-0002-0816-526X

Seema Agarwal: 0000-0002-3174-3152

Notes

The authors declare no competing financial interest.

ACKNOWLEDGMENTS

This work was supported by the project “Tree Gum Polymers and their Modified Bioplastics for Food Packaging Application” granted by Bavarian-Czech-Academic-Agency (BTHA) (registration numbers LTAB19007 and BTHA-JC-2019-26) and SFB 1357/C02 funded by Deutsche Forschungsgemeinschaft (DFG). The authors from Czech also acknowledge the assistance provided by the Research Infrastructures Nano-EnviCz (Project No. LM2015073), Pro NanoEnviCz (Project No. CZ.02.1.01/0.0/0.0/16_013/0001821), and Project Hybrid Materials for Hierarchical Structures (HyHi, Reg. No. CZ.02.1.01/0.0/0.0/16_019/0000843), supported by the Ministry of Education, Youth and Sports of the Czech Republic and European Union–European Structural and Investment Funds in the frames of Operational Program Research, Development and Education.

REFERENCES

- (1) Lambert, S.; Wagner, M. Environmental Performance of Bio-Based and Biodegradable Plastics: The Road Ahead. *Chem. Soc. Rev.* **2017**, *46* (22), 6855–6871.
- (2) Stürzel, M.; Mihan, S.; Mülhaupt, R. From Multisite Polymerization Catalysis to Sustainable Materials and All-Polyolefin Composites. *Chem. Rev.* **2016**, *116* (3), 1398–1433.
- (3) White, A. A.; Platz, M. S.; Aruguete, D. M.; Jones, S. L.; Madsen, L. D.; Wesson, R. D. The National Science Foundation's Investment in Sustainable Chemistry, Engineering, and Materials. *ACS Sustainable Chem. Eng.* **2013**, *1* (8), 871–877.
- (4) Siracusa, V.; Rocculi, P.; Romani, S.; Rosa, M. D. Biodegradable Polymers for Food Packaging: A Review. *Trends Food Sci. Technol.* **2008**, *19*, 634–643.
- (5) Pillai, C. K. S. Recent Advances in Biodegradable Polymeric Materials. *Mater. Sci. Technol.* **2014**, *30* (5), 558–566.

- (6) Dai, L.; Long, Z.; Chen, J.; An, X.; Cheng, D.; Khan, A.; Ni, Y. Robust Guar Gum/Cellulose Nanofibrils Multilayer Films with Good Barrier Properties. *ACS Appl. Mater. Interfaces* **2017**, *9* (6), 5477–5485.

- (7) Chowdhury, R. A.; Nuruddin, M.; Clarkson, C.; Montes, F.; Howarter, J.; Youngblood, J. P. Cellulose Nanocrystal (CNC) Coatings with Controlled Anisotropy as High-Performance Gas Barrier Films. *ACS Appl. Mater. Interfaces* **2019**, *11* (1), 1376–1383.

- (8) Österberg, M.; Vartiainen, J.; Lucenius, J.; Hippi, U.; Seppälä, J.; Serimaa, R.; Laine, J. A Fast Method to Produce Strong NFC Films as a Platform for Barrier and Functional Materials. *ACS Appl. Mater. Interfaces* **2013**, *5* (11), 4640–4647.

- (9) Rydz, J.; Musiol, M.; Zawidlak-Węgrzyńska, B.; Sikorska, W. Present and Future of Biodegradable Polymers for Food Packaging Applications. In *Biopolymers for Food Design*; Elsevier Inc.: 2018; pp 431–467.

- (10) Geueke, B.; Groh, K.; Muncke, J. Food Packaging in the Circular Economy: Overview of Chemical Safety Aspects for Commonly Used Materials. *J. Cleaner Prod.* **2018**, *193*, 491–505.

- (11) Tawakkal, I. S. M. A.; Cran, M. J.; Miltz, J.; Bigger, S. W. A Review of Poly(Lactic Acid)-Based Materials for Antimicrobial Packaging. *J. Food Sci.* **2014**, *79* (8), R1477–R1490.

- (12) Koppolu, R.; Lahti, J.; Abitbol, T.; Swerin, A.; Kuusipalo, J.; Toivakka, M. Continuous Processing of Nanocellulose and Poly(lactic acid) into Multilayer Barrier Coatings. *ACS Appl. Mater. Interfaces* **2019**, *11* (12), 11920–11927.

- (13) Masood, F. Polyhydroxyalkanoates in the Food Packaging Industry. In *Nanotechnology Applications in Food: Flavor, Stability, Nutrition and Safety*; Elsevier Inc.: 2017; pp 153–177.

- (14) Wang, C.; Sauvageau, D.; Elias, A. Immobilization of Active Bacteriophages on Polyhydroxyalkanoate Surfaces. *ACS Appl. Mater. Interfaces* **2016**, *8* (2), 1128–1138.

- (15) Wang, Q.; Cai, J.; Zhang, L.; Xu, M.; Cheng, H.; Han, C. C.; Kuga, S.; Xiao, J.; Xiao, R. A Bioplastic with High Strength Constructed from a Cellulose Hydrogel by Changing the Aggregated Structure. *J. Mater. Chem. A* **2013**, *1* (22), 6678–6686.

- (16) Hammi, N.; Wrońska, N.; Katir, N.; Lisowska, K.; Marcotte, N.; Cacciaguerra, T.; Bryszewska, M.; El Kadib, A. Supramolecular Chemistry-Driven Preparation of Nanostructured, Transformable, and Biologically Active Chitosan-Clustered Single, Binary, and Ternary Metal Oxide Bioplastics. *ACS Appl. Bio Mater.* **2019**, *2* (1), 61–69.

- (17) Wang, H.; Qian, J.; Ding, F. Emerging Chitosan-Based Films for Food Packaging Applications. *J. Agric. Food Chem.* **2018**, *66* (2), 395–413.

- (18) Perotto, G.; Ceseracciu, L.; Simonutti, R.; Paul, U. C.; Guzman-Puyol, S.; Tran, T.-N.; Bayer, I. S.; Athanassiou, A. Bioplastics from Vegetable Waste via an Eco-Friendly Water-Based Process. *Green Chem.* **2018**, *20* (4), 894–902.

- (19) Laufer, G.; Kirkland, C.; Cain, A. A.; Grunlan, J. C. Clay-Chitosan Nanobrick Walls: Completely Renewable Gas Barrier and Flame-Retardant Nanocoatings. *ACS Appl. Mater. Interfaces* **2012**, *4* (3), 1643–1649.

- (20) Nazarzadeh Zare, E.; Makvandi, P.; Borzacchiello, A.; Tay, F. R.; Ashtari, B.; Padil, V. V. T. Antimicrobial Gum Bio-Based Nanocomposites and Their Industrial and Biomedical Applications. *Chem. Commun.* **2019**, *55*, 14871–14885.

- (21) Nazarzadeh Zare, E.; Makvandi, P.; Tay, F. R. Recent Progress in the Industrial and Biomedical Applications of Tragacanth Gum: A Review. *Carbohydr. Polym.* **2019**, *212*, 450–467.

- (22) Hasnain, M. S.; Nayak, A. K. *Natural Polysaccharides in Drug Delivery and Biomedical Applications*; Hasnain, M. S., Nayak, A. K., Eds.; Academic Press: 2019.

- (23) Padil, V. V. T.; Waclawek, S.; Černík, M.; Varma, R. S. Tree Gum-Based Renewable Materials: Sustainable Applications in Nanotechnology, Biomedical and Environmental Fields. *Biotechnol. Adv.* **2018**, *36* (7), 1984–2016.

- (24) Wan, C.; Chen, B. Reinforcement and Interphase of Polymer/Graphene Oxide Nanocomposites. *J. Mater. Chem.* **2012**, *22* (8), 3637–3646.

- (25) Goh, K.; Heising, J. K.; Yuan, Y.; Karahan, H. E.; Wei, L.; Zhai, S.; Koh, J. X.; Htin, N. M.; Zhang, F.; Wang, R.; et al. Sandwich-Architected Poly(Lactic Acid)-Graphene Composite Food Packaging Films. *ACS Appl. Mater. Interfaces* **2016**, *8* (15), 9994–10004.
- (26) Wan, Y.; Chen, X.; Xiong, G.; Guo, R.; Luo, H. Synthesis and Characterization of Three-Dimensional Porous Graphene Oxide/Sodium Alginate Scaffolds with Enhanced Mechanical Properties. *Mater. Express* **2014**, *4* (5), 429–434.
- (27) Cheng, Q.-Y.; Zhou, D.; Gao, Y.; Chen, Q.; Zhang, Z.; Han, B.-H. Supramolecular Self-Assembly Induced Graphene Oxide Based Hydrogels and Organogels. *Langmuir* **2012**, *28* (5), 3005–3010.
- (28) Debnath, S.; Maity, A.; Pillay, K. Magnetic Chitosan–GO Nanocomposite: Synthesis, Characterization and Batch Adsorber Design for Cr(VI) Removal. *J. Environ. Chem. Eng.* **2014**, *2* (2), 963–973.
- (29) Zhang, J.; Cao, Y.; Feng, J.; Wu, P. Graphene-Oxide-Sheet-Induced Gelation of Cellulose and Promoted Mechanical Properties of Composite Aerogels. *J. Phys. Chem. C* **2012**, *116* (14), 8063–8068.
- (30) Padil, V. V. T.; Senan, C.; Waclawek, S.; Černík, M. Electrospun Fibers Based on Arabic, Karaya and Kondagogu Gums. *Int. J. Biol. Macromol.* **2016**, *91*, 299–309.
- (31) Kattimuttathu, S. I.; Chidambaram, K.; Vinod, V.; Rajender, N.; Venkateswara, R. M.; Miroslav, Č. Synthesis, Characterization and Optical Properties of Graphene Oxide-Polystyrene Nanocomposites. *Polym. Adv. Technol.* **2015**, *26* (3), 214–222.
- (32) Pan, G.; Yao, Y.; Zeng, X.; Sun, J.; Hu, J.; Sun, R.; Xu, J.-B.; Wong, C. P. Learning from Natural Nacre: Constructing Layered Polymer Composites with High Thermal Conductivity. *ACS Appl. Mater. Interfaces* **2017**, *9* (38), 33001–33010.
- (33) Yao, H.-B.; Fang, H.-Y.; Tan, Z.-H.; Wu, L.-H.; Yu, S.-H. Biologically Inspired, Strong, Transparent, and Functional Layered Organic-Inorganic Hybrid Films. *Angew. Chem., Int. Ed.* **2010**, *49* (12), 2140–2145.
- (34) Walther, A.; Bjurhager, I.; Malho, J.-M.; Ruokolainen, J.; Berglund, L.; Ikkala, O. Supramolecular Control of Stiffness and Strength in Lightweight High-Performance Nacre-Mimetic Paper with Fire-Shielding Properties. *Angew. Chem., Int. Ed.* **2010**, *49* (36), 6448–6453.
- (35) Pan, Y.; Wu, T.; Bao, H.; Li, L. Green Fabrication of Chitosan Films Reinforced with Parallel Aligned Graphene Oxide. *Carbohydr. Polym.* **2011**, *83* (4), 1908–1915.
- (36) Ionita, M.; Pandele, M. A.; Iovu, H. Sodium Alginate/Graphene Oxide Composite Films with Enhanced Thermal and Mechanical Properties. *Carbohydr. Polym.* **2013**, *94* (1), 339–344.
- (37) Aqlil, M.; Moussema Nzenguet, A.; Essamlali, Y.; Snik, A.; Larzek, M.; Zahouily, M. Graphene Oxide Filled Lignin/Starch Polymer Bionanocomposite: Structural, Physical, and Mechanical Studies. *J. Agric. Food Chem.* **2017**, *65* (48), 10571–10581.
- (38) Padil, V. V. T.; Černík, M. Green Synthesis of Copper Oxide Nanoparticles Using Gum Karaya as a Biotemplate and Their Antibacterial Application. *Int. J. Nanomed.* **2013**, *8*, 889–898.
- (39) Şişmanoğlu, T.; Karakuş, S.; Birer, O.; Soylu, G. S. P.; Kolan, A.; Tan, E.; Ürk, O.; Akdüt, G.; Kilislioglu, A. Preparation and Characterization of Antibacterial Senegalia (Acacia) Senegal/Iron–Silica Bio-Nanocomposites. *Appl. Surf. Sci.* **2015**, *354*, 250–255.
- (40) Abhilash, V.; Rajender, N.; Suresh, K. X-Ray Diffraction Spectroscopy of Polymer Nanocomposites. In *Spectroscopy of Polymer Nanocomposites*; Elsevier Inc.: 2016; pp 410–451.
- (41) Li, W.; Xu, Z.; Chen, L.; Shan, M.; Tian, X.; Yang, C.; Lv, H.; Qian, X. A Facile Method to Produce Graphene Oxide-g-Poly(L-Lactic Acid) as a Promising Reinforcement for PLLA Nanocomposites. *Chem. Eng. J.* **2014**, *237*, 291–299.
- (42) Padil, V. V. T.; Waclawek, S.; Černík, M. Green Synthesis: Nanoparticles and Nanofibres Based on Tree Gums for Environmental Applications. *Ecol. Chem. Eng. S* **2016**, *23* (4), 533–557.
- (43) Mao, A.; Zhang, D.; Jin, X.; Gu, X.; Wei, X.; Yang, G.; Liu, X. Synthesis of Graphene Oxide Sheets Decorated by Silver Nanoparticles in Organic Phase and Their Catalytic Activity. *J. Phys. Chem. Solids* **2012**, *73* (8), 982–986.
- (44) Rodríguez-González, C.; Martínez-Hernández, A. L.; Castaño, V. M.; Kharissova, O. V.; Ruoff, R. S.; Velasco-Santos, C. Polysaccharide Nanocomposites Reinforced with Graphene Oxide and Keratin-Grafted Graphene Oxide. *Ind. Eng. Chem. Res.* **2012**, *51* (9), 3619–3629.
- (45) Daher, C.; Paris, C.; Le Hô, A.-S.; Bellot-Gurlet, L.; Échard, J.-P. A Joint Use of Raman and Infrared Spectroscopies for the Identification of Natural Organic Media Used in Ancient Varnishes. *J. Raman Spectrosc.* **2010**, *41* (11), 1494–1499.
- (46) Tu, Z.; Wang, J.; Yu, C.; Xiao, H.; Jiang, T.; Yang, Y.; Shi, D.; Mai, Y.-W.; Li, R. K. Y. A Facile Approach for Preparation of Polystyrene/Graphene Nanocomposites with Ultra-Low Percolation Threshold through an Electrostatic Assembly Process. *Compos. Sci. Technol.* **2016**, *134*, 49–56.
- (47) Li, R.; Liu, C.; Ma, J. Studies on the Properties of Graphene Oxide-Reinforced Starch Biocomposites. *Carbohydr. Polym.* **2011**, *84* (1), 631–637.
- (48) El Achaby, M.; El Miri, N.; Snik, A.; Zahouily, M.; Abdelouahdi, K.; Fihri, A.; Barakat, A.; Solhy, A. Mechanically Strong Nanocomposite Films Based on Highly Filled Carboxymethyl Cellulose with Graphene Oxide. *J. Appl. Polym. Sci.* **2016**, *133* (2), 42356.
- (49) Habel, C.; Schöttle, M.; Daab, M.; Eichstaedt, N. J.; Wagner, D.; Bakhshi, H.; Agarwal, S.; Horn, M. A.; Breu, J. High-Barrier, Biodegradable Food Packaging. *Macromol. Mater. Eng.* **2018**, *303* (10), 1800333.
- (50) Edlund, U.; Ryberg, Y. Z.; Albertsson, A.-C. Barrier Films from Renewable Forestry Waste. *Biomacromolecules* **2010**, *11* (9), 2532–2538.
- (51) Vartiainen, J.; Vähä-Nissi, M.; Harlin, A. Biopolymer Films and Coatings in Packaging Applications—A Review of Recent Developments. *Mater. Sci. Appl.* **2014**, *05* (10), 708–718.
- (52) Rouf, T. B.; Kokini, J. L. Biodegradable Biopolymer–Graphene Nanocomposites. *J. Mater. Sci.* **2016**, *51*, 9915–9945.

3.2. Alkenyl succinic anhydride modified tree-gum kondagogu: A bio-based material with potential for food packaging

Abstract: Tree gums are a class of abundantly available carbohydrate polymers that have not been explored thoroughly in film fabrication for food packaging. Films obtained from pristine tree gums are often brittle, hygroscopic, and lack mechanical strength. This study focuses on the chemical modification of gum kondagogu using long-chain alkenyl groups of dodecenyl succinic anhydride (DDSA), an esterifying agent that introduces a 12-carbon hydrophobic chain to the kondagogu structure. The esterification reaction was confirmed by ^1H nuclear magnetic resonance and Fourier-transform infrared spectroscopy. The effect of nano-cellulose as an additive on various film properties was investigated. The developed films were characterized for their mechanical, morphological, optical, barrier, antibacterial, and biodegradable properties. The inclusion of long-chain carbon groups acted as internal plasticizers and resulted in an amorphous structure with better film-forming ability, improved hydrophobicity, and higher elongation at break values. The modified films exhibited antibacterial properties and excellent biodegradability under aerobic conditions.

Citation: **Abhilash Venkateshaiah**, Karel Havlíček, Renee L. Timmins, Maximilian Röhl, Stanislaw Waclawek, Nhung H.A. Nguyen, Miroslav Černík, Vinod V. T. Padil, and Seema Agarwal, “**Alkenyl succinic anhydride modified tree-gum kondagogu: A bio-based material with potential for food packaging.**” *Carbohydrate polymers* 266: 118126 [2021]



Alkenyl succinic anhydride modified tree-gum kondagogu: A bio-based material with potential for food packaging

Abhilash Venkateshaiah^a, Karel Havlíček^a, Renee L. Timmins^b, Maximilian Röhrl^b, Stanisław Waclawek^a, Nhung H.A. Nguyen^a, Miroslav Černík^a, Vinod V.T. Padil^{a,*}, Seema Agarwal^{c,*}

^a Institute for Nanomaterials, Advanced Technologies and Innovation (CXI), Technical University of Liberec (TUL), Studentská 1402/2, Liberec 1 461 17, Czech Republic

^b Inorganic Chemistry I, University of Bayreuth, Universitätsstraße 30, 95447 Bayreuth, Germany

^c Macromolecular Chemistry II, University of Bayreuth, Universitätsstraße 30, 95447 Bayreuth, Germany

ARTICLE INFO

Keywords:

Food packaging films
Gum Kondagogu
DDSA modification
Bioplastics
Biodegradable

ABSTRACT

Tree gums are a class of abundantly available carbohydrate polymers that have not been explored thoroughly in film fabrication for food packaging. Films obtained from pristine tree gums are often brittle, hygroscopic, and lack mechanical strength. This study focuses on the chemical modification of gum kondagogu using long-chain alkenyl groups of dodecyl succinic anhydride (DDSA), an esterifying agent that introduces a 12-carbon hydrophobic chain to the kondagogu structure. The esterification reaction was confirmed by ¹H nuclear magnetic resonance and Fourier-transform infrared spectroscopy. The effect of nano-cellulose as an additive on various film properties was investigated. The developed films were characterized for their mechanical, morphological, optical, barrier, antibacterial, and biodegradable properties. The inclusion of long-chain carbon groups acted as internal plasticizers and resulted in an amorphous structure with better film-forming ability, improved hydrophobicity, and higher elongation at break values. The modified films exhibited antibacterial properties and excellent biodegradability under aerobic conditions.

1. Introduction

The packaging industry is one of the major consumers of petro-sourced plastics, accounting for 40% of the total worldwide consumption (Porta et al., 2020). Traditionally, glass, metals, paper, and plastics are commonly used in packaging materials. However, conventional plastics remain a dominant wrapping material owing to their light weight, transparency, and high performance to cost ratio. Despite fulfilling the requirements of efficient packaging material, these materials are under constant scrutiny as they are nonrenewable and non-biodegradable. Raising environmental concerns over the adverse effects of these plastics and depleting fossil fuel reserves have prompted the development of new bioplastics derived from natural resources (Gasti et al., 2020; Goudar et al., 2021; Hiremani et al., 2020; Narasagoudr et al., 2020). These bioplastics are either chemically synthesized from bio-sourced chemicals or extracted directly from plants, trees, animals, and microorganisms. Currently, bioplastics that are naturally-sourced, biodegradable, or both account for only 1% of the total

plastics produced. However, their annual production capacity is estimated to increase from 2.11 million tons in 2019 to 2.43 million tons in 2024 (Market – European Bioplastics e.V., n.d.). Since their inception, bioplastics have been increasingly used in packaging, textiles, automotive, electronics, biomedical, agriculture toys, and many other sectors (Daemen et al., 2016; Venkateshaiah, Cheong, Habel, et al., 2020; Venkateshaiah, Cheong, Shin, et al., 2020; Venkateshaiah, Padil, Nagalakshmaiah, et al., 2020). Among these, bioplastics are used extensively in the packaging sector and accounted for more than 53% of the total production in 2019 (Market – European Bioplastics e.V., n.d.). Consequently, considerable research has been performed on bioplastics for food and non-food packaging in recent years.

Bioplastics derived from bio-based polymers offer sustainability and biodegradability, ideal for single-use packaging like in food packaging. Polysaccharides derived from agricultural and forest biomass have gained significant attention over the past decade, as they are one of the most abundant raw materials. They possess certain inherent characteristics such as biodegradability, non-toxicity, and biocompatibility,

* Corresponding authors.

E-mail addresses: vinod.padil@tul.cz (V.V.T. Padil), seema.agarwal@uni-bayreuth.de (S. Agarwal).

<https://doi.org/10.1016/j.carbpol.2021.118126>

Received 19 December 2020; Received in revised form 9 April 2021; Accepted 25 April 2021

Available online 28 April 2021

0144-8617/© 2021 Elsevier Ltd. All rights reserved.

which makes them well suited for food coatings and packaging. Several polysaccharides such as cellulose, starch, chitosan, alginate, gums, pectin, pullulan, and carrageenan have been studied for their ability to form films suitable for food packaging. Tree gum polysaccharides are a class of renewable, odorless, low-cost materials extracted from the exudates of trees that are secreted in response to any mechanical damage or microbial attack. These materials are usually water-soluble and are often referred to as hydrocolloids. They are capable of forming films via hydrogen bonding, ionic, hydrophobic, electrostatic interactions, and crosslinking (Saha et al., 2017). Gum kondagogu is one such polysaccharide extracted from the exudates of *Cochlospermum gossypium* tree barks. Sugar constituents of kondagogu include glucose, galactose, mannose, rhamnose, arabinose, gluconic acid, and galacturonic acid. This acidic gum is comprised of abundant carboxylic acid, hydroxyl, acetyl, and carbonyl functional groups (Padil et al., 2018). The physicochemical, compositional, morphological, rheological, and emulsifying properties of kondagogu are well studied and reported (Padil, Sashidhar, Sarma, & Vijaya Saradhi, 2008; Padil, Sashidhar, Suresh, et al., 2008). Toxicity studies have revealed kondagogu to be nontoxic and have the potential to be used as a food additive (Puskuri et al., 2017). Although the potential use of kondagogu in the biogenic synthesis of nanoparticles (Padil et al., 2011, 2018; Venkateshaiah et al., 2019), bio-based sponge for oil/organic solvent absorption, and biomedical applications (Ramakrishnan et al., 2021; Bera et al., 2017; Kumar et al., 2018; Nazarzadeh Zare et al., 2019; Padil et al., 2018) has been well established, the use of kondagogu as a packaging material has been scarcely explored. Kondagogu, in its pristine form, lacks any film-forming ability due to intermolecular and intramolecular hydrogen bonding interactions between the polymer chains. The films obtained after solvent evaporation are semicrystalline and brittle, lacking the required mechanical strength. This may be overcome by the use of external plasticizers such as glycerol; however, a high glycerol content is often associated with undesirably high moisture sensitivity. Furthermore, the higher dosage of plasticizer may result in the exudation and leaching out of the films, which may be detrimental to the packaged goods. Another strategy for overcoming these limitations is via modification and functionalization of kondagogu. To obtain good films, kondagogu may be blended with fillers (Venkateshaiah, Cheong, Habel, et al., 2020; Venkateshaiah, Cheong, Shin, et al., 2020; Venkateshaiah, Padil, Nagalakshmaiah, et al., 2020) and other polymers (Ramakrishnan et al., 2021; Padil et al., 2018) to improve its film-forming ability. The availability of abundant hydroxyl functional groups in kondagogu allows easy chemical modification and improved interactions with fillers.

Recently, chemically modifying polysaccharides with long-chain alkyl and alkenyl dicarboxylic acid anhydrides such as dodecyl succinic anhydride (DDSA) as an esterifying agent have gained significant attention (Shah et al., 2018). The long-chain alkenyl group imparts a hydrophobic character, while improving the film-forming property of polysaccharides (Shah et al., 2018). Liu et al. (2013) and Zhong et al. (2013) reported the plasticizing effect of long-chain alkenyl anhydrides after modifying the polysaccharides, thereby improving their film-forming property. The long alkenyl groups grafted onto the polysaccharides act as internal plasticizers by imparting steric hindrance into the polymeric chains, thereby inhibiting the formation of hydrogen bonds and chain aggregation (Liu et al., 2013; Zhong et al., 2013). Moreover, DDSA modified polysaccharides are known to show antibacterial properties (Inta et al., 2014; Padil, Nguyen, et al., 2015; Padil, Senan, & Černík, 2015). In this context, DDSA is ideally suited to be used in the modification of kondagogu. Additionally, the incorporation of nano-cellulose into the films is known to increase the strength of the films along with improving their barrier properties (Thomas et al., 2018). This natural nanomaterial is abundant and possesses superior mechanical strength and stiffness making it an ideal reinforcing agent in biopolymer systems (Thomas et al., 2018). As it is derived from natural biomass, it further contributes to the sustainability aspect by serving as an ecological alternative to obtain enhanced biopolymer composites.

Hydrophobically modifying kondagogu with DDSA may assist in overcoming the critical limiting factors for practical applications of kondagogu films in packaging. Despite being biorenewable and biodegradable biopolymers, the use of tree gums in the field of packaging is very limited. Only a handful of publications exploring the use of kondagogu for packaging applications are available. To the best of our knowledge, no studies on the effect of DDSA on kondagogu film properties have been reported. Furthermore, no reports are available on the use of hydrophobically modified kondagogu or its nanocomposites for food packaging. In this regard, this work aims to investigate the effects of hydrophobic modification of kondagogu on the properties of the resultant films for the first time. Furthermore, the synergistic effect of the modification in conjunction with the incorporation of nano-cellulose into the films was explored. This work emphasizes the valorization of kondagogu in the field of packaging by improving its hydrophobic character, as well as its barrier, mechanical, and film formability.

2. Experimental

2.1. Materials

Gum kondagogu was procured from Grijjan Cooperative society, Hyderabad, India. Gum purification and preparation have been reported earlier (Venkateshaiah, Cheong, Habel, et al., 2020; Venkateshaiah, Cheong, Shin, et al., 2020; Venkateshaiah, Padil, Nagalakshmaiah, et al., 2020). Cellulose nanofiber (nano-cellulose) was procured from Nanografi co. Ltd., Germany ($d = 10\text{--}20\text{ nm}$, $l = 2\text{--}3\text{ }\mu\text{m}$). Dodecyl succinic anhydride, ethanol absolute, sodium hydroxide, glutaraldehyde, hydrochloric acid, glycerol, cyclohexane ($\geq 99\%$), and other analytical-grade chemicals were purchased from Sigma-Aldrich.

2.1.1. Synthesis of DDSA modified kondagogu

Prior to the chemical modification, kondagogu was deacetylated as per the previous report (Padil et al., 2016). Briefly, 2 g of deacetylated kondagogu (GK) was dissolved in 100 ml of water under stirring at room temperature. After complete dissolution, the pH of the solution was adjusted to 8.5 with 2% NaOH solution. Subsequently, DDSA (30 wt% of GK) dissolved in 30 ml of ethanol was added slowly to the mixture under agitation using a peristaltic pump (Hotair BT300LC, China). The reaction was continued for 7 h once the pH was stable at 8.5. The reaction was terminated by adding 5% HCl to the reaction mixture to obtain a pH of 6. The product was then dialyzed against distilled water for 7 days to completely remove the residual salts. The resulting product was freeze-dried to yield a white powder, which was then purified by Soxhlet extraction for 6 h using cyclohexane as a solvent. The purified product was then dried in an oven overnight at 60 °C.

2.1.2. Fabrication of films

Hydrophobically modified GK (HMGK) films were prepared by the solution casting method. Briefly, 2 w/v% aqueous solutions of HMGK were prepared under magnetic stirring at 70 °C. After complete dissolution, 30 w/w% of glycerol was added to the solution and stirred for 30 min. To this, a few drops of 1 M HCl were added to obtain a pH of 3, and 10 w/w% of glutaraldehyde was added for crosslinking. The solution was stirred for another 1 h, and the solutions were poured onto polystyrene petri dishes and dried in an oven at 60 °C for 12 h. After cooling to room temperature, the films were peeled from the petri dishes and stored in zipper storage bags for further use. Similarly, a control sample of GK film was prepared using the same procedure. For the incorporation of nano-cellulose, before the addition of GK, different amounts of nano-cellulose (5%, 10%, and 15%) were dispersed in distilled water employing a homogenizer (IKA T 18 digital ULTRA-TURRAX, Germany) at 12,000 rpm for 3 min. Subsequently, the same procedure was followed as mentioned above. The films containing 5%, 10%, and 15% nano-cellulose were labelled HMGK/NC5, HMGK/NC10, and HMGK/NC15, respectively.

2.2. Characterization of materials and films

The functional groups of the GK and DDSA modified GK were analyzed by Attenuated Total Reflection-Fourier Transform Infrared spectroscopy (ATR-FTIR) (Nicolet IZ10, Thermo Scientific, USA) equipped with a multi-reflection, variable angle, and horizontal ATR accessory at a resolution of 4 cm^{-1} . An Ultrashield 500 plus Bruker (500 MHz) NMR spectrometer was used to record the ^1H nuclear magnetic resonance (NMR) spectra. The thermal stability of the materials was measured on a Thermogravimetric analyzer (TGA-4000, PerkinElmer, USA). The samples ($\sim 5\text{ mg}$) were analyzed under a nitrogen atmosphere at a flow rate of 50 ml/min to ensure an inert atmosphere. The thermal stability of the samples was measured at a temperature range of $30\text{ }^\circ\text{C}$ to $800\text{ }^\circ\text{C}$ and a heating rate of $10\text{ }^\circ\text{C/min}$. A scanning electron microscope (SEM, Zeiss LEO 1530) was employed to analyze the surface morphologies of the films. The instrument was operated at an acceleration voltage of 3 kV , and was equipped with an Everhart-Thornley secondary electron detector. Tensile properties of the films were determined by stress-strain tests on a Zwick/Roell BT1-FR 0.5TND14 at a tensile speed of 5 mm min^{-1} . The samples were cut to $3 \times 40\text{ mm}$ dimensions and conditioned at $20\text{ }^\circ\text{C}$ for 24 h before testing. Elastic modulus was obtained from the slope of the linear region of the stress-strain curves. The tests were performed on at least five specimens, and the average is reported as the result. The oxygen transmission rate of the film was measured on a Mocon OX-TRAN 2/21 (Mocon Inc. Minneapolis USA) with a lower detection limit of $0.05\text{ cm}^3\text{ m}^{-2}\text{ day}^{-1}\text{ bar}^{-1}$. Pure oxygen ($>99.95\%$, Linde Sauerstoff 3.5) was used as a permeant gas, and a mixture of 95% nitrogen and 5% hydrogen as a carrier gas. The tests were conducted at $23\text{ }^\circ\text{C}$ and relative humidity of 50% and 75%. Water vapor transmission tests were conducted on a Mocon PERMATRAN-W model 3/33 (Mocon Inc. Minneapolis USA) with a lower detection limit of $0.5\text{ g m}^{-2}\text{ day}^{-1}$. The tests were conducted at $23\text{ }^\circ\text{C}$ at a relative humidity of 50% and 75%.

2.2.1. Degree of substitution of DDSA by titration

The hydrophobic incorporation of DDSA onto GK was measured using the previously reported titration method (Melanie et al., 2020; Padil, Nguyen, et al., 2015; Padil, Senan, & Āerník, 2015). Briefly, 1 g of accurately weighed HMGK was dissolved in 50 ml of deionized water. After complete dissolution, the pH of the solution was adjusted to 9 through the addition of 0.05 M NaOH. The acid groups of HMGK were completely ionized by the addition of NaOH. This was then titrated against a 0.05 M HCl solution using phenolphthalein as an indicator. The same procedure was followed for GK as the blank. All titration reactions were performed in triplicate, and the average is reported. The degree of substitution was calculated using the following equation:

$$DS = \frac{266 \times C\Delta V}{W_{\text{sample}} - C\Delta V \times 266} \times 100\% \quad (1)$$

where 266 is the molecular weight of DDSA (g mol^{-1}), C is the molarity of HCl, ΔV (l) is the volume of the titer (sample – blank), and W_{sample} is the weight of the sample.

2.2.2. Equilibrium moisture content

Three specimens of each film were cut into $2\text{ cm} \times 2\text{ cm}$ dimensions, and the initial weight of the specimens was determined. The specimens were then oven-dried at $105\text{ }^\circ\text{C}$ for 24 h before measuring the final weight. The equilibrium moisture content was calculated using the following equation (Sukhija et al., 2016; Zhong et al., 2013):

$$EMC = \frac{\text{Initial weight} - \text{Final weight}}{\text{Initial weight}} \times 100\% \quad (2)$$

2.2.3. Water contact angle

The water contact angle (WCA) of the films was measured using a Ramehart contact angle goniometer. Briefly, $3\text{ }\mu\text{l}$ of deionized water

droplets was deposited on the film surface to determine the WCA of the films. The tests were performed on at least ten specimens, and the average is reported as the result.

2.2.4. Film opacity

The opacity of the films was characterized using a Jasco V630 UV-Vis spectrophotometer. The samples were placed inside 1 cm spectrophotometer cells and the transmittance was measured at 650 nm against an empty cell. The opacity (T) values were calculated using the following equation (Li et al., 2015; Zhu et al., 2014):

$$T = \frac{-\log T_{650}}{x} \quad (3)$$

where T_{650} is the fractional transmittance at 650 nm and x is the thickness of the film.

2.2.5. Antibacterial properties

The Gram-positive *Staphylococcus aureus* (CCM 3953) and Gram-negative *Escherichia coli* (CCM 3954) bacterial strains used in this analysis were procured from the Czech Collection of Microorganisms, Masaryk University, Brno, Czech Republic. Bacterial suspensions were freshly prepared in a nutrient broth by growing a single colony at $37\text{ }^\circ\text{C}$, overnight. The obtained bacterial culture was then centrifuged into a pellet, which was further washed and resuspended in physiological solution (0.85% NaCl) and adjusted to an optical density of 0.1 at 600 nm . The bacteria were spread homogeneously on nutrient broth agar plates [23.5 g/l , Plate Count Agar (M091), Himedia, India] and were immediately used for the tests. All of the plates with the samples were incubated for 24 h at $37\text{ }^\circ\text{C}$. All of the samples were tested in triplicates, and the average values are presented.

2.2.6. Biodegradation studies

The biodegradability of the unmodified and modified films was tested under aerobic conditions. The European standard method based on ISO 14851:1999 was used to study the biodegradation and prepare the medium and the samples (Venkateshaiah, Cheong, Habel, et al., 2020; Venkateshaiah, Cheong, Shin, et al., 2020; Venkateshaiah, Padil, Nagalakshmaiah, et al., 2020). Activated sludge from a wastewater treatment plant (WWTP) in Liberec was used as an inoculum at a concentration of 4.7 g/l with approximately $10,000\text{ CFU/ml}$. The test was performed by adding pre-weighed samples to 95 ml of biological medium (ISO 14851:1999) and 5 ml of inoculum. The mixture was dosed into a 250 ml respiration cell, and the test was begun straight away. As a control, only activated sludge (without any organic substrate) was used at the same concentration (blank). The measurements were conducted using a Micro-Oxymax respirometer with a paramagnetic oxygen sensor (Columbus Instruments International, USA). At the end of the 28-day test, the medium with the non-degradable residue of the samples was filtered through a filtration membrane with a pore size of $45\text{ }\mu\text{m}$ and dried at $80\text{ }^\circ\text{C}$ for 2 h, and the weight of the non-degraded material was determined. The weight difference corresponded to the degree of biodegradation of the sample. The test was conducted with cellulose as a positive control and polyethylene as a negative control under the same conditions.

3. Results and discussions

3.1. DDSA modification of GK and ^1H NMR spectroscopy

The base-catalyzed chemical modification of GK by DDSA was performed in an aqueous alkaline system at room temperature. The presence of abundant nucleophilic reactive functional groups in GK makes the DDSA esterification feasible. Fig. 1(a) represents the reaction between GK and DDSA during the modification process. The reaction proceeds with a nucleophilic substitution reaction between the GK

2.2. Characterization of materials and films

The functional groups of the GK and DDSA modified GK were analyzed by Attenuated Total Reflection-Fourier Transform Infrared spectroscopy (ATR-FTIR) (Nicolet IZ10, Thermo Scientific, USA) equipped with a multi-reflection, variable angle, and horizontal ATR accessory at a resolution limit of 4 cm^{-1} . An Ultrashield 500 plus Bruker (500 MHz) NMR spectrometer was used to record the ^1H nuclear magnetic resonance (NMR) spectra. The thermal stability of the materials was measured on a Thermogravimetric analyzer (TGA-4000, PerkinElmer, USA). The samples ($\sim 5\text{ mg}$) were analyzed under a nitrogen atmosphere at a flow rate of 50 ml/min to ensure an inert atmosphere. The thermal stability of the samples was measured at a temperature range of $30\text{ }^\circ\text{C}$ to $800\text{ }^\circ\text{C}$ and a heating rate of $10\text{ }^\circ\text{C/min}$. A scanning electron microscope (SEM, Zeiss LEO 1530) was employed to analyze the surface morphologies of the films. The instrument was operated at an acceleration voltage of 3 kV , and was equipped with an Everhart-Thornley secondary electron detector. Tensile properties of the films were determined by stress-strain tests on a Zwick/Roell BT1-FR 0.5TND14 at a tensile speed of 5 mm min^{-1} . The samples were cut to $3 \times 40\text{ mm}$ dimensions and conditioned at $20\text{ }^\circ\text{C}$ for 24 h before testing. Elastic modulus was obtained from the slope of the linear region of the stress-strain curves. The tests were performed on at least five specimens, and the average is reported as the result. The oxygen transmission rate of the film was measured on a Mocon OX-TRAN 2/21 (Mocon Inc. Minneapolis USA) with a lower detection limit of $0.05\text{ cm}^3\text{ m}^{-2}\text{ day}^{-1}\text{ bar}^{-1}$. Pure oxygen ($>99.95\%$, Linde Sauerstoff 3.5) was used as a permeant gas, and a mixture of 95% nitrogen and 5% hydrogen as a carrier gas. The tests were conducted at $23\text{ }^\circ\text{C}$ and relative humidity of 50% and 75% . Water vapor transmission tests were conducted on a Mocon PERMATRAN-W model 3/33 (Mocon Inc. Minneapolis USA) with a lower detection limit of $0.5\text{ g m}^{-2}\text{ day}^{-1}$. The tests were conducted at $23\text{ }^\circ\text{C}$ at a relative humidity of 50% and 75% .

2.2.1. Degree of substitution of DDSA by titration

The hydrophobic incorporation of DDSA onto GK was measured using the previously reported titration method (Melanie et al., 2020; Padil, Nguyen, et al., 2015; Padil, Senan, & Černík, 2015). Briefly, 1 g of accurately weighed HMGK was dissolved in 50 ml of deionized water. After complete dissolution, the pH of the solution was adjusted to 9 through the addition of 0.05 M NaOH . The acid groups of HMGK were completely ionized by the addition of NaOH . This was then titrated against a 0.05 M HCl solution using phenolphthalein as an indicator. The same procedure was followed for GK as the blank. All titration reactions were performed in triplicate, and the average is reported. The degree of substitution was calculated using the following equation:

$$DS = \frac{266 \times C\Delta V}{W_{\text{sample}} - C\Delta V \times 266} \times 100\% \quad (1)$$

where 266 is the molecular weight of DDSA (g mol^{-1}), C is the molarity of HCl , ΔV (l) is the volume of the titer (sample – blank), and W_{sample} is the weight of the sample.

2.2.2. Equilibrium moisture content

Three specimens of each film were cut into $2\text{ cm} \times 2\text{ cm}$ dimensions, and the initial weight of the specimens was determined. The specimens were then oven-dried at $105\text{ }^\circ\text{C}$ for 24 h before measuring the final weight. The equilibrium moisture content was calculated using the following equation (Sukhija et al., 2016; Zhong et al., 2013):

$$EMC = \frac{\text{Initial weight} - \text{Final weight}}{\text{Initial weight}} \times 100\% \quad (2)$$

2.2.3. Water contact angle

The water contact angle (WCA) of the films was measured using a Ramehart contact angle goniometer. Briefly, $3\text{ }\mu\text{l}$ of deionized water

droplets was deposited on the film surface to determine the WCA of the films. The tests were performed on at least ten specimens, and the average is reported as the result.

2.2.4. Film opacity

The opacity of the films was characterized using a Jasco V630 UV-Vis spectrophotometer. The samples were placed inside 1 cm spectrophotometer cells and the transmittance was measured at 650 nm against an empty cell. The opacity (T) values were calculated using the following equation (Li et al., 2015; Zhu et al., 2014):

$$T = \frac{-\log T_{650}}{x} \quad (3)$$

where T_{650} is the fractional transmittance at 650 nm and x is the thickness of the film.

2.2.5. Antibacterial properties

The Gram-positive *Staphylococcus aureus* (CCM 3953) and Gram-negative *Escherichia coli* (CCM 3954) bacterial strains used in this analysis were procured from the Czech Collection of Microorganisms, Masaryk University, Brno, Czech Republic. Bacterial suspensions were freshly prepared in a nutrient broth by growing a single colony at $37\text{ }^\circ\text{C}$, overnight. The obtained bacterial culture was then centrifuged into a pellet, which was further washed and resuspended in physiological solution (0.85% NaCl) and adjusted to an optical density of 0.1 at 600 nm . The bacteria were spread homogeneously on nutrient broth agar plates [23.5 g/l , Plate Count Agar (M091), Himedia, India] and were immediately used for the tests. All of the plates with the samples were incubated for 24 h at $37\text{ }^\circ\text{C}$. All of the samples were tested in triplicates, and the average values are presented.

2.2.6. Biodegradation studies

The biodegradability of the unmodified and modified films was tested under aerobic conditions. The European standard method based on ISO 14851:1999 was used to study the biodegradation and prepare the medium and the samples (Venkateshaiah, Cheong, Habel, et al., 2020; Venkateshaiah, Cheong, Shin, et al., 2020; Venkateshaiah, Padil, Nagalakshmaiah, et al., 2020). Activated sludge from a wastewater treatment plant (WWTP) in Liberec was used as an inoculum at a concentration of 4.7 g/l with approximately $10,0000\text{ CFU/ml}$. The test was performed by adding pre-weighed samples to 95 ml of biological medium (ISO 14851:1999) and 5 ml of inoculum. The mixture was dosed into a 250 ml respiration cell, and the test was begun straight away. As a control, only activated sludge (without any organic substrate) was used at the same concentration (blank). The measurements were conducted using a Micro-Oxymax respirometer with a paramagnetic oxygen sensor (Columbus Instruments International, USA). At the end of the 28-day test, the medium with the non-degradable residue of the samples was filtered through a filtration membrane with a pore size of $45\text{ }\mu\text{m}$ and dried at $80\text{ }^\circ\text{C}$ for 2 h , and the weight of the non-degraded material was determined. The weight difference corresponded to the degree of biodegradation of the sample. The test was conducted with cellulose as a positive control and polyethylene as a negative control under the same conditions.

3. Results and discussions

3.1. DDSA modification of GK and ^1H NMR spectroscopy

The base-catalyzed chemical modification of GK by DDSA was performed in an aqueous alkaline system at room temperature. The presence of abundant nucleophilic reactive functional groups in GK makes the DDSA esterification feasible. Fig. 1(a) represents the reaction between GK and DDSA during the modification process. The reaction proceeds with a nucleophilic substitution reaction between the GK

esterification reaction between GK and DDSA.

3.3. Film properties of GK and its derivatives

Upon dissolution in water, GK formed a homogenous solution, while the solubility of HMGK samples in water was limited at room temperature owing to the amphiphilic nature of the molecules due to the incorporation of long hydrophobic carbon chains. However, at elevated temperatures (70 °C), HMGK formed a uniform white suspension. For unmodified GK films, drying at 60 °C produced discontinuous films due to the rapid aggregation of GK molecules. Hence, the films needed to be dried at room temperature for 2–3 days for complete evaporation of water and to obtain continuous films. However, the drying process is a lot faster for HMGK samples as it was possible to dry them at elevated temperatures in the oven to obtain continuous, flexible films. This expedited the film fabrication process by alleviating the aggregation of GK molecules. Films prepared from unmodified GK were extremely brittle and lacked flexibility due to the strong intermolecular and intramolecular hydrogen bonding and the rigid sugar chains. However, the films obtained from HMGK were flexible and demonstrated a good film-forming ability. It is well known that the use of glycerol may improve the flexibility of the films by limiting the intermolecular interactions, while enhancing the mobility of the polymer chains. Since the same amount of plasticizer was added to all of the films, the improvement in the film-forming ability may be attributed to the change in the molecular structure brought about by the modification. Despite the addition of glycerol, the GK films were very stiff and fractured upon folding. HMGK, on the other hand, demonstrated good foldability. Additionally, nano-cellulose was added to the modified films to further enhance the film-forming ability, strength, and barrier properties. The use of nano-cellulose in packaging has seen a significant increase in recent years due to its abundance and biodegradability coupled with its unique properties. The surface hydroxyl and carboxyl functional groups present in nano-cellulose may interact with GK functional groups creating a dense network with enhanced mechanical and barrier properties. The incorporation of nano-cellulose into the gum solution clearly increased the viscosity of the solution. This is due to the gelling nature of

nano-cellulose, which forms an interconnected network that is swelled by water. A homogenous solution was formed after the complete dissolution of HMGK, indicating uniform mixing and dispersion.

3.4. Surface morphology analysis by SEM

The SEM micrographs of the different films are presented in Fig. 3. No macroscopic bubbles, cracks, or pores were observed in any of the films. The SEM image of HMGK shows a smoother surface compared to the films made by GK. Upon the addition of nano-cellulose, the surface roughness of the films re-emerged. As the nano-cellulose concentration in the film increased, more fibrils were observed on the film surface (Fig. 3c–e). The fibrils were found to be randomly oriented with a spaghetti-like structure and are uniformly dispersed and densely incorporated throughout the film. The gum matrix appears to be coated on the fibrils, implying a good adherence of the fibrils with the matrix, which may suggest an excellent interfacial interaction due to the hydrogen bonding between the hydroxyl groups of the components. Despite homogenizing the nano-cellulose solution at high rpm, partial aggregation of the fibrils was observed, which is further evident at higher concentrations. This may be due to the strong secondary interactions between the fibrils at higher concentrations (Zhang et al., 2019).

3.5. FTIR, moisture content, contact angle, and opacity of the films

The FTIR spectra of all of the films are presented in Fig. 4(a). The FTIR spectra of the films reveal the same peaks as observed for the GK and HMGK samples. The presence of glutaraldehyde was confirmed by the appearance of an absorption band at 1733 cm^{-1} in the GK film and its increased intensity in other films. This peak corresponds to the free aldehyde groups of glutaraldehyde. The band at 1100 cm^{-1} corresponding to the aliphatic groups of glutaraldehyde was masked by the absorption bands of the gums. Furthermore, crosslinking of the films was confirmed by an increase in the intensity of the absorption band at 1145 cm^{-1} , which suggests a reaction between the hydroxyl groups and the glutaraldehyde molecule. The equilibrium moisture content (EMC) and

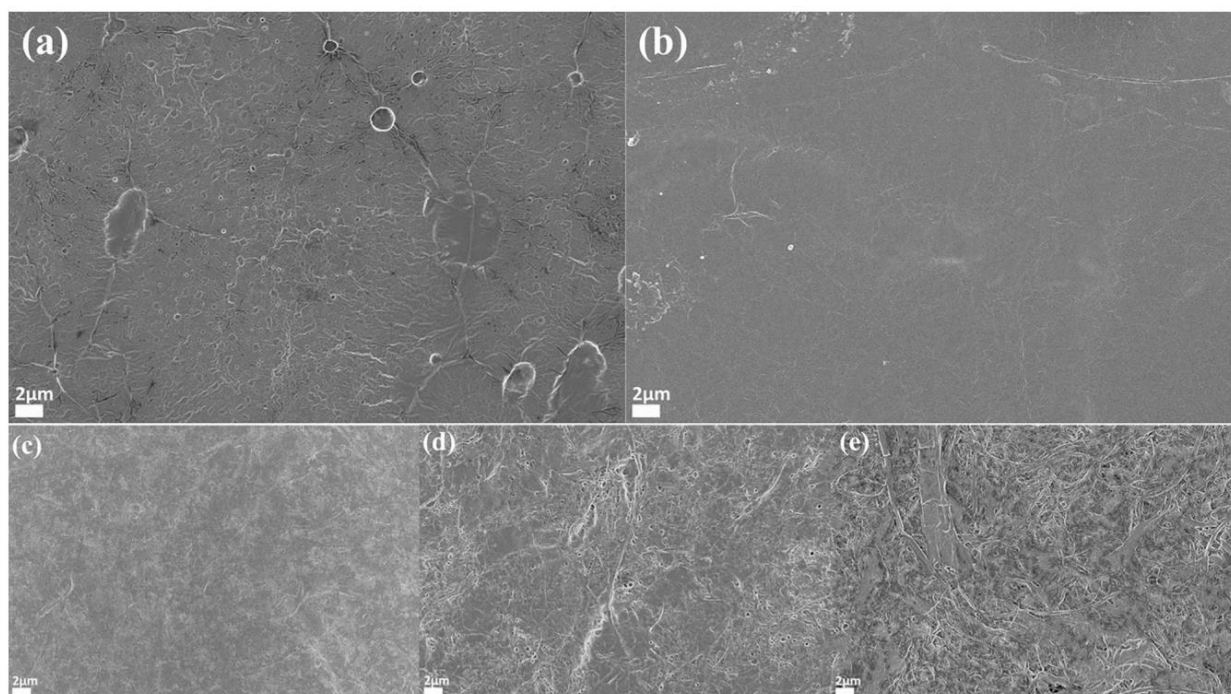


Fig. 3. SEM images of (a) GK, (b) HMGK, (c) HMGK/NC5, (d) HMGK/NC10 and (e) HMGK/NC15 (All images are taken at a scale of 2 μm).

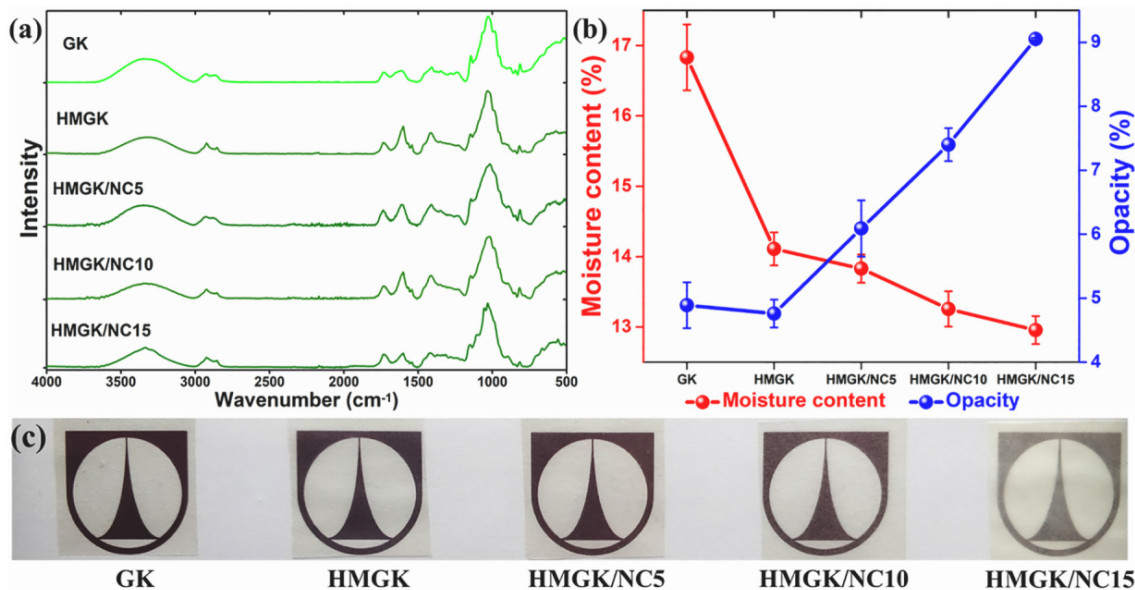


Fig. 4. (a) FTIR spectra of different modified and unmodified GK films, (b) Equilibrium moisture content and opacity of respective films, (c) Transparency of the films against the university logo.

the opacity of different films are depicted in Fig. 4(b). The chemical modification of GK brought about a reduction in the moisture retention ability of the films. It is well-known that polysaccharide films are hydrophilic due to their chemical composition. The abundant hydroxyl groups attract moisture and bind via hydrogen bonding. The inclusion of glycerol further contributes to increased hygroscopicity. This increased moisture may have a detrimental effect on the mechanical properties of the film and the shelf life of the packaged goods. Under the same conditions, GK films retained higher moisture compared to HMGK films. This change may be ascribed to the substitution of hydrophilic hydroxyl functional groups with lipophilic dodecyl groups, thereby reducing the hydrogen bonding interactions between the GK molecule and water molecules (Sweedman et al., 2013). This confirms an increase in the hydrophobicity of the films. Furthermore, a decreasing trend in the EMC was observed with the increase in the nano-cellulose content. This is due to the interactions between the gum molecule and the nano-cellulose. The formation of hydrogen bonds between HMGK and nano-cellulose leads to a decrease in the free -OH groups, hence retarding their ability to bind moisture in the films (Wang, Guo, et al., 2018). WCA measurements of GK and HMGK films clearly indicated an increase in the surface hydrophobicity of the films. GK films exhibited a WCA of $53.6^\circ \pm 3.9^\circ$, while the HMGK films showed an increased WCA of $61.8^\circ \pm 2.3^\circ$. This increase in WCA may be due to the decreased interaction of GK molecules with water molecules due to DDSA substitution (Li et al., 2015; Zhong et al., 2013). The WCA of HMGK/NC5, HMGK/NC10, and HMGK/NC15 were found to be $64.06^\circ \pm 3.2^\circ$, $65.5^\circ \pm 2.9^\circ$, and $66.5^\circ \pm 4.1^\circ$, respectively (Fig.S2). This slight increase in WCA is due to the increased surface roughness of the films arising from the inclusion of nano-cellulose as well as intercomponent hydrogen bonding between the filler and the matrix (Barnes et al., 2019; Kisonen et al., 2015; Mármol et al., 2020).

Transparency of the films plays an important role in the presentation of the packaged material. Transparent films are associated with low opacity values. The opacity values of different films calculated using Eq. (3) are presented in Fig. 4(b). No significant change in opacity was observed upon esterification of GK; however, the nanocomposite films showed higher opacity values (Fig. 4b). The presence of dispersed nano-cellulose hindered the transmittance of light through the films. This decrease in transmittance increased with the increase in filler concentration. This is in agreement with the previously reported studies (Fazeli

et al., 2018; Wang, Guo, et al., 2018).

3.6. Mechanical properties of the films

The packaging materials should possess sufficient mechanical strength to be able to withstand the wear and tear during transport and handling of the goods. Tensile strength (TS), elongation at break (ϵ), and modulus of the modified and unmodified films were analyzed to evaluate the mechanical properties of the films, and are presented in Fig. 5 and the values are tabulated in Table S1. After modification, the ϵ values of the HMGK films were considerably higher than the brittle GK films. However, a decline in the TS values of the HMGK films was also observed. While the ϵ values were three times the GK films, the TS values dropped by 50%. The strength and elongation of the films are predominantly dependent on the intermolecular interactions between the polymer chains in the film. As is well-known, the plasticizer has a significant effect on the reduction of intermolecular interactions between the chains. However, by using the same concentration of glycerol in all of the formulations, the effect of plasticizer has been eliminated. Furthermore, the plasticizing effect of water molecules by improving the polymer chain mobility in biopolymer films has been widely reported (Vieira et al., 2011). This suggests that the GK samples with higher moisture content (Fig. 4b) should have higher elongation than the HMGK samples. However, the opposite result was observed in this study. The HMGK films showed higher ϵ and lower TS despite having lower moisture content values. Hence, the changes in TS and ϵ observed in the present study are solely due to the chemical modification of GK and not due to external plasticization. This indicates that the pendant half ester groups of DDSA act as internal plasticizers contributing to the increased ϵ of the films (Liu et al., 2013). Also, the presence of long-chain carbon groups minimizes the intermolecular interactions, thereby reducing the hydrogen bonding between the polymer chains, thus sacrificing the TS of the films (Ren et al., 2010). The addition of nano-cellulose is known to improve the mechanical properties of the films (Wang et al., 2019). The addition of nano-cellulose into the HMGK matrix gradually increased the tensile strength and modulus of the films (Fig. 5). This may be attributed to the improved secondary interactions through hydrogen bonding between the hydroxyl groups of the filler and the matrix, giving rise to improved strength. The inherent stiffness, large surface area, and homogeneous distribution of nano-cellulose allow for the distribution of

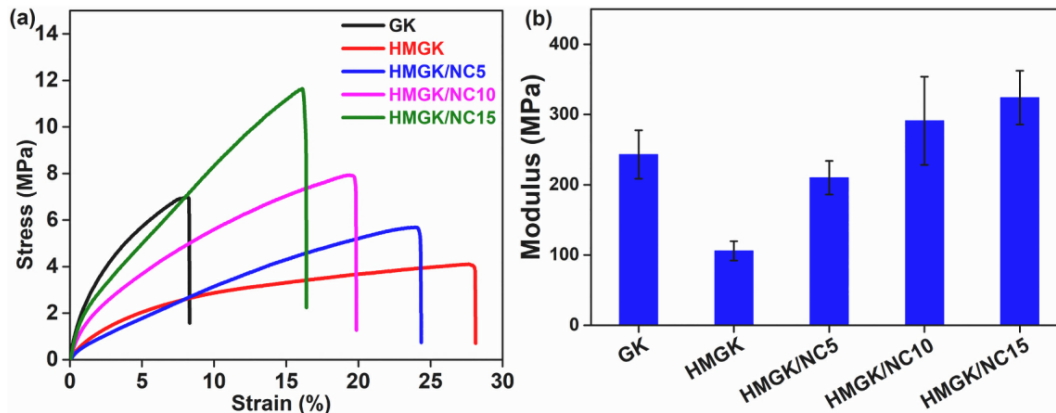


Fig. 5. (a) Stress vs. strain curves (b) Modulus of unmodified and modified films.

fibril networks and hydrogen bonding with GK molecules. This enabled the polysaccharide molecules in the films to form a rigid network with the nano-cellulose. These factors are likely to have assisted the transfer of stress from the GK matrix to the nano-cellulose fibrils, thereby increasing the tensile strength of the films. However, these increased interactions restricted the polymer chain mobility, thereby reducing the ϵ of the films (Movva & Kommineni, 2019).

3.7. Barrier properties of the films

Barrier properties play an essential role in determining the shelf life of the packaged goods. It is preferred that the packaging materials possess high barrier properties to maintain the quality of the packaged food. Nano-cellulose is widely known to improve the barrier properties of the films, especially in terms of the oxygen barrier. Nano-cellulose fibers are comprised of both crystalline and amorphous regions. The crystalline regions are completely impermeable to gas molecules; hence, the gas molecules have to go through a tortuous path to diffuse through the films. Additionally, the random entanglements of the fibers lead to higher density, further adding the tortuosity, thereby increasing the barrier properties. Herein, the barrier properties of the films containing the highest nano-cellulose content (HMGK/NC15) have been tested. The oxygen barrier and water vapor barrier properties were tested at 50% and 75% relative humidity (RH), and the results are tabulated in Table 1.

At 50% humidity, HMGK/NC15 exhibits good barrier properties with an oxygen transmission rate (OTR) of $10.94 \text{ cm}^3/\text{m}^2\cdot\text{day}\cdot\text{bar}$ and oxygen permeability (OP) value of $1049 \text{ cm}^3\cdot\mu\text{m}/\text{m}^2\cdot\text{day}\cdot\text{bar}$. These values are comparable and less than other conventional plastics such as polyethylene, polypropylene, polyethylene terephthalate used in packaging (Wang, Gardner, et al., 2018). Packaging materials with these oxygen barrier properties are ideal in the packaging of fresh meat, bakery products, fruits, and vegetables (Wang, Gardner, et al., 2018). The water vapor barrier properties of the films are comparatively lower than conventional plastics. This may be attributed to the affinity of the gum matrix and the nano-cellulose to water, resulting in a plasticization effect and swelling. Consequently, the mobility of the polymer chains increases and breaks the rigid structure, thereby creating pathways for the molecules to diffuse through the film (Ferrer et al., 2017; Nair et al.,

Table 1

Oxygen and moisture barrier properties of HMGK/NC15.

Relative humidity	OTR ^a	OP ^b	WVTR ^c	WVP ^d
50% RH	10.94	1049	70	2400
75% RH	630	60.4×10^{-3}	578	19.8×10^{-3}

OTR^a: oxygen transmission rate in $\text{cm}^3/\text{m}^2\cdot\text{day}\cdot\text{bar}$, OP^b: oxygen permeability in $\text{cm}^3\cdot\mu\text{m}/\text{m}^2\cdot\text{day}\cdot\text{bar}$, WVTR^c: water vapor transmission rate in $\text{g}/\text{m}^2\cdot\text{day}$, WVP^d: water vapor permeability in $\text{g}\cdot\mu\text{m}/\text{m}^2\cdot\text{day}\cdot\text{kPa}$.

2014; Wang, Gardner, et al., 2018). This is also the reason for the exponential drop in the barrier properties when the analysis was performed at 75% RH. Hence, these films are ideally suited for use as packaging under lower humidity conditions.

3.8. Antibacterial properties of the films

DDSA derivatives of polysaccharides have been known to exhibit antibacterial properties. Hence, the antibacterial properties of unmodified and modified GK samples were evaluated against Gram-positive *Staphylococcus aureus* and Gram-negative *Escherichia coli*. From Fig. 6, it is evident that the unmodified GK films do not show any antibacterial properties, while HMGK films show a clear zone of inhibition (ZOI). The mechanism involved in the antibacterial properties of HMGK films may be explained by the hydrophobic interactions of long dodecyl succinyl chains with the bacterial cell wall proteins. These interactions destroy the cell wall and cell membranes, consequently causing the leakage of intracellular proteins and nucleic acids leading to cell death (Olivetti et al., 2019; X. Zhang et al., 2015). The ZOI for *S. aureus* and *E. coli* were found to be $17.71 \pm 1.38 \text{ mm}$ and $7.85 \pm 1.02 \text{ mm}$, respectively. These data suggest that the HMGK films exhibit greater inhibition to Gram-positive bacteria compared to Gram-negative bacteria. The obtained results are in agreement with the previously reported antibacterial investigations of hydrophobically modified polysaccharides (Olivetti et al., 2019; Padil, Nguyen, et al., 2015; Padil, Senan, & Černík, 2015; X. Zhang et al., 2015).

3.9. Biodegradability of the films

Biodegradable packaging materials are considered to be a promising solution to curb the problems associated with the packaging waste from non-biodegradable plastics. Recently, many biodegradable polymers have been under scrutiny as their degradability in a reasonable time-frame under environmental conditions is under dispute. Therefore, biopolymers derived from natural sources are gaining much precedence. Oxygen accumulation graphs of modified and unmodified films are shown in Fig. S3. The preliminary results showed very similar biodegradability of GK and HMGK. Degradation of modified and unmodified samples in the inoculum may be attributed to covalent bond cleaving via active bacterial interactions and bacterial digestion, leading to the fragmentation of large molecular chains into low molecular weight fragments. No fragments of the GK film and negligibly small fragments from HMGK were observed on a $45 \mu\text{m}$ filter after 28 days in the biological medium containing activated sludge as an inoculum. The GK films exhibited 100% biodegradability with complete weight loss, while the HMGK film showed a biodegradability of $98.2 \pm 1.7\%$ under the same conditions. This may indicate that the chemical modification did

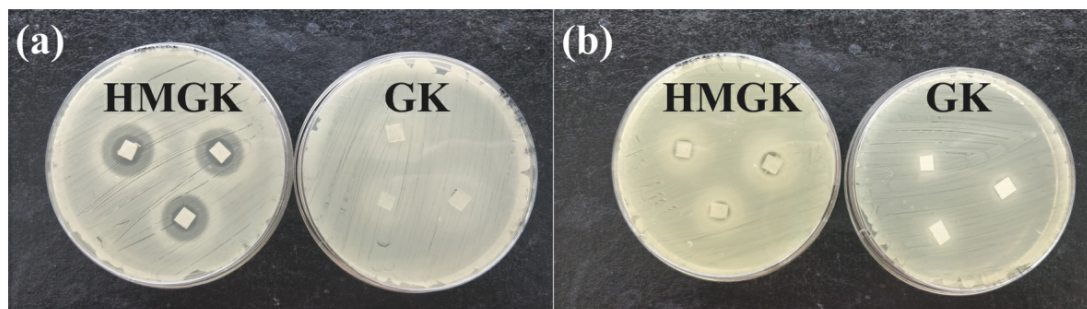


Fig. 6. The antibacterial properties of modified and unmodified films against (a) *Staphylococcus aureus* (b) *Escherichia coli*.

not affect the biodegradability of GK. Long-term biodegradation tests in different environmental media are underway.

4. Conclusion

Hydrophobically modified kondagogu films were fabricated by reacting GK and DDSA in aqueous media. The esterification of GK was confirmed using ^1H NMR and FTIR spectroscopy. It was evident that the chemical modification overcame the inherent brittle nature of the GK films while also reducing their moisture sensitivity. The grafted long-chain carbon groups act as an internal plasticizer and impart steric hindrance to the polymeric chains, and inhibit the formation of hydrogen bonds and chain aggregation. This significantly improved the elongation of the films while reducing their tensile strength. The incorporation of nano-cellulose enhanced the mechanical strength while further reducing the moisture sensitivity of the films. At 50% RH, the films demonstrated an excellent oxygen barrier with moderate water vapor barrier properties, which dropped exponentially at 75% RH. These films may be used for packaging under low humidity conditions. Furthermore, the films exhibited antibacterial properties against Gram-positive *Staphylococcus aureus* and Gram-negative *Escherichia coli*. The modified films retained the inherent biodegradability of GK and show excellent degradation of $98.2 \pm 1.7\%$ within 28 days. The present research highlights the development of biobased, biodegradable, antibacterial, mechanically robust films for environmental and food packaging industries.

Conflict of interest

The authors declare no conflict of interest.

CRediT authorship contribution statement

Abhilash Venkateshaiah: Conceptualization, Methodology, Analysis, Validation, Investigation, Writing – original draft. **Karel Havlíček:** Analysis and investigation. **Renee L. Timmins, Maximilian Röhr:** Analysis. **Stanislaw Waclawek:** Investigation. **Nhung H.A. Nguyen:** Analysis. **Miroslav Černík:** Supervision, Manuscript review and editing, Funding acquisition. **Vinod V.T. Padil:** Conceptualization, Supervision, Project administration, Manuscript review and editing. **Seema Agarwal:** Supervision, validation, Project administration, Manuscript review and editing.

Acknowledgments

This work was supported by the project “Tree Gum Polymers and their Modified Bioplastics for Food Packaging Application” granted by Bavarian-Czech-Academic-Agency (BTHA) (registration number LTAB19007 and BTHA-JC-2019-26) and SFB 1357/C02 funded by Deutsche Forschungsgemeinschaft (DFG). The authors would like to acknowledge the assistance provided by the Research Infrastructure

NanoEnviCz (Project No. LM2018124), and the “Inter Excellence Action Programme” within the framework of the project “Bio-based Porous 2D Membranes and 3D Sponges Based on Functionalized Tree Gum Polysaccharides and their Environmental Application” (registration number LTAUSA19091) – TUL internal No.: 18309/136, supported by the Ministry of Education, Youth and Sports of the Czech Republic. This work was also supported by the Ministry of Education, Youth and Sports of the Czech Republic and the European Union—European Structural and Investment Funds in the framework of the Operational Programme Research, Development and Education—Project Hybrid Materials for Hierarchical Structures (HyHi, Reg. No. CZ.02.1.01/0.0/0.0/16_019/0000843).

Appendix A. Supplementary data

Supplementary data to this article can be found online at <https://doi.org/10.1016/j.carbpol.2021.118126>.

References

- Barnes, E., Jefcoat, J. A., Alberts, E. M., McKechnie, M. A., Peel, H. R., Buchanan, J. P., ... Warner, C. M. (2019). Effect of cellulose nanofibrils and TEMPO-mediated oxidized cellulose nanofibrils on the physical and mechanical properties of poly(vinylidene fluoride)/cellulose nanofibril composites. *Polymers*, 11(7), 1091. <https://doi.org/10.3390/polym11071091>
- Bera, H., Nadimpalli, J., Kumar, S., & Vengala, P. (2017). Kondagogu gum-Zn+2-pectinate emulgel matrices reinforced with mesoporous silica for intragastric furbiprofen delivery. *International Journal of Biological Macromolecules*, 104, 1229–1237. <https://doi.org/10.1016/j.ijbiomac.2017.07.027>
- Biswas, A., Cheng, H. N., Kim, S., Alves, C. R., & Furtado, R. F. (2020). Hydrophobic modification of cashew gum with alkenyl succinic anhydride. *Polymers*, 12(3). <https://doi.org/10.3390/polym12030514>
- Daemen, S., van Zandvoort, M. A. M. J., Parekh, S. H., & Hesselink, M. K. C. (2016). Microscopy tools for the investigation of intracellular lipid storage and dynamics. In *5(3). Molecular metabolism* (pp. 153–163). Elsevier GmbH. <https://doi.org/10.1016/j.molmet.2015.12.005>.
- Fazeli, M., Keley, M., & Biazar, E. (2018). Preparation and characterization of starch-based composite films reinforced by cellulose nanofibers. *International Journal of Biological Macromolecules*, 116, 272–280. <https://doi.org/10.1016/j.ijbiomac.2018.04.186>
- Ferrer, A., Pal, L., & Hubbe, M. (2017). Nanocellulose in packaging: Advances in barrier layer technologies. In *95. Industrial crops and products* (pp. 574–582). Elsevier B.V.. <https://doi.org/10.1016/j.indcrop.2016.11.012>
- Gasti, T., Dixit, S., Sataraddi, S. P., Hiremani, V. D., Masti, S. P., Chougale, R. B., & Malabadi, R. B. (2020). Physicochemical and biological evaluation of different extracts of edible *Solanum nigrum* L. leaves incorporated chitosan/poly (vinyl alcohol) composite films. *Journal of Polymers and the Environment*, 28(11), 2918–2930. <https://doi.org/10.1007/s10924-020-01832-6>
- Goudar, N., Vanjeri, V. N., Kasai, D., Gouripur, G., Malabadi, R. B., Masti, S. P., & Chougale, R. B. (2021). ZnO NPs doped PVA/Spathodea campanulata thin films for food packaging. *Journal of Polymers and the Environment*, 1–16. <https://doi.org/10.1007/s10924-021-02070-0>
- Hermanson, G. T. (2013). The reactions of bioconjugation. In *Bioconjugate techniques* (3rd ed., pp. 229–258). Academic Press. <https://doi.org/10.1016/b978-0-12-382239-0.00003-0>.
- Hiremani, V. D., Sataraddi, S., Bayannavar, P. K., Gasti, T., Masti, S. P., Kamble, R. R., & Chougale, R. B. (2020). Mechanical, optical and antioxidant properties of 7-hydroxy-4-methyl coumarin doped polyvinyl alcohol/oxidized maize starch blend films. *SN Applied Sciences*, 2(11), 1–18. <https://doi.org/10.1007/s42452-020-03399-2>

- Inta, O., Yoksan, R., & Limtrakul, J. (2014). Hydrophobically modified chitosan: A bio-based material for antimicrobial active film. *Materials Science and Engineering C*, 42, 569–577. <https://doi.org/10.1016/j.msec.2014.05.076>
- Kisonen, V., Prakovna, K., Xu, C., Salminen, A., Mikkonen, K. S., Valtakari, D., ... Willför, S. (2015). Composite films of nanofibrillated cellulose and O-acetyl galactoglucomannan (GGM) coated with succinic esters of GGM showing potential as barrier material in food packaging. *Journal of Materials Science*, 50(8), 3189–3199. <https://doi.org/10.1007/s10853-015-8882-7>
- Kokubun, S., Ratcliffe, L., & Williams, P. A. (2013). Synthesis, characterization and self-assembly of biosurfactants based on hydrophobically modified inulins. *Biomacromolecules*, 14(8), 2830–2836. <https://doi.org/10.1021/bm4006529>
- Kumar, S. S. D., Mahesh, A., Antoniraj, M. G., Rathore, H. S., Houreld, N. N., & Kandasamy, R. (2018). Cellular imaging and folate receptor targeting delivery of gum kondagogu capped gold nanoparticles in cancer cells. *International Journal of Biological Macromolecules*, 109, 220–230. <https://doi.org/10.1016/j.ijbiomac.2017.12.069>
- Li, J., Ye, F., Liu, J., & Zhao, G. (2015). Effects of octenylsuccination on physical, mechanical and moisture-proof properties of stretchable sweet potato starch film. *Food Hydrocolloids*, 46, 226–232. <https://doi.org/10.1016/j.foodhyd.2014.12.017>
- Liu, Z., Liu, X., Cao, Y., Xie, W., Ma, X., & Yu, X. (2013). Edible starch sodium octenyl succinate film formation and its physical properties. *Journal of Applied Polymer Science*, 127(4), 2922–2927. <https://doi.org/10.1002/app.37773>
- Market – European Bioplastics e.V. (n.d.). Retrieved October 15, 2020, from <https://www.european-bioplastics.org/market/>
- Mármol, G., Gauss, C., & Fanguero, R. (2020). Potential of cellulose microfibers for PHA and PLA biopolymers reinforcement. *Molecules*, 25(20), 4653. <https://doi.org/10.3390/molecules25204653>
- Melanie, H., Taarji, N., Zhao, Y., Khalid, N., Neves, M. A., Kobayashi, I., ... Nakajima, M. (2020). Formulation and characterisation of O/W emulsions stabilised with modified seaweed polysaccharides. *International Journal of Food Science & Technology*, 55(1), 211–221. <https://doi.org/10.1111/ijfs.14264>
- Morros, J., Leveck, B., & Infante, M. R. (2010). Chemical hydrophobic modification of inulin in aqueous media: Synthesis of β -hydroxyalkyl ethers of inulin. *Carbohydrate Polymers*, 81(3), 681–686. <https://doi.org/10.1016/j.carbpol.2010.03.039>
- Movva, M., & Komminen, R. (2019). Effect of green gram husk nanocellulose on banana fiber composite. *Journal of Natural Fibers*, 16(2), 287–299. <https://doi.org/10.1080/15440478.2017.1414658>
- Nair, S. S., Zhu, J., Deng, Y., & Ragauskas, A. J. (2014). High performance green barriers based on nanocellulose. *Sustainable Chemical Processes*, 2(1), 1–7. <https://doi.org/10.1186/s40508-014-0023-0>
- Narasagoudr, S. S., Hegde, V. G., Chougale, R. B., Masti, S. P., Vootla, S., & Malabadi, R. B. (2020). Physico-chemical and functional properties of rutin induced chitosan/poly (vinyl alcohol) bioactive films for food packaging applications. *Food Hydrocolloids*, 109, 106096. <https://doi.org/10.1016/j.foodhyd.2020.106096>
- Nazarzadeh Zare, E., Makvandi, P., Borzacchiello, A., Tay, F. R., Ashtari, B., & Padil, V. T. V. (2019). Antimicrobial gum bio-based nanocomposites and their industrial and biomedical applications. *Chemical Communications*, 55(99), 14871–14885. <https://doi.org/10.1039/c9cc08207g>
- Olivetti, C., Alvarez Echazú, M. I., Perna, O., Perez, C. J., Mitarotonda, R., De Marzi, M., ... Alvarez, G. S. (2019). Dodecylsuccinic anhydride modified collagen hydrogels loaded with simvastatin as skin wound dressings. *Journal of Biomedical Materials Research. Part A*, 107(9), 1999–2012. <https://doi.org/10.1002/jbm.a.36713>
- Padil, V. T. V., Nguyen, N. H. A., Rožek, Z., Ševců, A., & Černík, M. (2015). Synthesis, fabrication and antibacterial properties of a plasma modified electrospon membrane consisting of gum Kondagogu, dodecyl succinic anhydride and poly (vinyl alcohol). *Surface and Coatings Technology*, 271, 32–38. <https://doi.org/10.1016/J.SURFCOAT.2015.01.035>
- Padil, V. T. V., Saravanan, P., Sreedhar, B., Devi, D. K., & Sashidhar, R. B. (2011). A facile synthesis and characterization of Ag, Au and Pt nanoparticles using a natural hydrocolloid gum kondagogu (*Cochlospermum gossypium*). *Colloids and Surfaces B: Biointerfaces*, 83(2), 291–298. <https://doi.org/10.1016/J.COLSURFB.2010.11.035>
- Padil, V. T. V., Sashidhar, R. B., Sarma, V. U. M., & Vijaya Saradhi, U. V. R. (2008). Compositional analysis and rheological properties of gum kondagogu (*Cochlospermum gossypium*): A tree gum from India. *Journal of Agricultural and Food Chemistry*, 56(6), 2199–2207. <https://doi.org/10.1021/jf072766p>
- Padil, V. T. V., Sashidhar, R. B., Suresh, K. I., Rama Rao, B., Vijaya Saradhi, U. V. R., & Prabhakar Rao, T. (2008). Morphological, physico-chemical and structural characterization of gum kondagogu (*Cochlospermum gossypium*): A tree gum from India. *Food Hydrocolloids*, 22(5), 899–915. <https://doi.org/10.1016/j.foodhyd.2007.05.006>
- Padil, V. T. V., Senan, C., & Černík, M. (2015). Dodecylsuccinic anhydride derivatives of gum karaya (*Sterculia urens*): Preparation, characterization, and their antibacterial properties. *Journal of Agricultural and Food Chemistry*, 63(14), 3757–3765. <https://doi.org/10.1021/jf505783e>
- Padil, V. T. V., Senan, C., Waclawek, S., & Černík, M. (2016). Electrospun fibers based on Arabic, karaya and kondagogu gums. *International Journal of Biological Macromolecules*, 91, 299–309. <http://www.ncbi.nlm.nih.gov/pubmed/27212218>
- Padil, V. T. V., Waclawek, S., Černík, M., & Varma, R. S. (2018). Tree gum-based renewable materials: Sustainable applications in nanotechnology, biomedical and environmental fields. In *Vol. 36, Issue 7, Biotechnology advances* (pp. 1984–2016). Elsevier Inc. <https://doi.org/10.1016/j.biotechadv.2018.08.008>
- Porta, R., Sabbah, M., & Di Pierro, P. (2020). Biopolymers as food packaging materials. *International Journal of Molecular Sciences*, 21(14), 4942. <https://doi.org/10.3390/ijms21144942>
- Puskuri, J., Katukam, V., & Sashidhar, R. B. (2017). Immunological evaluation of gum kondagogu (*Cochlospermum gossypium*): A tree gum with potential applications in food and pharma industry. *Bioactive Carbohydrates and Dietary Fibre*, 11, 48–52. <https://doi.org/10.1016/j.bcdf.2017.07.003>
- Ramakrishnan, R. K., Padil, V. T. V., Škodová, M., Waclawek, S., Černík, M., & Agarwal, S. (2021). Hierarchically porous bio-based sustainable conjugate sponge for highly selective oil/organic solvent absorption. *Advanced Functional Materials*, Article 202100640. <https://doi.org/10.1002/adfm.202100640>
- Ren, L., Jiang, M., Tong, J., Bai, X., Dong, X., & Zhou, J. (2010). Influence of surface esterification with alkenyl succinic anhydrides on mechanical properties of corn starch films. *Carbohydrate Polymers*, 82(3), 1010–1013. <https://doi.org/10.1016/j.carbpol.2010.05.041>
- Saha, A., Tyagi, S., Gupta, R. K., & Tyagi, Y. K. (2017). Natural gums of plant origin as edible coatings for food industry applications. *Critical Reviews in Biotechnology*, 37(8), 959–973. <https://doi.org/10.1080/07388551.2017.1286449>
- Shah, N. N., Soni, N., & Singhal, R. S. (2018). Modification of proteins and polysaccharides using dodecyl succinic anhydride: Synthesis, properties and applications—A review. In *Vol. 107, International journal of biological macromolecules* (pp. 2224–2233). Elsevier B.V. <https://doi.org/10.1016/j.ijbiomac.2017.10.099>
- Sukhija, S., Singh, S., & Riar, C. S. (2016). Analyzing the effect of whey protein concentrate and psyllium husk on various characteristics of biodegradable film from lotus (*Nelumbo nucifera*) rhizome starch. *Food Hydrocolloids*, 60, 128–137. <https://doi.org/10.1016/j.foodhyd.2016.03.023>
- Sweedman, M. C., Tizzotti, M. J., Schäfer, C., & Gilbert, R. G. (2013). Structure and physicochemical properties of octenyl succinic anhydride modified starches: A review. In *Vol. 92, Issue 1, Carbohydrate polymers* (pp. 905–920). Elsevier. <https://doi.org/10.1016/j.carbpol.2012.09.040>
- Thomas, B., Raj, M. K., Athira, B. K., Rubiyah, H. M., Joy, J., Moores, A., ... Sanchez, C. (2018). Nanocellulose, a versatile green platform: From biosources to materials and their applications. In *Vol. 118, Issue 24, Chemical reviews* (pp. 11575–11625). American Chemical Society. <https://doi.org/10.1021/acs.chemrev.7b00627>
- Venkateshaiah, A., Cheong, J. Y., Habel, C., Waclawek, S., Lederer, T., Černík, M., ... Agarwal, S. (2020). Tree gum–graphene oxide nanocomposite films as gas barriers. *ACS Applied Nano Materials*. <https://doi.org/10.1021/acsnanm.9b02166>
- Venkateshaiah, A., Cheong, J. Y., Shin, S. H., Akshaykumar, K. P., Yun, T. G., Bae, J., ... Varma, R. S. (2020). Recycling non-food-grade tree gum wastes into nanoporous carbon for sustainable energy harvesting. *Green Chemistry*, 22(4), 1198–1208. <https://doi.org/10.1039/c9gc04310a>
- Venkateshaiah, A., Padil, V. T. V., Nagalakshmaiah, M., Waclawek, S., Černík, M., & Varma, R. S. (2020). Microscopic techniques for the analysis of micro and nanostructures of biopolymers and their derivatives. *Polymers*, 12(3), 512. <https://doi.org/10.3390/polym12030512>
- Venkateshaiah, A., Silvestri, D., Ramakrishnan, R. K., Waclawek, S., Padil, V. T. V., Černík, M., & Varma, R. S. (2019). Gum kondagogu/reduced graphene oxide framed platinum nanoparticles and their catalytic role. *Molecules*, 24(20). <https://doi.org/10.3390/molecules24203643>
- Vieira, M. G. A., Da Silva, M. A., Dos Santos, L. O., & Beppu, M. M. (2011). Natural-based plasticizers and biopolymer films: A review. In *Vol. 47, Issue 3, European polymer journal* (pp. 254–263). Pergamon. <https://doi.org/10.1016/j.eurpolymj.2010.12.011>
- Wang, J., Liu, X., Jin, T., He, H., & Liu, L. (2019). Preparation of nanocellulose and its potential in reinforced composites: A review. *Journal of Biomaterials Science, Polymer Edition*, 30(11), 919–946. <https://doi.org/10.1080/09205063.2019.1612726>
- Wang, J., Gardner, D. J., Stark, N. M., Bousfield, D. W., Tajvidi, M., & Cai, Z. (2018). Moisture and oxygen barrier properties of cellulose nanomaterial-based films. In *Vol. 6, Issue 1, ACS sustainable chemistry and engineering* (pp. 49–70). American Chemical Society. <https://doi.org/10.1021/acscchemeng.7b03523>
- Wang, X., Guo, C., Hao, W., Ullah, N., Chen, L., Li, Z., & Feng, X. (2018). Development and characterization of agar-based edible films reinforced with nano-bacterial cellulose. *International Journal of Biological Macromolecules*, 118, 722–730. <https://doi.org/10.1016/j.ijbiomac.2018.06.089>
- Zhang, B., Huang, C., Zhao, H., Wang, J., Yin, C., Zhang, L., & Zhao, Y. (2019). Effects of cellulose nanocrystals and cellulose nanofibers on the structure and properties of polyhydroxybutyrate nanocomposites. *Polymers*, 11(12). <https://doi.org/10.3390/polym11122063>
- Zhang, X., Zhang, Y. W., Zhang, H., Yang, Q., Wang, H., & Zhang, G. (2015). Preparation, characterization and antibacterial activity of octenyl succinic anhydride modified inulin. *International Journal of Biological Macromolecules*, 78, 79–86. <https://doi.org/10.1016/j.ijbiomac.2015.03.067>
- Zhong, L. X., Peng, X. W., Yang, D., Cao, X. F., & Sun, R. C. (2013). Long-chain anhydride modification: A new strategy for preparing xylan films. *Journal of Agricultural and Food Chemistry*, 61(3), 655–661. <https://doi.org/10.1021/jf304818f>
- Zhu, G., Sheng, L., & Tong, Q. (2014). Preparation and characterization of carboxymethyl-gellan and pullulan blend films. *Food Hydrocolloids*, 35, 341–347. <https://doi.org/10.1016/j.foodhyd.2013.06.009>

3.3. High barrier, biodegradable nanocomposite films based on clay coated and chemically modified Gum Kondagogu

Abstract: Lately, environmentally benign packaging materials with biodegradability, flexibility, and high barrier properties are sought after as a substitute for conventional plastic packaging materials. Although natural polymers can be sustainable alternatives to petro-sourced, non-biodegradable plastics, they suffer from poor barrier and mechanical properties. In this study, a mechanically stable, biodegradable film of tree gum kondagogu with remarkable barrier properties was fabricated. The introduction of spray-coated, waterborne, large-aspect ratio sodium-hectorite dispersion on tree-gum films ensured very high barrier properties even at high relative humidity conditions (oxygen transmission rate (OTR) $\approx 1.7 \text{ cm}^3 \text{ m}^{-2} \text{ day}^{-1} \text{ bar}^{-1}$ at 75% relative humidity). The coating not only decreases gas permeability through the films but also minimizes the sensitivity of performance to humidity levels. The clay coated nanocomposite films outperformed various commercial polymers and were comparable to high-performance packaging films in terms of oxygen barrier properties. Further, the coating improved the mechanical properties of the films rendering them a prospective packaging material. These biodegradable, high-barrier and mechanically robust films are a promising advance in the field of sustainable packaging.

Citation: **Abhilash Venkateshaiah**, Renee L Timmins, Elmar Sehl, Stanisław Waclawek, Miroslav Černík, Vinod V. T. Padil, and Seema Agarwal. “**High Barrier, Biodegradable Nanocomposite Films based on Clay Coated and Chemically Modified Gum Kondagogu.**” *Macromolecular Materials and Engineering*. 2200008 [2022].

High Barrier, Biodegradable Nanocomposite Films Based on Clay-Coated and Chemically Modified Gum Kondagogu

Abhilash Venkateshaiah, Renee L. Timmins, Elmar Sehl, Stanisław Wacławek, Miroslav Černík, Vinod V. T. Padil,* and Seema Agarwal*

Lately, environmentally benign packaging materials with biodegradability, flexibility, and high barrier properties are sought after as a substitute for conventional plastic packaging materials due to increasing plastic pollution and microplastics in the environment. Although natural polymers can be sustainable alternatives to petro-sourced, non-biodegradable plastics, they suffer from the poor barrier and mechanical properties. In this study, a mechanically stable, biodegradable film of tree gum kondagogu with remarkable barrier properties is fabricated. The introduction of spray-coated, waterborne, large-aspect ratio sodium-hectorite dispersion on tree-gum films ensured very high barrier properties even at high relative humidity conditions (oxygen transmission rate (OTR) $\approx 1.7 \text{ cm}^3 \text{ m}^{-2} \text{ day}^{-1} \text{ bar}^{-1}$ at 75% relative humidity). The coating not only decreases gas permeability through the films but also minimizes the sensitivity of performance to humidity levels. The clay-coated nanocomposite films outperformed various commercial polymers and are comparable to high-performance packaging films in terms of oxygen barrier properties. Further, the coating improved the mechanical properties of the films rendering them a prospective packaging material. These biodegradable, high-barrier and mechanically robust films are a promising advance in the field of sustainable packaging.

1. Introduction

Synthetic, conventional plastics used in single-use applications such as food packaging, grocery bags, disposable utensils, and beverage containers are accumulating in landfills, posing a severe environmental threat. These materials, made of polymer multilayers, are often lined with aluminum and contaminated with food; thus are not recyclable.^[1] Plastic debris has become ubiquitous in the ecosystem and has even littered all the major ocean basins, rivers, and water bodies.^[2] Microplastics, a form of plastic debris, when ingested, might threaten wildlife and marine life by obstructing their digestive tracts. They can later be translocated to the circulatory system and other tissues and transferred from prey to predator through the food chain.^[3] These plastic wastes can be eliminated by utilizing extreme thermal processes like combustion and pyrolysis. However, these processes release greenhouse gases, which can be detrimental to the environment. These disastrous consequences can thus

be mitigated by using biomass-derived materials that degrade via naturally occurring pathways.^[4] Currently, there aren't any completely biodegradable, biomass-derived packaging materials that satisfy the barrier and mechanical property requirements while still being economically viable.^[5] As a result, researchers are looking for a bio-sourced, biodegradable material that can replace traditional plastics in single-use applications.^[6-9]

Bio-sourced polysaccharides, which are one of the most available raw materials in nature, have sparked a lot of interest in replacing single-use plastics. Their abundant availability, combined with their biodegradability, nontoxicity, and biocompatibility, can solve the aforementioned issue. Tree gums are one such polysaccharide that has recently gained interest as a packaging substitute.^[10-12] The potential of tree gums like Arabic, Karaya, Kondagogu, Cashew, and Tragacanth to form films appropriate for food packaging has been investigated.^[13] Tree gums are high molecular weight polysaccharides exuded from plants/trees as a defense mechanism against mechanical injury, chemical injury, microbial/insect attacks, and water stress. This process is called gummosis, and the obtained exudates form gels or viscous solutions in their respective solvents. Hydrocolloids, or water-soluble gums, have found applications in food, pharmaceutical,

A. Venkateshaiah, S. Wacławek, M. Černík, V. V. T. Padil
Institute for Nanomaterials
Advanced Technologies and Innovation (CXI)
Technical University of Liberec (TUL)
Studentská 1402/2, Liberec 1 461 17, Czech Republic
E-mail: vinod.padil@tul.cz

R. L. Timmins
Inorganic Chemistry I
University of Bayreuth
Universitätsstraße 30, Bayreuth 95447, Germany

E. Sehl, S. Agarwal
Macromolecular Chemistry II
University of Bayreuth
Universitätsstraße 30, Bayreuth 95447, Germany
E-mail: agarwal@uni-bayreuth.de

 The ORCID identification number(s) for the author(s) of this article can be found under <https://doi.org/10.1002/mame.202200008>

© 2022 The Authors. Macromolecular Materials and Engineering published by Wiley-VCH GmbH. This is an open access article under the terms of the Creative Commons Attribution License, which permits use, distribution and reproduction in any medium, provided the original work is properly cited.

DOI: 10.1002/mame.202200008

biomedical and cosmetic industries owing to their abundance, low cost, biocompatibility, nontoxicity, gelling ability, chemical inertness, water binding potential, and emulsion stabilization ability.^[14,15] Gum kondagogu is a polysaccharide obtained from the exudates of *Cochlospermum Gossypium*, a native Indian tree. Kondagogu has a high acidic sugar content, with glucuronic and galacturonic acids accounting for 52% of total carbohydrates, along with neutral sugars including glucose, rhamnose, galactose, and arabinose.^[16] The structural, physicochemical, morphological, rheological, and compositional characteristics of kondagogu have been studied and reported.^[17–22] The toxicological studies on kondagogu revealed that it is non-toxic, making it a suitable material for fabricating packaging films.^[23] The use of kondagogu to fabricate packaging films is minimal and yet to be thoroughly investigated. The films made from kondagogu, like most polysaccharide films, have intrinsic limitations that need to be addressed, such as high hydrophilicity, poor mechanical properties, and barrier properties. This could be overcome by combining kondagogu with different biopolymers,^[24] incorporating nanoparticles,^[25] and chemical modification.^[26]

We recently reported the use of dodeceny succinic anhydride (DDSA) modified kondagogu and cellulose nanofibers to fabricate packaging films.^[26] The chemical modification was clearly effective in overcoming the kondagogu films' intrinsic brittleness moisture sensitivity while retaining biodegradability. DDSA's long chain alkenyl groups function as an internal plasticizer, imparting steric hindrance to polysaccharide chains while inhibiting chain aggregation and hydrogen bond formation. This material's mechanical and barrier properties improved significantly when combined with cellulose nanofibers. However, even with the hydrophobic modification, the barrier properties of the films decreased exponentially at higher relative humidity (RH) levels. Despite the modification, kondagogu and cellulose nanofibers retain a certain affinity to moisture. This affinity causes self-association of water molecules which has plasticizing and/or swelling effect on the film. Due to the moisture-induced changes in polysaccharide chains' conformation, crystallinity, and mobility, these effects become much more pronounced at higher RH.^[25]

Single-layer biopolymer films seldom fulfill the industrial criteria for barrier characteristics specified for packaging, thus necessitating modifications. Biopolymer films' barrier properties have been enhanced by chemical and physical crosslinking and surface treatments such as grafting and coating.^[28,29] These approaches have been proven to enhance the barrier characteristics of biopolymers, and they are frequently employed in conjugation to meet commercial requirements. Coating of biopolymer films to improve barrier properties has recently gained significant attention.^[30–33] Studies on coating biopolymer films with graphene oxide,^[34] nanocellulose,^[31] chitin nanofibers,^[35] whey protein,^[36] polylactic acid,^[37] waxes,^[38] and inorganic materials^[39] have been reported. Inorganic two-dimensional (2D) nanosheets are proven to be impervious to gas molecules.^[40] Coating these inorganic dispersions onto biopolymer films yields a high aspect ratio lamellar structure. This creates a tortuous path for the gaseous molecular diffusion across polymeric materials, improving barrier characteristics. Breu and coworkers have proven this by using synthetic layered silicates like sodium

hectorite (NaHec), possessing a high aspect ratio, cation exchange capability, and osmotic swelling properties to improve the gas barrier properties of polymer films.^[41] Further, Habel et al. coated poly L-lactide (PLA) films with waterborne dispersions of NaHec and obtained biopolymer films with exceptional barrier properties.^[42] The authors observed that the clay coating improved the oxygen barrier properties by a factor of four while having no negative impact on the biodegradability of the PLA films. This improvement in the oxygen barrier was observed even at elevated RH, suggesting that the NaHec nanoparticles limit the diffusion of oxygen molecules through the film via the tortuous path mechanism regardless of RH. This would aid in improving the barrier qualities of biobased polymer films, which are strongly reliant on humidity conditions. In addition to excellent oxygen barrier properties, these waterborne clay dispersion coatings can even provide a water vapor barrier in a scalable manner. Based on this concept, we spray-coated NaHec onto hydrophobically modified kondagogu nanocomposites to produce high-barrier, biodegradable films with improved mechanical properties. The effects of cellulose nanofiber incorporation and NaHec coating on the barrier properties of the kondagogu films were analyzed at different humidity conditions. The resulting films had barrier properties that were superior to most conventional plastics.

2. Results and Discussion

2.1. Fabrication of KGNC/Hec Films

Our team has recently reported the detailed synthesis procedures and extensive characterization of DDSA modified kondagogu and cellulose nanofiber incorporated DDSA modified kondagogu (KGNC) films.^[24] We selected KGNC films with 10% and 15% cellulose nanofiber (CNF) in this study because they had the best mechanical and barrier properties^[26] and would be ideal for studying the combined effect of CNF incorporation and clay coating. Herein, we have used a melt-processed synthetic sodium hectorite (NaHec, $[\text{Na}_{0.5}]^{\text{inter}}[\text{Mg}_{2.5}\text{Li}_{0.5}]^{\text{oct}}[\text{Si}_4]^{\text{tet}}\text{O}_{10}\text{F}_2$) clay that can gently, osmotically delaminate into a high-aspect-ratio ($\approx 20\,000$) single layers when dispersed in water, without the need for ultrasonication. This enables uniform non-isotropic, nematic phases in the dispersion. A high barrier layer was created on the films by spray coating a 0.25 wt.% aqueous dispersion on a KGNC substrate (**Figure 1**). A total of 200 spraying/drying cycles were used to coat KGNC films with NaHec suspension to obtain the desired thickness of 3 μm . The suspension layer added in a single spraying process had a thickness of $\approx 1.5\ \mu\text{m}$, which corresponded to a dry film thickness of $\approx 20\ \text{nm}$. After 200 cycles, the final coating layer thickness was measured to be $3.144 \pm 0.193\ \mu\text{m}$ (Image)). The coatings were stable, and no loose powder was observed while handling the films. A slight decrease in transparency of the films was observed after NaHec coating (**Figure 1c**; Table S1, Supporting Information).

2.2. SEM and TEM analysis of the KGNC/Hec films

The surface morphology of the NaHec coated 15 wt.% cellulose nanofiber incorporated DDSA modified kondagogu (KGNC15)

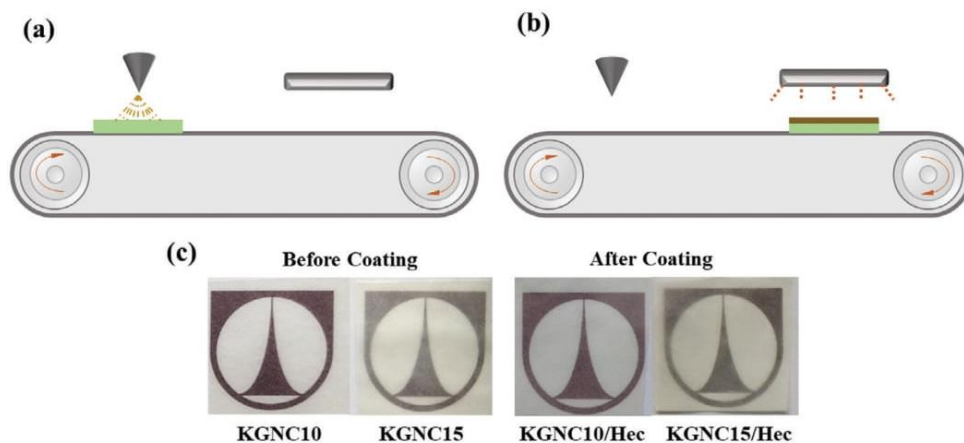


Figure 1. Schematic representation of the NaHec automated a) spray coating, b) drying process, and c) digital images of KGNC films before and after coating.

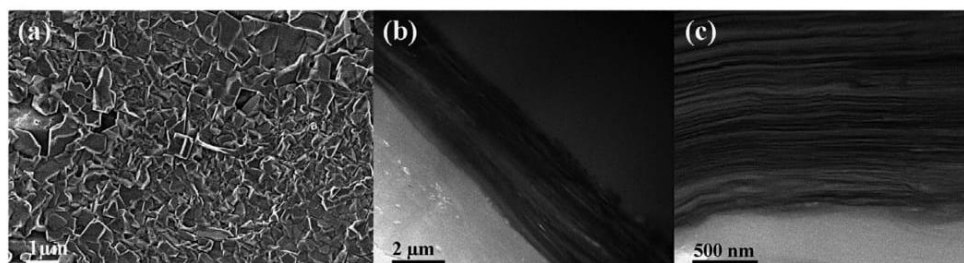


Figure 2. Morphology analysis of KGNC15/Hec film surface by a) SEM image and cross-section by b,c) TEM images.

film was observed by scanning electron microscopy (SEM) (Figure 2a). The image revealed the rough surface of the film with high aspect ratio clay nanoplatelets covering the film surface completely. Unlike the KGNC films, no cellulose nanofibers were observed on the film surface, suggesting that the NaHec suspension was evenly coated (Figure S2, Supporting Information; Figure 2a). The cross-sectional surface observed by transmission electron microscopy (TEM) analysis revealed a highly ordered orientation of clay nanoplatelets on the KGNC15 film substrate (Figure 2b,c). The light grey part is the KGNC film substrate, and the layered structure on top of it is the NaHec coating. Upon spraying the dilute dispersion of highly anisotropic NaHec platelets, the clay particles collide with the KGNC film substrate at high speeds. As a result of the collision, the droplets disperse on the film surface, while the 2D clay nanoplatelets tend to kinetically arrange themselves into dense parallel positions to the film surface.^[43] Furthermore, a thin liquid suspension film forms on the surface after each spraying phase, allowing for ample mobility of the particles. With 90 sec drying time, the nanoplatelets have enough time to align themselves in the most favorable parallel position. This could be clearly seen by the TEM images, wherein highly delaminated NaHec structures are arranged equidistantly on the film surface. This highly ordered parallel orientation of NaHec platelets ensues a tortuous pathway for gas diffusion, resulting in enhanced barrier properties.

2.3. Crystallinity and Thermal Analysis of the Films

X-ray diffraction (XRD) analysis revealed the perfectly aligned structure of the NaHec coatings on the KGNC substrates. Breu et al. have studied and reported the crystallographic data of NaHec in thorough detail.^[44,45] Figure 3a shows a sharp diffraction peak at $2\theta_{001} = 5.6^\circ$ for KGNC10/Hec and 5.05° for KGNC15/Hec, corresponding to monohydrated sodium cations in the interlayer space with a normal d-spacing of 1.67 and 1.72 nm, respectively. The 1D crystalline nanocomposite coatings have 0.96 nm thick NaHec platelets separated by 0.71 nm and 0.76 nm of PVA matrix for KGNC10/Hec and KGNC15/Hec, respectively. This implies that the nanocomposite coating is biphasic, predominantly consisting of 1D crystalline layers of clay domains intercalated by a secondary minor polyvinyl alcohol (PVA) phase (Figure 3a inset). In the case of KGNC15/Hec, a small diffraction peak corresponding to the second-order of the 1D crystal was also observed at $2\theta_{001} = 9.87^\circ$. Since the PVA volume in the interlayer spacing is small, their influence on the bulk properties can be negligible. Further, the thermogravimetric analysis (TGA) analysis of the samples was carried out and depicted in Figure 3b. All films exhibit an initial weight loss below 200°C as a result of loss of adsorbed moisture. The breaking of ester bonds between kondagogu and DDSA at 200°C causes the release of alkenyl chains, resulting in weight loss,^[22] followed by the degradation of gum polysaccharide chains above 250°C .^[21] From Fig-

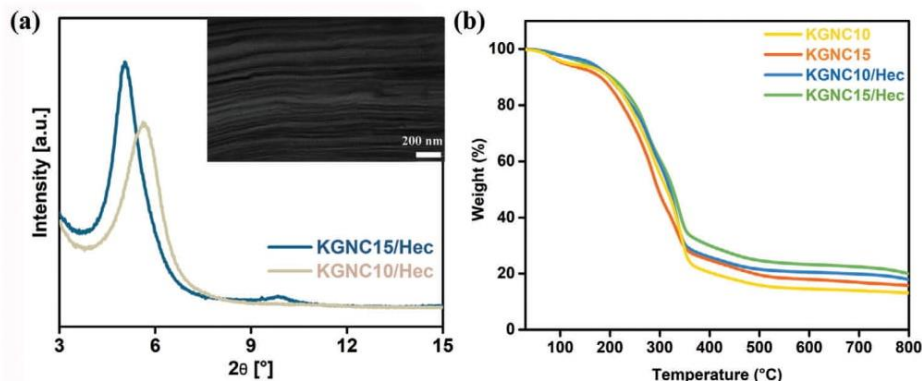


Figure 3. a) XRD pattern of the NaHec coating on KGNC film substrates. The inset is a TEM image of the NaHec coating with highly oriented PVA intercalated NaHec platelets on the KGNC15 substrate. b) TGA curves of uncoated and coated KGNC films.

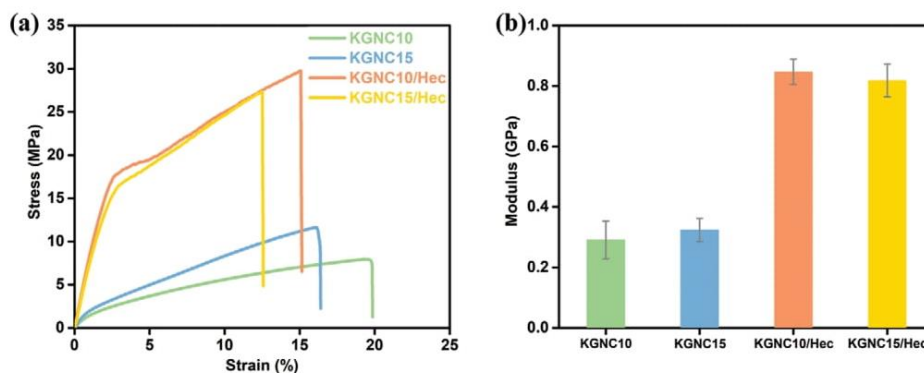


Figure 4. a) Stress-strain curves and b) Modulus of NaHec coated and uncoated films.

ure 3b, it can be seen that the NaHec coating has no significant effect on the thermal stability of the films. However, the KGNC/Hec samples show an increased leftover mass than the KGNC film samples. This increased leftover mass can be attributed to NaHec particles, which do not decompose below 800 °C.^[46]

2.4. Mechanical Properties of the Films

The mechanical performance of the uncoated and NaHec coated KGNC films were analyzed and presented in **Figure 4** and Table S2 (Supporting Information). The effect of NaHec coating on the mechanical properties of the films was determined by evaluating their tensile strength (TS), elongation at break (ϵ), and modulus. From **Figure 4a**, it is evident that the CNF loading increases the TS of the films. This increase in TS arises from the secondary interactions between the hydroxyl groups of CNFs and the matrix via hydrogen bonding. This enables a stiff network between the polysaccharide chains and the CNFs; as a result, a decrease in the ϵ was observed. NaHec coating significantly enhanced the tensile strength of the films. A three-fold increase in the tensile strength of the films was observed after coating. Additionally, the NaHec layer on the KGNC films serves as a stress transfer agent, increasing the tensile strength of composite films in general. However, unlike uncoated samples, KGNC10/Hec with lower CNF loading exhibits higher TS values than KGNC15/Hec. This could be due

to the aggregation of CNF at higher loadings.^[22] These aggregates may interfere with and inhibit the interactions between the Hec coating and the film, resulting in lower TS values. The coating further contributes to the stiffness of the films, which was evident by the decrease in the elongation at break values. A similar effect has been observed in other clay-biopolymer nanocomposites and coatings.^[47–49] In comparison to uncoated films, the modulus of the NaHec coated films increased by around 200%. This emphasizes the synergistic effect the clay coating has on the biocomposite films. Further, the films were subjected to repetitive bending deformation up to 50 times, and no delamination of the NaHec coating was observed. This suggests good compatibility between NaHec coating and KGNC films. Hydrophilic clay nanoparticles have been known to show affinity toward biopolymers like carrageenan,^[50] karaya,^[47] agar,^[51] and proteins.^[52]

2.5. Barrier Properties of the Films

The shelf life of products is primarily determined by the barrier properties of their packaging material, and hence high barrier properties are required in the packaging materials.^[53] Pristine biopolymer films have inferior barrier properties and thus would almost certainly need to be compounded with fillers that enhance barrier properties to gain prominence in the high-performance packaging industry.^[54] Since ISO 14663-2 specifies 65% RH as

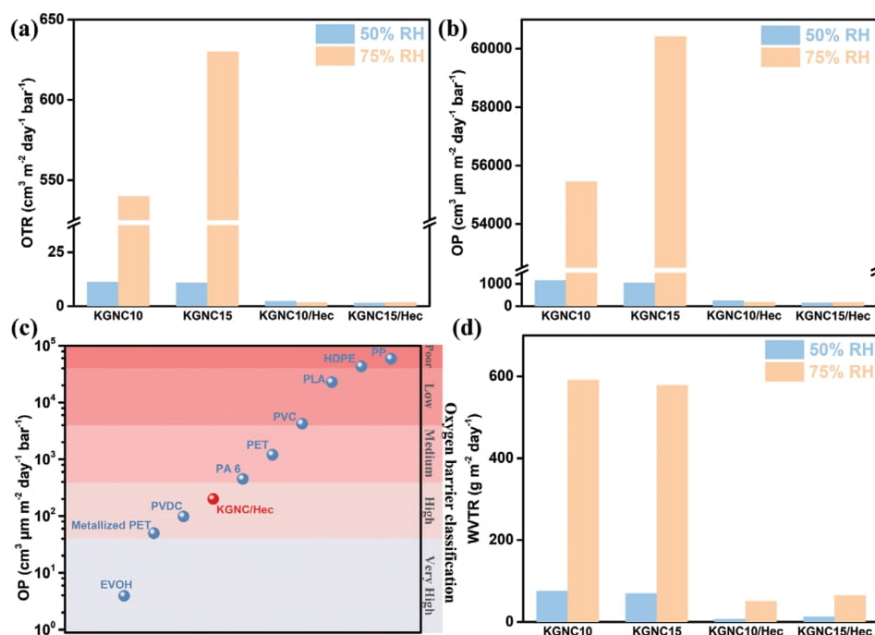


Figure 5. Barrier properties of the uncoated and NaHec coated KGNC films a) OTR, b) OP, c) comparison of OP values with common packaging materials, d) WVTR. EVOH, ethylene vinyl alcohol^[55]; HDPE, high-density polyethylene^[56]; PA 6, polyamide 6^[55]; PET, polyethylene terephthalate^[42]; PLA, polylactic acid^[42]; PP, polypropylene^[55]; PVC, polyvinyl chloride^[55]; PVDC, polyvinylidene chloride^[55]; Metallized PET, aluminum coated polyethylene terephthalate.^[56]

a standard measurement for PVA, we rely on a spectrum of RH (50% and 75% RH) enclosing this standard.

The KGNC films containing CNF exhibited good barrier properties at 50% RH; however, at 75% RH, an exponential drop in the barrier properties was observed (Figure 5 and Table S3, Supporting Information). This poor barrier performance at high RH could be due to the affinity of kondagogu and CNF to moisture leading to swelling and plasticization. As a result, the absorbed water molecules increase the polysaccharide chain mobility, thereby breaking the barrier structure and allowing the gas molecules to diffuse through the film.^[24] Due to their low barrier properties at high RH volumes, they may not be suitable for long-term storage in humid environments. The clay coating has been known to minimize not only the biopolymer film's permeability but also its susceptibility to water vapor concentrations. This ability of NaHec has been studied and established on several other polymer matrices.^[42,43,57] The nanocomposite coating's lamellar structure is comparable to natural nacre with low free inner volume arising from the large aspect ratio of the NaHec platelets. This, along with CNF and the high filler content, is beneficial in creating a tortuous path for gas diffusion, thereby enhancing the barrier properties (Figure S2, Supporting Information). Building on this idea, NaHec clay nanoplatelets delaminated in PVA solution were coated onto KGNC films. Prior to measuring the oxygen transmission rate (OTR) and water vapour transmission rate (WVTR) values, all films were carefully conditioned at room temperature and at different RH levels (50% and 75%). At 50% RH, the KGNC/Hec films with $\approx 3 \mu\text{m}$ NaHec coating demonstrate exceptional barrier properties (Figure 5). The OTR values of the films were as low as $\approx 2 \text{ cm}^3 \text{ m}^{-2} \text{ day}^{-1} \text{ bar}^{-1}$, a five-fold decrease from the uncoated films (Figure 5a). Further, as hypoth-

esized, increasing the RH to 75% had a negligible effect on the OTR values. The uncoated KGNC10 and KGNC15 films exhibited OTR values in the range of 540 and $630 \text{ cm}^3 \text{ m}^{-2} \text{ day}^{-1} \text{ bar}^{-1}$, respectively. Upon coating the films with NaHec dispersion, the OTR values decrease by more than two orders of magnitude with a $>99\%$ decrease in oxygen transmission. However, for a more accurate comparison of these findings, the transmission rates are converted into permeabilities as the thickness of the films has been known to influence the transmission rates significantly. Oxygen permeability (OP) can be defined as the rate of oxygen transmitted per unit thickness of the film. Based on these findings, the KGNC/Hec films clearly outperform the most widely used non-biodegradable traditional plastic packaging films, several coated and multilayered biopolymer films and are comparable to high-performance packaging materials like polyvinylidene chloride (PVDC) and aluminum-coated polyethylene terephthalate (PET) films (Figure 5c; Table S4, Supporting Information). The tortuous diffusion path formed by high aspect ratio NaHec platelets may be directly responsible for this improved oxygen barrier property. This is because in the absence of NaHec, PVA coatings have been shown to have significantly lower permeability reductions, and their efficiency is extremely sensitive to moisture.^[42] Further, the WVTR of the coated and uncoated films were evaluated and depicted in Figure 5d. The same trend observed in OTR holds well for the WVTR values of the coated and uncoated films. The NaHec coating significantly reduced water vapor transmission through the films. Even at an elevated RH of 75%, the WVTR values are reduced by a factor of 9, further emphasizing the lower moisture sensitivity arising from the high aspect ratio NaHec coating. Given the moisture sensitivity of kondagogu and CNF, as well as the water-based formulation of KGNC

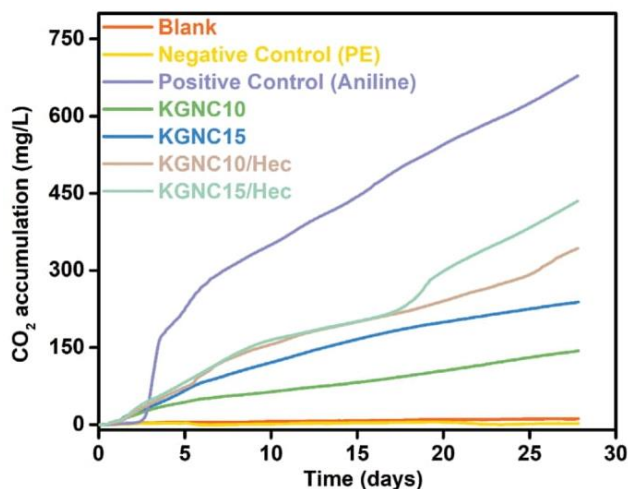


Figure 6. CO_2 accumulation as a function of time of KGNC films.

films and the NaHec coatings, the significant reduction in WVTR values was noteworthy.

2.6. Biodegradability of the Films

The biodegradation of the samples was carried out in an aqueous medium under aerobic conditions with polyethylene (PE) as negative control and aniline as a positive control. The cumulative CO_2 of each test sample was determined and plotted as a function of time to analyze the biodegradation rate (Figure 6). The microbes consume oxygen and degrade the polysaccharide chains generating carbon dioxide. As a result, monitoring CO_2 buildup in the cell could offer information on the biodegradation rate of samples. All the tested biopolymer film samples exhibit biodegradability, and the biodegradation increases with the increase in incubation time. The CO_2 accumulation trend suggests that the biodegradation rate increases quickly at the beginning of the test, which seems to level off as the test proceeds. This could be attributed to the increased availability of organic resources for microbial assimilation, resulting in an increase in the number of microbial colonies. As the test progresses, these resources get exhausted, slowing the rate of biodegradation. From the results, it was evident that the rate of degradation of coated samples was higher than the uncoated samples. The improved rate of biodegradation could be due to the ability of the clay to promote hydrolytic degradation. Furthermore, soaking the film in water causes the clay to swell, resulting in fragmentation of the film, which increases the surface area, thereby improving the biodegradation rate.^[58] This acceleration of biodegradability in the presence of clay nanoparticles has been observed in both conventional and biobased polymers.^[59–63]

3. Conclusions

High barrier, biodegradable packaging films based on gum kondagogu were prepared by spray coating kondagogu/CNF nanocomposite films with a waterborne dispersion of PVA and

NaHec. The entire film fabrication and coating process are water-based, making it environmentally friendly. The exfoliated NaHec platelets formed a thin layer ($\approx 3 \mu\text{m}$) of highly ordered nacre-like structure on the KGNC films. The coating improved the mechanical properties of the material, as shown by the increased tensile strength and modulus. Coating the films resulted in a threefold increase in tensile strength and a 200% improvement in modulus. The obtained flexible packaging films exhibit high barrier performance superior to many traditional plastics. The clay layer formed a tortuous path for gas molecules to diffuse across, dramatically limiting their permeability. The coated films had OTR values of $\approx 2 \text{ cm}^3 \text{ m}^{-2} \text{ day}^{-1} \text{ bar}^{-1}$, a fivefold improvement over the uncoated films. The enhanced barrier properties are negligibly affected by the increase in RH, as evidenced by a more than 99% decrease in oxygen transmission rates and a reduction in water vapor transmission rate by a factor of 9, even at 75% RH. Thus, KGNC/Hec films can be suitable for long-term packaging even in highly humid conditions.

4. Experimental Section

Materials: Gum Kondagogu (Grijjan Cooperative society, Hyderabad, India) was purified and deacetylated using the methods we previously reported.^[24] Melt synthesis was used to synthesize sodium hectorite (NaHec) $[\text{Na}_{0.5}]^{\text{inter}}[\text{Mg}_{2.5}\text{Li}_{0.5}]^{\text{oct}}[\text{Si}_4]^{\text{tet}}\text{O}_{10}\text{F}_2$, following a process described in the literature.^[47] The material had a 1.27 mmol g^{-1} cation exchange capacity (CEC) and a high aspect ratio >20000 . Cellulose nanofiber (CNF, $d = 10\text{--}20 \text{ nm}$, $l = 2\text{--}3 \mu\text{m}$) was purchased from Nanografi co. Ltd., Germany. Hydrochloric acid, Sodium hydroxide, DDSA, Polyvinyl alcohol (PVA, Mowiol 20–98 Mw ≈ 125000), ethanol absolute, glycerol, glutaraldehyde, cyclohexane ($\geq 99\%$), and other analytical-grade chemicals were procured from Merck company.

DDSA Modification of Kondagogu and Fabrication of Nanocomposite Films: Chemical modification of kondagogu and film fabrication was carried out using the methods we recently reported.^[24] Briefly, DDSA (30 wt.% of kondagogu, 30 mL) solution of absolute ethanol was slowly added to deacetylated kondagogu aqueous solution (2 g in 100 mL) at a pH of 8.5. After 7 h at constant pH of 8.5, 5% HCl was added to stop the reaction, and the product was purified by dialysis for 7 days against distilled water. The lyophilized product was further purified by Soxhlet extraction with cyclohexane and dried overnight in an oven at 60°C .

CNF reinforced gum films were prepared by dispersing CNF (10 and 15 wt.% of gum) in distilled water for 3 min at 12000 rpm using a homogenizer. 2 w/v% of modified kondagogu gum was mixed with the CNF dispersion at 70°C to ensure complete dissolution. Subsequently, glycerol (30 w/w%) was added as a plasticizer, followed by a few drops of 1 M HCl to achieve a pH of 3, and glutaraldehyde (10 w/w%) was added as a crosslinker. After 1 h of stirring to enable homogenous mixing, the solutions were cast into Petri dishes and dried for 12 h in an oven at 60°C . The DDSA modified kondagogu films containing 10 and 15% cellulose nanofibers were denoted as KGNC10 and KGNC15, respectively.

NaHec Clay Coating of Films: Delamination of dry NaHec (3 wt.%) was done in double-distilled water and allowed to mix for a week in an overhead mixer. This was added dropwise into PVA (5 wt.%) solution, and the total solid content was adjusted to 0.25% (50 wt.% NaHec, 50 wt.% PVA) using double distilled water, and the dispersion was mixed overnight. The dispersion was transferred to a speed mixer (Hauschild & Co. KG) to enhance the dispersion quality and eliminate gas bubbles under a vacuum just before coating. The dispersion was then transferred to a completely automated spray coating system (SATA 4000 LAB HVLP 1.0 mm spray gun, SATA GmbH & Co. KG, Germany). The obtained suspension was sprayed on the dry KGNC film substrate (4 bar, 1 mL s^{-1}) attached to a conveyor belt by means of a stationary airbrush (Figure 1a). The sample was then dried for 90 s under an IR lamp at 40°C (Figure 1b) for each spray cycle (a total of 200 cycles). The films were then dried in an oven at 40°C for 48 h

to ensure complete water removal. KGNC10/Hec and KGNC15/Hec were the designations for the coated KGNC10 and KGNC15 films, respectively.

Characterization Techniques: The surface morphology of the films was studied using a scanning electron microscope (SEM, UHR FE-SEM Carl Zeiss ULTRA Plus, Germany) with an acceleration voltage of 0.5–2.5 kV. Transmission electron microscopy (TEM) images were obtained on JEM-2200 FS (JEOL GmbH, Germany). An Ion Slicer EM09100IS (JEOL GmbH, Germany) was used to prepare thin cross-sections of the nanocomposite films with coating. A Jasco V630 UV-Vis spectrophotometer was used to determine the transparency of the films. X-ray diffraction (XRD) analysis was carried out on a Bragg-Bertano type diffractometer (Empyrean, Malvern Analytical BV, The Netherlands) equipped with a Pixel-1D detector using nickel filtered Cu-K α radiation ($\lambda = 1.54187 \text{ \AA}$). A Thermogravimetric analyzer (TGA-4000, PerkinElmer, USA) was used to determine the films' thermal stability. The samples (5 mg) were analyzed in an inert atmosphere with a nitrogen flow rate of 50 mL min^{-1} . The analysis was done at a temperature range of 30–800 °C with a heating rate of $10 \text{ }^\circ\text{C min}^{-1}$. Stress-strain analysis on a Zwick/Roell BT1-FR 0.5TND14 was used to evaluate the mechanical properties of the films. The samples were cut into $3 \text{ mm} \times 30 \text{ mm}$ dimensions and conditioned at 20°C for 24 h prior to testing. A Mitutoyo 293–805 optical micrometer with a precision of $1 \text{ }\mu\text{m}$ was used to measure the thickness of each specimen. The width of the specimens was measured using a Zeiss digital microscope, Smartzoom 5 equipped with a Zeiss PlanApo D 1.6x/0.1 FWD 36 mm objective ($36 \times$ magnification) with a precision of $\approx 3 \text{ }\mu\text{m}$ (2 pixels), taking the average of the different positions in the gauge area as the final width. The samples were tested at a tensile speed of 5 mm min^{-1} with a pristine gauge length of 10 mm. The slope of the linear region of the stress-strain curves was used to calculate the elastic modulus. The analysis was performed on at least ten specimens, and the statistical average is reported as a result. Mocon OX-TRAN 2/21 instrument was used in the measurement of oxygen transmission rates (OTR) with a lower detection limit of $0.05 \text{ cm}^3 \text{ m}^{-2} \text{ day}^{-1} \text{ bar}^{-1}$. As a carrier gas, a combination of 98% nitrogen and 2% hydrogen was used, with pure oxygen (>99.95%, Linde Sauerstoff 3.5) as the permeant gas. The tests were performed at a temperature of 23°C and relative humidity of 50% and 75%. Mocon PERMATRAN-W 3/33 instrument with a lower detection limit of $0.5 \text{ g m}^{-2} \text{ day}^{-1}$ was used to determine the water vapor transmission rates (WVTR). The analysis was performed at 23°C and relative humidity of 50% and 75%.

The materials were evaluated for biodegradability under aerobic circumstances according to European standard technique based on ISO 14851:1999. As an inoculum, 4.7 g L^{-1} activated sludge from a wastewater treatment plant (WWTP; Liberec, Czech Republic) containing about $100\,000 \text{ CFU mL}^{-1}$ was utilized. The inorganic medium was prepared by a mixture of four different solutions. Solution 1 had a mixture of 8.5 g L^{-1} of KH_2PO_4 , 21.75 g L^{-1} of K_2HPO_4 , 33.4 g L^{-1} of $\text{Na}_2\text{HPO}_4 \cdot 2\text{H}_2\text{O}$, and 0.5 g L^{-1} of NH_4Cl measuring a pH of 7.4; Solution 2 contained 22.5 g L^{-1} of $\text{MgSO}_4 \cdot 7\text{H}_2\text{O}$; solution 3 contained 36.4 g L^{-1} of $\text{CaCl}_2 \cdot 2\text{H}_2\text{O}$; solution 4 contained 0.25 g L^{-1} of $\text{FeCl}_3 \cdot 6\text{H}_2\text{O}$. The medium was prepared by adding 10 mL of solution 1 to 500 mL of distilled water along with 1 mL each of solution 2–4 and made up to 1000 mL. Pre-weighed samples (50 mg) were added to the biological mixture of 95 mL of inorganic medium and 5 mL of inoculum, then dosing the mixture into a 250 mL respiration cell and starting the test immediately for 28 days. At the same concentration, activated sludge containing no organics was utilized as a blank. A Micro-Oxymax respirometer (Columbus Instruments International, USA) with a paramagnetic oxygen sensor was used for measurements.

Supporting Information

Supporting Information is available from the Wiley Online Library or from the author.

Acknowledgements

Financial support for the project was provided by SFB 1357/C02 funded by Deutsche Forschungsgemeinschaft (DFG) and Bavarian-Czech-Academic

Agency (BTHA) (registration number LTAB19007 and BTHA-JC-2019-26). The authors would like to acknowledge the assistance provided by the Research Infrastructure NanoEnviCz (Project No. LM2018124) and the "Inter Excellence Action Programme" within the framework of the project "Bio-based Porous 2D Membranes and 3D Sponges Based on Functionalized Tree Gum Polysaccharides and their Environmental Application" (registration number LTAUSA19091) – TUL internal No.: 18309/136, supported by the Ministry of Education, Youth and Sports of the Czech Republic. The Ministry of Education also supported this work, Youth and Sports of the Czech Republic and the European Union—European Structural and Investment Funds in the framework of the Operational Programme Research, Development and Education—Project Hybrid Materials for Hierarchical Structures (HyHi, Reg. No. CZ.02.1.01/0.0/0.0/16_019/0000843).

Open access funding enabled and organized by Projekt DEAL.

Conflict of Interest

The authors declare no conflict of interest.

Data Availability Statement

The data that support the findings of this study are available in the supplementary material of this article.

Keywords

biodegradable polymers, bioplastics, clay coatings, high barrier, tree-gums

Received: January 4, 2022

Revised: February 17, 2022

Published online:

- [1] R. Geyer, J. R. Jambeck, K. L. Law, *Sci. Adv.* **2017**, *3*, e1700782.
- [2] A. Chamas, H. Moon, J. Zheng, Y. Qiu, T. Tabassum, J. H. Jang, M. Abu-Omar, S. L. Scott, S. Suh, *ACS Sustainable Chem. Eng.* **2020**, *8*, 3494.
- [3] M. N. Issac, B. Kandasubramanian, *Environ. Sci. Pollut. Res.* **2021**, *28*, 19544.
- [4] S. Singha, M. Mahmutovic, C. Zamalloa, L. Stragier, W. Verstraete, A. J. Svagan, O. Das, M. S. Hedenqvist, *ACS Sustainable Chem. Eng.* **2021**, *9*, 6337.
- [5] Z. Yu, Y. Ji, V. Bourg, M. Bilgen, J. C. Meredith, *Emergent Mater.* **2020**, *3*, 919.
- [6] L. S. F. Leite, C. Pham, S. Bilatto, H. M. C. Azeredo, E. D. Cranston, F. K. Moreira, L. H. C. Mattoso, J. Bras, *ACS Sustainable Chem. Eng.* **2021**, *9*, 8539.
- [7] L. Guo, T. Qiang, Y. Ma, L. Ren, C. Zhu, *ACS Sustainable Chem. Eng.* **2021**, *9*, 8393.
- [8] Y. Qiu, J. Fu, B. Sun, X. Ma, *e-Polymers* **2021**, *21*, 072.
- [9] X. u Yan, W. Zhou, X. Ma, B. Sun, *e-Polymers* **2021**, *21*, 038.
- [10] C. Zhang, Y. Zhang, R. Cha, K. Long, J. Li, X. Jiang, *ACS Sustainable Chem. Eng.* **2019**, *7*, 15404.
- [11] Q. Ma, L. Cao, T. Liang, J. Li, L. A. Lucia, L. Wang, *ACS Sustainable Chem. Eng.* **2018**, *6*, 8926.
- [12] V. V. T. Padil, C. Senan, S. Wacławek, M. Černík, S. Agarwal, R. S. Varma, *ACS Sustainable Chem. Eng.* **2019**, *7*, 5900.
- [13] A. Khezerlou, H. Zolfaghari, S. A. Banihashemi, S. Forghani, A. Ehsani, *Polym. Adv. Technol.* **2021**, *32*, 2306.
- [14] M. S. Amiri, V. Mohammadzadeh, M. E. T. Yazdi, M. Barani, A. Rahdar, G. Z. Kyzas, *Molecules* **2021**, *26*, 1770.

- [15] S. Barak, D. Mudgil, S. Taneja, *J. Sci. Food Agric.* **2020**, *100*, 2828.
- [16] Venkateshaiah, Silvestri, Ramakrishnan, Wactawek, Padil, Černík, Varma, *Molecules* **2019**, *24*, 3643.
- [17] B. Janaki, R. B. Sashidhar, *Food Chem.* **1998**, *61*, 231.
- [18] V. T. P. Vinod, R. B. Sashidhar, *Food Chem.* **2009**, *116*, 686.
- [19] V. T. P. Vinod, R. B. Sashidhar, K. I. Suresh, B. Rama Rao, U. V. R. Vijaya Saradhi, T. Prabhakar Rao, *Food Hydrocoll* **2008**, *22*, 899.
- [20] V. T. P. Vinod, R. B. Sashidhar, V. U. M. Sarma, U. V. R. Vijaya Saradhi, *J. Agric. Food Chem.* **2008**, *56*, 2199.
- [21] V. T. P. Vinod, R. B. Sashidhar, V. U. M. Sarma, S. S. Raju, *Food Chem.* **2010**, *123*, 57.
- [22] V. T. P. Vinod, R. B. Sashidhar, *Indian J. Nat. Prod. Resour.* **2010**, *1*, 181.
- [23] B. Janaki, R. B. Sashidhar, *Food Chem. Toxicol.* **2000**, *38*, 523.
- [24] R. K. Ramakrishnan, S. Wactawek, M. Černík, V. V. T. Padil, *Int. J. Biol. Macromol.* **2021**, *177*, 526.
- [25] A. Venkateshaiah, J. Y. Cheong, C. Habel, S. Wactawek, T. Lederer, M. Černík, I. - D. Kim, V. V. T. Padil, S. Agarwal, *ACS Appl. Nano Mater* **2020**, *3*, 633.
- [26] A. Venkateshaiah, K. Havlíček, R. L. Timmins, M. Röhr, S. Wactawek, N. H. A. Nguyen, M. Černík, V. V. T. Padil, S. Agarwal, *Carbohydr. Polym.* **2021**, *266*, 118126.
- [27] M. Kurek, A. Guinault, A. Voilley, K. Galić, F. Debeaufort, *Food Chem.* **2014**, *144*, 9.
- [28] A. M. Youssef, S. M. El-Sayed, *Carbohydr. Polym.* **2018**, *193*, 19.
- [29] S. M. El-Sayed, H. S. El-Sayed, O. A. Ibrahim, A. M. Youssef, *Carbohydr. Polym.* **2020**, *239*, 116234.
- [30] P. Tyagi, K. S. Salem, M. A. Hubbe, L. Pal, L. Pal, *Trends Food Sci. Technol.* **2021**, *115*, 461.
- [31] P. Tyagi, L. A. Lucia, M. A. Hubbe, L. Pal, L. Pal, *Carbohydr. Polym.* **2019**, *206*, 281.
- [32] V. T. Thuy, L. T. Hao, H. Jeon, J. M. o Koo, J. Park, E. S. Lee, S. Y. Hwang, S. Choi, J. Park, D. X. Oh, *Green Chem.* **2021**, *23*, 2658.
- [33] T. Zhang, Q. Yu, L. Fang, J. Wang, T. Wu, P. Song, *ACS Appl. Polym. Mater.* **2019**, *1*, 3470.
- [34] C. Sharma, P. H. Manepalli, A. Thatte, S. Thomas, N. Kalarikkal, S. Alavi, *Colloid Polym. Sci.* **2017**, *295*, 1695.
- [35] C. C. Satam, C. W. Irvin, A. W. Lang, J. C. R. Jallorina, M. L. Shofner, J. R. Reynolds, J. C. Meredith, *ACS Sustainable Chem. Eng.* **2018**, *6*, 10637.
- [36] P. Cinelli, M. Schmid, E. Bugnicourt, J. Wildner, A. Bazzichi, I. Anguillesi, A. Lazzeri, *Polym. Degrad. Stab.* **2014**, *108*, 151.
- [37] R. Koppolu, J. Lahti, T. Abitbol, A. Swerin, J. Kuusipalo, M. Toivakka, *ACS Appl. Mater. Interfaces* **2019**, *11*, 11920.
- [38] M. O. Reis, J. B. Olivato, A. P. Bilck, J. Zanela, M. V. E. Grossmann, F. Yamashita, *Ind. Crops Prod.* **2018**, *112*, 481.
- [39] J. Vartiainen, K. Rose, Y. Kusano, J. Mannila, L. Wikström, J. *Coatings Technol. Res.* **2019** *171* **2019**, *17*, 305.
- [40] Y. Cui, S. Kumar, B. Rao Kona, D. Van Houcke, *RSC Adv.* **2015**, *5*, 63669.
- [41] M. W. Möller, D. A. Kunz, T. Lunkenbein, S. Sommer, A. Nennemann, J. Breu, *Adv. Mater.* **2012**, *24*, 2142.
- [42] C. Habel, M. Schöttle, M. Daab, N. J. Eichstaedt, D. Wagner, H. Bakhshi, S. Agarwal, M. A. Horn, J. Breu, *Macromol. Mater. Eng.* **2018**, *303*, 1800333.
- [43] E. S. Tsurko, P. Feicht, C. Habel, T. Schilling, M. Daab, S. Rosenfeldt, J. Breu, *J. Memb. Sci.* **2017**, *540*, 212.
- [44] H. Kalo, W. Milius, J. Breu, *RSC Adv.* **2012**, *2*, 8452.
- [45] M. Stöter, D. A. Kunz, M. Schmidt, D. Hirsemann, H. Kalo, B. Putz, J. Senker, J. Breu, *Langmuir* **2013**, *29*, 1280.
- [46] E. S. Tsurko, P. Feicht, F. Nehm, K. Ament, S. Rosenfeldt, I. Pietsch, K. Roschmann, H. Kalo, J. Breu, *Macromolecules* **2017**, *50*, 4344.
- [47] T. L. Cao, K. B. Song, K. Bin Song, *Food Hydrocoll* **2019**, *89*, 453.
- [48] J. Zhu, A. Kumar, P. Hu, C. Habel, J. Breu, S. Agarwal, *Glob. Challenges* **2020**, *4*, 2000030.
- [49] J. Zhu, C. Habel, T. Schilling, A. Greiner, J. Breu, S. Agarwal, *Macromol. Mater. Eng.* **2019**, *304*, 1800779.
- [50] M. J. Sanchis, M. Carsí, M. Culebras, C. M. Gómez, S. Rodriguez, F. G. Torres, *Carbohydr. Polym.* **2017**, *176*, 117.
- [51] J. - W. Rhim, S. - B. Lee, S.-I.n Hong, *J. Food Sci.* **2011**, *76*, N40.
- [52] J.-H. Lee, N. - B. Song, W. - S. Jo, K. B. Song, K. Bin Song, *Int. J. Food Sci. Technol.* **2014**, *49*, 1869.
- [53] E. Ruggeri, D. Kim, Y. Cao, S. Farè, L. De Nardo, B. Marelli, *ACS Sustainable Chem. Eng.* **2020**, *8*, 14312.
- [54] S. Davoodi, S. M. Davachi, A. Ghorbani Golkhajeh, A. S. Shekarabi, A. Abbaspourrad, *ACS Sustainable Chem. Eng.* **2020**, *8*, 1487.
- [55] J. Wang, D. J. Gardner, N. M. Stark, D. W. Bousfield, M. Tajvidi, Z. Cai, *ACS Sustainable Chem. Eng.* **2018**, *6*, 49.
- [56] J. Lange, Y. Wyser, *Packag. Technol. Sci.* **2003**, *16*, 149.
- [57] E. Doblhofer, J. Schmid, M. Rieß, M. Daab, M. Süntinger, C. Habel, H. Bargel, C. Hugenschmidt, S. Rosenfeldt, J. Breu, T. Scheibel, *ACS Appl. Mater. Interfaces* **2016**, *8*, 25535.
- [58] R. L. Timmins, A. Kumar, M. Röhr, K. Havlíček, S. Agarwal, J. Breu, *Macromol. Mater. Eng.* **2021**, 2100727.
- [59] E. Chiellini, A. Corti, S. D'antone, R. Solaro, *Prog. Polym. Sci.* **2003**, *28*, 963.
- [60] T. O. Kumanayaka, R. Parthasarathy, M. Jollands, *Polym. Degrad. Stab.* **2010**, *95*, 672.
- [61] H. Qin, Z. Zhang, M. Feng, F. Gong, S. Zhang, M. Yang, *J. Polym. Sci. Part B Polym. Phys.* **2004**, *42*, 3006.
- [62] S. Mohanty, S. K. Nayak, *J. Polym. Environ.* **2012**, *20*, 195.
- [63] E. Castro-Aguirre, R. Auras, S. Selke, M. Rubino, T. Marsh, *Polymers (Basel)* **2018**, *10*, 202.

3.4. Dialdehyde Modified Tree Gum Karaya: A Sustainable Green Crosslinker for Gelatin-Based Edible Films.

Abstract: Natural biopolymers, which are environmentally friendly materials, are an appealing resource for producing edible films. Edible packaging films may be consumed with the food or beverage that they hold since they are made from edible components derived from plants and animals. Even if they are not consumed, they disintegrate quickly, significantly reducing the waste disposal problem. In this work, karaya dialdehyde (KDA) with a variable aldehyde content is effectively produced through the periodate oxidation of gum karaya and subsequently used as an eco-friendly crosslinking agent for edible gelatin films. Chemical crosslinking between the gelatin protein chains is generated when KDA is added, producing a water-stable film. The mechanical properties are found to be significantly improved as a result of the covalent bonding between the two polymers. Excessive oxidation, on the other hand, has a detrimental effect on the film properties. Despite the crosslinking, the films are biodegradable, suggesting that composite films made in an environmentally benign manner in an aqueous media using polymers derived from biosources may be utilizable in the edible film-based packaging sector.

Citation: **Abhilash Venkateshaiah**, Elmar Sehl, Renee L Timmins, Stanisław Waclawek, Miroslav Černík, Seema Agarwal, and Vinod V. T. Padil. “**Dialdehyde Modified Tree Gum Karaya: A Sustainable Green Crosslinker for Gelatin-Based Edible Films.**” *Advanced Sustainable Systems*. 2100423 [2022].

Dialdehyde Modified Tree Gum Karaya: A Sustainable Green Crosslinker for Gelatin-Based Edible Films

Abhilash Venkateshaiah, Elmar Sehl, Renee L. Timmins, Stanisław Wacławek, Miroslav Černík, Seema Agarwal, and Vinod V. T. Padil*

Natural biopolymers, which are environmentally friendly materials, are an appealing resource for producing edible films. Edible packaging films may be consumed with the food or beverage that they hold since they are made from edible components derived from plants and animals. Even if they are not consumed, they disintegrate quickly, significantly reducing the waste disposal problem. In this work, karaya dialdehyde (KDA) with a variable aldehyde content is effectively produced through the periodate oxidation of gum karaya and subsequently used as an eco-friendly crosslinking agent for edible gelatin films. Chemical crosslinking between the gelatin protein chains is generated when KDA is added, producing a water-stable film. The mechanical properties are found to be significantly improved as a result of the covalent bonding between the two polymers. Excessive oxidation, on the other hand, has a detrimental effect on the film properties. Despite the crosslinking, the films are biodegradable, suggesting that composite films made in an environmentally benign manner in an aqueous media using polymers derived from biosources may be utilizable in the edible film-based packaging sector.

1. Introduction

Due to the growing interest in environmentally responsible packaging materials and depletion of petroleum resources, the development of alternative forms of packaging is increasing worldwide.^[1–6] Biopolymer-based edible films and coatings have gained popularity in recent years as they are environmentally benign and cost-efficient.^[7–10] Food preservation using edible films or coatings is not a novel technique; for decades, they have been employed to keep food safe from deterioration. The

most common and widely known examples include coating cellulose on meat and wax coatings on fruits and vegetables to preserve freshness.^[11] Concerns over single-use conventional plastic packaging and its environmental repercussions have inspired the revival of these techniques. Edible films are fabricated utilizing edible ingredients and are used to wrap food products. They protect the food products from contamination, inhibit mass transfer (gases, water vapor, and solutes), and facilitate ease of handling of the food product while extending its shelf life. Edible films produced from naturally derived materials are nontoxic, biodegradable, and may also be consumed with the food it holds. This helps alleviate the problem of single-use plastic packaging materials accumulating in landfills, thereby reducing pollution. Despite their numerous benefits, edible films are unlikely to completely replace

traditional packaging materials. However, they may be considered a green alternative for food wrapping in order to increase food stability, prevent contamination, and ensure safety during storage and transportation.^[12] Edible films based on various polysaccharides, proteins, fruits, vegetables, and other plant and animal-derived components have been evaluated for packaging applications utilizing a wide variety of analytical techniques.^[13–17]

Among the numerous materials investigated, gelatin stands out as one of the widely studied animal-derived proteins for the production of edible films. Gelatin is a partially denatured derivative of insoluble fibrous collagen and is isolated from the skin, bones, and tissues of various animals. Regardless of its source, gelatin is nontoxic, biodegradable, biocompatible, easily soluble in hot water, and has exceptional film-forming ability, and is therefore suitable for food applications.^[18] Despite these benefits, gelatin films swell and dissolve when exposed to excessive humidity due to their hydrophilic nature. As a result, crosslinking is an essential step to improve the properties and stability of gelatin films. Crosslinking ensues the formation of covalent bonds between the gelatin molecular segments by means of its functional side groups like amino, carboxyl, and guanidine groups, resulting in enhanced physical and chemical characteristics of the film. Several crosslinkers have been explored for gelatin-based systems including, glutaraldehyde, formaldehyde, genipin, transglutaminase,

A. Venkateshaiah, S. Wacławek, M. Černík, V. V. T. Padil
Institute for Nanomaterials
Advanced Technologies and Innovation (CXI)
Technical University of Liberec (TUL)
Studentská 1402/2, Liberec 1, Liberec 461 17, Czech Republic
E-mail: vinod.padil@tul.cz

E. Sehl, S. Agarwal
Macromolecular Chemistry II
University of Bayreuth
Universitätsstraße 30, 95447 Bayreuth, Germany

R. L. Timmins
Inorganic Chemistry I
University of Bayreuth
Universitätsstraße 30, 95447 Bayreuth, Germany

DOI: 10.1002/adsu.202100423

tannic acid, ferulic acid, 1-ethyl-3-(3-dimethylaminopropyl) carbodiimide, polydopamine, and proanthocyanidin.^[19–21] However, these crosslinking approaches have disadvantages, such as toxicity, high cost, quicker deactivation, poor stability, and so on. As a result, these crosslinking systems are not ideal for the fabrication of gelatin-based edible packaging since they raise concerns on the edibility of the films. This has prompted the development of novel natural crosslinkers based on dialdehyde-modified polysaccharides. By employing suitable oxidation systems, aldehyde groups may be introduced into polysaccharide chains via oxidation of the polysaccharide's adjacent diols. These dialdehyde groups are reactive and may crosslink ϵ -amino groups of lysine or hydroxyllysine groups of gelatin protein via Schiff's base formation. This allows for the development of stable gelatin systems in a more environmentally friendly, nontoxic, and cost-effective manner, utilizing a biosustainable alternative crosslinker. Many polysaccharides, including starch,^[22] cellulose,^[23] xanthan gum,^[24] pullulan,^[25] and alginates,^[26] have been modified and utilized to crosslink gelatin films.

Gum karaya (GK) is a partially acetylated tree gum polysaccharide obtained from the exudates of *sterculia urens* trees and other *sterculia* species. Native to India and northern Africa, GK is a complex polysaccharide with a highly branched structure made up of acidic sugars like D-galacturonic acid, and D-glucuronic acid, as well as neutral sugars like D-galactose, and L-rhamnose.^[27] GK has a poor water solubility arising from the presence of acetyl groups and high viscosity and swellability, and is used mainly in food, pharmaceutical, and cosmetic applications.^[28] However, upon the deacetylation of karaya using sodium hydroxide, an improvement in the solubility is observed.^[28] GK possesses several desirable characteristics including biorenewability, biocompatibility, high acidic stability, and low cost.^[29] Moreover, GK is biodegradable and nontoxic without any allergenic, mutagenic, or teratogenic effects and is therefore an ideal choice for use in edible films.^[29] Despite these advantages, the application of GK in food packaging and coatings has received little attention. Furthermore, dialdehyde modification of GK and its influence on gelatin film crosslinking has not been reported yet.

The primary objective of this study is to develop environmentally safe edible films made from materials derived from natural sources. This is the first-ever study to be reported on the dialdehyde modification of karaya and its use in the crosslinking of edible gelatin films. Herein, dialdehyde modified karaya (KDA) with various different contents of aldehyde was effectively produced via chemical oxidation by sodium periodate (SP). The obtained KDA was used to crosslink gelatin films, and the effect of the aldehyde content on the physicochemical properties of the gelatin films was studied. The dialdehyde modification of GK and its crosslinking effect on gelatin was confirmed via Fourier-transform infrared (FTIR) spectroscopy. Furthermore, it was observed that the degree of oxidation and aldehyde content had a significant impact on the mechanical properties of the films. Despite the crosslinking, the biodegradation of the components remained unchanged. This opens up new possibilities for GK in the development of edible films for food packaging applications.

2. Results and Discussions

GK is a botanical gum polysaccharide with a complex branched structure, and with abundant hydrophilic polar moieties such as hydroxyl groups. Sodium periodate (SP) oxidation may selectively cleave the carbon–carbon bond between the adjacent hydroxyl groups of GK, yielding a dialdehyde derivative of GK (KDA). The periodate ion selectively oxidizes the hydroxyl groups on the C2 and C3 of the GK repeating unit resulting in a ring-opened structure with two aldehyde groups (**Figure 1a**). The introduced aldehyde groups may form reversible hemiacetal linkages with the hydroxyl groups existing within the same molecule or with adjacent molecules (**Figure 1b,c**). The formation of these hemiacetal linkages between the oxidized and unoxidized molecules has been shown to inhibit sodium periodate from further oxidizing the polysaccharide chains.^[30] Furthermore, degradation of the oxidized polysaccharide chains has been observed to occur in conjunction with the periodate oxidation (**Figure 1d**). This may be because dialdehyde polysaccharides are more susceptible to hydrolytic attack than their unmodified counterparts.^[24,31]

Periodate oxidation allows a large number of aldehyde groups to be introduced into GK polysaccharide chains, potentially making it a nontoxic, bio-based crosslinker for gelatin films. The degree of oxidation of GK may be controlled by varying the amount of SP, and therefore KDA with different aldehyde contents may be produced. Thereby, the reaction was carried out using 25%, 50%, and 100% (wt% of GK), and the products were denoted KDA2, KDA5, and KDA10, respectively.

The oxidation of the GK structure by periodate was confirmed by FTIR spectroscopy (**Figure 2a**). The FTIR spectra of deacetylated GK reveals peaks at 3320, 2925, and 1035 cm^{-1} corresponding to the $-\text{OH}$, $\text{C}-\text{H}$, and $\text{C}-\text{O}-\text{C}$ stretching vibrations, respectively, and the peaks at 1600 and 1410 cm^{-1} are due to the carboxylate groups of uronic acids.^[32] The 1730–1740 cm^{-1} range in the FTIR spectrum of the oxidized polysaccharide is a fingerprint region of the aldehyde groups introduced during the oxidation process.^[26] The FTIR spectra of KDA with varying SP concentrations exhibit small peaks of varying intensity at 1733 cm^{-1} , suggesting the successful dialdehyde modification of GK. Furthermore, the intensity of the peak increases with an increase in the SP concentration. This indicates that when the concentration of sodium periodate in the reaction mixture increases, so does the aldehyde content. Despite the formation of reversible intramolecular and intermolecular hemiacetal connections, the signal at 1733 cm^{-1} implies that some free aldehyde groups capable of crosslinking gelatin molecules persist. The degree of oxidation corresponding to the aldehyde content was further quantified via hydroxylamine hydrochloride titration, and the results are shown in **Figure 2b**. As shown in **Figure 2b**, the degree of oxidation increases as the concentration of SP increases, confirming the results obtained from FTIR. **Figure 3a** shows the solid-state carbon-13 cross-polarization magic angle spinning nuclear magnetic resonance (^{13}C CP-MAS NMR) spectra of GK and KDA with varying degrees of oxidation. The signals at 160–180 ppm are due to the carboxylic groups of uronic acids, and the changes occurring are likely due to the intermolecular interactions of carboxylic groups.^[33] The broad and increasing intensity signals appearing

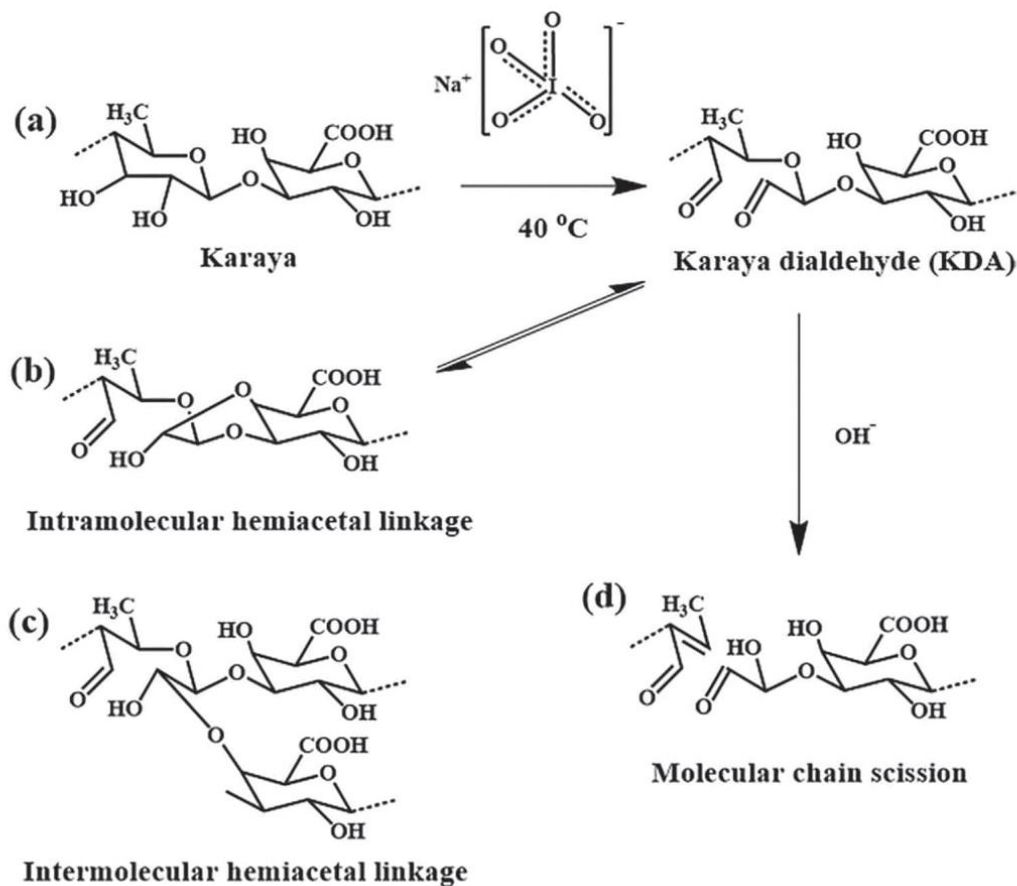


Figure 1. Reactions involved in the sodium periodate oxidation of gum karaya a) Dialdehyde modification of gum karaya, formation of reversible b) intramolecular and c) intermolecular hemiacetal linkages, and d) molecular chain scission.

at 90–100 ppm suggest that the GK has been successfully oxidized, and the aldehyde groups of the KDA are hydrated or have reversibly formed hemiacetal linkages.^[34,35] The signal intensity is further seen to be increasing as a function of SP concentration, which is consistent with the previously reported

studies.^[36,37] The molecular weight of the deacetylated GK and various KDA was analyzed by gel permeation chromatography (GPC) (Figure 3b; and Figure S1, Supporting Information). The oxidation of polysaccharides by periodate is known to cause a reduction in their molecular weight. This decrease in molecular

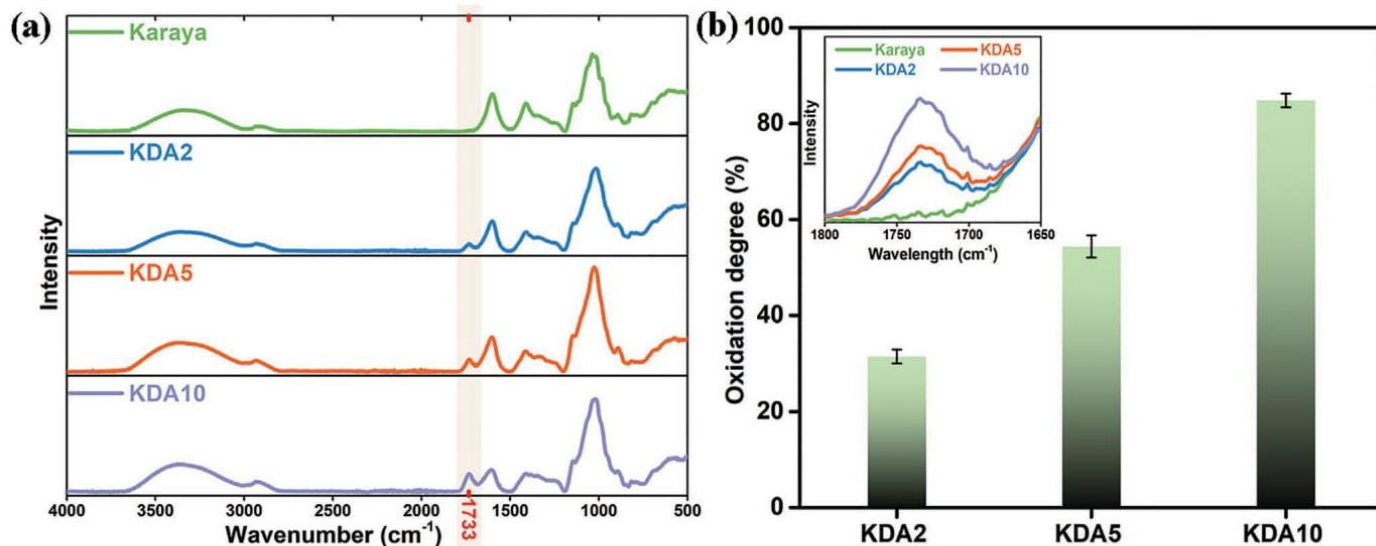


Figure 2. a) FTIR spectra of the aldehyde derivatives of gum karaya, b) degree of oxidation determined by hydroxylamine-hydrochloride titration method (inset: increase in the intensity of the FTIR peak at 1733 cm^{-1} , with the increase in the sodium periodate concentration).

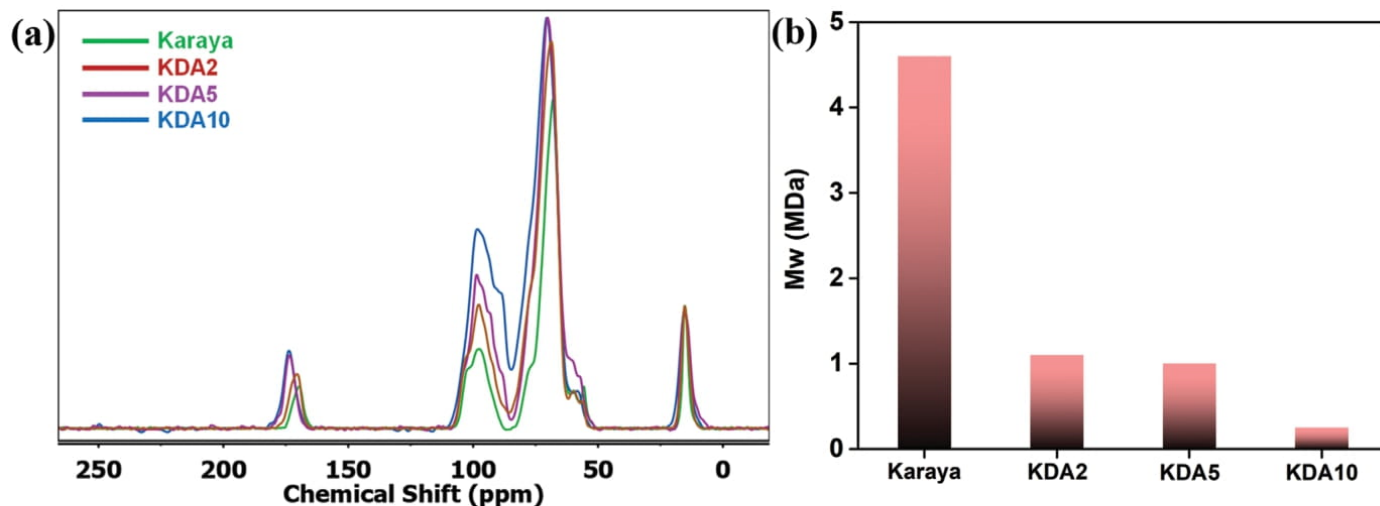


Figure 3. a) ¹³C CP-MAS NMR spectra of aldehyde derivatives of gum karaya, b) Molecular weight of gum karaya and its derivatives determined by GPC.

weight is due to the cleaving of polymer chains, which co-occurs with the introduction of aldehyde groups into the molecular chains. The results indicate that the molecular weight of GK decreases significantly due to oxidation, and a further decrease in the molecular weight was observed with the increase in SP dosage. The molecular weight of the deacetylated GK was found to be 4.5 MDa, which upon oxidation decreased to 1.1, 1, and 0.25 MDa for KDA2, KDA5, and KDA10, respectively.

The obtained KDA of varying oxidation degrees and aldehyde content was used to crosslink gelatin-based edible films. Through Schiff's base formation, the aldehyde groups of KDA may react with the ϵ -amino groups of gelatin protein, forming a crosslinked structure (Figure 4a). The nucleophilic nitrogen in the amino group of the gelatin attacks the electrophilic carbon of the KDA aldehyde group, resulting in the formation of Schiff's base. The reaction proceeds in an aqueous solution under physiological conditions without generating any toxic byproducts.^[38] This enables the fabrication of stable, nontoxic, edible films made entirely of biopolymers. The gelatin-to-GK ratio was kept constant at 5:1, and the effect of the oxidation degree of KDA on the physicochemical properties of the gelatin films was analyzed. From Figure 4b, it is evident that all the films obtained were transparent. However, the color of the films changed with the addition of KDA of various different oxidation degrees. The color of the samples varied from yellow for G-KDA2 to brown for G-KDA10. A shift in color from white/colorless to yellow or brown distinguishes the reaction between gelatin and an aldehyde based crosslinker.^[26] The creation of an imine bond and the formation of Schiff's base between the ϵ -amino groups of gelatin protein and the aldehyde groups of the KDA brings about this change in color.

FTIR spectroscopy was used to confirm the interactions between gelatin and KDA. Figure 4c shows the FTIR spectra of neat gelatin film and KDA incorporated crosslinked gelatin films. The FTIR spectra of all the films show peaks corresponding to gelatin functional groups (Figure 4c). The peak at $\approx 3284\text{ cm}^{-1}$ corresponds to the N–H and O–H stretching of amide A group; the peak at $\approx 1630\text{ cm}^{-1}$ arises due to the C=O stretching of the amide I group; the peak at $\approx 1540\text{ cm}^{-1}$ may be assigned to the C–N stretching and N–H bending of the amide

II group; the peak at 1238 cm^{-1} is due to the N–H in-plane bending and C–N stretching of the amide III group; and the peak at 1033 cm^{-1} corresponds to the C–O stretching.^[39] Because of the presence of KDA, the peak intensity of the composite films at 1033 cm^{-1} is greater than that of the neat gelatin film, which may be ascribed to the C–O stretching arising from the KDA.^[40] The absence of KDA's distinctive aldehyde peak at 1733 cm^{-1} in all the composite films implies that these groups were consumed in the formation of Schiff's base, whereby crosslinking the gelatin films.^[25,41] The fingerprint peak of Schiff's base, formed by the reaction between the aldehyde and ϵ -amino groups, is generally visible around 1630 cm^{-1} . However, the C=O stretching in the amide I group of gelatin also exhibits a peak in the same region, making it difficult to discern the formation of Schiff's base.^[26] Moreover, the decreased relative intensity of the peak $\approx 1540\text{ cm}^{-1}$ of the characteristic amide II group of gelatin suggests the involvement of this group in the crosslinking reaction.^[30,39]

Furthermore, the thermal stability of the films was evaluated via thermogravimetric analysis (TGA). The TGA and DTG curves of gelatin and films crosslinked with different KDAs are given in Figure 4d; and Figure S2 (Supporting Information). Gelatin film in the absence of KDA shows maximum degradation at $320\text{ }^\circ\text{C}$. All the crosslinked films exhibit similar thermal degradation stages in the examined temperature range. The first stage of thermal degradation occurs at around $40\text{--}130\text{ }^\circ\text{C}$, which may be attributed to the evaporation of adsorbed and bound water. The second degradation step is around $\approx 260\text{ }^\circ\text{C}$, which may be assigned to the removal of glycerol and the degradation of oxidized karaya chains. The final degradation step corresponds to the degradation of gelatin molecular chains. The temperature of 50% degradation (T_{50}) was found to be $332\text{ }^\circ\text{C}$ for gelatin and $\approx 320\text{ }^\circ\text{C}$ for the other films. This may be due to the difference in the degradation temperatures (T_{max}) of karaya and gelatin. The degradation temperature of karaya is around $\approx 288\text{ }^\circ\text{C}$, while the degradation temperature of gelatin is $\approx 320\text{ }^\circ\text{C}$.^[42,43] Owing to this difference in the degradation temperatures of the two components, the thermal stability of the composite films is lower than that of neat gelatin films.

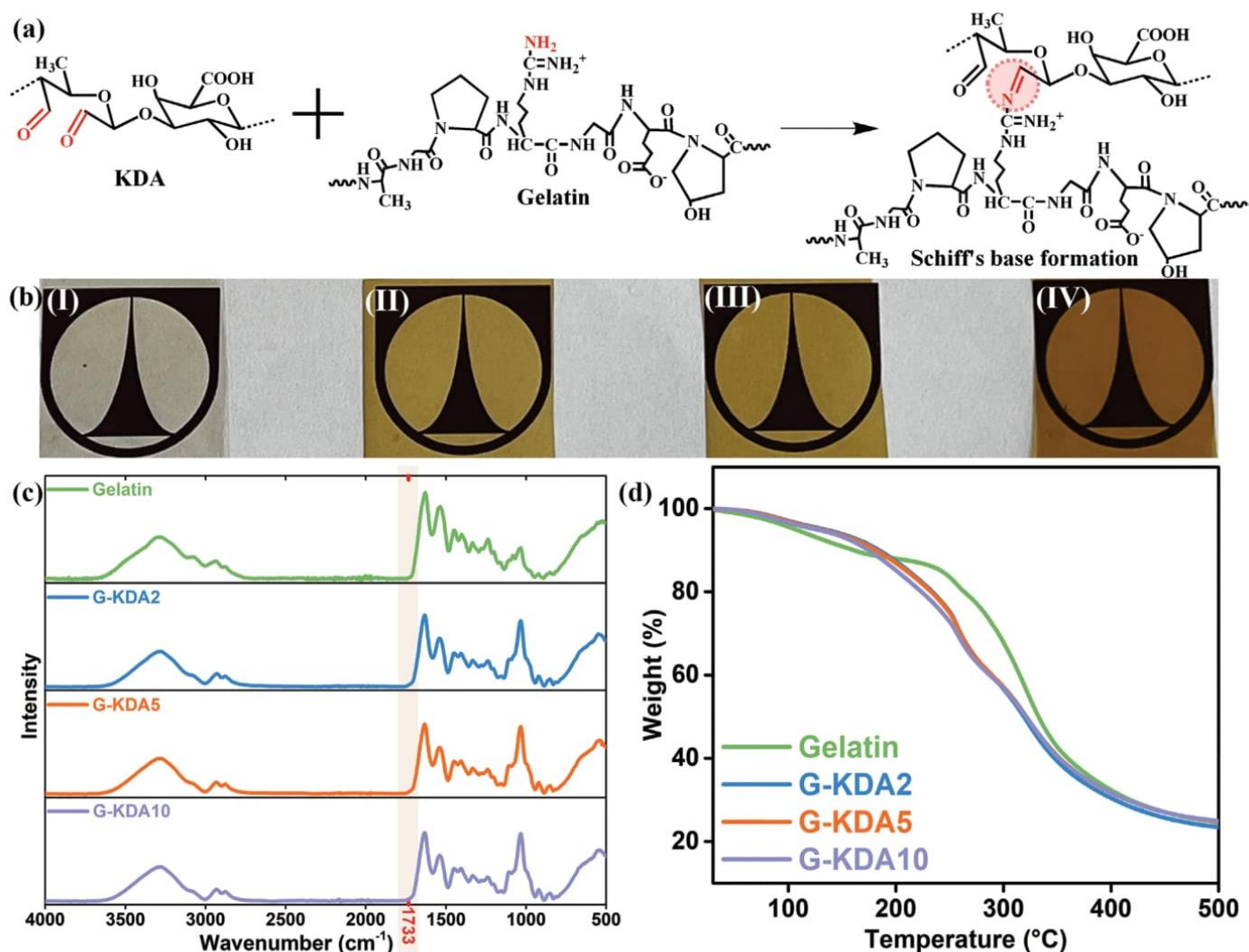


Figure 4. a) Schematic illustration of the reaction between KDA and gelatin to produce Schiff's base, b) Optical images of (I) gelatin, (II) G-KDA2, (III) G-KDA5, and (IV) G-KDA10, c) FTIR spectra of different composite films produced by crosslinking gelatin with KDA, d) TGA curves of different films.

The mechanical strength and flexibility of the packaging films are critical for ensuring safe packaging, storing, and handling of the product, which further influences the product's shelf life. The influence of the KDA incorporation and its crosslinking effect on the mechanical performance of edible gelatin films were evaluated via tensile tests, and the results are depicted in **Figure 5a**; and **Figure S4** (Supporting Information). The tensile strength (TS) of neat gelatin films plasticized with glycerol is 5.9 ± 0.7 MPa with an elongation at break (EB) value of $242 \pm 37\%$. Upon incorporation of KDA, a significant increase in the tensile strength of the films was observed. This may be attributed to the chemical crosslinking of the gelatin films by KDA. The incorporation of KDA2 resulted in the highest increase in tensile strength, with a TS value of 18 ± 1.93 , while the G-KDA5 and G-KDA10 films had TS values of 13.1 ± 2.01 , and 15 ± 2.31 , respectively. The addition of KDA to the gelatin films increased the tensile strength of the films by more than twofold. However, it was observed that the addition of KDA lowered the EB values of the films (**Figure 5b**). This suggests that the stretchability of the films was negatively affected by the crosslinking action of KDA. This is a common phenomenon observed in gelatin films

crosslinked with oxidized polysaccharides.^[24,25] Furthermore, it is also worth mentioning that no positive correlation was observed between the oxidation degree and the TS of the films (**Figure 5b**). A significant increase in the TS was observed after crosslinking gelatin with KDA with a lower oxidation degree of 31.5%. However, as the oxidation degree increased, a decrease in the TS was observed. This may be due to the different types of crosslinks formed in edible films. It is well known that SP oxidation reduces the length of the polysaccharide chains as well as the molecular weight of the dialdehyde modified product.^[44] This change in chain length gives rise to different types of crosslinks. This is supported by the crosslinking index calculated by the ninhydrin assay (**Figure S3**, Supporting Information). It was observed that as the molecular weight of the KDA decreased, the crosslinking degree of the film increased. This is due to the increase in the diffusion coefficient of the low molecular weight of KDA, which allows for more crosslinks between the gelatin chains. KDA with a low oxidation degree has more extended and flexible chains, allowing for long-range crosslinking between gelatin molecules. By connecting more gelatin molecules while maintaining extended gaps between

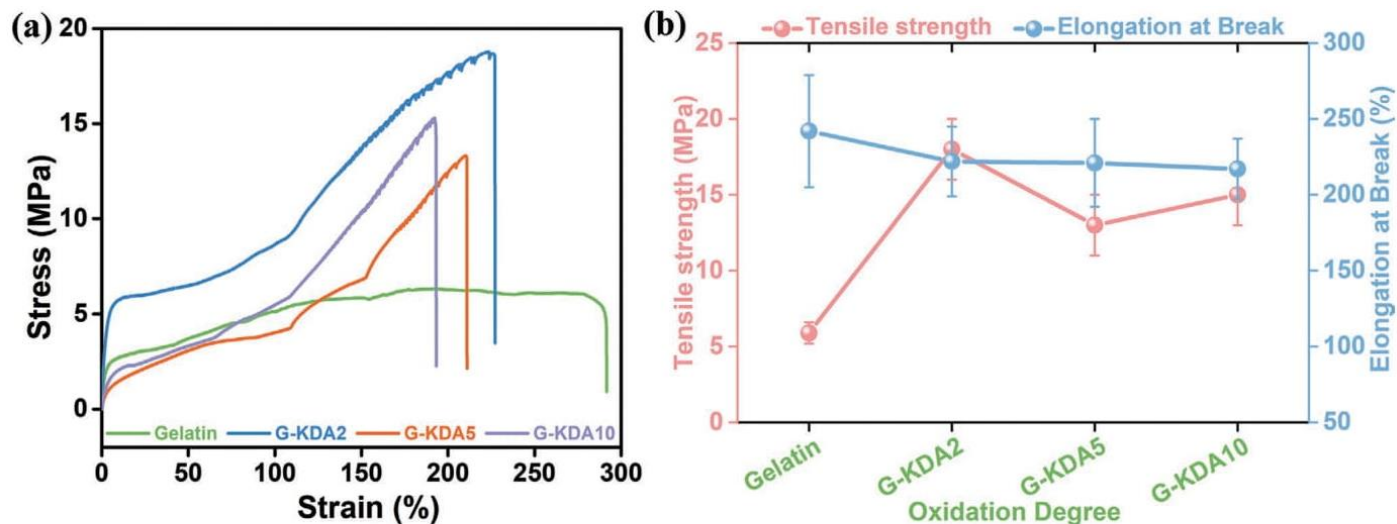


Figure 5. Mechanical properties of the edible films. a) Stress–strain curves of different films, b) Influence of the incorporation of KDA with varying degrees of oxidation on the mechanical performance of edible gelatin films.

crosslinking sites, this long-range crosslinking generates an optimum network between KDA and gelatin with improved characteristics. In contrast, KDA with a higher oxidation degree has shorter chain lengths, which leads to short-range crosslinks, resulting in a poor network and crosslinking. Similar observations were made previously when using crosslinking agents with different molecular weights.^[25,45]

Oxygen, as is widely known, may induce food oxidation, affecting a variety of food characteristics, such as odor, color, flavor, and nutritional content. The ability of the packaging film to prevent oxidation or deterioration of a product is a key parameter that influences the quality of the finished product and the shelf life of the food. Therefore, it is crucial to evaluate the oxygen barrier (OB) properties of the films. Prior to the measurement, the edible films were conditioned at 50% and 75% relative humidity (RH) at 23 °C. Since the biopolymeric films are sensitive to humidity levels, the oxygen transmission rates (OTR) were evaluated at two different RH (Figure 6a). In addition, the OTR values were converted into oxygen permeability (OP) values, which take the thickness of the films into account, enabling a more reasonable assessment of the OB characteris-

tics (Figure 6b). Overall, the KDA crosslinked films exhibited higher OB properties than the neat gelatin film. This increase in the OB values may be attributed to the development of chemical crosslinks between gelatin protein chains and KDA, which creates a compact film structure slowing oxygen permeability through the film. The OB properties of the films were considerably reduced when the RH was raised to 75%. This is a typical phenomenon with biopolymer films owing to their affinity to moisture and its subsequent plasticizing effect and increased gas permeation.^[46,47] Due to its optimal networking produced by long-range crosslinks, G-KDA2 exhibits superior OB properties to G-KDA5 and G-KDA10 at both 50% and 75% RH. This accentuates the effect of crosslinking in terms of the film barrier characteristics.^[48] The water vapor transmission rates (WVTR) of the films follow a similar pattern to the OB characteristics (Figure S5, Supporting Information). At 50% RH, G-KDA2 demonstrated lower WVTR values than the other films. However, at 75% RH, there was no positive correlation between the WVTR values of the films. This may be due to the higher sensitivity of the biopolymer films to water vapor and humidity, resulting in a considerable loss of water vapor barrier characteristics.

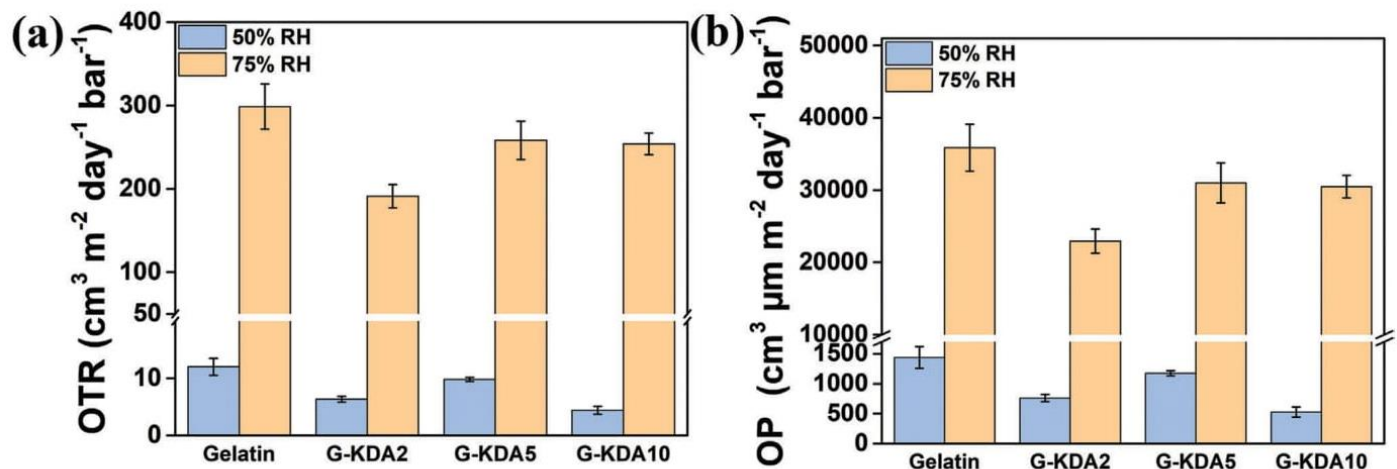


Figure 6. Barrier properties of the edible films. a) Oxygen transmission rate, and b) Oxygen permeability.

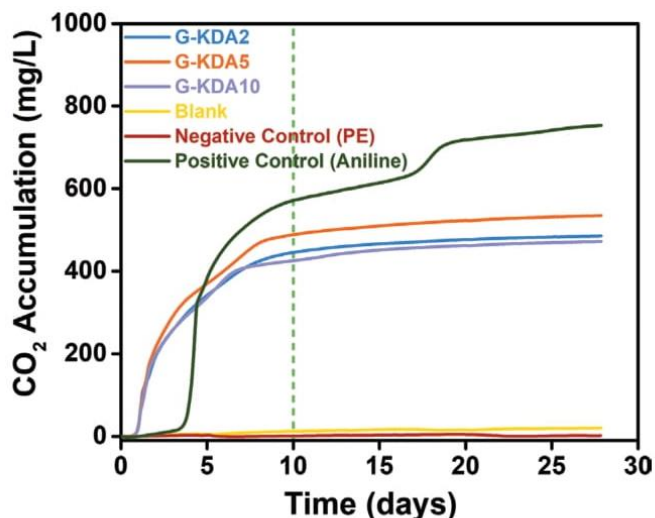


Figure 7. Biodegradation of the edible films represented by CO₂ accumulation as a function of time.

The edible films were tested for biodegradation using the ISO 14 851:1999 European standard technique, with aniline as a positive control and polyethylene as a negative control. One of the key characteristics that distinguish edible films is their inherent biodegradability. In this study, the influence of gelatin and KDA crosslinking on the biodegradation of the otherwise inherently biodegradable materials was analyzed under aerobic conditions. Gelatin is an animal-sourced protein material composed of oligopeptides, and karaya is a tree-sourced polysaccharide, both of which are inherently biodegradable.^[29,49] In the presence of oxygen, microbes break down the material into smaller molecules, which are then subsequently converted to carbon dioxide through metabolic or enzymatic processes. It is possible to assess the material's biodegradability under aerobic conditions by monitoring the carbon dioxide (CO₂) generated during the degradation process. **Figure 7** shows the evolution of CO₂ during the biodegradation test period of the samples, which correlates to the biodegradation rate. It is evident from the results that all the samples exhibit biodegradation with a short incubation time (<1 day). The CO₂ buildup pattern indicates that the biodegradation rate increases rapidly at the start of the test, which is associated with the abundant availability of nutrients in the form of organic materials. The microbes assimilate these organic resources and multiply while generating large quantities of CO₂. However, as time progresses, the CO₂ accumulation plateaus, suggesting the depletion of the resources and completion of degradation. It is worth noting that all the samples are entirely biodegraded within ten days of the test period, indicating excellent biodegradability. This suggests that even after crosslinking, the films retain the biodegradability of their individual components.

3. Conclusions

This work elucidates the development of eco-friendly biopolymer edible films based on gelatin and GK. GK was oxidized with SP to obtain KDA containing aldehyde groups,

which was then used as a “green” crosslinking agent for gelatin. Through the formation of Schiff's base, the resulting crosslinked structure improved the stability of the films. The enhanced compaction of gelatin protein chains induced by crosslinking resulted in a substantial improvement in the mechanical properties of the films. The mechanical characteristics were also found to be dependent on the degree of oxidation. Furthermore, crosslinking with KDA also improved the oxygen barrier characteristics of the gelatin films. Despite the crosslinking, the materials retained their inherent biodegradability and were found to degrade entirely within ten days. The obtained results highlight GK as a sustainable green alternative for crosslinking edible gelatin films.

4. Experimental Section

Materials: Partially acetylated GK with M_w of $\approx 9.5 \times 10^6$ g mol⁻¹ was procured from Sigma-Aldrich. Deacetylation of GK was performed following a procedure previously reported.^[50] Gelatin (bovine skin, Type B), sodium periodate, hydroxylamine hydrochloride (99%), glycerol, and other analytical grade chemicals were obtained from Sigma-Aldrich.

Dialdehyde Modification of GK: Dialdehyde modification of deacetylated GK was performed using different concentrations of sodium periodate. Briefly, 1 g of deacetylated GK was dissolved in 80 mL of distilled water. Then, 20 mL of a SP solution of different concentrations (25, 50, and 100 wt% of GK) was added to this solution, followed by adjusting the pH of the reaction mixture to 4 using 1 M sulfuric acid. The reaction mixture was heated to 40 °C and stirred continuously in the dark for 4 h. The obtained product was dialyzed against distilled water for 5 days. The dialyzed solution was then frozen overnight and lyophilized to obtain dialdehyde modified GK (KDA). The obtained products were denoted as KDA2, KDA5, and KDA10, corresponding to the SP concentrations of 25, 50, and 100 wt%, respectively.

Oxidation Degree of KDA: The oxidation degree of KDA was determined employing the hydroxylamine hydrochloride titration method.^[26] The process involves the conversion of KDA to oxime via the reaction of Schiff's base with hydroxylamine hydrochloride. The procedure involved the dissolution of a 0.1 g KDA sample in 25 mL of 0.25 M hydroxylamine hydrochloride solution, and the released hydrochloric acid was titrated against 0.1 M NaOH. Methyl orange (0.1%), which changes color from red to yellow at the endpoint, was used as an indicator. Titration was performed in triplicates. The aldehyde content was calculated using the following equation

$$\text{Degree of oxidation (\%)} = \frac{C_{\text{NaOH}}(V_{\text{sample}} - V_{\text{blank}}) \times M_{\text{GK}}}{m} \times 100 \quad (1)$$

where C_{NaOH} is the concentration of NaOH = 0.1 mol L⁻¹, $V_{\text{sample}} - V_{\text{blank}}$ is the volume of NaOH consumed (L), M_{GK} is the approximate molecular weight of the GK repeating unit, and m is the dry weight of the KDA sample (g).

Preparation of KDA Crosslinked Gelatin Films: A gelatin solution (3 w/v%) was prepared by dissolving gelatin in distilled water at 50 °C under constant stirring for 30 min. After complete dissolution, glycerol (25 wt% of gelatin) was added to the solution and stirring continued for 30 min. Simultaneously, the KDA solution was prepared by dissolving KDA in distilled water at 70 °C under vigorous stirring. Finally, the two solutions were mixed in a 5:1 (gelatin: KDA) weight ratio and continued stirring for 1 h. The film-forming solution was then poured onto polystyrene petri dishes and dried in an oven at 60 °C for 12 h. The films were peeled off the petri dishes and placed in zipper storage bags for further use. The films prepared using KDA2, KDA5, and KDA10 were denoted as G-KDA2, G-KDA5, G-KDA10, respectively. A neat gelatin control film was prepared using the same procedure without the addition of KDA.

Characterization Techniques: Attenuated total reflection Fourier transform infrared spectroscopy (ATR-FTIR, Nicolet IZ10, Thermo Scientific, USA) with a multireflection, variable angle, and horizontal ATR accessory was used to examine the functional groups of the obtained materials at a resolution of 4 cm⁻¹. A thermogravimetric analyzer (TGA-4000, PerkinElmer, USA) was used to determine the thermal stability of the materials at temperatures ranging from 30 to 500 °C at a heating rate of 10 °C min⁻¹. To ensure an inert atmosphere, the samples (≈5 mg) were analyzed in a nitrogen atmosphere at a flow rate of 50 mL min⁻¹. Solid-state NMR (JEOL 400YH, Japan) was used to analyze the samples, utilizing ¹³C CP-MAS NMR techniques with 9216 scans and analyzed using Delta v6.0 software. The spectra were referenced with the external standard γ -glycine (δ 174.1), and intensities normalized to the signal from -CH₃ within the samples. GPC measurements were performed on the Dionex Ultimate 3000 system with an LPG-3400SD quaternary gradient pump. An Agilent 1260 infinity II MDS RALS/LALS detector was used for light scattering detection. A Varian 385-LC detector was used for ELSD detection. A Shodex Asahipak GF-7M HQ column with a particle size of 9 μ m, pore size of 10⁴ Å, length of 300 mm, and internal diameter of 7.5 mm was used to determine the molecular weight. The mobile phase (200 \times 10⁻³ M ammonium acetate in 3% acetonitrile) flow rate was maintained at 0.6 mL min⁻¹, and the column temperature was kept at 35 °C. The sample injection volume was 30 μ L. Shodex P-82 pullulan standards of the molecular weights 800, 400, and 200 kDa were used to calibrate the column.

A Ninhydrin assay was used to determine the degree of crosslinking by estimating the percentage of free amino groups present in the samples.^[51] Briefly, 5 mg of the film was rehydrated in distilled water, followed by the addition of 1 mL of ninhydrin solution. This solution was heated at 100 °C for 30 min. The solution was then cooled to room temperature and diluted using 50% v/v ethanol. The absorbance of these solutions was measured on an Ultraviolet–visible spectrometer (UV–Vis; Hach Lange DR 3900) with matching at 570 nm. The crosslinking index was calculated using the following equation^[52]

$$\text{Crosslinking index \%} = \left(1 - \frac{\text{Absorbance of films}}{\text{Absorbance of pure gelatin film}} \right) \times 100 \quad (2)$$

The mechanical performance was determined by stress-strain testing on a Zwick/Roell BT1-FR 0.5TND14. The samples were cut to a size of 3 \times 30 mm². The thickness of each sample was measured with a Mitutoyo Series 293 (0–25 mm) digital micrometer. The samples were conditioned at 23 °C for 24 h before testing. The samples were tested at a speed of 10 mm min⁻¹ with a pristine gauge length of 10 mm. The slope of the linear region of the stress–strain curves was used to calculate the elastic modulus. All samples were measured seven times, and the statistical average is reported as the result.

The OTR were measured using a Mocon OX-TRAN 2/21 instrument, with a lower detection limit of 0.05 cm³ m⁻² day⁻¹ bar⁻¹. Pure oxygen (>99.95%, Linde Sauerstoff 3.5) was used as the permeant gas, with a carrier gas comprising 98% nitrogen and 2% hydrogen. The barrier properties were analyzed at a temperature of 23 °C and 50% and 75% RH. A Mocon PERMATRAN-W 3/33 instrument (0.5 g m⁻² day⁻¹ lower detection limit) was used to determine the WVTR.

The biodegradability of the films was assessed under aerobic conditions according to the European standard technique based on ISO 14 851:1999, as reported previously.^[46] Activated sludge obtained from the Liberec wastewater treatment plant at a concentration of 4.7 g L⁻¹ and 100 000 CFU was used as an inoculum. The test was conducted for 28 days in a 250 mL respiration cell with preweighed samples added to a mixture of 95 mL of a medium and 5 mL of the inoculum. The medium was made up of four different solutions. Solution 1 was a mixture of KH₂PO₄ (8.5 g L⁻¹), K₂HPO₄ (21.75 g L⁻¹), Na₂HPO₄·2H₂O (33.4 g L⁻¹), and NH₄Cl (0.5 g L⁻¹) with a pH of 7.4. Solutions 2, 3, and 4 consisted of MgSO₄·7H₂O (22.5 g L⁻¹), CaCl₂·2H₂O (36.4 g L⁻¹), and FeCl₃·6H₂O (0.25 g L⁻¹), respectively. A total of 10 mL of solution 1 and 1 mL each of solutions 2, 3, and 4 was added to 500 mL of distilled water and made up to 1000 mL. A Micro-Oxymax respirometer (Columbus Instruments

International, USA) with a paramagnetic oxygen sensor was utilized for the measurements.

Supporting Information

Supporting Information is available from the Wiley Online Library or from the author.

Acknowledgements

The authors would like to acknowledge the assistance provided by the Research Infrastructure NanoEnvicZ (Project No. LM2018124) and the “Inter Excellence Action Programme” within the framework of the project “Bio-Based Porous 2D Membranes and 3D Sponges Based on Functionalized Tree Gum Polysaccharides and their Environmental Application” (registration number LTAUSA19091) — TUL internal No.: 18309/136, supported by the Ministry of Education, Youth and Sports of the Czech Republic. The Ministry of Education, Youth and Sports of the Czech Republic and the European Union — European Structural and Investment Funds also supported this work in the framework of the Operational Programme Research, Development and Education — Project Hybrid Materials for Hierarchical Structures (HyHi, Reg. No. CZ.02.1.01/0.0/0.0/16_019/0000843). The authors would like to thank Dr. Christopher Hobbs for measuring ¹³C CP-MAS NMR of aldehyde derivatives of gum karaya.

Conflict of Interest

The authors declare no conflict of interest.

Data Availability Statement

Research data are not shared.

Keywords

biodegradable, dialdehyde modification, edible films, gelatin, karaya, natural crosslinkers, tree gum

Received: October 30, 2021

Revised: January 26, 2022

Published online:

- [1] Y. Liu, S. Ahmed, D. E. Sameen, Y. Wang, R. Lu, J. Dai, S. Li, W. Qin, *Trends Food Sci. Technol.* **2021**, *112*, 532.
- [2] L. Marangoni Júnior, R. P. Vieira, E. Jamróz, C. A. R. Anjos, *Carbohydr. Polym.* **2021**, *252*, 117221.
- [3] Y. Pei, L. Wang, K. Tang, D. L. Kaplan, *Adv. Funct. Mater.* **2021**, *31*, 2008552.
- [4] N. Attias, M. Reid, S. C. Mijowska, I. Dobryden, M. Isaksson, B. Pokroy, Y. J. Grobman, T. Abitbol, *Adv. Sustainable Syst.* **2021**, *5*, 2000196.
- [5] A. Nag, M. A. Ali, H. Kawaguchi, S. Saito, Y. Kawasaki, S. Miyazaki, H. Kawamoto, D. T. N. Adi, K. Yoshihara, S. Masuo, Y. Katsuyama, A. Kondo, C. Ogino, N. Takaya, T. Kaneko, Y. Ohnishi, *Adv. Sustainable Syst.* **2021**, *5*, 2000193.

- [6] S. Gopalakrishnan, J. Xu, F. Zhong, V. M. Rotello, *Adv. Sustainable Syst.* **2021**, 5, 2000167.
- [7] Z. Wang, L. Tang, F. Lin, Y. Shen, Y. Chen, X. Chen, B. Huang, B. Lu, *Adv. Sustainable Syst.* **2020**, 4, 2000043.
- [8] V. Mihalca, A. D. Kerezi, A. Weber, C. Gruber-Traub, J. Schmucker, D. C. Vodnar, F. V. Dulf, S. A. Socaci, A. Fărcaș, C. I. Mureșan, R. Suharoschi, O. L. Pop, *Polymers* **2021**, 13, 769.
- [9] I. F. Olawuyi, S. R. Kim, W. Y. Lee, *Carbohydr. Polym.* **2021**, 272, 118371.
- [10] W. Zhang, Y. Zhang, J. Cao, W. Jiang, *Int. J. Biol. Macromol.* **2021**, 166, 288.
- [11] A.-P. Bizymis, C. Tzia, *Crit. Rev. Food Sci. Nutr.* **2021**, 1, <https://doi.org/10.1080/10408398.2021.1934652>.
- [12] S. A. A. Mohamed, M. El-Sakhawy, M. A. M. El-Sakhawy, *Carbohydr. Polym.* **2020**, 238, 116178.
- [13] R. Zibaei, S. Hasanvand, Z. Hashami, Z. Roshandel, M. Rouhi, J. T. de Guimarães, A. M. Mortazavian, Z. Sarlak, R. Mohammadi, *Carbohydr. Polym.* **2021**, 256, 117554.
- [14] A. Lisitsyn, A. Semenova, V. Nasonova, E. Polishchuk, N. Revutskaia, I. Kozyrev, E. Kotenkova, *Polymers* **2021**, 13, 1592.
- [15] A. Khezerlou, H. Zolfaghari, S. A. Banihashemi, S. Forghani, A. Ehsani, *Polym. Adv. Technol.* **2021**, 32, 2306.
- [16] A. Yadav, N. Kumar, A. Upadhyay, Pratibha, R. K. Anurag, *Food Rev. Int.* **2021**, 1, <https://doi.org/10.1080/87559129.2021.1940198>.
- [17] S. Paidari, N. Zamindar, R. Tahergorabi, M. Kargar, S. Ezzati, N. Shirani, S. H. Musavi, *J. Food Meas. Charact.* **2021**, 15, 4205.
- [18] N. S. Said, N. K. Howell, N. Sarbon, *Food Rev. Int.* **2021**, 1, <https://doi.org/10.1080/87559129.2021.1929298>.
- [19] A. Ehrmann, *Polymers* **2021**, 13, 1973.
- [20] G. Yang, Z. Xiao, H. Long, K. Ma, J. Zhang, X. Ren, J. Zhang, *Sci. Rep.* **2018**, 8, 1616.
- [21] C. E. Campiglio, N. C. Negrini, S. Farè, L. Draghi, *Materials* **2019**, 12, 2476.
- [22] O. Moreno, J. Cárdenas, L. Atarés, A. Chiralt, *Carbohydr. Polym.* **2017**, 178, 147.
- [23] H. W. Kwak, H. Lee, S. Park, M. E. Lee, H. J. Jin, *Int. J. Biol. Macromol.* **2020**, 146, 332.
- [24] J. Guo, L. Ge, X. Li, C. Mu, D. Li, *Food Hydrocolloids* **2014**, 39, 243.
- [25] J. Liu, L. Zhang, C. Liu, X. Zheng, K. Tang, *LWT* **2021**, 138, 110607.
- [26] J. Park, J. Nam, H. Yun, H. J. Jin, H. W. Kwak, *Carbohydr. Polym.* **2021**, 254, 117317.
- [27] A. Venkateshaiah, J. Y. Cheong, S.-H. Shin, A. K. K. P., T. G. Yun, J. Bae, S. Waclawek, M. Černík, S. Agarwal, A. Greiner, V. V. T. Padil, I.-D. Kim, R. S. Varma, *Green Chem.* **2020**, 22, 1198.
- [28] V. V. T. Padil, S. Waclawek, M. Černík, R. S. Varma, *Biotechnol. Adv.* **2018**, 36, 1984.
- [29] V. Raj, J. H. Lee, J. J. Shim, J. Lee, *Carbohydr. Polym.* **2021**, 258, 117687.
- [30] B. Sarker, D. G. Papageorgiou, R. Silva, T. Zehnder, F. Gul-E-Noor, M. Bertmer, J. Kaschta, K. Chrissafis, R. Detsch, A. R. Boccaccini, *J. Mater. Chem. B* **2014**, 2, 1470.
- [31] H. Li, B. Wu, C. Mu, W. Lin, *Carbohydr. Polym.* **2011**, 84, 881.
- [32] S. C. C. C. Silva, E. M. de Araujo Braz, F. A. de Amorim Carvalho, C. A. R. de Sousa Brito, L. M. Brito, H. M. Barreto, E. C. da Silva Filho, D. A. da Silva, *Int. J. Biol. Macromol.* **2020**, 164, 606.
- [33] H. Amer, T. Nypelö, I. Sulaeva, M. Bacher, U. Henniges, A. Potthast, T. Rosenau, *Biomacromolecules* **2016**, 17, 2972.
- [34] U. J. Kim, S. Kuga, M. Wada, T. Okano, T. Kondo, *Biomacromolecules* **2000**, 1, 488.
- [35] H. Yang, D. Chen, T. G. M. van de Ven, *Cellulose* **2015**, 22, 1743.
- [36] J. Leguy, Y. Nishiyama, B. Jean, L. Heux, *ACS Sustainable Chem. Eng.* **2019**, 7, 412.
- [37] J. Lindh, D. O. Carlsson, M. Strømme, A. Mihranyan, *Biomacromolecules* **2014**, 15, 1928.
- [38] C. Mo, L. Xiang, Y. Chen, *Macromol. Rapid Commun.* **2021**, 42, 2100025.
- [39] L. Zhang, J. Liu, X. Zheng, A. Zhang, X. Zhang, K. Tang, *Carbohydr. Polym.* **2019**, 216, 45.
- [40] Y. Jiang, G. Li, J. Liu, M. Li, Q. Li, K. Tang, *ACS Appl. Bio Mater.* **2021**, 4, 1536.
- [41] G. Li, Y. Jiang, M. Li, W. Zhang, Q. Li, K. Tang, *Int. J. Biol. Macromol.* **2021**, 168, 233.
- [42] L. Wang, L. Lin, Y. Guo, J. Long, R. J. Mu, J. Pang, *Food Hydrocolloids* **2020**, 108, 105863.
- [43] A. Venkateshaiah, J. Y. Cheong, C. Habel, S. Waclawek, T. Lederer, M. Černík, I.-D. Kim, V. V. T. Padil, S. Agarwal, *ACS Appl. Nano Mater.* **2020**, 3, 633.
- [44] T. Nypelö, B. Berke, S. Spirk, J. A. Sirviö, *Carbohydr. Polym.* **2021**, 252, 117105.
- [45] J. Liu, E. Brown, C.-K. Liu, Tang, *J. Am. Leather Chem. Assoc.* **2018**, 113, 96.
- [46] A. Venkateshaiah, K. Havlíček, R. L. Timmins, M. Röhr, S. Waclawek, N. H. A. Nguyen, M. Černík, V. V. T. Padil, S. Agarwal, *Carbohydr. Polym.* **2021**, 266, 118126.
- [47] J. Wang, D. J. Gardner, N. M. Stark, D. W. Bousfield, M. Tajvidi, Z. Cai, *ACS Sustainable Chem. Eng.* **2018**, 6, 49.
- [48] F. Garavand, M. Rouhi, S. H. Razavi, I. Cacciotti, R. Mohammadi, *Int. J. Biol. Macromol.* **2017**, 104, 687.
- [49] M. Held, A. Pichler, J. Chabeda, N. Lam, P. Hindenberg, C. Romero-Nieto, G. Hernandez-Sosa, *Adv. Sustainable Syst.* <https://doi.org/10.1002/adsu.202100035>.
- [50] V. V. T. Padil, C. Senan, S. Waclawek, M. Černík, *Int. J. Biol. Macromol.* **2016**, 91, 299.
- [51] J. M. Zatorski, A. N. Montalbina, J. E. Ortiz-Cárdenas, R. R. Pompano, *Anal. Bioanal. Chem.* **2020**, 412, 6211.
- [52] S. Kim, D. Jeong, H. Lee, D. Kim, S. Jung, *Int. J. Biol. Macromol.* **2020**, 149, 281.

3.5. Recycling non-food-grade tree gum wastes into nanoporous carbon for sustainable energy harvesting

Abstract: The disposal of natural wastes has become a global problem and the use of lower-grade gums is very limited owing to their impurities as well as sticky nature. Rather than disposing these wastes, nanoporous carbon (nC) has instead been synthesized by carbonization and exfoliation. The synthesized nC exhibits a substantially high surface area along with abundant micro/mesopores. This desirable and useful nature of nC is well-suited for water-driven effective electrical energy conversion, which enables the fast evaporation of water via a capillary action through nanopores. Under asymmetric wetting in a water container and ambient conditions, the nC-based energy harvesters showed high capability of electricity production and reliable output generation, easily turning on a blue light-emitting diode (2.5 V and 20 mA) using a stored power source. In summary, many energy harvesters can be manufactured for the scale-up of electricity, and the suitability of regenerated carbon nanomaterials for green energy harvesting can contribute toward alleviating chronic environmental issues.

Citation: **Abhilash Venkateshaiah**, Jun Young Cheong, Sung-Ho Shin, Akshay Kumar K. P, Tae Gwang Yun, Jaehyeong Bae, Stanislaw Waclawek, et al. **“Recycling Non-Food-Grade Tree Gum Wastes into Nanoporous Carbon for Sustainable Energy Harvester.”** *Green Chemistry* 22 (4): 1198–1208 [2020]



Cite this: DOI: 10.1039/c9gc04310a

Recycling non-food-grade tree gum wastes into nanoporous carbon for sustainable energy harvesting†

Abhilash Venkateshaiah,^{‡a} Jun Young Cheong,^{‡b} Sung-Ho Shin,^{‡b} K. P. Akshaykumar,^c Tae Gwang Yun,^b Jaehyeong Bae,^{id b} Stanisław Wacławek,^{id a} Miroslav Černík,^a Seema Agarwal,^{id d} Andreas Greiner,^{id d} Vinod V. T. Padil,^{id *a} Il-Doo Kim^{id *b} and Rajender S. Varma^{id *e}

The disposal of natural wastes has become a global problem and the use of lower-grade gums is very limited owing to their impurities as well as sticky nature. Rather than disposing these wastes, nanoporous carbon (nC) has instead been synthesized by carbonization and exfoliation. The synthesized nC exhibits a substantially high surface area along with abundant micro/mesopores. This desirable and useful nature of nC is well-suited for water-driven effective electrical energy conversion, which enables the fast evaporation of water *via* a capillary action through nanopores. Under asymmetric wetting in a water container and ambient conditions, the nC-based energy harvesters showed high capability of electricity production and reliable output generation, easily turning on a blue light-emitting diode (2.5 V and 20 mA) using a stored power source. In summary, many energy harvesters can be manufactured for the scale-up of electricity, and the suitability of regenerated carbon nanomaterials for green energy harvesting can contribute toward alleviating chronic environmental issues.

Received 17th December 2019,
Accepted 22nd January 2020

DOI: 10.1039/c9gc04310a

rsc.li/greenchem

Introduction

Polysaccharides isolated from tree exudates, seeds and seaweeds and from microbial origin are a class of biomaterials garnering prominent research interest. These natural biopolymers are well established in food and pharmaceutical industries as stabilizing, suspending, gelling, emulsifying, binding, thickening and coating agents.^{1,2} Amongst various biomaterials, many naturally derived gums are modified to tailor their properties for controlled drug delivery, tissue reconstruction,

pH-sensitive hydrogels, and biosorbents for heavy metals.^{1,3,4} In all the aforementioned applications, however, the utilized gums are only of higher grade with better purity and the lower grade contaminated gums often end up being discarded, thus increasing waste biomass. Nowadays, owing to rising environmental concerns, there is a need for utilizing this biomass waste to generate beneficial products with potential end-use applications. In particular, the synthesis of carbon-based materials from zero-value waste biomass is a new area of focus and swiftly gaining precedence as these low-value materials often possess a high carbon content. Recently, a number of results have been reported that utilize various agricultural residues and sea food wastes for functional applications.⁵ Waste biomass including lignin,⁶ rice husk,⁷ and wheat straws⁸ has been used in the synthesis of carbonaceous materials. The ensuing carbon materials from waste biomass have found their applications in environmental remediation,^{9,10} catalysis,¹¹ energy storage,¹² and electrochemical energy storage and sensors.^{13,14} By designing a suitable scalable process, it is possible to exploit these undervalued discarded waste materials.

Compared with other bio-wastes, gum wastes [Grade II and III types of gum arabic (GA), guar gum (GG), gum karaya (GK)] present significant problems as they are viscous and readily attach to various substrates and powders unlike other bio-

^aDepartment of Nanomaterials in Natural Sciences, Institute for Nanomaterials, Advanced Technologies and Innovation (CXI), Technical University of Liberec (TUL), Studencká 1402/2, Liberec 1, 461 17, Czech Republic. E-mail: vinod.padil@tul.cz

^bDepartment of Materials Science and Engineering, Korea Advanced Institute of Science and Technology, 291 Daehak-ro, Yuseong-gu, Daejeon 34141, Republic of Korea. E-mail: idkim@kaist.ac.kr

^cCentral European Institute of Technology, Brno University of Technology, Purkyňova 123, 613 00 Brno, Czech Republic

^dMacromolecular Chemistry II, University of Bayreuth, Universitatstraße 30, 95447 Bayreuth, Germany

^eRegional Centre of Advanced Technologies and Materials, Department of Physical Chemistry, Faculty of Science, Palacký University in Olomouc, Šlechtitelů 27, 783 71 Olomouc, Czech Republic. E-mail: Varma.Rajender@epa.gov

†Electronic supplementary information (ESI) available. See DOI: 10.1039/c9gc04310a

‡These authors contributed equally to this work.

wastes that can be decomposed in a controlled fashion. Moreover, these gum wastes cannot be used for food and pharmaceutical applications due to their highly acidic nature, and they are disposed as bio-wastes of no commercial value. On the other hand, there are significant merits in utilizing low-grade gum wastes (both grade II and grade III): the inherent presence of carbon-rich substances can be exploited in the presence of metal impurities that can be co-doped to fabricate carbon-based materials. These gum wastes possess multi-branched structures with enhanced physicochemical and mechanical properties, which can be adopted for various potential applications. Therefore, it is an enticing strategy to develop a facile and general synthetic process to recycle these gum wastes for functional use rather than perpetually throwing the wastes in already overburdened disposal sites.

In this work, we have successfully developed a generalized synthetic method to fabricate nanoporous carbon (nC) by heat treatment and exfoliation. This method is highly versatile and applicable to a wide variety of lower-grade gums (GA, GG, and GK) and a commercial xanthan gum (XG), which were all transformed into nC with high surface area and pore volume. In view of their abundant micropores and mesopores, assisting in the fast ion transport kinetics with low-resistance pathways and short ion channels, they can be deployed for various applications, including energy harvesting that generates power. The nC-based fabricated energy harvesters have shown the capability of generating an output voltage of ~ 0.4 V and current of ~ 3 μ A attributed to the capillary action through the nanopores in nC. The charged power source from the nC-based energy harvester was demonstrated to turn on a commercial blue LED with an operation voltage of 2.5 V. Moreover, such energy harvester device can be scaled up, being capable of turning on objects requiring higher voltages and currents, such as a university logo.

Experimental section

Materials

Isopropanol, potassium hydroxide (KOH), hydrochloric acid (35 wt%), and sulfuric acid (96 wt%) were purchased from Penta, Czech Republic. Distilled water was obtained by an ELGA purelab flex system (ELGA, Veolia Water, Marlow, UK). Gum samples of different types (grades II and III), such as gum arabic (GA), gum karaya (GK), guar gum (GG), were procured from the Girijan Cooperative society (GCC), Hyderabad, India. These gums are non-edible tree gums that are usually considered as waste biomaterials, which were labeled as Grade II and III, respectively. Xanthan gum, a commercial gum, was obtained from Sigma-Aldrich. Poly(acrylic acid) (PAA) and carboxymethyl cellulose (CMC) were purchased from Sigma Aldrich.

Synthesis of nC

Lower grade gums (such as GA, GK and GG), procured as bio-waste, were cleaned by washing thoroughly with distilled water

to remove any dirt and impurities. In addition to tree-based gums (GA, GK and GG – all are Grade II and III), a commercial xanthan gum from bacteria has been used to make nC. These gums were then dried overnight at 80 °C to remove residual water and moisture. The dried gums were then powdered in a high-speed mechanical blender followed by sieving (mesh size – 250 μ m) to obtain a fine sample. The powdered samples were then pyrolyzed in a furnace at 800 °C under a nitrogen atmosphere for a period of 2 h at a heating rate of 3 °C min^{-1} . This yielded a carbonized product, which was then washed with isopropanol followed by distilled water to remove any organic impurities. The carbonized product was further mixed homogeneously with KOH in a ratio of 1 : 3 by weight using a mortar and pestle. The mixture was again heated to 800 °C in a furnace under nitrogen atmosphere for 1 h at a heating rate of 5 °C min^{-1} . The resulting product was washed with 1 : 1 HCl solution to remove any residual KOH, and again washed with distilled water to neutralize the product. Furthermore, the product was dried at 80 °C overnight. The exfoliation of the final product was accomplished in 10% H_2SO_4 solution using a probe sonicator. The exfoliation was carried out for 1 h with a pulse “on” and “off” time of 5 seconds with a power of 25 W. The solution was placed in an ice bath to reduce the heat generated during the process. The final product was washed several times with distilled water to attain neutrality followed by drying overnight at 80 °C. The micro/mesoporous renewable carbons obtained were generally called nanoporous carbon (nC). The carbon obtained from Gum Arabic, Gum Guar, Gum Karaya, Gum Xanthan were denoted by GAnC (Gum Arabic Nanoporous Carbon), GGnC (Gum Guar Nanoporous Carbon), GKnC (Gum Karaya Nanoporous Carbon), and XGnC (Gum Xanthan Nanoporous Carbon), respectively.

Characterizations

Fourier transform infrared spectroscopy (FTIR) was carried out on a NICOLET IZ10, Thermo Scientific, USA, Attenuated total – reflection Fourier transform infrared spectroscope (ATR-FTIR) employing a germanium ATR crystal provided with a 45° single reflection angle horizontal ATR accessory. Raman spectroscopy was performed on a Raman DXR microscope, Thermo Fisher Scientific, USA, at a laser excitation wavelength of 514 nm from an Argon laser with 1 cm^{-1} spectral resolution. The surface area and pore volumes of the samples were determined by nitrogen adsorption–desorption analysis on a Quantachrome Instruments NOVA3200 analyzer using NovaWin software, 5 points of Brunauer–Emmett–Teller (BET) analysis for the total surface area, and a nonlocal density functional theory (NLDFT) technique for the pore size distribution. The samples were degassed at liquid nitrogen temperature for 15 h prior to measurement. The sample surface morphology and the elemental composition were assessed on a UHR FE-SEM instrument (Carl Zeiss ULTRA Plus, Germany), operating at 0.5–2.5 kV acceleration voltage. X-ray diffraction spectroscopy was carried out on a Bruker AXS/8 instrument (Berlin, Germany), and the diffraction spectra were obtained using $\text{Cu-K}\alpha$ radiation (40 kV, 60 mA). The XPS analysis was carried out

using a PHI VersaProbe III scanning XPS microprobe (Kanagawa, 253-8522, Japan).

Dye adsorption tests

The dye adsorption studies were carried out on an anionic dye (methyl orange) and a cationic dye (methylene blue). The adsorption experiments were performed in 25 ml glass vials under ambient conditions. The vials were filled with dye solutions such that the final concentration was 50 mg L^{-1} , to which 0.1 g L^{-1} of nCs was added. At the specified time intervals, 1.5 ml of the solution was taken and centrifuged at 14 000 rpm for 3 min to separate the solid and liquid phase. The supernatant was then diluted and analyzed for dye adsorption in a UV-Vis spectrophotometer (Hach Lange DR 3900) with 1 cm quartz cuvettes. The adsorption of MO (methyl orange) and MB (methylene blue) were determined by measuring the absorbance at $\lambda_{\text{max}} = 464 \text{ nm}$ and $\lambda_{\text{max}} = 664 \text{ nm}$, respectively. The adsorption of the dye per unit mass of the adsorbent (q_t mg g^{-1}) was calculated using the following eqn (1):

$$q_t = (C_0 - C_t)V/m \quad (1)$$

where C_0 and C_t are the initial concentration (mg L^{-1}) and concentration at time t (mg L^{-1}), V is the volume of the dye solution, and m is the mass of the adsorbent.

The adsorption mechanism was further analyzed by utilizing the kinetic models to evaluate the experimental data. The pseudo-first-order kinetic model and the pseudo-second-order kinetic model are the most commonly used models to quantify the process of adsorption and to study their kinetics. The linear form of the pseudo-first-order kinetic model is expressed as:

$$\log(q_e - q_t) = \log(q_e) - k_1 t \quad (2)$$

where q_e is the quantity of dye adsorbed at equilibrium (mg g^{-1}), q_t is the quantity of dye adsorbed at time t (mg g^{-1}), and k_1 is the pseudo-first-order rate constant.

The pseudo-second-order kinetic model is usually expressed as:

$$t/q_t = 1/k_2 q_e^2 + t/q_e \quad (3)$$

where k_2 is the pseudo-second-order rate constant.

Preparation of energy harvesting devices and electrical tests

The energy harvesters were fabricated as follows: first, glass substrates ($25 \text{ mm} \times 75 \text{ mm}$, Sigma Aldrich) were cleaned using acetone, IPA, and DI water. Subsequently, the mixture consisting of nC (0.02 g), PAA (0.01 g), and CMC (0.01 g) in DI water was coated on the pre-cleaned glass substrates using slurry casting, followed by drying on a hot plate at $90 \text{ }^\circ\text{C}$ for 5 min. Then, the nC-coated glass was placed in a vacuum oven at $150 \text{ }^\circ\text{C}$ for 1 h to fully remove any residual flammable solvents. The low-pressure environment also minimized oxidation during the drying step. Lastly, the water-wettable hydrophilic surface of nC was formed by subjecting it to O_2 plasma treatment (O_2 , 100 sccm, 100 W, 120 s). The output voltage and

current were measured using a high resistance electrometer (Keithley 6517a). A custom-built water container was used to transfer the input water energy.

Results and discussion

Synthesis and characterizations of nC

Typically, different gums [gum Arabic (GA), Guar gum (GG), gum Karaya (GK), xanthan gum (XG)], are high molecular weight macromolecules comprising long chain monosaccharides. To start with, GA is a branched polysaccharide, which is either slightly acidic or neutral and is a mixture of calcium, magnesium and potassium salts of arabic acid. It is obtained from the exudates of *Acacia Senegal* and *Acacia seyal* trees, and has a backbone of 1,3-linked β -D-galactopyranosyl units with side chains of two to five 1,3-linked β -D-galactopyranosyl units connected to the main chain by 1,6-linkages.¹⁵ GG is a branched nonionic polysaccharide obtained from the seeds of the leguminous shrub *Cyamopsis tetragonoloba*. It consists of repeating units of galactose and mannose with straight chain mannose units joined by β -D-(1 \rightarrow 4) linkages having α -D-galactopyranose units.¹⁶ GK is a partially acetylated polysaccharide obtained from the exudates of *Sterculia urens* trees with a high molecular mass of $\sim 1.6 \times 10^6 \text{ Da}$ and under the substituted rhamnogalacturonoglycan (pectic)-type tree gums.¹⁷ GK is composed of 60% of neutral sugars, including rhamnose and galactose, along with 40% of acidic sugars like glucuronic acid and galacturonic acids.¹⁸ Moreover, XG is an anionic polysaccharide of high molecular weight obtained by aerobic submerged fermentation from *Xanthomonas campestris*. It has a backbone made of β -(1 \rightarrow 4)-D-glucopyranose glucan and side chains of [β -(1 \rightarrow 3)-mannose- α -(1 \rightarrow 2)-glucuronic acid- β -(1 \rightarrow 4)-mannose] on alternating residues.¹⁹ All these gums consist of carbon chains with various functional groups (carboxyl ($-\text{COO}^-$), hydroxyl (OH^-), ether (C-O-C), acetyl ($\text{CH}_3\text{CO}-$), aliphatic ($-\text{CH}$) and carbonyl ($-\text{C=O}$) groups), with carbon being a very rich and abundant component ($\sim 70\%$). Various factors (such as tapping time, seasonal variations, frequency of rainfall and maximum temperature) govern the gum grades at gum collection. A schematic illustration on the synthesis of various types of nC is presented in Fig. 1a. By utilizing low-grade inexpensive gum wastes, we have designed a synthesis procedure to obtain functional nC with low cost. Consequently, the strategy suggested in this work offers a simple, cost-effective, and sustainable route to fabricate the energy device utilizing tap water readily available in our living environment. Discarded gum wastes of no commercial value can be transformed into nC to generate electricity. Afterwards, nC can be disposed into the soil again to plant the gum trees (Fig. 1a). In the synthetic procedure, the gums were pre-carbonized followed by potassium hydroxide (KOH) activation in a furnace. Pre-carbonization offers certain textural advantages over the conventional one-step activation, although KOH can activate the material in a single step.^{20,21} Pre-carbonization can provide a much higher surface area and some initial nano-

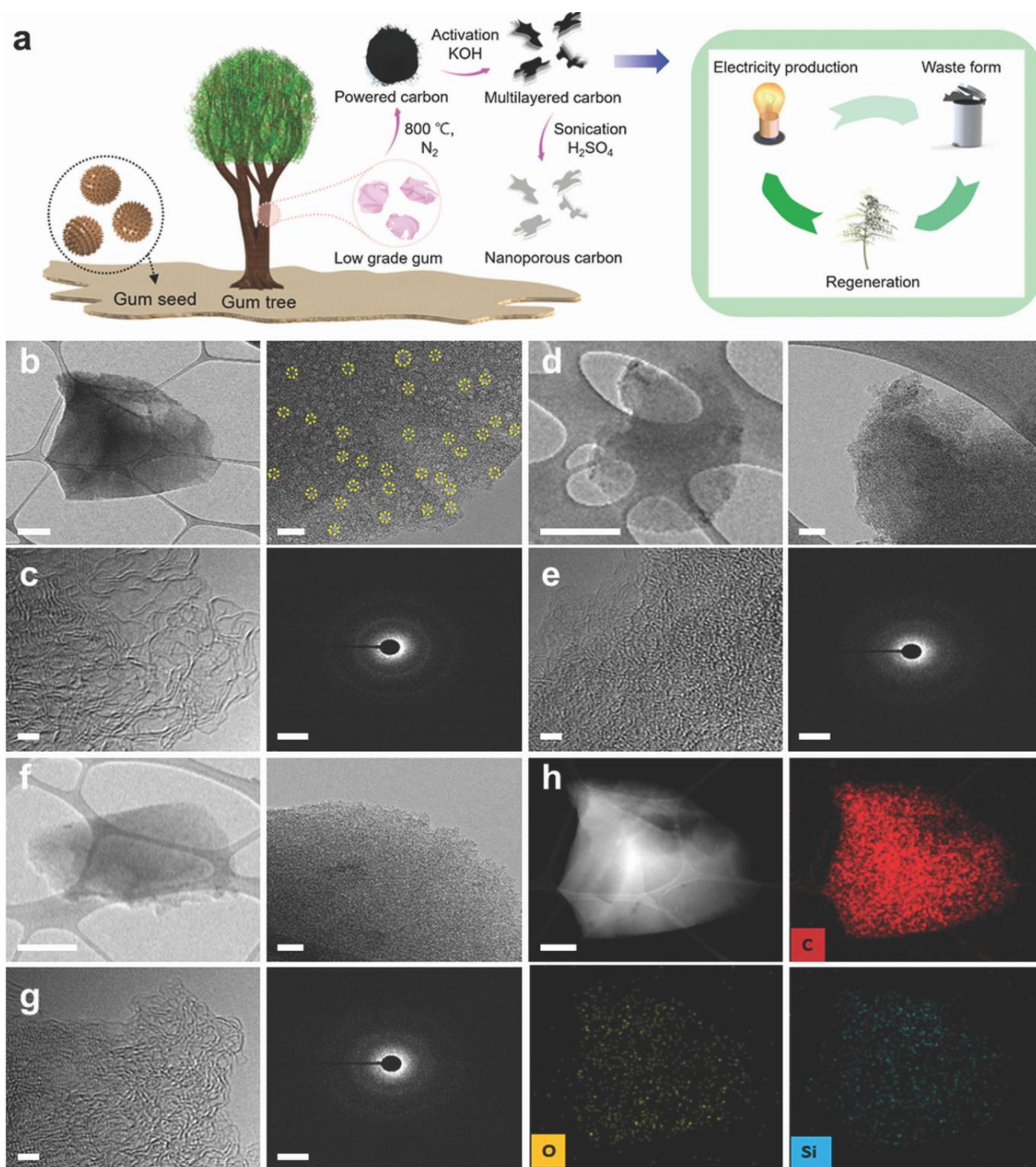


Fig. 1 (a) Schematic illustration for the synthetic process of gum-derived carbon and sustainable strategy to generate power. TEM images in low and medium magnification of (b) GAnC, (d) GGnC, and (f) GKnC. HRTEM image and SAED patterns of (c) GAnC, (e) GGnC, and (g) GKnC. (h) HAADF-STEM image and elemental mapping of GAnC. (Scale bars: (b) 1 μm , (b), (d), (f) 0.5 μm and 50 nm, (c), (e), (g) 2 nm and 5 1/nm, (h) 0.5 μm .)

pore development (mesopores and micropores), thus enabling KOH to have enhanced contact with the precursor materials, which may even penetrate into the pores.²² In addition, KOH reacts rather violently with the carbon structure and rips apart

the layers of carbon. The use of high temperature is necessary to ensure complete carbonization and activation of the sample. However, it has been observed from several studies that temperatures above 800 °C can lead to a lower yield, as

well as a lower surface area.^{20,23,24} This may likely be the result of collapsing micropores into mesopores, and eventually lead to the formation of macropores.²⁵

Aqueous exfoliation is a well-known technique to obtain graphene-like materials as they assist in the separation of carbon layers. By employing a probe sonicator, we could accelerate the aqueous exfoliation of the carbon structures in H₂SO₄, as it provides a definite power delivery into the aqueous systems better than the bath sonicators.²⁶ Exfoliation can assist in the development of a high surface area by breaking down the carbon structure, as well as the macropores. For the synthesis of a graphene-like material, 10 g of the dried gum powders was initially taken, and the final product weights and yields are tabulated in Table S1.† The morphological transitions from the pristine gum to the finalized nC is presented in Fig. S1,† and were obtained through scanning electron microscopy (SEM). As can be seen, the pristine GK sample was first carbonized, and then it was activated with KOH to form the large multilayered carbon. Through sonication, the smaller nC was successfully created. Based on the final SEM image, nC with a rough surface can be observed. The energy-dispersive X-ray spectroscopy (EDX) (Fig. S2†) results for various types of nC (nC derived from GA, GG, GK, and XG, which are designated as GAnC, GGnC, GKnC, and XGnC) revealed the presence of the abundant carbon content with some presence of oxygen. The elemental composition also revealed the presence of silicon (Si) in all nCs, except for XGnC. This can be due to the fact that the native gums contain a certain number of other elements depending on the soil where they originate from.^{27,28} Transmission electron microscopy (TEM) analysis of GAnC, GGnC, and GKnC was conducted (Fig. 1b–g), revealing a porous morphology for all samples with amorphous carbon. Fig. 1b, d and f show the typical TEM images of the nCs at two different magnifications. The TEM images reveal a highly porous light structure for the nCs, where the ‘white’ bright spots are indicative of pore sites and the black region represents the carbon matrix. The pores were uniformly distributed throughout the material, indicating a three-dimensional (3D) porous network. The presence of such 3D porous network imparts a large surface area and promotes ion storage, and thus assists in the quick penetration of electrolytes and fast ion diffusion. As for the pore structure, GGnC and GKnC show uniform microporous structure. However, the presence of mesopores can be clearly observed in GAnCs (Fig. 1b) and XGnC (Fig. S3†). High-resolution TEM (HRTEM) and the selected area diffraction (SAED) patterns of the nCs are shown in Fig. 1c, e and g, which reveal wavy layered and distorted graphitic sheets with no ordered structure. This is consistent for all nCs. In the SAED patterns of the nCs, no obvious speckles can be observed in the diffraction patterns, suggesting that they exhibit a very low degree of crystallinity and consist of predominantly amorphous regions with many defects. The high-angle annular dark field-scanning transmission electron microscopy (HAADF-STEM) and its corresponding STEM mapping were acquired to analyze the presence and distribution of different elements in the nCs (Fig. 1h and Fig. S4†),

which indicate the carbon matrix and uniform presence of oxygen and silicon throughout the material.

To confirm the carbonization process and analyze the functional groups present in the final product, Fourier-transform infrared (FT-IR) spectroscopy was used (Fig. S5 and Table S2†). All gums showed similar bands and intensities. The FT-IR spectra of GA reveal bands at 3382 cm⁻¹, 2933 cm⁻¹, 1737 cm⁻¹, 1249 cm⁻¹, and 1029 cm⁻¹, corresponding to the –OH stretch, C–H stretch, C=O stretch, C–OH and C–O–C stretching modes, respectively. The FT-IR spectra of GG reveal bands at 3384 cm⁻¹, 2938 cm⁻¹, 1735 cm⁻¹, 1261 cm⁻¹, and 1027 cm⁻¹, corresponding to the –OH stretch, C–H stretch, C=O stretch, C–OH and C–O–C stretching modes, respectively. In addition, a band at 1644 cm⁻¹ corresponds to the associated water molecule. The GK spectra show bands at 3399 cm⁻¹, 2937 cm⁻¹, 1718 cm⁻¹, 1415 cm⁻¹, 1251 cm⁻¹, and 1041 cm⁻¹, corresponding to the –OH stretch, C–H stretch, C=O stretch, C–O stretch, C–OH and C–O–C stretching modes, respectively. The XG FT-IR spectra have bands at 3380 cm⁻¹, 2938 cm⁻¹, and 1035 cm⁻¹ corresponding to the –OH stretch, C–H stretch, and C–O–C stretch, respectively. Bands at 1722 cm⁻¹ and 1608 cm⁻¹ correspond to the asymmetrical stretch of carboxylate and carbonyl group, respectively. Based on the FT-IR results, it is evident that most of these bands either disappeared or weakened, suggesting the successful carbonization of the gums. The nC sample consists of bands at ~2940 cm⁻¹, ~1730 cm⁻¹, and 1040 cm⁻¹, corresponding to the C–H stretch, C=O stretch and C–O–C stretching vibrations, respectively. The XPS analysis data (Fig. S6†) provide the atomic ratios of different elements present in the nCs. XGnC had the highest carbon content of 88% and GKnC had the least with only 57%, while GGnC and GAnC had a carbon content of 60% and 79%, respectively. The chemical composition obtained from XPS also revealed the presence of 7%, 3%, 8% of Si in GAnC, GGnC and GKnC, respectively. This affirms that the elemental composition is in accordance with the EDX results. Residual oxygen contents of 32%, 35%, 18% and 12% were found in GAnC, GGnC, GKnC, and XGnC, respectively. Even though the presence of oxygen content reduces the conductivity of the prepared nCs, it contributes to the improvement of wettability with aqueous electrolytes.²⁹ The deconvoluted C 1s XPS spectra (Fig. S7†) of the nCs can be resolved into four peaks at 284.8 eV, 284.3 eV, 286.6 eV and 288.2 eV. The distinguishable main peak at 284.8 eV corresponds to the sp² hybridized carbon, while the small peaks at 284.3 eV, 286.6 eV and 288.2 eV represent the sp³ carbon, C–O–C and C=O, respectively. Among nCs, XGnC showed the highest content of graphitic carbon.

The crystalline structure and composition of the nCs were analyzed by Raman spectroscopy (Fig. 2a), which revealed two peaks for all the nCs at ~1340 cm⁻¹ and ~1590 cm⁻¹ corresponding to the D-band and G-band, respectively. The D-band arises due to the A_{1g} phonon breathing vibrations from disordered graphite, while the G-band appears as a result of the first-order scattering of the E_{2g} phonon of sp² carbon atoms in 2D graphite.^{30,31} Furthermore, additional peaks are observed

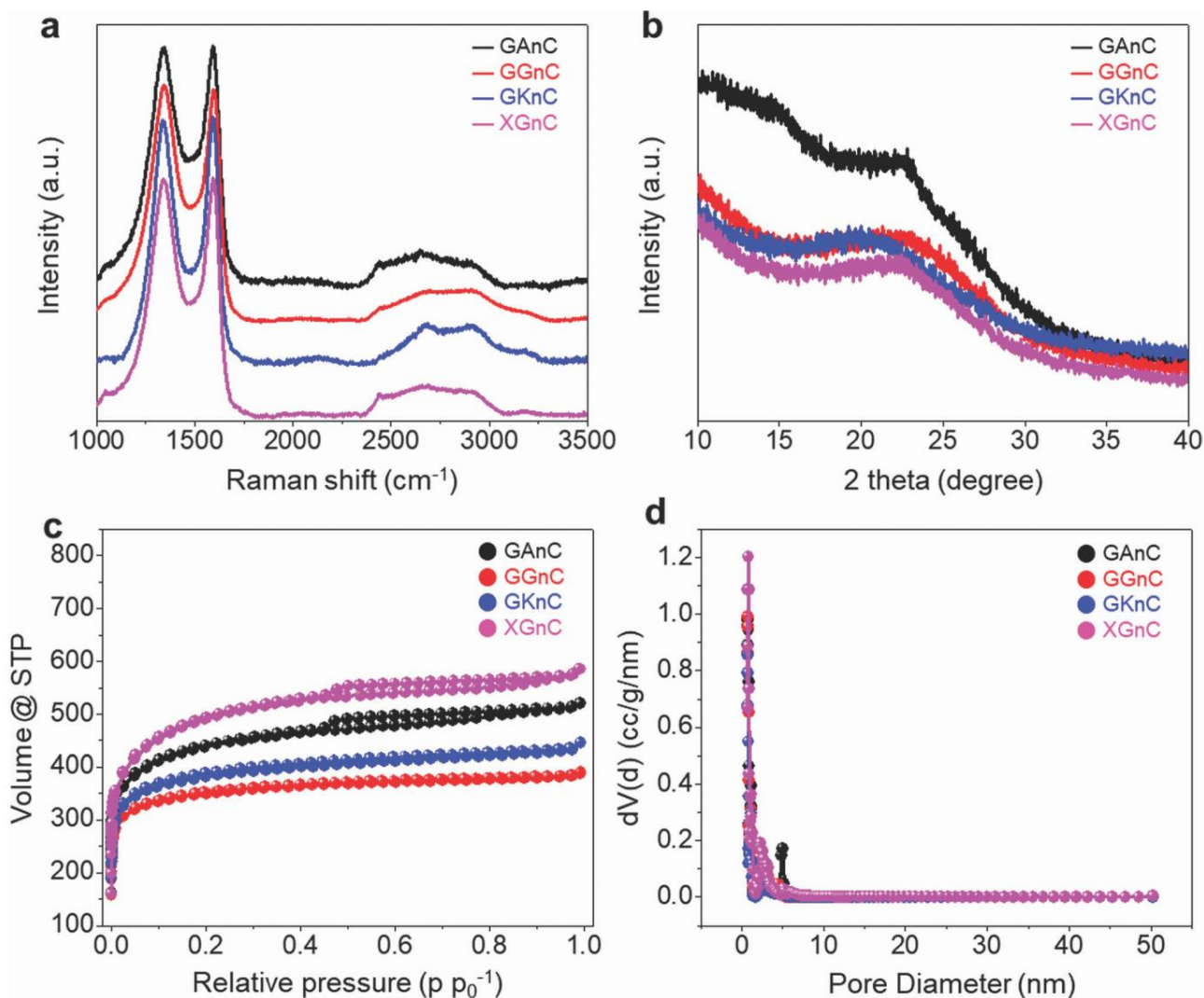


Fig. 2 (a) Raman spectra, (b) XRD patterns, (c) N_2 adsorption–desorption isotherms, and (d) pore size distributions of GAnC, GGnC, GKnC, and XGnC.

at $\sim 2700\text{ cm}^{-1}$ and $\sim 2850\text{ cm}^{-1}$ that can be assigned to 2D band and S3 bands, respectively. This indicates a certain degree of graphitization of the gums.³² The ratio between the intensity of the G-band to the D-band (I_G/I_D) is proportional to the degree of crystallinity of the carbonaceous materials. The I_G/I_D values for all nCs are tabulated in Table S3.† The I_G/I_D values of all materials are ~ 1 , indicating a certain degree of graphitization in the materials. Furthermore, the nC was studied by X-ray diffraction (Fig. 2b). The pattern showed a broad peak at $2\theta = \sim 22\text{--}25^\circ$, which can be attributed to the characteristic reflection from the graphitic plane. This further reaffirmed the graphitization of the materials. The Brunauer–Emmett–Teller (BET) surface area of the materials were determined, and their nitrogen adsorption–desorption isotherms are depicted in Fig. 2c. The N_2 adsorption–desorption isotherm of nC derived from GA and XG shows mixed type II and type III curves, indicating the presence of a mix of microporosity

and mesoporosity. The curve also shows a H_2 -type hysteresis loop at a relative pressure region of $0.5\text{--}0.9P/P_0$. This type of hysteresis curve is typical of a material with a high mesopore-to-micropore ratio. However, the nCs derived from GG and GK show no hysteresis loop, which suggests that the ratio of micropores to mesopores is high in these materials. The steep increase in the nitrogen intake at low P/P_0 indicates the presence of a large number of micropores. These results are in accordance with the TEM results, which showed the clear presence of mesopores in GAnC and XGnC and a majority of micropores in GGnC and GKnC. The BET surface area and pore volume were also determined for nC, and are tabulated in Table S4.† The nC derived from XG had the highest surface area of $1780\text{ m}^2\text{ g}^{-1}$ with a pore volume of $0.88\text{ cm}^3\text{ g}^{-1}$. The pore size distribution, calculated from the adsorption branch of the isotherm by the nonlocal density functional theory (NLDFT) method, is depicted in Fig. 2d, which shows that the

maximum pore volume is in the micropore region. However, the mesopores were also observed in the nC samples. This is a direct result of the activation by KOH, which results in a structure comprising both micropores and mesopores. The high surface-to-volume ratio and abundant pores present in the materials promote ion adsorption by providing numerous adsorption sites and ion diffusion pathways.

Dye adsorption characteristics of nC

The micro/mesoporosity of the synthesized nCs were evaluated by gauging their ability to remove toxic pollutants from water (Fig. 3) – this test is conducted to verify the effect of surface area of different nCs in their adsorption capabilities. The study involved an anionic dye, methyl orange (MO) (Fig. 3a–c), and a cationic dye, methylene blue (MB) (Fig. 3d–f). The nC did adsorb large quantities of both dyes at a very low adsorbent concentration of 0.1 g L^{-1} . When the nC was introduced into the glass vials, the respective orange and blue colors of the MO and MB dyes decreased over time as confirmed by the decrease in the intensity of the UV-Vis peaks at 464 nm and 664 nm for MO and MB, respectively. The adsorption capacity of the nC was in accordance with its surface area. XGnC showed the highest adsorption capacity for both MO and MB followed by GAnC, GKnC, and GGnC. XGnC had an adsorption capacity of 483 mg g^{-1} and 500 mg g^{-1} for MO and MB, respectively. Even though the nCs had a higher adsorption capacity for both dyes, the adsorption capability for MB was found to be higher and displayed a faster adsorption rate. This

can be attributed to the certain degree of graphitization in the nCs, which provides favorable conditions for MB adsorption. The π -electrons from the C=C bonds of the MB interact with the π -electrons from the nCs, resulting in a π - π stacking interaction.^{33,34} Additionally, the presence of a negative charge from the residual oxygen functionalities attracts the positively charged MB, thus increasing the binding of the MB with the nCs.³⁵ The adsorption kinetics were determined to glean more information pertaining to the mechanism and the adsorption rate. The pseudo-first-order and pseudo-second-order kinetic models for both MO and MB are plotted in Fig. 3b, c, e and f. The correlation coefficient of the pseudo-second-order model obtained from linear fittings of the graphs is higher than the pseudo-first-order model for all nCs. This suggests that chemisorption is the rate-controlling step in the dye adsorption onto nCs, which is typical for adsorbents with a graphitic structure.^{36,37} Furthermore, the nCs could be easily separated from the media *via* centrifugation, and the nCs retained their adsorption capacity for up to five cycles with only a slight reduction ($\sim 10\%$) in their adsorption capacity. As demonstrated by dye adsorption tests, the effect of the surface area in the adsorption capacity was confirmed. The nCs with higher surface areas attained enhanced adsorption capabilities.

nC as a practical energy harvester

Recently, the water-induced energy conversion applications using water (such as evaporation³⁸ and moisture absorption³⁹) have been widely investigated owing to their clean, abundant,

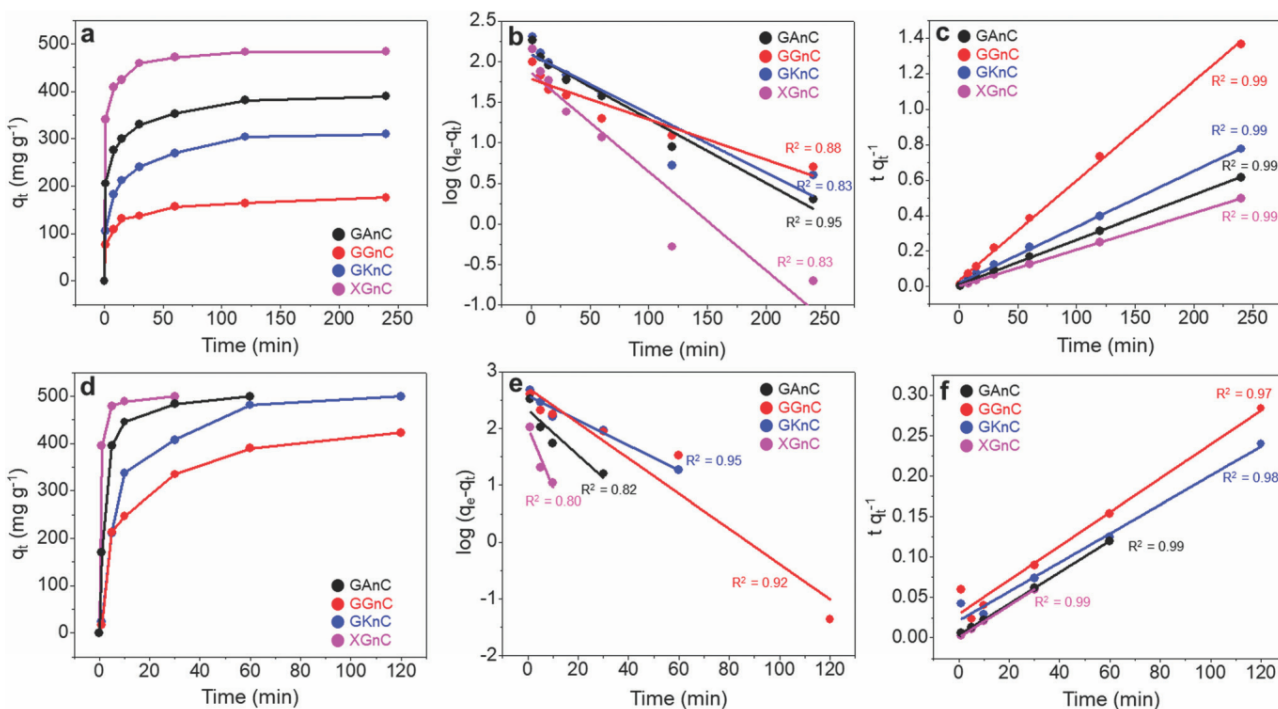


Fig. 3 (a) Adsorption of MO on nCs, (b) pseudo-first-order kinetic model for the MO adsorption, and (c) pseudo-second-order kinetic model for the MO adsorption. (d) Adsorption of MB on nCs, (e) pseudo-first-order kinetic model for the MB adsorption, and (f) pseudo-second-order kinetic model for the MB adsorption.

and easily exploitable attributes. In particular, the water evaporation-induced electricity production using carbon nanomaterials has been regarded as one of the most promising approaches to reliably convert water energy into a direct output signal for a long term. In this regard, the prepared nC that has uniform micropores of ~ 2 nm is envisaged to be an appropriate material for driving the fast evaporation *via* capillary action through the micropores and in turn, contributes to the high-performance electricity energy conversion. Furthermore, the preparation of nC using gum waste is suitable for a recyclable, low-cost, and large-scale production, especially in the developing world where these materials are predominantly produced, thus reflecting the sustainable use of local resources.

The schematic process is shown in Fig. 4a. Briefly, in the fabrication of energy harvesters, GAnC was coated onto a glass substrate by slurry casting using a mixture consisting of nC (0.02 g), PAA (0.01 g), and CMC (0.01 g). Details of the process are described in the Experimental section. Here, GAnC was chosen as a suitable candidate as it exhibits the highest surface area and porosity among the nCs fabricated from raw gum wastes (excluding XGnC), which were synthesized from

the commercial powder. In Fig. 4b–d, the electricity generation was based on GAnC and induced by asymmetric wetting. Prior to the measurement, the surfaces of the energy harvesters were treated by O_2 plasma exposure, ensuring the hydrophilicity of carbon after the O_2 plasma treatment (Fig. S8†). As shown in Fig. 4b, water was simply well absorbed in this case along the carbon surface as the partial bottom area of the device was dipped into a water container (red dashed line, Fig. 4b). Subsequently, the water molecules were actively desorbed by natural evaporation from the top side of the carbon surface area that was exposed to air, in comparison to the bottom side that was dipped in water. Thus, a potential difference is formed between the top and the bottom electrode areas, induced by the difference in the evaporation rate. As a result, to refill water for the more quickly evaporated top area, the water at the bottom continuously and quickly flows by capillary action through the high-density nanopores of carbon. Also, to generate a DC electrical current, electrons directionally move to balance the potential difference through an external circuit. As shown in Fig. 4d, there is an output voltage of ~ 0.4 V and DC output of ~ 3 μ A from a device with the dimensions of 1.0 cm \times 2.5 cm. Notably, the output current was 20-fold

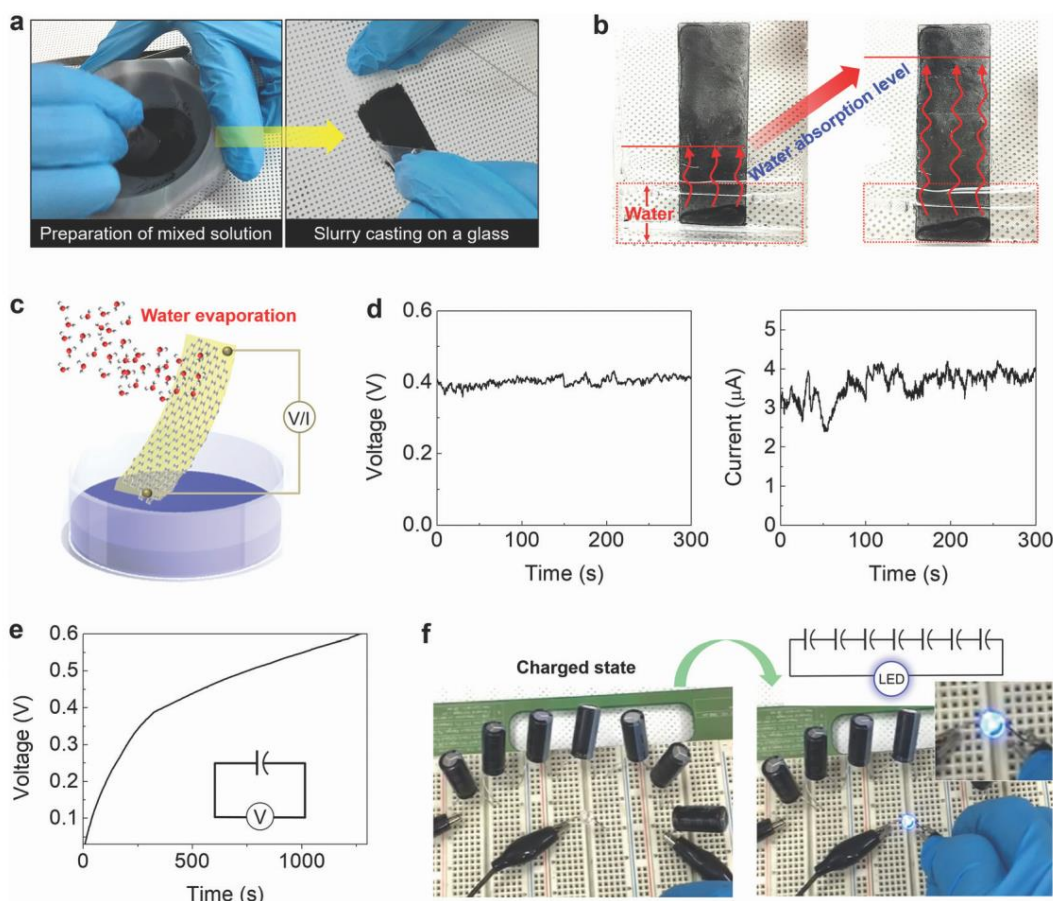


Fig. 4 (a) Schematic representation of the fabrication process for the nC-based energy harvester. (b) Photograph showing the asymmetric water-wetting of the energy harvester in a water container. (c) Schematic illustration on the evaporation-induced electricity generation. (d) Output voltage and current measurements. (e) Charging test using a capacitor of 470 μ F. (f) Demonstration of driving a commercial blue light emitting diode.

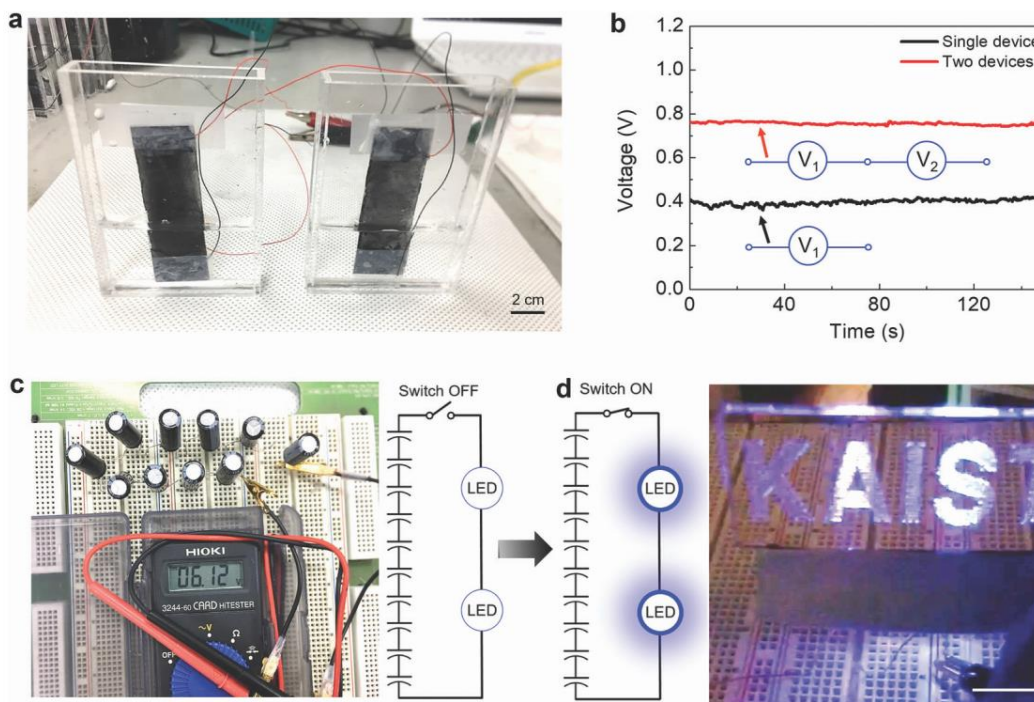


Fig. 5 (a) Scale-up of electricity using serially connected devices. (b) Comparison of output voltage using a single device and two devices. (c) Photograph showing a charged output of up to 6.1 V. (d) Visual demonstration (the scale bar is 1 cm).

higher than previously reported evaporation-driven electricity devices using carbon without nanopores.³⁸ To further confirm the effectiveness of nanoporous carbon, we measured outputs using a binder-based sample alone without nC, which showed negligible output performance (Fig. S9†). Moreover, the output performance of the nC-based sample was noticeably higher when compared to an energy harvester using carbon black nanoparticles,³⁸ generating an output voltage of ~ 0.16 V and current of ~ 300 nA (Fig. S11†). These results demonstrate that the nanopores in each nC coated on the glass, indeed, play a crucial role in quickly transporting the water molecules for high output performance due to the high capillary pressure.⁴⁰ Also, to examine the reliability of the developed energy harvesters, the long-term output generation was measured over 2.5 h (Fig. S10†). Next, we attempted to store the generated electricity using a capacitor with 470 μ F and 0.6 V that was charged for 1300 s (Fig. 4e). The electrical energy stored up to 2.6 V (Fig. S12†). Using the harvested electrical power, it can be utilized to turn on a commercial blue light-emitting diode that consumes 2.5 V and 20 mA (Fig. 4f).

Simply, such nC can also scale up the output voltage by increasing the number of devices (Fig. 5), which could also be shown through visual demonstration. As shown in Fig. 5a, two nC-based energy harvesters were easily combined in a serial configuration. Thus, as shown in Fig. 5b, the output voltage was proportionally increased by up to 0.77 V, indicating that the scale-up of outputs can be easily realized. Finally, Fig. 5c shows the electricity charging up to 6.1 V using 10 serially connected capacitors. Attributed to the increased electrical energy,

the “KAIST” logo can be visualized by turning on the blue LEDs that consume 6 V and 20 mA (Fig. 5d and Movie S1†). Based on all of these results and demonstrations, it is suggested that a sustainable strategy can be adopted towards gum wastes, as shown in this work, which builds up a milestone for utilizing various worthless biowastes into sustainable power production. The burgeoning demand for increasing global population and energy consumption can possibly be addressed using local resources that are of practically no use for humans or animals. Furthermore, the occurrence of these wastes in the developing world bodes well for their exploitation locally, thus reinforcing the true tenets of sustainability.

Conclusion

In summary, we have first demonstrated a simple and efficient method to synthesize nC from low-grade gum wastes *via* a synthetic process that can be applied to a wide variety of gum wastes, culminating in the fabrication of assorted nCs with varied chemical compositions and bonding. After synthesis, the high density of the pores was successfully attained in the nCs with a large surface area, and the effect of the nC surface area was clearly demonstrated *via* dye adsorption tests. In view of their high surface areas with abundant micropores, the fabricated nC was evaluated as an energy harvester where it exhibited significant current and voltage generation by simply using water, and was capable of turning on the light for a commercial LED. Such fabricated nC-based energy harvester can

also be scaled up, with improved performance proportional to the number of nCs used. Using tap water, the fabricated nC energy harvester is capable of turning the university logo on, showing its practicality in harnessing electrical energy. Significantly, our study establishes an initial milestone in building up a sustainable solution to overcome the energy deficiency in the world, by utilizing local biodegradable and non-toxic gum wastes into a source of energy harvester, which can be scalable, renewable, and practical.

Author contributions

A. V., J. Y. C., and S.-H. S. contributed equally to this work. A. V., A. K. K. P., V. V. T. P. and S. W. initiated the experiments and synthesized MCs. A. V. and A. K. K. P. conducted the dye adsorption characteristics of the MC microsheets. A. V., J. Y. C. and V. V. T. P. conducted the characterizations of MCs. J. Y. C. and S.-H. S. prepared and conducted the energy harvesting tests and discussed the results with T. G. Y., J. B., J. Y. C., and S.-H. S. further extended the applications and the impact of MCs throughout this work. J. Y. C. and S.-H. S. were supervised under I.-D. K., M. C., V. V. T. P., J. Y. C., and S.-H. S. wrote the manuscript. S. A., A. G. and R. S. V. reviewed and edited the manuscript.

Conflicts of interest

There are no conflicts to declare.

Acknowledgements

This work was supported by Samsung Electronics (no. G01190324), the Ministry of Education, Youth and Sports, in the framework of the targeted support of the “National Program for Sustainability I” LO 1201 and the OPR & DI project “Extension of CxI facilities” (CZ.1.05/2.1.00/19.0386), the Research Infrastructure NanoEnviCz, supported by the Ministry of Education, Youth and Sports of the Czech Republic in the framework of Project No. LM2015073, Ministry of Education, Youth and Sports of the Czech Republic and the European Union – European Structural and Investment Funds in the frames of Operational Program Research, Development and Education–project Hybrid Materials for Hierarchical Structures (HyHi, Reg. No. CZ.02.1.01/0.0/0.0/16_019/0000843), NRF grant funded by the Korean Government (NRF-2017H1A2A1042006-Global Ph.D. Fellowship Program), and NRF grant funded by the Korean Government the (NRF-2018R1A6A3A01013461-Postdoctoral Fellowship Program). This work was also supported by the project “Tree Gum Polymers and their Modified Bioplastics for Food Packaging Application” granted by the Bavarian-Czech-Academic-Agency (BTHA) (registration numbers LTAB19007 and BTHA-JC-2019-26) and another project “Bio-based Porous 2D Membranes and 3D Sponges Based on Functionalized Tree Gum Polysaccharides and their Environmental Application” (regis-

tration number LTAUSA19091- TUL internal No. 18309/136) by the Ministry of Education, Youth and Sports in the Czech Republic under the “Inter Excellence – Action programme”.

References

- 1 D. Verbeken, S. Dierckx and K. Dewettinck, *Appl. Microbiol. Biotechnol.*, 2003, **63**, 10–21.
- 2 V. V. T. Padil, S. Waclawek, M. Černík and R. S. Varma, *Biotechnol. Adv.*, 2018, **36**, 1984–2016.
- 3 D. A. Silva, J. P. A. Feitosa, J. S. Maciel, H. C. B. Paula and R. C. M. de Paula, *Carbohydr. Polym.*, 2006, **66**, 16–26.
- 4 G. O. Aspinall, *Pure Appl. Chem.*, 1967, **14**, 43–56.
- 5 J. C. Colmenares, R. S. Varma and P. Lisowski, *Green Chem.*, 2016, **18**, 5736–5750.
- 6 S. Irvani and R. S. Varma, *Green Chem.*, 2020, **22**, DOI: 10.1039/C9GC02835H.
- 7 K. Ojha, B. Kumar and A. K. Ganguli, *J. Chem. Sci.*, 2017, **129**, 397–404.
- 8 F. Chen, J. Yang, T. Bai, B. Long and X. Zhou, *J. Electroanal. Chem.*, 2016, **768**, 18–26.
- 9 S. Karagöz, T. Tay, S. Ucar and M. Erdem, *Bioresour. Technol.*, 2008, **99**, 6214–6222.
- 10 C. Akmil-Başar, E. Köseoğlu and Y. Önal, *Part. Sci. Technol.*, 2016, **34**, 526–532.
- 11 T. Tsoncheva, I. Genova, I. Stoycheva, I. Spassova, R. Ivanova, B. Tsyntsarski, G. Issa, D. Kovacheva and N. Petrov, *J. Porous Mater.*, 2015, **22**, 1127–1136.
- 12 Z. Liu, Z. Zhu, J. Dai and Y. Yan, *ChemistrySelect*, 2018, **3**, 5726–5732.
- 13 D. Chen, H. Zhou, H. Li, J. Chen, S. Li and F. Zheng, *Sci. Rep.*, 2017, **7**, 14985, DOI: 10.1038/s41598-017-15129-7.
- 14 Z. Gao, Y. Zhang, N. Song and X. Li, *Mater. Res. Lett.*, 2017, **5**, 69–88.
- 15 B. H. Ali, A. Ziada and G. Blunden, *Food Chem. Toxicol.*, 2009, **47**, 1–8.
- 16 Y. Zheng, Y. Zhu, G. Tian and A. Wang, *Int. J. Biol. Macromol.*, 2015, **73**, 39–44.
- 17 V. V. T. Padil and M. Černík, *Int. J. Nanomed.*, 2013, **8**, 889–898.
- 18 G. O. Aspinall, L. Khondo and B. A. Williams, *Can. J. Chem.*, 1987, **65**, 2069–2076.
- 19 H. Jian, L. Zhu, W. Zhang, D. Sun and J. Jiang, *Carbohydr. Polym.*, 2012, **87**, 2176–2182.
- 20 L. Muniandy, F. Adam, A. R. Mohamed and E. P. Ng, *Microporous Mesoporous Mater.*, 2014, **197**, 316–323.
- 21 Q. Yu, M. Li, P. Ning, H. Yi and X. Tang, *Sep. Sci. Technol.*, 2014, **49**, 2366–2375.
- 22 M. A. A. Zaini and M. J. Kamaruddin, *J. Anal. Appl. Pyrolysis*, 2013, **101**, 238–241.
- 23 I. Okman, S. Karagöz, T. Tay and M. Erdem, *Appl. Surf. Sci.*, 2014, **293**, 138–142.
- 24 H. Guo and X. L. Deng, *Adv. Mater. Res.*, 2013, **787**, 46–51.
- 25 S. E. Abechi, C. E. Gimba, A. Uzairu and U. A. Dallatu, *Res. J. Chem. Sci.*, 2013, **3**, 54–61.

- 26 P. He, C. Zhou, S. Tian, J. Sun, S. Yang, G. Ding, X. Xie and M. Jiang, *Chem. Commun.*, 2015, **51**, 4651–4654.
- 27 D. M. W. Anderson and W. Weiping, *Int. Tree Crops J.*, 1992, **7**, 167–179.
- 28 B. N. Chikamai and W. B. Banks, *Food Hydrocolloids*, 1993, **7**, 521–534.
- 29 E. Raymundo-Piñero, F. Leroux and F. Béguin, *Adv. Mater.*, 2006, **18**, 1877–1882.
- 30 L. Bokobza, J.-L. Bruneel and M. Couzi, *C*, 2015, **1**, 77–94.
- 31 C. A. Amarnath, C. E. Hong, N. H. Kim, B. C. Ku, T. Kuila and J. H. Lee, *Carbon*, 2011, **49**, 3497–3502.
- 32 I. K. Moon, J. Lee, R. S. Ruoff and H. Lee, *Nat. Commun.*, 2010, **1**, 73, DOI: 10.1038/ncomms1067.
- 33 L. A. Mercante, M. H. M. Facure, D. A. Locilento, R. C. Sanfelice, F. L. Migliorini, L. H. C. Mattoso and D. S. Correa, *New J. Chem.*, 2017, **41**, 9087–9094.
- 34 X. He, K. B. Male, P. N. Nesterenko, D. Brabazon, B. Paull and J. H. T. Luong, *ACS Appl. Mater. Interfaces*, 2013, **5**, 8796–8804.
- 35 S. Bai, X. Shen, X. Zhong, Y. Liu, G. Zhu, X. Xu and K. Chen, *Carbon*, 2012, **50**, 2337–2346.
- 36 X. Zhang, J. Shen, N. Zhuo, Z. Tian, P. Xu, Z. Yang and W. Yang, *ACS Appl. Mater. Interfaces*, 2016, **8**, 24273–24280.
- 37 L. Chen, Y. Li, Q. Du, Z. Wang, Y. Xia, E. Yedinak, J. Lou and L. Ci, *Carbohydr. Polym.*, 2017, **155**, 345–353.
- 38 G. Xue, Y. Xu, T. Ding, J. Li, J. Yin, W. Fei, Y. Cao, J. Yu, L. Yuan, L. Gong, J. Chen, S. Deng, J. Zhou and W. Guo, *Nat. Nanotechnol.*, 2017, **12**, 317–321.
- 39 Y. Huang, H. Cheng, C. Yang, P. Zhang, Q. Liao, H. Yao, G. Shi and L. Qu, *Nat. Commun.*, 2018, **9**, 4166, DOI: 10.1038/s41467-018-06633-z.
- 40 Y. Li, H. Chen, S. Xiao, M. A. Alibakhshi, C. W. Lo, M. C. Lu and C. Duan, *ACS Nano*, 2019, **13**, 3363–3372.



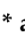

3.6. Gum Kondagogu/Reduced Graphene Oxide Framed Platinum Nanoparticles and Their Catalytic Role

Abstract: This study investigates an environmentally benign approach to generate platinum nanoparticles (Pt NP) supported on the reduced graphene oxide (RGO) by non-edible gum waste of gum kondagogu (GK). The reaction adheres to the green chemistry approach by using an aqueous medium and a nontoxic natural reductant—GK—whose abundant hydroxyl groups facilitate in the reduction process of platinum salt and helps as well in the homogenous distribution of ensued Pt NP on RGO sheets. Scanning Electron Microscopy (SEM) confirmed the formation of kondagogu gum/reduced graphene oxide framed spherical platinum nanoparticles (RGO-Pt) with an average particle size of 3.3 ± 0.6 nm, as affirmed by Transmission Electron Microscopy (TEM). X-ray Diffraction (XRD) results indicated that the Pt NPs formed are crystalline with a face-centered cubic structure, while morphological analysis by XRD and Raman spectroscopy revealed a simultaneous reduction of GO and Pt. The hydrogenation of 4-nitrophenol could be accomplished in the superior catalytic performance of RGO-Pt. The current strategy emphasizes a simple, fast and environmentally benign technique to generate low-cost gum waste supported nanoparticles with a commendable catalytic activity that can be exploited in environmental applications.

Citation: **Abhilash Venkateshaiah**, Daniele Silvestri, Rohith K. Ramakrishnan, Stanislaw Wacławek, Vinod V.T. Padil, Miroslav Černík, and others, “**Gum Kondagoagu/Reduced Graphene Oxide Framed Platinum Nanoparticles and Their Catalytic Role**”, *Molecules*, 24 (2019)

Article

Gum Kondagoagu/Reduced Graphene Oxide Framed Platinum Nanoparticles and Their Catalytic Role

Abhilash Venkateshaiah ¹, Daniele Silvestri ¹, Rohith K. Ramakrishnan ¹,
Stanislaw Waclawek ¹, Vinod V. T. Padil ^{1,*}, Miroslav Černík ^{1,*} and Rajender S. Varma ^{2,*}

¹ Department of Nanomaterials in Natural Sciences, Institute for Nanomaterials, Advanced Technologies and Innovation (CXI), Technical University of Liberec (TUL), Studentská 1402/2, 46117 Liberec 1, Czech Republic; abhilash.venkateshaiah@tul.cz (A.V.); daniele.silvestri@tul.cz (D.S.);

rohith.kunjiparambil.ramakrishnan@tul.cz (R.K.R.); stanislaw.waclawek@tul.cz (S.W.)

² Regional Centre of Advanced Technologies and Materials, Department of Physical Chemistry, Faculty of Science, Palacký University in Olomouc, Šlechtitelů 27, 78371 Olomouc, Czech Republic

* Correspondence: vinod.padil@tul.cz (V.V.T.P.); miroslav.cernik@tul.cz (M.Č.);

Varma.Rajender@epa.gov (R.S.V.)

Academic Editor: M. Concepción Gimeno

Received: 6 September 2019; Accepted: 8 October 2019; Published: 9 October 2019



Abstract: This study investigates an environmentally benign approach to generate platinum nanoparticles (Pt NP) supported on the reduced graphene oxide (RGO) by non-edible gum waste of gum kondagogu (GK). The reaction adheres to the green chemistry approach by using an aqueous medium and a nontoxic natural reductant—GK—whose abundant hydroxyl groups facilitate in the reduction process of platinum salt and helps as well in the homogenous distribution of ensued Pt NP on RGO sheets. Scanning Electron Microscopy (SEM) confirmed the formation of kondagogu gum/reduced graphene oxide framed spherical platinum nanoparticles (RGO-Pt) with an average particle size of 3.3 ± 0.6 nm, as affirmed by Transmission Electron Microscopy (TEM). X-ray Diffraction (XRD) results indicated that the Pt NPs formed are crystalline with a face-centered cubic structure, while morphological analysis by XRD and Raman spectroscopy revealed a simultaneous reduction of GO and Pt. The hydrogenation of 4-nitrophenol could be accomplished in the superior catalytic performance of RGO-Pt. The current strategy emphasizes a simple, fast and environmentally benign technique to generate low-cost gum waste supported nanoparticles with a commendable catalytic activity that can be exploited in environmental applications.

Keywords: greener catalysts; kondagogu gum; RGO; Pt nanoparticle; 4-nitrophenol reduction

1. Introduction

Metal nanoparticles have gained considerable attention over the past few years owing to their remarkable physical and chemical properties—which is a stark contrast from their bulk counterparts. The properties arising due to the nano realm have made it possible for them to be used in a wide array of applications including catalysis [1,2], sensors [3], biomedicine [4–6], and drug delivery applications [7–9]. Over the years, different approaches have been developed for the synthesis of metal nanoparticles to obtain different sizes, structures, and morphologies. Conventional synthesis uses chemical reducing agents such as sodium borohydride (NaBH_4), hydrazine, and dimethylformamide (DMF) to reduce metal cations to produce nanoparticles, with the inherent drawback that these chemicals are highly reactive and raise serious concerns regarding potential environmental impact and associated biological threats [10]. Extensive research has gone into developing new environmentally benign techniques to synthesize metal nanoparticles without the use of hazardous chemicals and solvents and preferably utilizing materials of biological origins, thus adhering to the principles of

green chemistry. In addition to being eco-friendly, green synthesis offers several advantages over the conventional means, which include cost-effectiveness, simple experimental design, minimal to zero toxic chemicals, and byproducts [11] wherein precursors derived from various biological sources have been deployed successfully [12–18].

Biorenewable natural gums extruded from trees or extracted from seaweeds, and bacteria are a class of polysaccharides that have recently gained attention due to their ability to reduce metal salts to produce nanoparticles [19–22]. The complex polysaccharides and protein structures encompassing the gums provide a non-toxic alternative pathway to effectively reduce and stabilize the nanoparticles. Although numerous polysaccharides have been used in the greener assembly of nanoparticles, the use of gum kondagogu (GK) was much less explored; GK is a non-toxic, naturally occurring polysaccharide, readily available from the exudates of *Cochlospermum Gossypium* (Bixaceae family) tree [23]. GK contains a highly acidic sugar content, including galacturonic and glucuronic acids, which make up 52% of the total carbohydrates, while the remaining are neutral sugars such as glucose, galactose, rhamnose, and arabinose [24]. Upon toxicological evaluation, GK has been declared a non-toxic material, with potential applications as food additives [25] and can be an ideal reducing and stabilizing agent owing to its low cost, biorenewable nature, and availability of plentiful functional groups (hydroxyl, acetyl, carbonyl, carboxylic) with metal biosorption properties [16].

4-Nitrophenol (4-NP) is a toxic chemical often found in industrial and agricultural wastewaters. Various methods have been developed for the reduction and removal of 4-NP from these wastewaters and the reduction of 4-NP by NaBH_4 is one of the simplest and most popular methods. However, the presence of a high kinetic barrier between 4-NP and BH_4^- requires an effective catalyst in order for the reaction to proceed. Hence, researchers have been developing newer effective catalysts capable of assisting in the effective reduction of 4-NP. Additionally, the reduction of 4-NP by NaBH_4 is often considered as a model reaction to assess the catalytic performance of novel catalysts.

Platinum (Pt) is one of the most extensively used catalyst elements in many chemical and electrochemical reactions [26], especially Pt nanoparticles with large surface area and greatly higher active sites, which have garnered significant attention due to their promising potential in the field of environmental and energy-related catalysis. With its unfilled 5d orbital and rich electronic structure, it is a well-established catalytic system in multifarious applications [27,28]. Thus, careful control and design of the surface and interface of the Pt nanoparticles with its in-depth analysis and comprehension of the structural aspects plays a pivotal role in optimizing the catalytic performance. Despite having an excellent catalytic ability, Pt nanoparticles are often associated with severe agglomeration, which reduces its catalytic performance [29]. To minimize agglomeration and to attain good dispersibility and stability, Pt nanoparticles are often deposited on support materials [30–32] that possess high specific surface area, abundant anchoring sites, high stability and high electric conductivity (for electrocatalytic applications). Carbon-based materials are the most commonly used ones for this purpose as they fulfill the requirement mentioned above [33–39]. Graphene, an atomically thin 2D material, suits all the above descriptions required for the deposition of Pt nanoparticles. Since its isolation in its pure form from graphite in 2004 [40], graphene has garnered significant attention for various applications. It can be synthesized by different methods including mechanical exfoliation [40,41], chemical vapor deposition [42,43], unzipping of carbon nanotubes [44,45], and synthesis on SiC [46,47]. Since these techniques are associated with high production costs, alternatively graphene oxide (GO) or reduced graphene oxide (RGO) can provide a low-cost scalable option and the presence of abundant oxygen functionalities offer anchoring sites for the metal nanoparticles to obtain NP decorated graphene sheets.

In the current study, we propose a simple, fast, inexpensive, and environmentally friendly process to deposit Pt nanoparticles on the graphene sheets. GO prepared by using the modified Hummers method [48] is conventionally reduced by hydrazine hydrate, NaBH_4 or ethylene glycol [49–52]. In the present work, however, a green chemistry approach entails the simultaneous reduction of Pt salt and GO using GK waste to generate Pt nanoparticle adorning the RGO sheets. We have thoroughly characterized the obtained Pt nanoparticle decorated graphene sheets (Pt-RGO) using scanning electron

microscopy (SEM), transmission electron microscopy (TEM), X-ray diffraction analysis (XRD), and Raman spectroscopy. Furthermore, the catalytic performance of the Pt-RGO catalysts was assessed in the hydrogenation of 4-nitrophenol (4-NP).

2. Results and Discussion

To optimize the process of NPs preparation on the GO surface, we carried out the synthesis at different reaction conditions and reagent concentrations (Details are presented in Table S1). From the results obtained, it was concluded that the optimum conditions were: 30 min reaction time, a temperature of 150 °C, and PtCl₄ 1 mM. In other tested conditions, the reaction remains incomplete, which could be ascertained visually as the material does not completely precipitate (Figures S2 and S3).

The surface morphology of the thus prepared Pt-RGO was analyzed using SEM images. All the SEM images of the Pt-RGO from different metal salt concentrations (Figure S4) indicated folded structures on both, the surface and the edges, which suggests the typical morphology of few-layered RGO. It is evident from the images that at a lower PtCl₄ concentration of 0.5 mM, only a few isolated nanoparticles can be seen. However, when the concentration was increased to 2 mM, a clear agglomeration of nanoparticles was discerned on the surface. At a concentration of 1 mM, a uniform finely dispersed Pt NPs deposition on the RGO surface can be detected.

Furthermore, to analyze the morphology and to obtain insights into the particle size and distribution, TEM and HRTEM analysis were carried out (Figure 1) confirming that the GK had assisted in the formation and decoration of Pt nanoparticles on the RGO surface. The NPs were evenly dispersed throughout the surface with negligible agglomeration, which can be attributed to the presence of GK in the reaction medium.

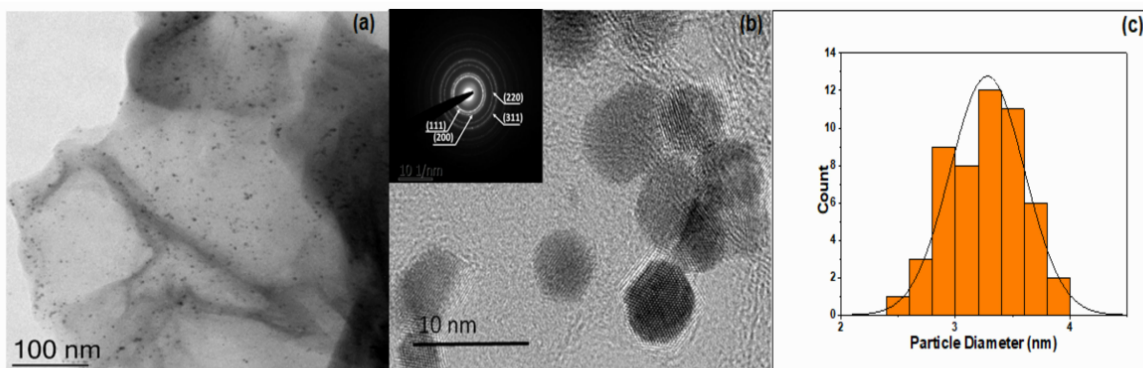


Figure 1. (a) TEM and (b) HRTEM image of the Pt-RGO; inset image corresponds to the SAED pattern of the Pt-RGO; (c) histogram depicting the size distribution of nanoparticles.

The particles were mainly spherical shaped with a mean diameter of around 3.3 ± 0.6 nm. HRTEM images clearly show the lattice fringes and the d spacing was calculated to be around 0.22 nm corresponding to the (111) plane distance of face-centered cubic (fcc) crystalline Pt NP [53] with the SAED pattern showing diffraction rings corresponding to (111), (200), (220) and (311) reflections of fcc platinum crystals [53].

Furthermore, to analyze the crystal structure of the nanoparticles, the X-ray diffraction pattern of the Pt-RGO samples was recorded, as shown in Figure 2. GO before reduction shows a sharp diffraction peak at $2\theta = 11^\circ$, which is a characteristic of GO and is associated with the chemical exfoliation of graphite [54], the appearance of a sharp plane (002) confirms the formation of exfoliated GO sheets [55]. Upon reduction, this peak is shifted to 23.5° , which affirms the formation of RGO [55] as evidenced by the XRD graphs of Pt-RGO (Figure 2). Additionally, five more major peaks were observed in Pt-RGO at 39.5 , 45.6 , 66.8 , 80.7 , and 85° , which corresponds to the (111), (200), (220), (311) and (222) planes of Pt, respectively [56]. These results are in accordance with the results obtained from SAED analysis and are

consistent with the fcc structure of the platinum (JCPDS #040802), thus confirming the formation of crystalline Pt [56].

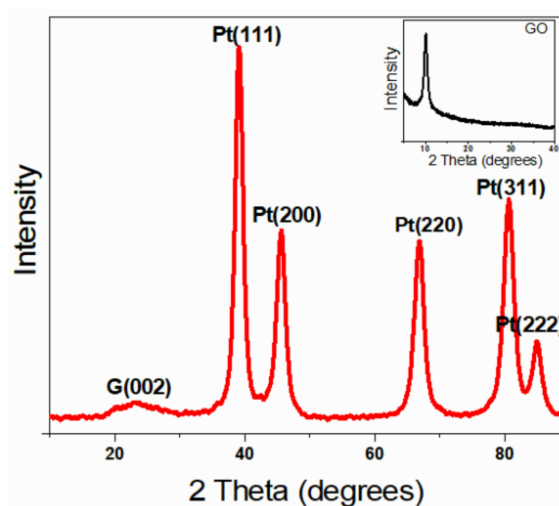


Figure 2. XRD pattern of the green synthesized Pt-RGO catalyst. The inset image is the XRD pattern of GO.

Raman analysis of the Pt-RGO provides information on the nature of RGO and the formation of defects during the reduction of GO; Figure 3 displays the Raman spectra of GO and Pt-RGO catalysts. Before the reduction, GO show the major peaks at 1353 and 1594 cm^{-1} corresponding to D and G bands [57]. G band corresponds to the first-order scattering of the E_{2g} mode and the D band arises due to the defects and asymmetrical breaking at the graphene edges. The lesser intensity bands at 2691 and 2930 cm^{-1} can be assigned to the 2D and D + D' bands, respectively [58]. In the case of Pt-RGO, the same major and minor bands reappear, however, an obvious blue shift associated with RGO is observed. The D and G bands are shifted to 1345 and 1580 cm^{-1} respectively, while the 2D and D + D' bands appear at 2674 and 2918 cm^{-1} respectively. The intensity ratio of D and G bands (I_D/I_G) for GO and Pt-RGO were found to be 0.96 and 1.34, respectively, and this increase in intensity indicated a reduction in the average domain size of the sp^2 -hybridized carbon atoms upon reduction of exfoliated GO [59].

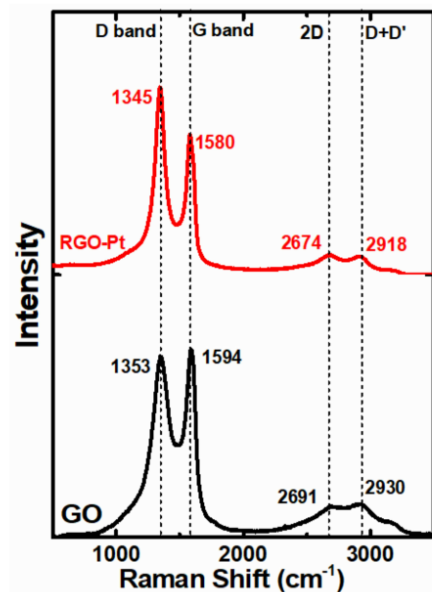


Figure 3. Raman spectra of GO and Pt-RGO.

The catalytic performance of the prepared green catalyst was assessed by studying its ability to catalyze the reduction of 4-NP to 4-aminophenol. While 4-NP shows the maximum absorbance at ~ 317 nm, after the addition of sodium borohydride, this peak shifts to 401 nm due to the formation of 4-nitrophenolate, intermediate of 4-NP deprotonation. Due to the high energetic barrier, hydrogenation to 4-aminophenol does not proceed without a catalyst, which was confirmed by the unchanged intensity at 401 nm in time (data not shown). However, upon the addition of the Pt-RGO catalyst, the intensity at 401 nm continuously decreased and 4-aminophenol is formed. In an excess of NaBH_4 (12 mM of NaBH_4 and 0.12 mM of 4-NP) the catalytic activity of Pt-RGO was described by the pseudo-first-order kinetic model [60]; the experiment being performed for four different Pt-RGO concentrations (0.0012 to 0.01 g/L).

The absorbance A can be considered linearly proportional to the concentration of C of 4-NP, and A/A_0 is proportional to C/C_0 , and thus the rate constant of the pseudo-first-order kinetic reaction can be calculated using Equation (1).

$$\ln\left(\frac{A_t}{A_0}\right) = -kt. \quad (1)$$

By following Equation (1), the rate constants (k_{app}) were determined to be 0.13, 0.20, 0.35 and 0.71 min^{-1} for the Pt-RGO catalyst concentration of 0.0012, 0.0025, 0.005 and 0.01 g/L, respectively (Figure 4b). The performance of the catalyst is linearly proportional to the concentration of catalyst used, hence, upon increasing the concentration of the catalyst, the k_{app} increased as well. This can be explained by the fact that when the concentration of the catalyst increased, the total surface area increased along with the number of active sites available for the catalytic reactions (Figure 4a) corroborating the earlier reports on the linear increase of k_{app} value with the increase in catalyst concentration. Lara et al. [61] reported an increase of k_{app} when the palladium-based catalyst concentration was increased. Similarly, Kastner and Thunemann [62] reported in their work that increasing the catalyst concentration (Ag NP) could increase the k_{app} in a linear way.

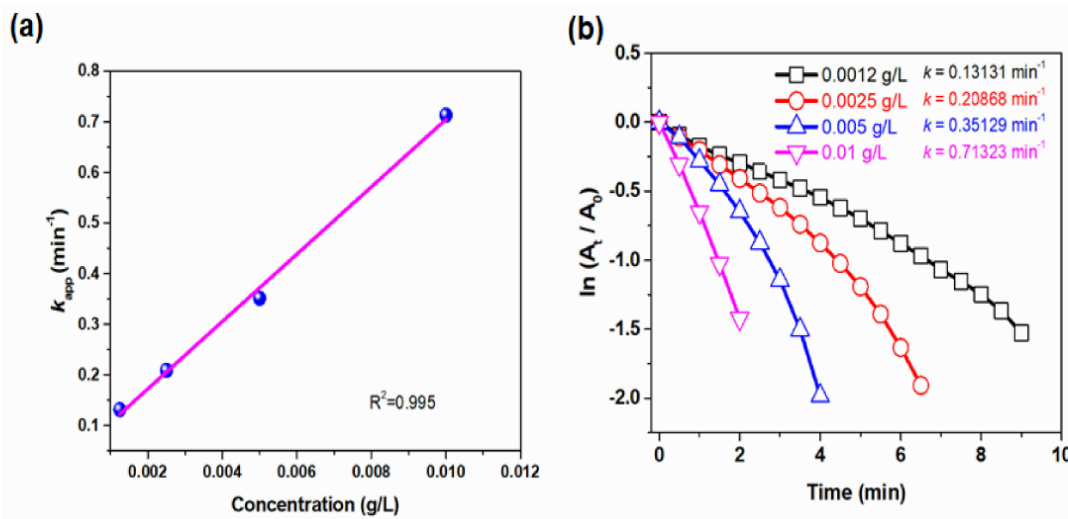


Figure 4. (a) k_{app} (min^{-1}) vs. concentration (g/L) of Pt-RGO used, (b) plot of $\ln(A_t/A_0)$ versus reaction time for different Pt-RGO concentrations (0.0012 to 0.01 g/L) for the reduction of 4-NP.

4-NP is one of the most used compounds for testing the catalytic activity of the catalysts; therefore, it should be easy to compare the catalytic performance of different catalysts. Further, to emphasize on the good catalytic performance of the Pt-RGO green catalysts, we have tabulated the k_{app} values of different studies in comparison with our study in Table 1.

Table 1. Comparison between different catalysts with our present study.

Catalysts	4-NP Concentration (mM)	NaBH ₄ Concentration (mM)	Reducing/ Supporting Material	Reaction Time (min)	Rate Constant (k_{app}) min ⁻¹	Reference
Pt-RGO	0.12	12	GK	2	0.71	This work
Pd-RGO/GA	5	0.5	Gum Arabic	5	0.12	[63]
Au ₅₃ Pd ₄₇ /Graphene nanosheets	0.05	5	-	3.5	0.86	[64]
GPt-RGONPs	0.024	0.024	Guar gum	240	0.42	[21]
AgNPs@MWCNTs	0.1	5	Chitosan	5	0.47	[65]
XG/Ag	1×10^{-4}	0.1	Xanthan gum	1440	0.90	[20]
LrGO-Ag ₂₀ Au ₈₀	9.6×10^{-5}	0.1	<i>Cetraria Islandica</i>	1.7	0.45	[66]

3. Materials and Methods

3.1. Chemicals and Materials

GK, a grade III non-edible gum waste (Figure S1), was collected from Girijan Co-operative Corporation, Hyderabad, India. Graphite with particle size < 50 μm was purchased from Merck. PtCl₄ (96%), sodium borohydride (98%), 4-nitrophenol (ReagentPlus > 99%) were procured from Sigma Aldrich. Sulfuric acid (96 wt%), hydrochloric acid (35 wt%), hydrogen peroxide (30 wt%), potassium permanganate, sodium nitrate was procured from Penta, Czech Republic. Deionized water (18.2 M Ω -cm⁻¹, ELGA, Veolia Water, Marlow, UK) was to carry out the experiments.

3.2. Synthesis of Pt-RGO Nanoparticles

GK was thoroughly cleaned by three washings with distilled water. To remove water and residual moisture from the gum samples, they were dried overnight in an oven at 80 °C. Completely dried gum samples were then powdered using a high-speed mechanical blender and then sieved using a mesh size of 250 μm to obtain a uniform fine powder.

Graphene Oxide (GO) was produced from graphite flakes using the modified Hummers method [48,67] In a typical process, 69 mL of concentrated sulfuric acid along with 1.5 g of sodium nitrate was taken in a two-necked round-bottomed flask to which 3 g of graphite powder was added gradually over 30 min period under constant stirring. The flask was then kept on an ice bath and 9 g of potassium permanganate powder was added very slowly for over 30 min; the temperature of the reaction was maintained so that it does not exceed 20 °C. After the addition, the ice bath was removed and the mixture was stirred at 35 °C for 12 h. Then, 138 mL of deionized water was poured into the solution, which raised the temperature up to 98 °C and turned the solution dark brown in color. The stirring was continued for another 2 h, after which 30 mL of 30% hydrogen peroxide was added to convert MnO₂ to soluble MnSO₄; the color of the mixture changed to golden yellow and the reaction was continued for another 30 min. Then, the mixture was washed with 5% HCl several times to remove sulfate salts. The product was made alkaline by washing it with 5% solution of sodium carbonate and the ensuing solid product was isolated by filtration and dried in an oven for 24 h at 75 °C.

Pt-RGO was prepared using the one-pot synthesis strategy via simultaneous reduction of both PtCl₄ salt and GO by GK waste. Briefly, GO dispersed in water, was added into PtCl₄ water solution (0.25–2 mM) under constant stirring such that the final GO concentration is 1 g/L. Then, the mixture was sonicated for 30 min to enable fine dispersion. A 2.5 mL of the above mixture was mixed with 2.5 mL GK solution (processed GK via deacetylation protocol; stock solution = 20 g L⁻¹) [24] under vigorous stirring in a sealed ampoule. The reaction was allowed to proceed for 30 min under heating (120–150 °C) in a dry bath, when reduced graphene oxide precipitated as a black solid; solution color became clear, as opposed to the initial light yellow color of PtCl₄, indicating the complete reduction of the metal salt. The ensuing product was isolated by centrifuging and washed with deionized water. Finally, the product was dried in an oven overnight to remove any residual moisture. The synthesis

was conducted under different reaction conditions by varying time, temperature and concentration of PtCl_4 to optimize the synthetic protocol.

3.3. Characterization Techniques

Scanning Electron Microscopy (SEM) of the samples was assessed on UHR FE-SEM Carl Zeiss ULTRA Plus, Germany, operating at 0.5–2.5 kV acceleration voltage. Further, to analyze the morphology and selected area electron diffraction (SAED) patterns field emission transmission electron microscopy (FE-TEM) JEM-2100F, JEOL Ltd., Japan, operating at 200 kV, was used. The particle size distribution was calculated by measuring 50 particles using HRTEM images by using ImageJ. The obtained micrographs were processed by using the digital image processing software Gatan Digital Micrograph. The crystallographic structures of the material were determined using X-ray diffraction (XRD) spectroscopy, which was performed on Bruker, AXS/8, Berlin, Germany and the diffraction spectrum over 2θ range of 0 to 80° was obtained using $\text{Cu-K}\alpha$ radiation (40 kV, 60 mA) to identify the crystal phase and composition. Raman Spectroscopy was carried out using a Raman DXR microscope (Thermo Fisher, Waltham, MA, USA), with a laser excitation wavelength of 514 nm on an Argon laser with 1 cm^{-1} spectral resolution. The spectra were recorded at ambient conditions in the range $1000\text{--}3000\text{ cm}^{-1}$. UV-vis spectroscopy was performed on Hach Lange DR 3900 UV-vis spectrophotometer, UK using 1 cm quartz cuvettes.

3.4. Catalytic Reduction of 4-Nitrophenol (4-NP)

The catalytic prowess of Pt-RGO catalysts was evaluated in hydrogenation of 4-NP to 4-aminophenol using NaBH_4 , where the procedure was followed on the lines previously reported by Baruah et al. [68]. Initially, 24 μL of 4-NP (5 mM) was taken in an Eppendorf tube to which the prerequisite amount of Pt-RGO was added (0.0012 to 0.01 g/L). To this mixture, 120 μL of NaBH_4 (0.1 M) was added followed by the addition of DI water to adjust the volume to 1 mL. This solution mixture was thoroughly mixed and immediately transferred to a clean quartz cuvette (1 cm path length), and the absorbance was recorded continuously over regular time intervals using a UV-Vis spectrometer.

4. Conclusions

A one-pot co-reduction method was uncovered successfully to obtain RGO sheets decorated uniformly with Pt nanoparticles using biorenewable GK waste as a reducing agent. Even though GK has been used in the synthesis of metal nanoparticles, its ability to simultaneously reduce GO and metal salts has not been studied until now, to directly generate nanocomposite from a readily available and eco-friendly precursor. Furthermore, the proposed synthesis is fairly expeditious as compared to other reported methods [63,69,70] GK has not only successfully reduced Pt salt and GO simultaneously, but also assisted in the fine dispersion of Pt on the RGO surface; hydroxyl groups on the GO surface provide anchoring sites for the deposition of Pt nanoparticles. The obtained Pt-RGO nanoparticles were further analyzed by SEM, TEM, XRD, and Raman spectroscopy, where morphological studies showed that the ensuing nanoparticles were spherical in shape with an average particle size of $3.3 \pm 0.6\text{ nm}$ and the Raman studies and XRD results established the successful reduction of GO by GK. In addition, XRD results indicated the formation of crystalline Pt nanoparticles with fcc geometry. The Pt-RGO thus obtained, displayed good catalytic performance in the hydrogenation of 4-nitrophenol, wherein the hydrogenation of 4-nitrophenol occurred in 2 min reaction time with a rate constant (k_{app}) of 0.71 min^{-1} . The superior catalytic performance of the Pt-RGO catalyst can be attributed to the synergistic effect of Pt nanoparticles anchored on the RGO surface. The simple and easy synthesis of Pt-RGO follows greener synthesis protocols and offers attractive possibilities to be used in the production of efficient green catalysts for the reduction of toxic and hazardous chemicals in various fields.

Supplementary Materials: The following are available online at <http://www.mdpi.com/1420-3049/24/20/3643/s1>, Figure S1: Image of the gum kondagogu (grade III-non-edible gum). Figure S2: SEM images of Pt-RGO with different PtCl_4 concentration. (a) 0.25, (b) 0.5, (c) 1, and (d) 2 mM. Figure S3: Images of the final products of

different temperature (I) 120, (II) 130, (III) 140, and (IV) 150 °C. Figure S4: Images of the final products of different time (I) 15, (II) 30, and (III) 60 min. Figure S5: EDX profile of Pt-RGO. Figure S6: Plot of $\ln(A_t/A_0)$ versus reaction time of G-Pt of varying concentrations (a) 0.0012, (b) 0.0025, (c) 0.005 and (d) 0.01 g/L. Table S1: Different reaction conditions and concentrations for the optimization of the reaction conditions.

Author Contributions: Conceptualization, A.V.; methodology, A.V., D.S., R.K.R.; investigation, A.V., D.S., R.K.R., S.W.; writing—original draft preparation, A.V., D.S.; writing—review and editing, S.W., V.V.T.P., R.S.V., M.Č.; supervision, V.V.T.P., S.W., R.S.V.; project administration, M.Č.; funding acquisition, M.Č.

Funding: The authors acknowledge the support rendered by the Ministry of Education, Youth and Sports (MEYS) in the framework of the targeted support of the OPR&DI project ‘Extension of CxI facilities’ (CZ.1.05/2.1.00/19.0386), and the Research Infrastructure NanoEnviCz (Project No. LM2015073); and MEYS and the European Structural and Investment Funds in the frames of Operational Program Research, Development and Education for the Project Hybrid Materials for Hierarchical Structures (HyHi), Registration Number CZ.02.1.01/0.0/0.0/16_019/0000843). This work was also supported by the Student Grant Scheme 2019 project of the Technical University in Liberec.

Conflicts of Interest: The authors declare no conflict of interest.

References

- Schauermaier, S.; Nilius, N.; Shaikhutdinov, S.; Freund, H.-J. Nanoparticles for heterogeneous catalysis: New mechanistic insights. *Acc. Chem. Res.* **2013**, *46*, 1673–1681. [[CrossRef](#)] [[PubMed](#)]
- Polshettiwar, V.; Varma, R.S. Green chemistry by nano-catalysis. *Green Chem.* **2010**, *12*, 743. [[CrossRef](#)]
- Lee, K.S.; El-Sayed, M.A. Gold and silver nanoparticles in sensing and imaging: Sensitivity of plasmon response to size, shape, and metal composition. *J. Phys. Chem. B* **2006**, *110*, 19220–19225. [[CrossRef](#)] [[PubMed](#)]
- McNamara, K.; Tofail, S.A.M. Nanoparticles in biomedical applications. *Adv. Phys. X* **2017**, *2*, 54–88. [[CrossRef](#)]
- Azharuddin, M.; Zhu, G.H.; Das, D.; Ozgur, E.; Uzun, L.; Turner, A.P.F.; Patra, H.K. A repertoire of biomedical applications of noble metal nanoparticles. *Chem. Commun.* **2019**, *55*, 6964–6996. [[CrossRef](#)] [[PubMed](#)]
- Iravani, S.; Varma, R.S. Biofactories: Engineered nanoparticles via genetically engineered organisms. *Green Chem.* **2019**, *21*, 4583–4603. [[CrossRef](#)]
- Iravani, S.; Varma, R.S. Plant-derived edible nanoparticles and miRNAs: Emerging frontier for therapeutics and targeted drug-delivery. *ACS Sustain. Chem. Eng.* **2019**, *7*, 8055–8069. [[CrossRef](#)]
- Mei, W.; Wu, Q. Applications of metal nanoparticles in medicine/metal nanoparticles as anticancer agents. In *Metal Nanoparticles*; Wiley-VCH Verlag GmbH & Co. KGaA: Weinheim, Germany, 2017; pp. 169–190.
- Rai, M.; Ingle, A.P.; Gupta, I.; Brandelli, A. Bioactivity of noble metal nanoparticles decorated with biopolymers and their application in drug delivery. *Int. J. Pharm.* **2015**, *496*, 159–172. [[CrossRef](#)]
- Varma, R.S. Greener approach to nanomaterials and their sustainable applications. *Curr. Opin. Chem. Eng.* **2012**, *1*, 123–128. [[CrossRef](#)]
- Gawande, M.B.; Bonifácio, V.D.B.; Luque, R.; Branco, P.S.; Varma, R.S. Benign by design: Catalyst-free in-water, on-water green chemical methodologies in organic synthesis. *Chem. Soc. Rev.* **2013**, *42*, 5522–5551. [[CrossRef](#)]
- Silvestri, D.; Waclawek, S.; Sobel, B.; Torres-Mendieta, R.; Novotny, V.; Nguyen, N.H.A.; Ševců, A.; Padil, V.T.P.; Mullerova, J.; Stuchlik, M.; et al. A poly(3-hydroxybutyrate)–chitosan polymer conjugate for the synthesis of safer gold nanoparticles and their applications. *Green Chem.* **2018**, *20*, 4975–4982. [[CrossRef](#)]
- Gour, A.; Jain, N.K. Advances in green synthesis of nanoparticles. *Artif. Cells Nanomed. Biotechnol.* **2019**, *47*, 844–851. [[CrossRef](#)]
- Iravani, S. Green synthesis of metal nanoparticles using plants. *Green Chem.* **2011**, *13*, 2638. [[CrossRef](#)]
- Mohammadinejad, R.; Shavandi, A.; Raie, D.S.; Sangeetha, J.; Soleimani, M.; Hajibehzad, S.S.; Thangadurai, D.; Hospet, R.; Popoola, J.O.; Arzani, A.; et al. Plant molecular farming: Production of metallic nanoparticles and therapeutic proteins using green factories. *Green Chem.* **2019**, *21*, 1845–1865. [[CrossRef](#)]
- Padil, V.V.T.; Waclawek, S.; Černík, M.; Varma, R.S. Tree gum-based renewable materials: Sustainable applications in nanotechnology, biomedical and environmental fields. *Biotechnol. Adv.* **2018**, *36*, 1984–2016. [[CrossRef](#)] [[PubMed](#)]
- Virkutyte, J.; Varma, R.S. Green synthesis of metal nanoparticles: Biodegradable polymers and enzymes in stabilization and surface functionalization. *Chem. Sci.* **2011**, *2*, 837–846. [[CrossRef](#)]

18. Mohammadinejad, R.; Karimi, S.; Iravani, S.; Varma, R.S. Plant-derived nanostructures: Types and applications. *Green Chem.* **2015**, *18*, 20–52. [[CrossRef](#)]
19. Thekkae Padil, V.V.; Černík, M.; Padil, V.V.T.; Černík, M. Green synthesis of copper oxide nanoparticles using gum karaya as a biotemplate and their antibacterial application. *Int. J. Nanomed.* **2013**, *8*, 889–898.
20. Xu, W.; Jin, W.; Lin, L.; Zhang, C.; Li, Z.; Li, Y.; Song, R.; Li, B. Green synthesis of xanthan conformation-based silver nanoparticles: Antibacterial and catalytic application. *Carbohydr. Polym.* **2014**, *101*, 961–967. [[CrossRef](#)]
21. Pandey, S.; Mishra, S.B. Catalytic reduction of p-nitrophenol by using platinum nanoparticles stabilised by guar gum. *Carbohydr. Polym.* **2014**, *113*, 525–531. [[CrossRef](#)]
22. Chen, X.; Han, W.; Zhao, X.; Tang, W.; Wang, F. Epirubicin-loaded marine carrageenan oligosaccharide capped gold nanoparticle system for pH-triggered anticancer drug release. *Sci. Rep.* **2019**, *9*, 6754. [[CrossRef](#)] [[PubMed](#)]
23. Vinod, V.T.P.; Sashidhar, R.B.; Sarma, V.U.M.; Vijaya Saradhi, U.V.R. Compositional analysis and rheological properties of gum kondagogu (*Cochlospermum gossypium*): A tree gum from India. *J. Agric. Food Chem.* **2008**, *56*, 2199–2207. [[CrossRef](#)] [[PubMed](#)]
24. Vinod, V.T.P.; Sashidhar, R.B.; Suresh, K.I.; Rama Rao, B.; Saradhi, U.V.R.V.; Rao, T.P. Morphological, physico-chemical and structural characterization of gum kondagogu (*Cochlospermum gossypium*): A tree gum from India. *Food Hydrocoll.* **2008**, *22*, 899–915. [[CrossRef](#)]
25. Janaki, B.; Sashidhar, R. Subchronic (90-day) Toxicity Study in Rats Fed gum Kondagogu (*Cochlospermum gossypium*). *Food Chem. Toxicol.* **2000**, *38*, 523–534. [[CrossRef](#)]
26. Waclawek, S.; Padil, V.V.T.; Černík, M. Major advances and challenges in heterogeneous catalysis for environmental applications: A review. *Ecol. Chem. Eng. S* **2018**, *25*, 9–34. [[CrossRef](#)]
27. Chen, A.; Holt-Hindle, P. Platinum-based nanostructured materials: Synthesis, properties, and applications. *Chem. Rev.* **2010**, *110*, 3767–3804. [[CrossRef](#)]
28. Xu, Y.; Zhang, B. Recent advances in porous Pt-based nanostructures: Synthesis and electrochemical applications. *Chem. Soc. Rev.* **2014**, *43*, 2439. [[CrossRef](#)]
29. Kim, K.W.; Kim, S.M.; Choi, S.; Kim, J.; Lee, I.S. Electroless Pt deposition on Mn₃O₄ nanoparticles via the galvanic replacement process: Electrocatalytic nanocomposite with enhanced performance for oxygen reduction reaction. *ACS Nano* **2012**, *6*, 5122–5129. [[CrossRef](#)]
30. Dendooven, J.; Ramachandran, R.K.; Solano, E.; Kurttepel, M.; Geerts, L.; Heremans, G.; Ronge, J.; Minjauw, M.M.; Doobelaere, T.; Devloo-Casier, K.; et al. Independent tuning of size and coverage of supported Pt nanoparticles using atomic layer deposition. *Nat. Commun.* **2017**, *8*, 1074. [[CrossRef](#)]
31. Attard, G.A.; Ahmadi, A.; Jenkins, D.J.; Hazzazi, O.A.; Wells, P.B.; Griffin, K.G.; Johnston, P.; Gillies, J.E. The characterisation of supported platinum nanoparticles on carbon used for enantioselective hydrogenation: A combined electrochemical-stm approach. *Chem. Phys. Chem.* **2003**, *4*, 123–130. [[CrossRef](#)]
32. Wang, Y.-J.; Zhao, N.; Fang, B.; Li, H.; Bi, X.T.; Wang, H. Carbon-supported Pt-based alloy electrocatalysts for the oxygen reduction reaction in polymer electrolyte membrane fuel cells: Particle size, shape, and composition manipulation and their impact to activity. *Chem. Rev.* **2015**, *115*, 3433–3467. [[CrossRef](#)]
33. Wang, J.; Wang, Z.; Li, S.; Wang, R.; Song, Y. Surface and interface engineering of FePt/C nanocatalysts for electro-catalytic methanol oxidation: Enhanced activity and durability. *Nanoscale* **2017**, *9*, 4066–4075. [[CrossRef](#)]
34. Zhang, B.-W.; Zhang, Z.-C.; Liao, H.-G.; Gong, Y.; Gu, L.; Qu, X.-M.; You, L.-X.; Liu, S.; Huang, L.; Tian, X.-C.; et al. Tuning Pt-skin to Ni-rich surface of Pt₃Ni catalysts supported on porous carbon for enhanced oxygen reduction reaction and formic electro-oxidation. *Nano Energy* **2016**, *19*, 198–209. [[CrossRef](#)]
35. Yang, G.; Frenkel, A.I.; Su, D.; Teng, X. Enhanced electrokinetics of C–C bond splitting during ethanol oxidation by using a Pt/Rh/Sn catalyst with a partially oxidized Pt and Rh core and a SnO₂ shell. *ChemCatChem* **2016**, *8*, 2876–2880. [[CrossRef](#)]
36. Li, B.; Fan, H.; Cheng, M.; Song, Y.; Li, F.; Wang, X.; Wang, R. Porous Pt–NiO_x nanostructures with ultrasmall building blocks and enhanced electrocatalytic activity for the ethanol oxidation reaction. *RSC Adv.* **2018**, *8*, 698–705. [[CrossRef](#)]
37. Seselj, N.; Engelbrekt, C.; Zhang, J. Graphene-supported platinum catalysts for fuel cells. *Sci. Bull.* **2015**, *60*, 864–876. [[CrossRef](#)]

38. Yarar Kaplan, B.; Haghmoradi, N.; Biçer, E.; Merino, C.; Alkan Gürsel, S. High performance electrocatalysts supported on graphene based hybrids for polymer electrolyte membrane fuel cells. *Int. J. Hydrogen Energy* **2018**, *43*, 23221–23230. [[CrossRef](#)]
39. Takenaka, S.; Miyamoto, H.; Utsunomiya, Y.; Matsune, H.; Kishida, M. Catalytic activity of highly durable Pt/CNT catalysts covered with hydrophobic silica layers for the oxygen reduction reaction in PEFCs. *J. Phys. Chem. C* **2014**, *118*, 774–783. [[CrossRef](#)]
40. Novoselov, K.S.; Geim, A.K.; Morozov, S.V.; Jiang, D.; Zhang, Y.; Dubonos, S.V.; Grigorieva, I.V.; Firsov, A.A. Electric field effect in atomically thin carbon films. *Science* **2004**, *306*, 666–669. [[CrossRef](#)]
41. Geim, A.K.; Novoselov, K.S. The rise of graphene. *Nat. Mater.* **2007**, *6*, 183–191. [[CrossRef](#)]
42. Guermoune, A.; Chari, T.; Popescu, F.; Sabri, S.S.; Guillemette, J.; Skulason, H.S.; Szkopek, T.; Siaj, M. Chemical vapor deposition synthesis of graphene on copper with methanol, ethanol, and propanol precursors. *Carbon N. Y.* **2011**, *49*, 4204–4210. [[CrossRef](#)]
43. Habib, M.R.; Liang, T.; Yu, X.; Pi, X.; Liu, Y.; Xu, M. A review of theoretical study of graphene chemical vapor deposition synthesis on metals: Nucleation, growth, and the role of hydrogen and oxygen. *Rep. Prog. Phys.* **2018**, *81*, 036501. [[CrossRef](#)] [[PubMed](#)]
44. Kosynkin, D.V.; Higginbotham, A.L.; Sinitiskii, A.; Lomeda, J.R.; Dimiev, A.; Price, B.K.; Tour, J.M. Longitudinal unzipping of carbon nanotubes to form graphene nanoribbons. *Nature* **2009**, *458*, 872–876. [[CrossRef](#)] [[PubMed](#)]
45. Akhavan, O.; Ghaderi, E.; Emamy, H.; Akhavan, F. Genotoxicity of graphene nanoribbons in human mesenchymal stem cells. *Carbon N.Y.* **2013**, *54*, 419–431. [[CrossRef](#)]
46. Novoselov, K.S.; Fal'ko, V.I.; Colombo, L.; Gellert, P.R.; Schwab, M.G.; Kim, K. A roadmap for graphene. *Nature* **2012**, *490*, 192–200. [[CrossRef](#)] [[PubMed](#)]
47. Warner, J.H.; Schaffel, F.; Rummeli, M.; Bachmatiuk, A. *Graphene: Fundamentals and Emergent Applications*; Elsevier: Amsterdam, The Netherlands, 2013.
48. Kattimuttathu, S.I.; Chidambaram, K.; Vinod, V.; Rajender, N.; Venkateswara, R.M.; Cernik, M. Synthesis, characterization and optical properties of graphene oxide-polystyrene nanocomposites. *Polym. Adv. Technol.* **2015**, *26*, 214–222.
49. Gao, X.; Jang, J.; Nagase, S. Hydrazine and thermal reduction of graphene oxide: Reaction mechanisms, product structures, and reaction design. *J. Phys. Chem. C* **2010**, *114*, 832–842. [[CrossRef](#)]
50. Yang, Z.; Zheng, Q.; Qiu, H.; Li, J.; Yang, J. A simple method for the reduction of graphene oxide by sodium borohydride with CaCl₂ as a catalyst. *New Carbon Mater.* **2015**, *30*, 41–47. [[CrossRef](#)]
51. Liu, Y.; Zhang, Y.; Ma, G.; Wang, Z.; Liu, K.; Liu, H. Ethylene glycol reduced graphene oxide/polypyrrole composite for supercapacitor. *Electrochim. Acta* **2013**, *88*, 519–525. [[CrossRef](#)]
52. Xu, C.; Yuan, R.; Wang, X. Selective reduction of graphene oxide. *New Carbon Mater.* **2014**, *29*, 61–66. [[CrossRef](#)]
53. Li, Z.; Gao, Q.; Zhang, H.; Tian, W.; Tan, Y.; Qian, W.; Liu, Z. Low content Pt nanoparticles anchored on N-doped reduced graphene oxide with high and stable electrocatalytic activity for oxygen reduction reaction. *Sci. Rep.* **2017**, *7*, 43352. [[CrossRef](#)] [[PubMed](#)]
54. Abhilash, V.; Rajender, N.; Suresh, K. X-ray diffraction spectroscopy of polymer nanocomposites. In *Spectroscopy of Polymer Nanocomposites*; Elsevier Inc.: Amsterdam, The Netherlands, 2016; pp. 410–451.
55. Moon, I.K.; Lee, J.; Ruoff, R.S.; Lee, H. Reduced graphene oxide by chemical graphitization. *Nat. Commun.* **2010**, *1*, 73. [[CrossRef](#)] [[PubMed](#)]
56. Sen, F.; Karatas, Y.; Gulcan, M.; Zahmakiran, M. Amylamine stabilized platinum(0) nanoparticles: Active and reusable nanocatalyst in the room temperature dehydrogenation of dimethylamine-borane. *RSC Adv.* **2014**, *4*, 1526–1531. [[CrossRef](#)]
57. Stankovich, S.; Dikin, D.A.; Piner, R.D.; Kohlhaas, K.A.; Kleinhammas, A.; Jia, Y.; Wu, Y.; Nguyen, S.T.; Ruoff, R.S. Synthesis of graphene-based nanosheets via chemical reduction of exfoliated graphite oxide. *Carbon N.Y.* **2007**, *45*, 1558–1565. [[CrossRef](#)]
58. Muhammad Hafiz, S.; Ritikos, R.; Whitcher, T.J.; Md. Razib, N.; Bien, D.C.S.; Chanlek, N.; Nakajima, H.; Saisopa, T.; Songsiriritthigul, P.; Huang, N.M.; et al. A practical carbon dioxide gas sensor using room-temperature hydrogen plasma reduced graphene oxide. *Sensors Actuators B Chem.* **2014**, *193*, 692–700. [[CrossRef](#)]
59. Tuinstra, F.; Koenig, J.L. Raman spectrum of graphite. *J. Chem. Phys.* **1970**, *53*, 1126–1130. [[CrossRef](#)]

60. Stumm, W.; Morgan, J.J. *Aquatic Chemistry: Chemical Equilibria and Rates in Natural Waters*; John Wiley & Sons: Hoboken, NJ, USA, 1996.
61. Lara, L.R.S.; Zottis, A.D.; Elias, W.C.; Faggion, D.; Campos, C.E.M.; Acuna, J.J.S.; Domingos, J.B. The catalytic evaluation of in situ grown Pd nanoparticles on the surface of Fe₃O₄@dextran particles in the p-nitrophenol reduction reaction. *RSC Adv.* **2015**, *5*, 8289–8296. [[CrossRef](#)]
62. Kästner, C.; Thünemann, A.F. Catalytic reduction of 4-nitrophenol using silver nanoparticles with adjustable activity. *Langmuir* **2016**, *32*, 7383–7391. [[CrossRef](#)] [[PubMed](#)]
63. Vilian, A.T.E.; Choe, S.R.; Giribabu, K.; Jang, S.-C.; Roh, C.; Huh, Y.S.; Han, Y.-K. Pd nanospheres decorated reduced graphene oxide with multi-functions: Highly efficient catalytic reduction and ultrasensitive sensing of hazardous 4-nitrophenol pollutant. *J. Hazard. Mater.* **2017**, *333*, 54–62. [[CrossRef](#)] [[PubMed](#)]
64. Chen, X.; Cai, Z.; Chen, X.; Oyama, M. AuPd bimetallic nanoparticles decorated on graphene nanosheets: Their green synthesis, growth mechanism and high catalytic ability in 4-nitrophenol reduction. *J. Mater. Chem. A* **2014**, *2*, 5668–5674. [[CrossRef](#)]
65. Alshehri, S.M.; Almuqati, T.; Almuqati, N.; Al-Farraj, E.; Alhokbany, N.; Ahamad, T. Chitosan based polymer matrix with silver nanoparticles decorated multiwalled carbon nanotubes for catalytic reduction of 4-nitrophenol. *Carbohydr. Polym.* **2016**, *151*, 135–143. [[CrossRef](#)] [[PubMed](#)]
66. Çıplak, Z.; Getiren, B.; Gökalp, C.; Yıldız, A.; Yıldız, N. Green synthesis of reduced graphene oxide-AgAu bimetallic nanocomposite: Catalytic performance. *Chem. Eng. Commun.* **2019**, 1–15. [[CrossRef](#)]
67. Hummers, W.S.; Offeman, R.E. Preparation of graphitic oxide. *J. Am. Chem. Soc.* **1958**, *80*, 1339. [[CrossRef](#)]
68. Baruah, B.; Gabriel, G.J.; Akbashev, M.J.; Booher, M.E. Facile synthesis of silver nanoparticles stabilized by cationic polynorbornenes and their catalytic activity in 4-nitrophenol reduction. *Langmuir* **2013**, *29*, 4225–4234. [[CrossRef](#)] [[PubMed](#)]
69. Raju, M.M.; Pattanayak, D.K. A platinum supported reduced graphene catalyst to enhance the hydrogenation of nitro compound activity. *RSC Adv.* **2015**, *5*, 59541–59549. [[CrossRef](#)]
70. Nie, R.; Wang, J.; Wang, L.; Qin, Y.; Chen, P.; Hou, Z. Platinum supported on reduced graphene oxide as a catalyst for hydrogenation of nitroarenes. *Carbon N.Y.* **2012**, *50*, 586–596. [[CrossRef](#)]

Sample Availability: Samples of the gum and their functionalized nanoparticles are available from the authors.



© 2019 by the authors. Licensee MDPI, Basel, Switzerland. This article is an open access article distributed under the terms and conditions of the Creative Commons Attribution (CC BY) license (<http://creativecommons.org/licenses/by/4.0/>).

4. Conclusions

The work carried out in this thesis is aimed to investigate the potential of exudate tree gums for various applications, with an emphasis on food packaging application. Due to their intrinsic shortcomings, tree gum polysaccharides do not fulfill food packaging requirements. The methods adopted in this study appear to overcome these limitations, enhancing the potential of these gums to be used as a substitute for conventional packaging material.

The incorporation of graphene oxide (GO) into the gum matrix resulted in the enhancement of the film-forming ability of the gums via secondary interactions. The gums intercalated the GO layers forming highly ordered freestanding films with enhanced mechanical properties. This improvement in the properties arises from the interactions between the functional groups of the components via hydrogen bonding. The addition of GO created a tortuous path for the diffusion of gas molecules through the films, thus enhancing the barrier properties to levels equivalent to traditional packing materials.

The hygroscopic nature of kondagogu gum was reduced by its chemical modification using long-chain alkenyl groups of dodecenyl succinic anhydride (DDSA). The introduction of a 12-carbon hydrophobic chain was confirmed by ^1H nuclear magnetic resonance and Fourier-transform infrared spectroscopy. The long-chain carbon groups served as internal plasticizers, resulting in an amorphous structure with improved film-forming ability, hydrophobicity, and flexibility. Furthermore, the addition of nanocellulose fibres enhanced the mechanical strength and barrier characteristics of the films. The modified films exhibited antibacterial properties and excellent biodegradability under aerobic conditions.

Despite these modifications, the films exhibited humidity-induced property deterioration. To overcome this, the films were coated with aqueous dispersions of PVA and sodium hectorite clay nanoparticles. The coating enhanced the material's mechanical characteristics, such as tensile

strength and modulus, while also creating a tortuous path for decreased gas diffusion. The resulting flexible packaging films outperform several conventional polymers in terms of barrier performance. The improved barrier characteristics remain unaffected by the increase in relative humidity as high as 75%.

Furthermore, edible films based on dialdehyde modified karaya crosslinked gelatin films were fabricated. The chemical modification and the crosslinking were confirmed by ^{13}C nuclear magnetic resonance and Fourier-transform infrared spectroscopy. These chemically crosslinked biopolymer composite films exhibited excellent stability with improvement in mechanical and barrier properties. The films retain biodegradability despite the crosslinking, the films are biodegradable, implying that these bioplastics are environmentally sustainable and might be useful in the edible film-based packaging sector.

Additionally, the lower grade tree gum wastes were used to obtain value-added nanostructures for advanced applications. The carbon-rich structure of the gum wastes was carbonized to obtain high surface area nanoporous structures. These resulting materials allow for rapid water evaporation via capillary action, making them ideal for water-driven efficient electrical energy harvesters. Under asymmetric wetting and ambient conditions, the energy harvesters demonstrated excellent capability to generate electricity reliably with tremendous potential to scale up. The abundant hydroxyl functional groups present in the non-edible KG wastes were used in the synthesis of reduced graphene oxide (RGO) supported platinum nanoparticles. KG aided in the simultaneous reduction of Pt salt and GO, as well as homogenous nanoparticle dispersion over the RGO surface. The supported nanoparticles exhibited superior catalytic performance in the hydrogenation of 4-nitrophenol, wherein the reduction of 4-nitrophenol to 4-aminophenol was achieved very quickly.

5. Future prospects

Exudate gums possess a unique set of properties which makes them an ideal material for the development of biodegradable packaging material. One of the important outcomes of the present investigation is the potential ability of the tree gums in the development of packaging films with remarkable properties. Nevertheless, the research presented in this thesis was conducted on a laboratory scale and there is still a need for the scaling up of the process. In a large-scale sector like food packaging, solution casting may not be an optimal option for film fabrication. Extrusion is one example of a scalable process that should be investigated in future. To be employed in thermal processing procedures such as extrusion, the thermal profile of tree gums must be extensively researched. Gums can be mixed with other biopolymers such as starches, which have already been validated in the extrusion technique, to improve their thermal processability.

The development of edible films using tree gum polysaccharides is another prospective application with tremendous potential. Edible films incorporated with bioactive materials could be developed for the active packaging of food and pharmaceuticals. Furthermore, the sustainable bioplastics developed using tree gums can be extended to other applications including biomedical, energy and environmental applications. The non-toxicity, biocompatibility and non-mutagenic properties of the tree gums could be explored in biomedical applications. Bioinks based on tree gums could be developed for 3D printing structures for use in biomedical applications, biosensors and food areas.

6. Publications

Thesis related publications:

- [1] **A. Venkateshaiah**, J.Y. Cheong, C. Habel, S. Waclawek, T. Lederer, M. Černík, I.-D. Kim, V.V.T. Padil, S. Agarwal, “*Tree Gum-Graphene Oxide Nanocomposite Films as Gas Barriers*”, *ACS Appl. Nano Mater.* 3 (2020). <https://doi.org/10.1021/acsanm.9b02166>.
- [2] **A. Venkateshaiah**, K. Havlíček, R.L. Timmins, M. Röhrl, S. Waclawek, N.H.A. Nguyen, M. Černík, V.V.T. Padil, S. Agarwal, “*Alkenyl succinic anhydride modified tree-gum kondagogu: A bio-based material with potential for food packaging*”, *Carbohydr. Polym.* 266 (2021) 118126. <https://doi.org/10.1016/j.carbpol.2021.118126>.
- [3] **A. Venkateshaiah**, R.L. Timmins, E. Sehl, S. Waclawek, M. Černík, V.V.T. Padil, and S. Agarwal. “*High Barrier, Biodegradable Nanocomposite Films based on Clay Coated and Chemically Modified Gum Kondagogu.*” *Macromolecular Materials and Engineering.* 2200008 [2022]. <https://doi.org/10.1002/mame.202200008>
- [4] **A. Venkateshaiah**, E. Sehl, R.L. Timmins, S. Waclawek, M. Černík, S. Agarwal, and V.V. T. Padil. “*Dialdehyde Modified Tree Gum Karaya: A Sustainable Green Crosslinker for Gelatin-Based Edible Films.*” *Advanced Sustainable Systems.* 2100423 [2022]. <https://doi.org/10.1002/adsu.202100423>.
- [5] **A. Venkateshaiah**, J.Y. Cheong, S.H. Shin, K.P. Akshaykumar, T.G. Yun, J. Bae, S. Waclawek, M. Černík, S. Agarwal, A. Greiner, V.V.T. Padil, I.D. Kim, R.S. Varma, “*Recycling non-food-grade tree gum wastes into nanoporous carbon for sustainable energy harvesting*”, *Green Chem.* 22 (2020) 1198–1208. <https://doi.org/10.1039/c9gc04310a>.
- [6] **A. Venkateshaiah**, D. Silvestri, R.K. Ramakrishnan, S. Waclawek, V.V.T. Padil, M. Černík, R.S. Varma, “*Gum kondagoagu/reduced graphene oxide framed platinum nanoparticles and their catalytic role*”, *Molecules.* 24 (2019) 3643. <https://doi.org/10.3390/molecules24203643>.
- [7] **A. Venkateshaiah**, V.V.T. Padil, M. Nagalakshmaiah, S. Waclawek, M. Černík, R.S. Varma, “*Microscopic Techniques for the Analysis of Micro and Nanostructures of Biopolymers and Their Derivatives*”, *Polymers (Basel).* 12 (2020) 512. <https://doi.org/10.3390/polym12030512>.

Additional publications:

- [8] **A. Venkateshaiah**, D. Silvestri, S. Waclawek, R.K. Ramakrishnan, K. Krawczyk, P. Saravanan, M. Pawlyta, V.V.T. Padil, M. Černík, D.D. Dionysiou, “*A comparative study of the degradation efficiency of chlorinated organic compounds by bimetallic zero-valent iron nanoparticles*”, *Environ. Sci. Water Res. Technol.* (2022).

<https://doi.org/10.1039/D1EW00791B>.

- [9] J.Y. Cheong, **A. Venkateshaiah**, T.G. Yun, S.-H. Shin, M. Černík, V.V.T. Padil, I.-D. Kim, R.S. Varma, “*Transforming gum wastes into high tap density micron-sized carbon with ultra-stable high-rate Li storage*”, *Electrochim. Acta.* (2020) 137419. <https://doi.org/10.1016/j.electacta.2020.137419>.
- [10] D. Silvestri, S. Waclawek, **A. Venkateshaiah**, K. Krawczyk, B. Sobel, V.V.T. Padil, M. Černík, R.S. Varma, “*Synthesis of Ag nanoparticles by a chitosan-poly(3-hydroxybutyrate) polymer conjugate and their superb catalytic activity*”, *Carbohydr. Polym.* 232 (2020). <https://doi.org/10.1016/j.carbpol.2019.115806>.
- [11] D. Silvestri, S. Waclawek, R. K. Ramakrishnan, **A. Venkateshaiah**, K. Krawczyk, V.V.T. Padil, B. Sobel, M. Černík, “*The Use of a Biopolymer Conjugate for an Eco-Friendly One-Pot Synthesis of Palladium-Platinum Alloys*”, *Polymers (Basel)*. 11 (2019) 1948. <https://doi.org/10.3390/polym11121948>.
- [12] S.H. Shin, J.Y. Cheong, H. Lim, V.V.T. Padil, **A. Venkateshaiah**, I.D. Kim, “*Carbon anchored conducting polymer composite linkage for high performance water energy harvesters*”, *Nano Energy*. 74 (2020) 104827. <https://doi.org/10.1016/j.nanoen.2020.104827>.
- [13] E.N. Zare, V.V.T. Padil, B. Mokhtari, **A. Venkateshaiah**, S. Waclawek, M. Černík, F.R. Tay, R.S. Varma, P. Makvandi, “*Advances in biogenically synthesized shaped metal- and carbon-based nanoarchitectures and their medicinal applications*”, *Adv. Colloid Interface Sci.* 283 (2020) 102236. <https://doi.org/10.1016/j.cis.2020.102236>.

7. References

- 1 PlasticsEurope, <https://www.plasticseurope.org/en>, (accessed 21 September 2021).
- 2 A. Chamas, H. Moon, J. Zheng, Y. Qiu, T. Tabassum, J. H. Jang, M. Abu-Omar, S. L. Scott and S. Suh, Degradation Rates of Plastics in the Environment, *ACS Sustain. Chem. Eng.*, 2020, **8**, 3494–3511.
- 3 P. Li, X. Wang, M. Su, X. Zou, L. Duan and H. Zhang, Characteristics of Plastic Pollution in the Environment: A Review, *Bull. Environ. Contam. Toxicol.* 2020, 2020, **1**, 1–8.
- 4 M. N. Issac and B. Kandasubramanian, Effect of microplastics in water and aquatic systems, *Environ. Sci. Pollut. Res.*, 2021, **28**, 19544–19562.
- 5 Q. Chen, A. Allgeier, D. Yin and H. Hollert, Leaching of endocrine disrupting chemicals from marine microplastics and mesoplastics under common life stress conditions, *Environ. Int.*, 2019, **130**, 104938.
- 6 L. Lu, T. Luo, Y. Zhao, C. Cai, Z. Fu and Y. Jin, Interaction between microplastics and microorganism as well as gut microbiota: A consideration on environmental animal and human health, *Sci. Total Environ.*, 2019, **667**, 94–100.
- 7 R. Geyer, J. R. Jambeck and K. L. Law, Production, use, and fate of all plastics ever made, *Sci. Adv.*, 2017, **3**, e1700782.
- 8 A. Venkateshaiah, V. V. T. Padil, M. Nagalakshmaiah, S. Waclawek, M. Černík and R. S. Varma, Microscopic Techniques for the Analysis of Micro and Nanostructures of Biopolymers and Their Derivatives, *Polymers (Basel)*, 2020, **12**, 512.
- 9 R. Gheorghita, L. Anchidin-Norocel, R. Filip, M. Dimian and M. Covasa, Applications of Biopolymers for Drugs and Probiotics Delivery, *Polym. 2021, Vol. 13, Page 2729*, 2021, **13**, 2729.
- 10 A. S. A. Mohammed, M. Naveed and N. Jost, Polysaccharides; Classification, Chemical Properties, and Future Perspective Applications in Fields of Pharmacology and Biological Medicine (A Review of Current Applications and Upcoming Potentialities), *J. Polym. Environ.* 2021 298, 2021, **29**, 2359–2371.
- 11 S. Barak, D. Mudgil and S. Taneja, Exudate gums: chemistry, properties and food applications – a review, *J. Sci. Food Agric.*, 2020, **100**, 2828–2835.
- 12 F. Bouaziz, M. Koubaa, R. Ellouz Ghorbel and S. Ellouz Chaabouni, Recent advances in Rosaceae gum exudates: From synthesis to food and non-food applications, *Int. J. Biol. Macromol.*, 2016, **86**, 535–545.
- 13 C. F. Abib, M. Ntoupka, R. Peltier, J. M. Harmand and P. Thaler, Ethephon: A tool to boost gum arabic production from *Acacia senegal* and to enhance gummosis processes, *Agrofor. Syst.*, 2013, **87**, 427–438.

- 14 L. N. Harsh, J. C. Tewari, H. A. Khan and M. Ram, Ethephon-induced gum Arabic exudation technique and its sustainability in arid and semi-arid regions of India, *For. Trees Livelihoods*, 2013, **22**, 204–211.
- 15 R. B. Sashidhar, D. Raju and R. Karuna, in *Polysaccharides: Bioactivity and Biotechnology*, eds. K. G. Ramawat and J.-M. Mérillon, Springer, Cham, 2015, pp. 185–217.
- 16 M. A. Cerqueira, A. I. Bourbon, A. C. Pinheiro, J. T. Martins, B. W. S. Souza, J. A. Teixeira and A. A. Vicente, Galactomannans use in the development of edible films/coatings for food applications, *Trends Food Sci. Technol.*, 2011, **22**, 662–671.
- 17 M. A. Cerqueira, M. J. Sousa-Gallagher, I. Macedo, R. Rodriguez-Aguilera, B. W. S. Souza, J. A. Teixeira and A. A. Vicente, Use of galactomannan edible coating application and storage temperature for prolonging shelf-life of “Regional” cheese, *J. Food Eng.*, 2010, **97**, 87–94.
- 18 P. Varela and S. M. Fiszman, Hydrocolloids in fried foods. A review, *Food Hydrocoll.*, 2011, **25**, 1801–1812.
- 19 J. M. Li and S. P. Nie, The functional and nutritional aspects of hydrocolloids in foods, *Food Hydrocoll.*, 2016, **53**, 46–61.
- 20 A. M. Hamdani, I. A. Wani and N. A. Bhat, Sources, structure, properties and health benefits of plant gums: A review, *Int. J. Biol. Macromol.*, 2019, **135**, 46–61.
- 21 V. Raj, J. H. Lee, J. J. Shim and J. Lee, Recent findings and future directions of grafted gum karaya polysaccharides and their various applications: A review, *Carbohydr. Polym.*, 2021, **258**, 117687.
- 22 M. S. Amiri, V. Mohammadzadeh, M. E. T. Yazdi, M. Barani, A. Rahdar and G. Z. Kyzas, Plant-Based Gums and Mucilages Applications in Pharmacology and Nanomedicine: A Review, *Mol. 2021, Vol. 26, Page 1770*, 2021, **26**, 1770.
- 23 V. D. Prajapati, G. K. Jani, N. G. Moradiya and N. P. Randeria, Pharmaceutical applications of various natural gums, mucilages and their modified forms, *Carbohydr. Polym.*, 2013, **92**, 1685–1699.
- 24 I. Inamuddin, M. I. Ahamed, R. Boddula and T. Altalhi, *Polysaccharides : properties and applications*, John Wiley & Sons, Ltd., 2021.
- 25 A. Khezerlou, H. Zolfaghari, S. A. Banihashemi, S. Forghani and A. Ehsani, Plant gums as the functional compounds for edible films and coatings in the food industry: A review, *Polym. Adv. Technol.*, 2021, **32**, 2306–2326.
- 26 V. V. T. Padil, S. Waclawek, M. Černík and R. S. Varma, Tree gum-based renewable materials: Sustainable applications in nanotechnology, biomedical and environmental fields, *Biotechnol. Adv.*, 2018, **36**, 1984–2016.
- 27 A. Nussinovitch, in *Plant Gum Exudates of the World*, CRC Press, 2009, pp. 1–22.

- 28 D. Verbeken, S. Dierckx and K. Dewettinck, Exudate gums: Occurrence, production, and applications, *Appl. Microbiol. Biotechnol.*, 2003, **63**, 10–21.
- 29 P. A. Williams, in *Gum Arabic*, eds. J. F. Kennedy, G. O. Phillips and P. A. Williams, Royal Society of Chemistry, Cambridge, 2011, pp. 179–187.
- 30 B. H. Ali, A. Ziada and G. Blunden, Biological effects of gum arabic: A review of some recent research, *Food Chem. Toxicol.*, 2009, **47**, 1–8.
- 31 A. Abuarra, R. Hashim, S. Bauk, S. Kandaiya and E. T. Tousi, Fabrication and characterization of gum Arabic bonded *Rhizophora* spp. particleboards, *Mater. Des.*, 2014, **60**, 108–115.
- 32 S. P. Egadu, P. Mucunguzi and J. Obua, Uses of tree species producing gum arabic in Karamoja, Uganda, *Afr. J. Ecol.*, 2007, **45**, 17–21.
- 33 H. H. Musa, A. A. Ahmed and T. H. Musa, in *Bioactive Molecules in Food*, eds. J.-M. Mérillon and K. G. Ramawat, Springer, Cham, 2019, pp. 797–814.
- 34 F. Thevenet, in *Polymer Science: A Comprehensive Reference*, eds. K. Matyjaszewski and M. Möller, Elsevier, 2012, vol. 10, pp. 205–212.
- 35 S. Patel and A. Goyal, Applications of Natural Polymer Gum Arabic: A Review, *Int. J. Food Prop.*, 2015, **18**, 986–998.
- 36 R. C. Randall, G. O. Phillips and P. A. Williams, Fractionation and characterization of gum from *Acacia senegal*, *Food Hydrocoll.*, 1989, **3**, 65–75.
- 37 S. Al-Assaf, G. O. Phillips, H. Aoki and Y. Sasaki, Characterization and properties of *Acacia senegal* (L.) Willd. var. *senegal* with enhanced properties (*Acacia* (sen) SUPER GUM™): Part 1—Controlled maturation of *Acacia senegal* var. *senegal* to increase viscoelasticity, produce a hydrogel form and convert a poor into a good emulsifier, *Food Hydrocoll.*, 2007, **21**, 319–328.
- 38 C. Flindt, S. Al-Assaf, G. O. Phillips and P. A. Williams, Studies on acacia exudate gums. Part V. Structural features of *Acacia seyal*, *Food Hydrocoll.*, 2005, **19**, 687–701.
- 39 N. E. Siddig, M. E. Osman, S. Al-Assaf, G. O. Phillips and P. A. Williams, Studies on acacia exudate gums, part IV. Distribution of molecular components in *Acacia seyal* in relation to *Acacia senegal*, *Food Hydrocoll.*, 2005, **19**, 679–686.
- 40 E. A. Hassan, S. Al-Assaf, G. O. Phillips and P. A. Williams, Studies on *Acacia* gums: Part III molecular weight characteristics of *Acacia seyal* var. *seyal* and *Acacia seyal* var. *fistula*, *Food Hydrocoll.*, 2005, **19**, 669–677.
- 41 S. Al-Assaf, G. O. Phillips and P. A. Williams, Studies on acacia exudate gums. Part I: the molecular weight of *Acacia senegal* gum exudate, *Food Hydrocoll.*, 2005, **19**, 647–660.
- 42 A. K. Ray, P. B. Bird, G. A. Iacobucci and B. C. Clark, Functionality of gum arabic. Fractionation, characterization and evaluation of gum fractions in citrus oil emulsions and

- model beverages, *Food Hydrocoll.*, 1995, **9**, 123–131.
- 43 M. Dhiman, A. Singh and M. M. Sharma, A review on *Sterculia urens* Roxb.: a boon to the livelihood for tribal people and industry, *Ind. Crops Prod.*, 2019, **130**, 341–351.
- 44 A. Nussinovitch, in *Plant Gum Exudates of the World*, ed. A. Nussinovitch, CRC Press, 2009.
- 45 V. B. Kuruwanshi, P. Katiyar and S. Khan, Scientific Approaches of Gum Tapping in Gum Karaya (*Sterculia urens* Roxb.) for High Gum Production, *Int.J.Curr.Microbiol.App.Sci.*, 2017, **6**, 3366–3374.
- 46 H. Postulkova, I. Chamradova, D. Pavlinak, O. Humpa, J. Jancar and L. Vojtova, Study of effects and conditions on the solubility of natural polysaccharide gum karaya, *Food Hydrocoll.*, 2017, **67**, 148–156.
- 47 B. Janaki and R. B. Sashidhar, Physico-chemical analysis of gum kondagogu (*Cochlospermum gossypium*): A potential food additive, *Food Chem.*, 1998, **61**, 231–236.
- 48 V. T. P. Vinod and R. B. Sashidhar, Solution and conformational properties of gum kondagogu (*Cochlospermum gossypium*) – A natural product with immense potential as a food additive, *Food Chem.*, 2009, **116**, 686–692.
- 49 V. T. P. Vinod, R. B. Sashidhar, K. I. Suresh, B. Rama Rao, U. V. R. Vijaya Saradhi and T. Prabhakar Rao, Morphological, physico-chemical and structural characterization of gum kondagogu (*Cochlospermum gossypium*): A tree gum from India, *Food Hydrocoll.*, 2008, **22**, 899–915.
- 50 V. T. P. Vinod, R. B. Sashidhar, V. U. M. Sarma and U. V. R. Vijaya Saradhi, Compositional Analysis and Rheological Properties of Gum Kondagogu (*Cochlospermum gossypium*): A Tree Gum from India, *J. Agric. Food Chem.*, 2008, **56**, 2199–2207.
- 51 V. T. P. Vinod, R. B. Sashidhar, V. U. M. Sarma and S. S. Raju, Comparative amino acid and fatty acid compositions of edible gums kondagogu (*Cochlospermum gossypium*) and karaya (*Sterculia urens*), *Food Chem.*, 2010, **123**, 57–62.
- 52 V. T. P. Vinod and R. B. Sashidhar, Surface morphology, chemical and structural assignment of gum Kondagogu (*Cochlospermum gossypium* DC.): An exudate tree gum of India, *Indian J. Nat. Prod. Resour.*, 2010, **1**, 181–192.
- 53 V. T. P. Vinod, R. B. Sashidhar and M. Černík, Morphology and Metal Binding Characteristics of a Natural Polymer—Kondagogu (*Cochlospermum gossypium*) Gum, *Mol. 2013, Vol. 18, Pages 8264-8274*, 2013, **18**, 8264–8274.
- 54 A. Venkateshaiah, D. Silvestri, R. K. Ramakrishnan, S. Waclawek, V. V. T. Padil, M. Černík and R. S. Varma, Gum kondagoagu/reduced graphene oxide framed platinum nanoparticles and their catalytic role, *Molecules*, 2019, **24**, 3643.
- 55 A. Mortensen, F. Aguilar, R. Crebelli, A. Di Domenico, M. J. Frutos, P. Galtier, D. Gott, U. Gundert-Remy, C. Lambré, J. Leblanc, O. Lindtner, P. Moldeus, P. Mosesso, A.

- Oskarsson, D. Parent-Massin, I. Stankovic, I. Waalkens-Berendsen, R. A. Woutersen, M. Wright, M. Younes, L. Brimer, P. Peters, J. Wiesner, A. Christodoulidou, F. Lodi, A. Tard and B. Dusemund, Re-evaluation of karaya gum (E 416) as a food additive, *EFSA J.*, 2016, **14**, 4598.
- 56 D. M. W. Anderson and M. A. Eastwood, The safety of gum arabic as a food additive and its Energy Value as an ingredient: a brief review, *J. Hum. Nutr. Diet.*, 1989, **2**, 137–144.
- 57 D. M. W. Anderson, Evidence for the safety of gum karaya (*Sterculia* spp.) as a food additive, *Food Addit. Contam.*, 1989, **6**, 189–199.
- 58 A. Mortensen, F. Aguilar, R. Crebelli, A. Di Domenico, M. J. Frutos, P. Galtier, D. Gott, U. Gundert-Remy, C. Lambré, J. Leblanc, O. Lindtner, P. Moldeus, P. Mosesso, A. Oskarsson, D. Parent-Massin, I. Stankovic, I. Waalkens-Berendsen, R. A. Woutersen, M. Wright, M. Younes, L. Brimer, A. Christodoulidou, F. Lodi, A. Tard and B. Dusemund, Re-evaluation of acacia gum (E 414) as a food additive, *EFSA J.*, 2017, **15**, 4741.
- 59 B. Janaki and R. B. Sashidhar, Subchronic (90-day) Toxicity Study in Rats Fed gum Kondagogu (*Cochlospermum gossypium*), *Food Chem. Toxicol.*, 2000, **38**, 523–534.
- 60 F. Thevenet, in *Encapsulation and Controlled Release of Food Ingredients*, eds. S. J. Risch and G. A. Reineccius, 1995, pp. 51–59.
- 61 F. Shahidi and X. Han, Encapsulation of food ingredients, *Crit. Rev. Food Sci. Nutr.*, 2009, **33**, 501–547.
- 62 B. R. Bhandari, E. D. Dumoulin, H. M. J. Richard, I. Noleau and A. M. Lebert, Flavor Encapsulation by Spray Drying: Application to Citral and Linalyl Acetate, *J. Food Sci.*, 1992, **57**, 217–221.
- 63 S. M. Jafari, E. Assadpoor, Y. He and B. Bhandari, Encapsulation Efficiency of Food Flavours and Oils during Spray Drying, *Dry. Technol.*, 2008, **26**, 816–835.
- 64 S. Singh, R. Ranjan and A. Kumar Gupta, Role of Exudates in Food System: A mini-review, *J. Food Agric. Res.*, 2021, **1**, 109–121.
- 65 M. D. Ranken, R. C. Kill and C. Baker, Sugar and Chocolate Confectionery, *Food Ind. Man.*, 1997, 406–443.
- 66 M. A. Montenegro, M. L. Boiero, L. Valle and C. D. Borsarelli, in *Products and Applications of Biopolymers*, ed. J. Verbeek, IntechOpen, 2012, pp. 3–26.
- 67 E. W. Gakuru, M. N. Omwamba, B. N. Chikamai and S. M. Mahungu, Sensory Analysis of Sugar Reduced Jam Containing Gum Arabic from *Acacia senegal* var. *kerensis*, *Food Nutr. Sci.*, 2019, **10**, 1277–1286.
- 68 M. E. El-Sayed, A. S. Bakr, A. M. Gaafar, A. I. Ismaiel and M. M. Salem, Production low-fat beef burger by using gum arabic as fat replacer, *Menoufia J. Food Dairy Sci.*, 2020, **5**, 17–33.

- 69 R. Babiker, T. H. Merghani, K. Elmusharaf, R. M. Badi, F. Lang and A. M. Saeed, Effects of gum Arabic ingestion on body mass index and body fat percentage in healthy adult females: Two-arm randomized, placebo controlled, double-blind trial, *Nutr. J.*, 2012, **11**, 1–7.
- 70 S. J. Reiner, G. A. Reineccius and T. L. Peppard, A Comparison of the Stability of Beverage Cloud Emulsions Formulated with Different Gum Acacia- and Starch-Based Emulsifiers, *J. Food Sci.*, 2010, **75**, E236–E246.
- 71 B. Ebrahimi, A. Homayouni Rad, B. Ghanbarzadeh, M. Torbati and P. M. Falcone, The emulsifying and foaming properties of Amuniacum gum (*Dorema ammoniacum*) in comparison with gum Arabic, *Food Sci. Nutr.*, 2020, **8**, 3716–3730.
- 72 K. S. Minhas, J. S. Sidhu, G. S. Mudahar and A. K. Singh, Flow behavior characteristics of ice cream mix made with buffalo milk and various stabilizers, *Plant Foods Hum. Nutr.* 2002 **57**, 2002, **57**, 25–40.
- 73 S. Featherstone, in *A Complete Course in Canning and Related Processes*, ed. S. Featherstone, Woodhead Publishing, 14th edn., 2015, pp. 147–211.
- 74 J. N. BeMiller, in *Carbohydrate chemistry for food scientists*, ed. J. N. BeMiller, AACC International Press, 3rd edn., 2019, pp. 313–321.
- 75 A. M. El Shafey, Green synthesis of metal and metal oxide nanoparticles from plant leaf extracts and their applications: A review, *Green Process. Synth.*, 2020, **9**, 304–339.
- 76 P. K. Dikshit, J. Kumar, A. K. Das, S. Sadhu, S. Sharma, S. Singh, P. K. Gupta and B. S. Kim, Green Synthesis of Metallic Nanoparticles: Applications and Limitations, *Catalysts*, 2021, **11**, 902.
- 77 C. Vanlalveni, S. Lallianrawna, A. Biswas, M. Selvaraj, B. Changmai and S. L. Rokhum, Green synthesis of silver nanoparticles using plant extracts and their antimicrobial activities: a review of recent literature, *RSC Adv.*, 2021, **11**, 2804–2837.
- 78 A. Rana, K. Yadav and S. Jagadevan, A comprehensive review on green synthesis of nature-inspired metal nanoparticles: Mechanism, application and toxicity, *J. Clean. Prod.*, 2020, **272**, 122880.
- 79 S. Jadoun, R. Arif, N. K. Jangid and R. K. Meena, Green synthesis of nanoparticles using plant extracts: a review, *Environ. Chem. Lett.*, 2021, **19**, 355–374.
- 80 H. Duan, D. Wang and Y. Li, Green chemistry for nanoparticle synthesis, *Chem. Soc. Rev.*, 2015, **44**, 5778–5792.
- 81 H. R. El-Seedi, R. M. El-Shabasy, S. A. M. Khalifa, A. Saeed, A. Shah, R. Shah, F. J. Iftikhar, M. M. Abdel-Daim, A. Omri, N. H. Hajrahand, J. S. M. Sabir, X. Zou, M. F. Halabi, W. Sarhan and W. Guo, Metal nanoparticles fabricated by green chemistry using natural extracts: biosynthesis, mechanisms, and applications, *RSC Adv.*, 2019, **9**, 24539–24559.
- 82 V. V. T. Padil, E. N. Zare, P. Makvandi and M. Černík, Nanoparticles and nanofibres based

- on tree gums: Biosynthesis and applications, *Compr. Anal. Chem.*, 2021, **94**, 223–265.
- 83 A. Anwar, A. Masri, K. Rao, K. Rajendran, N. A. Khan, M. R. Shah and R. Siddiqui, Antimicrobial activities of green synthesized gums-stabilized nanoparticles loaded with flavonoids, *Sci. Rep.*, 2019, **9**, 1–12.
- 84 M. Eskandari-Nojehdehi, H. Jafarizadeh-Malmiri and A. Jafarizad, Microwave Accelerated Green Synthesis of Gold Nanoparticles Using Gum Arabic and their Physico-Chemical Properties Assessments, *Zeitschrift fur Phys. Chemie*, 2018, **232**, 325–343.
- 85 I. Rocha, E. Lucht, I. C. Riegel-Vidotti, M. Vidotti and E. S. Orth, Kinetic approach to elucidate size controllable features in nanocomposites of gold nanoparticles and poly(3,4-ethylenedioxythiophene) in aqueous dispersion stabilized by gum acacia, *J. Phys. Chem. C*, 2014, **118**, 25756–25764.
- 86 Y. M. Mohan, K. M. Raju, K. Sambasivudu, S. Singh and B. Sreedhar, Preparation of acacia-stabilized silver nanoparticles: A green approach, *J. Appl. Polym. Sci.*, 2007, **106**, 3375–3381.
- 87 V. Kattumuri, K. Katti, S. Bhaskaran, E. J. Boote, S. W. Casteel, G. M. Fent, D. J. Robertson, M. Chandrasekhar, R. Kannan and K. V. Katti, Gum Arabic as a Phytochemical Construct for the Stabilization of Gold Nanoparticles: In Vivo Pharmacokinetics and X-ray-Contrast-Imaging Studies, *Small*, 2007, **3**, 333–341.
- 88 C. C. Wu and D. H. Chen, Facile green synthesis of gold nanoparticles with gum arabic as a stabilizing agent and reducing agent, *Gold Bull.*, 2010, **43**, 234–240.
- 89 H. Kong, J. Yang, Y. Zhang, Y. Fang, K. Nishinari and G. O. Phillips, Synthesis and antioxidant properties of gum arabic-stabilized selenium nanoparticles, *Int. J. Biol. Macromol.*, 2014, **65**, 155–162.
- 90 D. Keerthi Devi, S. Veera Pratap, R. Haritha, K. Samba Sivudu, P. Radhika and B. Sreedhar, Gum acacia as a facile reducing, stabilizing, and templating agent for palladium nanoparticles, *J. Appl. Polym. Sci.*, 2011, **121**, 1765–1773.
- 91 P. Chawla, N. Kumar, A. Bains, S. B. Dhull, M. Kumar, R. Kaushik and S. Punia, Gum arabic capped copper nanoparticles: Synthesis, characterization, and applications, *Int. J. Biol. Macromol.*, 2020, **146**, 232–242.
- 92 S. Kothaplamoottil Sivan, A. K. K. Padinjareveetil, V. V. T. Padil, R. Pilankatta, B. George, C. Senan, M. Černík and R. S. Varma, Greener assembling of MoO₃ nanoparticles supported on gum arabic: cytotoxic effects and catalytic efficacy towards reduction of p-nitrophenol, *Clean Technol. Environ. Policy*, 2019, **21**, 1549–1561.
- 93 M. Venkatesham, D. Ayodhya, A. Madhusudhan, A. Santoshi Kumari, G. Veerabhadram and K. Giriya Mangatayaru, A Novel Green Synthesis of Silver Nanoparticles Using Gum Karaya: Characterization, Antimicrobial and Catalytic Activity Studies, *J. Clust. Sci.*, 2014, **25**, 409–422.
- 94 B. R. Gangapuram, R. Bandi, R. Dadigala, G. M. Kotu and V. Guttena, Facile Green

- Synthesis of Gold Nanoparticles with Carboxymethyl Gum Karaya, Selective and Sensitive Colorimetric Detection of Copper (II) Ions, *J. Clust. Sci.*, 2017, **28**, 2873–2890.
- 95 V. V. T. Padil and M. Černík, Green synthesis of copper oxide nanoparticles using gum karaya as a biotemplate and their antibacterial application., *Int. J. Nanomedicine*, 2013, **8**, 889–98.
- 96 N. H. A. Nguyen, V. V. T. Padil, V. I. Slaveykova, M. Černík and A. Ševců, Green Synthesis of Metal and Metal Oxide Nanoparticles and Their Effect on the Unicellular Alga *Chlamydomonas reinhardtii*, *Nanoscale Res. Lett.*, 2018, **13**, 1–13.
- 97 V. V. T. Padil, S. Waclawek, C. Senan, J. Kupčík, K. Pešková, M. Černík and H. M. Somashekarappa, Gum karaya (*Sterculia urens*) stabilized zero-valent iron nanoparticles: characterization and applications for the removal of chromium and volatile organic pollutants from water, *RSC Adv.*, 2017, **7**, 13997–14009.
- 98 A. J. Kora, R. B. Sashidhar and J. Arunachalam, Gum kondagogu (*Cochlospermum gossypium*): A template for the green synthesis and stabilization of silver nanoparticles with antibacterial application, *Carbohydr. Polym.*, 2010, **82**, 670–679.
- 99 G. B. Reddy, A. Madhusudhan, D. Ramakrishna, D. Ayodhya, M. Venkatesham and G. Veerabhadram, Green chemistry approach for the synthesis of gold nanoparticles with gum kondagogu: characterization, catalytic and antibacterial activity, *J. Nanostructure Chem.*, 2015, **5**, 185–193.
- 100 V. T. P. Vinod, P. Saravanan, B. Sreedhar, D. K. Devi and R. B. Sashidhar, A facile synthesis and characterization of Ag, Au and Pt nanoparticles using a natural hydrocolloid gum kondagogu (*Cochlospermum gossypium*), *Colloids Surfaces B Biointerfaces*, 2011, **83**, 291–298.
- 101 K. S. Saranya, V. V. T. Padil, C. Senan, R. Pilankatta, Sk. Saranya, B. George, S. Waclawek and M. Černík, Green Synthesis of High Temperature Stable Anatase Titanium Dioxide Nanoparticles Using Gum Kondagogu: Characterization and Solar Driven Photocatalytic Degradation of Organic Dye, *Nanomaterials*, 2018, **8**, 1002.
- 102 D. Raju, U. J. Mehta and S. R. Beedu, Biogenic green synthesis of monodispersed gum kondagogu (*Cochlospermum gossypium*) iron nanocomposite material and its application in germination and growth of mung bean (*Vigna radiata*) as a plant model, *IET Nanobiotechnology*, 2016, **10**, 141–146.
- 103 L. Rastogi, S. R. Beedu and A. J. Kora, Facile synthesis of palladium nanocatalyst using gum kondagogu (*Cochlospermum gossypium*): a natural biopolymer, *IET Nanobiotechnology*, 2015, **9**, 362–367.
- 104 D. Silvestri, J. Mikšíček, S. Waclawek, R. Torres-Mendieta, V. V. T. Padil and M. Černík, Production of electrospun nanofibers based on graphene oxide/gum Arabic, *Int. J. Biol. Macromol.*, 2019, **124**, 396–402.
- 105 V. V. T. Padil, C. Senan, S. Waclawek, M. Černík, S. Agarwal and R. S. Varma, Bioplastic Fibers from Gum Arabic for Greener Food Wrapping Applications, *ACS Sustain. Chem.*

- Eng.*, 2019, **7**, 5900–5911.
- 106 V. V. T. Padil, C. Senan, S. Wacławek and M. Černík, Electrospun fibers based on Arabic, karaya and kondagogu gums, *Int. J. Biol. Macromol.*, 2016, **91**, 299–309.
- 107 V. V. T. Padil, N. H. A. Nguyen, Z. Rožek, A. Ševců and M. Černík, Synthesis, fabrication and antibacterial properties of a plasma modified electrospun membrane consisting of gum Kondagogu, dodecyl succinic anhydride and poly (vinyl alcohol), *Surf. Coatings Technol.*, 2015, **271**, 32–38.
- 108 C. Zhang, P. Wang, J. Li, H. Zhang and J. Weiss, Characterization of core-shell nanofibers electrospun from bilayer gelatin/gum Arabic O/W emulsions crosslinked by genipin, *Food Hydrocoll.*, 2021, **119**, 106854.
- 109 R. Y. Tsai, T. Y. Kuo, S. C. Hung, C. M. Lin, T. Y. Hsien, D. M. Wang and H. J. Hsieh, Use of gum arabic to improve the fabrication of chitosan–gelatin-based nanofibers for tissue engineering, *Carbohydr. Polym.*, 2015, **115**, 525–532.
- 110 C. Zhang, Y. Li, P. Wang, A. Zhang, F. Feng and H. Zhang, Electrospinning of bilayer emulsions: The role of gum Arabic as a coating layer in the gelatin-stabilized emulsions, *Food Hydrocoll.*, 2019, **94**, 38–47.
- 111 V. Raj, J. H. Lee, J. J. Shim and J. Lee, Recent findings and future directions of grafted gum karaya polysaccharides and their various applications: A review, *Carbohydr. Polym.*, 2021, **258**, 117687.
- 112 S. Ahmad, M. Ahmad, K. Manzoor, R. Purwar and S. Ikram, A review on latest innovations in natural gums based hydrogels: Preparations & applications, *Int. J. Biol. Macromol.*, 2019, **136**, 870–890.
- 113 R. Mohammadinejad, A. Kumar, M. Ranjbar-Mohammadi, M. Ashrafizadeh, S. S. Han, G. Khang and Z. Roveimiab, Recent Advances in Natural Gum-Based Biomaterials for Tissue Engineering and Regenerative Medicine: A Review, *Polymers (Basel)*, 2020, **12**, 176.
- 114 M. S. Amiri, V. Mohammadzadeh, M. E. T. Yazdi, M. Barani, A. Rahdar and G. Z. Kyzas, Plant-Based Gums and Mucilages Applications in Pharmacology and Nanomedicine: A Review, *Molecules*, 2021, **26**, 1770.
- 115 A. T. Paulino, M. R. Guilherme, L. H. C. Mattoso and E. B. Tambourgi, Smart Hydrogels Based on Modified Gum Arabic as a Potential Device for Magnetic Biomaterial, *Macromol. Chem. Phys.*, 2010, **211**, 1196–1205.
- 116 B. Jamoussi, R. Chakroun, C. Jablaoui and L. Rhazi, Efficiency of Acacia Gummifera powder as biosorbent for simultaneous decontamination of water polluted with metals, *Arab. J. Chem.*, 2020, **13**, 7459–7481.
- 117 R. B. Sashidhar, S. K. Selvi, V. V. T. Padil, T. Kosuri, D. Raju and R. Karuna, Bioprospecting of gum kondagogu (*Cochlospermum gossypium*) for bioremediation of uranium (VI) from aqueous solution and synthetic nuclear power reactor effluents, *J. Environ. Radioact.*, 2015, **148**, 33–41.

- 118 V. V. T. Padil, R. B. Sashidhar and B. Sreedhar, Biosorption of nickel and total chromium from aqueous solution by gum kondagogu (*Cochlospermum gossypium*): A carbohydrate biopolymer, *J. Hazard. Mater.*, 2010, **178**, 851–860.
- 119 V. V. T. Padil, R. B. Sashidhar, N. Sivaprasad, V. U. M. Sarma, N. Satyanarayana, R. Kumaresan, T. N. Rao and P. Raviprasad, Bioremediation of mercury (II) from aqueous solution by gum karaya (*Sterculia urens*): A natural hydrocolloid, *Desalination*, 2011, **272**, 270–277.
- 120 V. V. T. Padil, R. B. Sashidhar, B. Sreedhar, B. Rama Rao, T. Nageswara Rao and J. T. Abraham, Interaction of Pb²⁺ and Cd²⁺ with gum kondagogu (*Cochlospermum gossypium*): A natural carbohydrate polymer with biosorbent properties, *Carbohydr. Polym.*, 2009, **78**, 894–901.
- 121 Standard Test Method for Determination of Oxygen Gas Transmission Rate, Permeability and Permeance at Controlled Relative Humidity Through Barrier Materials Using a Coulometric Detector, <https://www.astm.org/f1927-14.html>, (accessed 9 December 2021).
- 122 Standard Test Methods for Water Vapor Transmission of Materials, https://www.astm.org/e0096_e0096m-05.html, (accessed 9 December 2021).
- 123 Standard Test Method for Oxygen Gas Transmission Rate Through Plastic Film and Sheeting Using a Coulometric Sensor, <https://www.astm.org/d3985-02e01.html>, (accessed 9 December 2021).
- 124 L. Halim, M. A. Pascall, J. Lee and B. Finnigan, Effect of Pasteurization, High-Pressure Processing, and Retorting on the Barrier Properties of Nylon 6, Nylon 6/Ethylene Vinyl Alcohol, and Nylon 6/Nanocomposites Films, *J. Food Sci.*, 2009, **74**, N9–N15.
- 125 A. Blanchard, F. Gouanvé and E. Espuche, Effect of humidity on mechanical, thermal and barrier properties of EVOH films, *J. Memb. Sci.*, 2017, **540**, 1–9.
- 126 C. Maes, W. Luyten, G. Herremans, R. Peeters, R. Carleer and M. Buntinx, Recent Updates on the Barrier Properties of Ethylene Vinyl Alcohol Copolymer (EVOH): A Review, *Polym. Rev.*, 2018, **58**, 209–246.
- 127 E. Doblhofer, J. Schmid, M. Rieß, M. Daab, M. Suntinger, C. Habel, H. Bargel, C. Hugenschmidt, S. Rosenfeldt, J. Brey and T. Scheibel, Structural Insights into Water-Based Spider Silk Protein–Nanoclay Composites with Excellent Gas and Water Vapor Barrier Properties, *ACS Appl. Mater. Interfaces*, 2016, **8**, 25535–25543.
- 128 F. Wu, M. Misra and A. K. Mohanty, Challenges and new opportunities on barrier performance of biodegradable polymers for sustainable packaging, *Prog. Polym. Sci.*, 2021, **117**, 101395.
- 129 H. L. Calambas, A. Fonseca, D. Adames, Y. Aguirre-Loredo and C. Caicedo, Physical-Mechanical Behavior and Water-Barrier Properties of Biopolymers-Clay Nanocomposites, *Mol. 2021, Vol. 26, Page 6734*, 2021, **26**, 6734.
- 130 Z. Shen, A. Rajabi-Abhari, K. Oh, G. Yang, H. J. Youn and H. L. Lee, Improving the Barrier

- Properties of Packaging Paper by Polyvinyl Alcohol Based Polymer Coating—Effect of the Base Paper and Nanoclay, *Polymers (Basel)*, 2021, **13**, 1334.
- 131 J. Wang, D. J. Gardner, N. M. Stark, D. W. Bousfield, M. Tajvidi and Z. Cai, Moisture and Oxygen Barrier Properties of Cellulose Nanomaterial-Based Films, *ACS Sustain. Chem. Eng.*, 2018, **6**, 49–70.
- 132 L. Meng, F. Xie, B. Zhang, D. K. Wang and L. Yu, Natural Biopolymer Alloys with Superior Mechanical Properties, *ACS Sustain. Chem. Eng.*, 2019, **7**, 2792–2802.
- 133 E. Jamróz, P. Kulawik and P. Kopel, The Effect of Nanofillers on the Functional Properties of Biopolymer-Based Films: A Review, *Polymers (Basel)*, 2019, **11**, 675.
- 134 S. Agarwal, Major factors affecting the characteristics of starch based biopolymer films, *Eur. Polym. J.*, 2021, **160**, 110788.
- 135 M. G. A. Vieira, M. A. Da Silva, L. O. Dos Santos and M. M. Beppu, Natural-based plasticizers and biopolymer films: A review, *Eur. Polym. J.*, 2011, **47**, 254–263.
- 136 A. Kocira, K. Kozłowicz, K. Panasiewicz, M. Staniak, E. Szpunar-Krok and P. Hortyńska, Polysaccharides as Edible Films and Coatings: Characteristics and Influence on Fruit and Vegetable Quality—A Review, *Agronomy*, 2021, **11**, 813.
- 137 Y. Cheng, W. Tian, Q. Mi, X. Zheng and J. Zhang, Highly Transparent All-Polysaccharide Composite Films with Tailored Transmission Haze for Light Manipulation, *Adv. Mater. Technol.*, 2020, **5**, 2000378.
- 138 L. C. Tomé, N. H. C. S. Silva, H. R. Soares, A. S. Coroadinha, P. Sadocco, I. M. Marrucho and C. S. R. Freire, Bioactive transparent films based on polysaccharides and cholinium carboxylate ionic liquids, *Green Chem.*, 2015, **17**, 4291–4299.
- 139 P. Suppakul, J. Miltz, K. Sonneveld and S. W. Bigger, Active Packaging Technologies with an Emphasis on Antimicrobial Packaging and its Applications, *J. Food Sci.*, 2003, **68**, 408–420.
- 140 M. Ozdemir and J. D. Floros, Active Food Packaging Technologies, *Crit. Rev. Food Sci. Nutr.*, 2010, **44**, 185–193.
- 141 V. A. Jideani and K. Vogt, Antimicrobial Packaging for Extending the Shelf Life of Bread—A Review, *Crit. Rev. Food Sci. Nutr.*, 2015, **56**, 1313–1324.
- 142 Z. Fang, Y. Zhao, R. D. Warner and S. K. Johnson, Active and intelligent packaging in meat industry, *Trends Food Sci. Technol.*, 2017, **61**, 60–71.
- 143 I. Ahmed, H. Lin, L. Zou, A. L. Brody, Z. Li, I. M. Qazi, T. R. Pavase and L. Lv, A comprehensive review on the application of active packaging technologies to muscle foods, *Food Control*, 2017, **82**, 163–178.
- 144 K. A. Roche, Food Labeling: Applications, *Encycl. Food Heal.*, 2016, 49–55.

- 145 A. Morinval and L. Averous, Systems Based on Biobased Thermoplastics: From Bioresources to Biodegradable Packaging Applications, *Polym. Rev.*, 2021, 1–69.
- 146 U. Pagga, D. B. Beimborn and M. Yamamoto, Biodegradability and compostability of polymers—test methods and criteria for evaluation, *J. Environ. Polym. Degrad.*, 1996, **4**, 173–178.
- 147 A. Magnin, E. Pollet, V. Phalip and L. Avérous, Evaluation of biological degradation of polyurethanes, *Biotechnol. Adv.*, 2020, **39**, 107457.
- 148 T. Kijchavengkul and R. Auras, Compostability of polymers, *Polym. Int.*, 2008, **57**, 793–804.
- 149 V. V. T. Padil, N. H. A. Nguyen, A. Ševcu° and M. Černík, Fabrication, Characterization, and Antibacterial Properties of Electrospun Membrane Composed of Gum Karaya, Polyvinyl Alcohol, and Silver Nanoparticles, *J. Nanomater.*, 2015, **2015**, 10.
- 150 T. L. Cao and K. Bin Song, Active gum karaya/Cloisite Na⁺ nanocomposite films containing cinnamaldehyde, *Food Hydrocoll.*, 2019, **89**, 453–460.
- 151 R. K. Ramakrishnan, S. Waclawek, M. Černík and V. V. T. Padil, Biomacromolecule assembly based on gum kondagogu-sodium alginate composites and their expediency in flexible packaging films, *Int. J. Biol. Macromol.*, 2021, **177**, 526–534.